

The Formation of an Infection-related Membrane Domain is Controlled by the Sequential Recruitment of Scaffold and Receptor Proteins

Dissertation

der Fakultät für Biologie der
Ludwig-Maximilians-Universität München

vorgelegt von

THOMAS FRANZ STRATIL

aus München

15. Dezember 2015



The Formation of an Infection-related Membrane Domain is Controlled by the Sequential Recruitment of Scaffold and Receptor Proteins

Dissertation

der Fakultät für Biologie der
Ludwig-Maximilians-Universität München

vorgelegt von

THOMAS FRANZ STRATIL
aus München

15. Dezember 2015

Die vorliegende Arbeit wurde im Bereich Genetik der Arbeitsgruppe von Herrn Prof. Dr. Thomas Ott angefertigt.

Erstgutachter: Prof. Dr. Thomas Ott

Zweitgutachter: Prof. Dr. Marc Bramkamp

Dissertation eingereicht am 15. Dezember 2015

Tag der mündlichen Prüfung: 28. April 2016

Eidesstattliche Versicherung

Hiermit erkläre ich an Eides statt, dass ich die vorliegende Arbeit selbstständig, und ohne unerlaubte Hilfe von Dritten angefertigt habe.

München, den

(Thomas F. Stratil)

Erklärung

Ich habe weder anderweitig versucht, eine Dissertation einzureichen oder mich einer Doktorprüfung zu unterziehen, noch habe ich diese Dissertation oder Teile derselben einer anderen Prüfungskommission vorgelegt.

München, den

(Thomas F. Stratil)

Contents

Eidesstattliche Versicherung	iii
Contents	iv
List of Figures	vii
Frequently Used Abbreviations	ix
Summary	1
Zusammenfassung	2
1 Introduction	3
1.1 The Context of Research	3
1.2 Symbiotic Plant Microbe-Interactions	4
1.2.1 Arbuscular Mycorrhiza	4
1.2.2 Root Nodule Symbiosis	4
1.3 Symbiotic Signaling at the Plasma Membrane During RNS	9
1.3.1 The Role of the Receptor-like Kinases.....	9
1.3.2 Downstream Targets of the Receptor-like Kinases	11
1.3.3 Symbiotic Flotillins	12
1.3.4 Symbiotic Remorin	13
1.4 Plasma Membrane Compartmentalization	14
1.4.1 The Fluid Mosaic Model	14
1.4.2 The Picket Fence Model	15
1.4.3 Membrane Rafts	16
1.4.4 The Plasma Membrane - Cell Wall Continuum	19
1.5 Microdomains in the Plant's Plasma Membrane	20
1.5.1 The Casparian Strip Domain.....	21
1.5.2 Microdomains in Plant Development	21
1.5.3 Microdomains in Plant-Biotic Interactions.....	22
1.5.4 Remorins as Markers for Plant Microdomains.....	23
1.6 Root Nodule Symbiosis Specific Microdomains	24
2 Aim of This Study	27
3 Results	28
3.1 FLIM-FRET Microscopy as a Tool to Identify Microdomains	28
3.1.1 LjSYMREM1 Interacts with NFR1 in Microdomains.....	28
3.1.2 MtSYMREM1 SLiM Mutants Interact with LYK3.....	30

3.1.3	FLIM-FRET in <i>Arabidopsis thaliana</i>	31
3.2	Identification of Components Required for SYMREM1-labeled Microdomains	33
3.2.1	SYMREM1-labeled Microdomains are Actin Dependent	33
3.2.2	SYMREM1 Domains Co-localize with Actin Filaments	35
3.3	SYMREM1 mis-localizes in the LYK3 Mutant Allele <i>hcl-1</i>.....	37
3.4	The Actin Cytoskeleton is Altered in <i>Medicago truncatula hcl-1</i>.....	40
3.5	SYMREM1 Localization is Dependent on FLOT4 in the Homologous <i>Medicago truncatula</i> Root System.....	44
3.5.1	SYMREM1 and FLOT4 Co-localize in <i>Medicago truncatula</i>	44
3.5.2	<i>SYMREM1</i> and <i>FLOT4</i> Promoters are Active at the Same Time.....	46
3.5.3	SYMREM1 Microdomains are Reduced upon RNAi of <i>FLOT4</i>	48
3.6	Artificial Assembly of a Root- and Symbiosis- Specific Microdomain	49
3.6.1	FLOT4 induces SYMREM1 Compartmentalization in <i>Nicotiana benthamiana</i>	50
3.6.2	LYK3 is Required for SYMREM1 and FLOT4 Localization Into Microdomains in <i>N. benthamiana</i>	56
4	Discussion	61
4.1	Stability of SYMREM1-labeled Microdomains	61
4.2	Flotillins Compartmentalize the Plasma Membrane	64
4.3	Cytoskeleton Defect in <i>hcl-1</i>.....	66
4.4	The Cell Wall and the Immobilization of LYK3	68
4.5	A Model for Microdomain-Assembly	71
4.6	Hypothesis on the Biological Meaning of Root Nodule Symbiosis Specific Microdomains	72
4.6.1	GTPases	73
4.6.2	E3 Ubiquitin Ligases	74
4.6.3	Proteins Required for Exocytosis	75
4.6.4	Cell-wall-degrading Enzymes	76
4.6.5	Exopolysaccharides Receptors.....	76
4.6.6	DMI2/ SYMRK and Its Interactors	77
4.6.7	NADPH Oxidases	78
4.7	Outlook	79
5	Methods	80
5.1	Cultivation Methods	80
5.1.1	Bacterial Growth Conditions.....	80
5.1.2	Rhizobial Inoculation of <i>Medicago truncatula</i>	80
5.1.3	<i>Nicotiana benthamiana</i> Growth Conditions	80
5.1.4	<i>Medicago truncatula</i> Growth Conditions	80
5.2	Transformation Methods.....	81
5.2.1	Transformation of <i>Escherichia coli</i>	81
5.2.2	Transformation of <i>Agrobacterium</i> Strains.....	81
5.2.3	Transient Transformation of <i>Nicotiana benthamiana</i> Leaves	81
5.2.4	Sterilization and Germination of <i>Medicago truncatula</i> Seeds.....	82
5.2.5	Transient Transformation of <i>Medicago truncatula</i>	82
5.3	Confocal Microscopy	82

Contents

5.4 FLIM-FRET Microscopy	83
5.4.1 Interaction Between SYMREM1 and NFR1/LYK3	83
5.4.2 Interaction Between Strubbelig and Quirky	84
5.5 Image Processing	84
5.5.1 Co-localization Analysis	84
5.5.2 Domain Counting	86
5.5.3 Determination of Actin Orientation	86
5.6 Cytoskeleton Disruption	87
5.7 Molecular Biology Methods	87
5.7.1 PCRs	87
5.7.2 Cloning	87
5.7.3 Western Blot	88
5.7.4 Constructs Used/Generated in This Study	89
5.7.5 Primer Used in This Study	91
6 References	93
Contributions to Publications	123
Acknowledgments	124
Curriculum Vitae	125

List of Figures

Figure 1 Scheme of the symbiotic, epidermal infection process.	6
Figure 2 Simplified model of plasma membrane compartmentalization.....	18
Figure 3 FLIM-FRET reveals interaction between SYMREM1 and NFR1 in precise areas of the plasma membrane.	29
Figure 4 FLIM-FRET in <i>Arabidopsis thaliana</i> reveals plasmodesmata-localized interaction between SUB and QKY.	32
Figure 5 Depolymerisation of microtubules and actin filaments in <i>Medicago truncatula</i> A17 roots.	34
Figure 6 SYMREM1 microdomains are dependent on the actin cytoskeleton.....	35
Figure 7 SYMREM1-labeled microdomains co-localize with actin filaments.	37
Figure 8 YFP:SYMREM1 localizes into microdomains in root hairs of <i>Medicago truncatula</i> RLKs mutants.	38
Figure 9 Patterns of SYMREM1-labelled MDs are altered in the <i>hcl-1</i> mutant allele.	39
Figure 10 The <i>Medicago truncatula</i> LYK3 mutant <i>hcl-1</i> shows a strong root hair elongation defect.	41
Figure 11 Transgenic roots of <i>hcl-1</i> show a strongly altered actin pattern.....	42
Figure 12 Actin patterns are altered throughout <i>hcl-1</i> roots.....	43
Figure 13 SYMREM1 and Lifeact co-localize in <i>hcl-1</i>	44
Figure 14 FLOT4 localization in transgenic <i>Medicago truncatula</i> root cells.....	45
Figure 15 FLOT4 is an essential building block of SYMREM1-labelled microdomains.	46
Figure 16 The <i>SYMREM1</i> and <i>FLOT4</i> promoters are active in the epidermis.....	47
Figure 17 Microdomain-labeling by SYMREM1 is FLOT4-dependent.....	49
Figure 18 SYMREM1 and FLOT4 exclude each other locally in <i>Nicotiana benthamiana</i>	51
Figure 19 Microtubules tracks exclude SYMREM1.....	52
Figure 20 YFP:SYMREM1 is compartmentalized by FLOT4 and not by LYK3.	52
Figure 21 Compartmentalization of SYMREM1 in leaf epidermal cells is FLOT4 dependent.	53

List of Figures

Figure 22 Controls for FLOT4-mCherry induced compartmentalization in <i>Nicotiana benthamiana</i>	55
Figure 23 <i>Arabidopsis thaliana</i> Flotillin1a does not induce SYMREM1-compartmentalization in <i>Nicotiana benthamiana</i>	55
Figure 24 Artificial reconstitution of a symbiosis-related MD in <i>Nicotiana benthamiana</i>	57
Figure 25 LYK3 is recruited into a symMD in a SYMREM1-dependent manner.	58
Figure 26 FLOT2 does not induce the formation of microdomains in <i>Nicotiana benthamiana</i>	59
Figure 27 Model depicting steps in microdomain assembly during Root Nodule Symbiosis.	71
Figure 28 The procedure of co-localization analysis and verification by randomization.	85
Figure 29 The steps for domain counting.	86

Frequently Used Abbreviations

AM	Arbuscular Mycorrhiza
BiFC	Bimolecular Fluorescence Complementation
CLSM	Confocal Laser Scanning Microscopy
Compl.	Complemented
DIM	Detergent insoluble membrane
DMI2	Doesn't Make Infections 2
dpi	Days post infiltration
DRM	Detergent resistant membrane
EPS	Exopolysaccharides
FLIM	Fluorescent Lifetime Imaging Microscopy
FLOT	Flotillin
FRET	Foerster Resonance Energy Transfer
GFP	Green fluorescent protein
HA	Hemagglutinin epitope
<i>hcl</i>	Hair curling (LYK3 allele)
ID	Intrinsic disorder
IT	Infection thread
<i>L.</i>	<i>Lotus</i>
LCO	Lipo-chitoooligosaccharide
LYK3	LysM Receptor-like Kinase 3
<i>M.</i>	<i>Medicago</i>
MAP4	Microtubule binding domain of MAP4
MD	Mesoscale microdomain
MoRF	Molecular recognition feature
<i>N.</i>	<i>Nicotiana</i>
n=	Sample number
NF	Nodulation factor
NFP	Nod Factor Perception (Receptor-like kinase)
NFR1	Nod Factor Receptor 1
NFR5	Nod Factor Receptor 5
NLS	Nuclear localization signal
ns	Nanosecond
p	Promoter
p=	P value
p35S	Cauliflower Mosaic Virus 35s promoter
PD	Plasmodesmata
PIT	Preinfection thread

Frequently Used Abbreviations

PM	Plasma membrane
PPA	Prepenetration apparatus
ps	Picosecond
pUbi	Polyubiquitin promoter
QKY	Quirky
rd Rr	Randomized Pearson correlation coefficient
REM	Remorin
RemCa	Remorin C-terminal membrane anchor
RLK	Receptor like kinase
RNAi	RNA interference
RNS	Root Nodule Symbiosis
ROS	Reactive oxygen species
Rr	Pearson correlation coefficient
SE	Standard error
SLiM	Short linear motif
SUB	Strubbelig
SYMRK	Symbiosis Receptor Kinase
UTR	Untranslated region
YFP	Yellow fluorescent protein
τ	Fluorescence lifetime

Summary

The plasma membrane (PM) is a spatially highly organized organelle in which membrane proteins are clustered in so-called microdomains (MD). These are thought to function as hubs for condensing relevant signaling proteins. During Root Nodule Symbiosis, a beneficial interaction of legumes with nitrogen fixing bacteria, key signaling components at the plasma membrane localize into such microdomains. These include the receptor-like kinase LYK3, the flotillin FLOT4, and the remorin SYMREM1.

In this work, we show the requirements for the formation of SYMREM1-labeled MDs. We establish that the stability of these MD depends on the actin cytoskeleton, and we show, statistically, that the SYMREM1 and FLOT4- labeled MDs greatly co-localize in the homologous *Medicago truncatula* system. Silencing of endogenous *FLOT4* by RNAi reduces the number of SYMREM1-labeled MD, demonstrating FLOT4 also is required for MD stability. Studies on the *FLOT4* and *SYMREM1* promoter activity reveal similar induction in timely and spatial manner. Therefore, FLOT4 and SYMREM1 may target identical MDs. In the *Medicago* LYK3 mutant allele *hcl-1*, SYMREM1-, and FLOT4-labeled MDs mis-localize at the PM, which results from a previously non-described defect in the organization of the actin cytoskeleton.

In the heterologous overexpression system, *Nicotiana benthamiana*, SYMREM1 by itself does not label MD. Thus, this system lacks components that are required for the formation of such MDs. The step-wise addition of differently tagged FLOT4 and LYK3 constructs, reveal a FLOT4-dependent compartmentalization of SYMREM1 in *Nicotiana*, confirming data from the homologous system. Furthermore, the presence of LYK3 induced the formation of clear, co-localizing FLOT4/SYMREM1-labeled MD. The co-expression of other flotillins could not induce the formation of such a MD. This demonstrated that we were able to re-constitute a core of a symbiosis-related MD in a heterologous system, and indicates that SYMREM1, FLOT4 and LYK3 localize to the same MD to regulate signaling during root nodule symbiosis.

Zusammenfassung

In der hochorganisierten Plasmamembran lokalisieren Proteine in sogenannten Mikrodomänen. Während der Wurzelknöllchensymbiose, einer Interaktion zwischen Leguminosen und Stickstoff-fixierenden Bakterien, sind essentielle Signalkomponenten in solchen Mikrodomänen organisiert. Dies trifft zu auf die Rezeptor-ähnliche Kinase LYK3, das Flotillin FLOT4, und das Remorin SYMREM1.

In dieser Arbeit wird gezeigt, wie die SYMREM1-beinhaltenden Mikrodomänen stabilisiert sind. Für die Stabilität dieser SYMREM1-markierten Mikrodomänen ist das Aktin Zytoskelett zuständig. Weitergehend, wird statistisch deutlich, dass SYMREM1 und FLOT4 im homologen System *Medicago* in Mikrodomänen co-lokalisieren. Reduzierung des *FLOT4*-Transkripts durch RNA-Interferenz verursacht eine Verringerung an SYMREM1-markierten Mikrodomänen. Dies verdeutlicht, dass FLOT4 auch essentiell ist damit SYMREM1 in Mikrodomänen lokalisieren kann. Eine Analyse der Promoteraktivität zeigt, dass *SYMREM1* und *FLOT4* zeitgleich, und in den gleichen Zelltypen exprimiert werden. Demnach wird vermutet, dass diese beiden Proteine in identischen Mikrodomänen lokalisieren. In einer Mutanten LYK3 *Medicago* Linie, nämlich *hcl-1*, fehllokalisieren sowohl SYMREM1-, als auch FLOT4-markierte Mikrodomänen in der PM, was wir auf ein zuvor unentdecktes, strukturell verändertes Aktin Zytoskelett in dieser Linie zurückführen.

In dem heterologen Expressionssystem *Nicotiana benthamiana*, markiert SYMREM1 keine Mikrodomänen. In diesem System fehlen also Komponenten die nötig sind um diese Mikrodomänen zu bilden. Eine schrittweise erfolgende additive co-expression von SYMREM1 mit FLOT4 und/oder LYK3 zeigt, dass sich eine Mikrodomänen-Population nur bildet wenn alle drei Proteine gleichzeitig anwesend sind. Substitution von FLOT4 durch andere Flotilline konnte keine Bildung solcher Domänen herbeiführen. Somit wurde erstmals gezeigt, dass eine potenziell symbiose-spezifische Mikrodomäne in einem heterologen System rekonstituiert werden konnte. Dies deutet darauf hin, dass SYMREM1, FLOT4 und LYK3 alle in der gleichen Mikrodomäne vorhanden sind, und gemeinsam Signalprozesse während der Etablierung der Wurzelknöllchensymbiose regulieren.

1 Introduction

1.1 The Context of Research

Feeding the world's growing population is one of today's greatest challenges. In the past, food production has relied heavily on agricultural expansion and new technologies, developed in the Industrial and Agricultural Revolutions of the 18th and 19th century. Later, during the Green Revolution of the 20th century, the generation of high-yield crops, as well as the extensive use of pesticides and fertilizers, resulted in a large increase in crop yields. Food production in the past half century was able to keep up with a rapidly growing world population (currently 7.3 billion.)

This type of agricultural production has, however, been detrimental to the environment. It has had a significant negative impact on: global warming, the loss of biodiversity, loss or eutrophication of (fresh) water resources, deforestation and soil salinization, and it is non-sustainable (Foley et al., 2005; Power, 2010).

The world's population is projected to near, or even surpass, the 10 billion mark by the year 2050: a plus of 3 billion added to today's population (Gerland et al., 2014). Feeding these people will require a multitude of efforts, including, among many other things: a change in eating habits, less wasting of agricultural products, more modern equipment and irrigation and distribution systems (Foley et al., 2011). Ultimately, sustainability will have to be the foundation of agricultural production in the future.

Nitrogen is one limiting factor in the cultivation of plants designated for food production. The extensive application of industrial nitrogenous fertilizers to boost plant growth is the cause of major environmental problems (Rockstrom et al., 2009). The amount of fertilizers used has gone up by more than 800% over the course of the last 50 years (Tilman et al., 2001).

Some plants, the legumes, do not require extensive nitrogen fertilization. They undergo a symbiotic relationship with bacteria, commonly termed 'rhizobia', making these plants less dependent on nitrate in the soil. This so-called root nodule symbiosis (RNS) is of great interest to scientists in the field of molecular research. The discovery of the genetic prerequisites for the plant's compatibility to undergo RNS, and, therefore, the potential genetic transfer of this ability

to non-symbiotic economic plants may provide part of the solution to more sustainable agricultural practices.

1.2 Symbiotic Plant Microbe-Interactions

In order to cope with the limited availability of nutrients, most land plants have the ability to undergo endosymbiosis with either fungi and/or bacteria. These symbioses are in fact so common that they are the default mechanism with which plants acquire their mineral nutrients and are thought to be prerequisites for the plants survival under limiting or harsh environmental conditions (Wang and Qiu, 2006; Bunn et al., 2009; Al-Yahya'ei et al., 2011).

1.2.1 Arbuscular Mycorrhiza

The evolutionary, more ancient type of endosymbiosis, termed 'arbuscular mycorrhiza' (AM) occurs between most land plants and fungi of the genus *Glomeromycota* (AM), named so for the intracellular accommodation of highly branched 'tree-like structures' (arbuscules) of the fungus within the cortical cell layers of the host plant (Parniske, 2008).

AM symbiosis is initiated when the plant detects signals, the 'myc factors' (Maillet et al., 2011), from the fungal hyphopodia and reacts by generating a prepenetration apparatus (PPA) (Genre et al., 2005; Genre et al., 2008) that precedes epidermal infection of the plant by the fungus. The PPA is made up of cytoskeletal and endoplasmic reticulum components; it contains a cytoplasmic bridge linked to the nucleus and forms an organized structure just beneath the site of contact between the fungus and the plant. The PPA has been shown to function as a guide for the intracellular path (in *Medicago truncatula*; intercellular in *Lotus japonicus*) of fungal infection through the epidermal and the cortical cell layers (Genre et al., 2005; Genre et al., 2008). In the cortex, the fungus grows along the apoplast and subsequently enters a host cell through a PPA-like structure, where it branches and forms the mature arbuscule. The arbuscule is completely surrounded by both the fungal and the plant plasma membrane (PM) (Genre et al., 2008), which establishes the arbuscule 'symbiotic interface', the place of nutrient exchange. The fungus provides (among other nutrients) phosphorus to the plant and in return receives up to a fifth of the plants produced photosynthates (Bago et al., 2000).

1.2.2 Root Nodule Symbiosis

Legumes, e.g. the model plants *Medicago truncatula* and *Lotus japonicus* additionally have the ability to establish a symbiotic relationship with bacteria, which are capable of reducing

atmospheric nitrogen. This so-called ‘root nodule symbiosis’ (RNS) shares a genetic pathway with AM signaling, the genes of which are termed ‘common symbiosis genes’ (Parniske, 2008; Popp and Ott, 2011; Oldroyd, 2013). During RNS the symbiotic interface is formed between compatible (nitrogen fixing) rhizobia and the plant.

The Infection Process

The establishment of RNS begins when bacteria recognize plant-derived signals. Legume roots secrete a mixture of flavonoids into the rhizosphere, a process that is dependent on and, therefore, an indicator of phosphorus and nitrogen availability in the soil (Coronado et al., 1995; Juszczuk et al., 2004). The flavonoids function as attractants of rhizobia and activate the expression of rhizobial *nod* genes resulting in the production of Nodulation-factors (NF) (Oldroyd and Downie, 2004; Peck et al., 2006). NFs are lipochitooligosaccharides (LCOs) with an N-acetylglucosamine backbone, but depending on the rhizobial species, they come in various lengths and with several modifications. This diversity in the NFs is one determinant for the observed specificity of the rhizobia-host plant interaction (Roche et al., 1991, Miller, 2012; Denarie et al., 1996).

Responsible for the recognition of the NFs are LysM-domain-containing receptor-like kinases (RLKs) in the plasma membrane (PM) of the plant. These are NOD FACTOR PERCEPTION (NFP) and LysM-DOMAIN-CONTAINING RECEPTOR-LIKE KINASE (LYK3) of *M. truncatula* (Ben Amor et al., 2003; Limpens et al., 2003; Arrighi et al., 2006) and NOD FACTOR RECEPTOR 5 (NFR5) and NOD FACTOR RECEPTOR 1 (NFR1) of *L. japonicus* (Madsen et al., 2003; Radutoiu et al., 2003).

The LysM-domain is a motif typically found in proteins of bacteria and can attach to chitin (or chitin-like compounds) or peptidoglycans (Buist et al., 2008), to which NFs are very similar in structure and chemical composition. LysM-domain-containing-RLKs are plant specific (Zhang et al., 2009) and are also key players in immunity responses (Kaku et al., 2006; Miya et al., 2007; Wan et al., 2008; Iizasa et al., 2010; Petutschnig et al., 2010; Nakagawa et al., 2011; Willmann et al., 2011; Gust et al., 2012; Wan et al., 2012; Tanaka et al., 2013). The signal is then transduced via a Leucin-rich repeat containing RLK DOESN'T MAKE INFECTIONS 2 (DMI2) of *M. truncatula*/SYMBIOSIS RECEPTOR-LIKE KINASE (SYMRK) of *L. japonicus* (Endre et al., 2002a; Stracke et al., 2002).

NF-detection ultimately results in specific calcium fluxes at the root hair tip and specific nuclear calcium oscillations (‘spiking’): first in epidermal cells, and later in cortical cells the spiking signature prime the plant for infection (Ehrhardt et al., 1996; Oldroyd and Downie, 2004; Oldroyd, 2013) and active activates nodulation specific genes (Miwa et al., 2006b). Root hair cells begin to swell, then curl to enclose rhizobia, which then form a microcolony (van Brussel et

al., 1992a; Heidstra et al., 1994; Esseling et al., 2003; Gage, 2004). The calcium flux may serve as a key signal that leads to a reorientation of the polar outward directed growth of the root-hair cell in such a way that an inward growing invagination is formed (Walker and Downie, 2000; Miwa et al., 2006a). This structure will lead to the formation of an infection thread (IT).

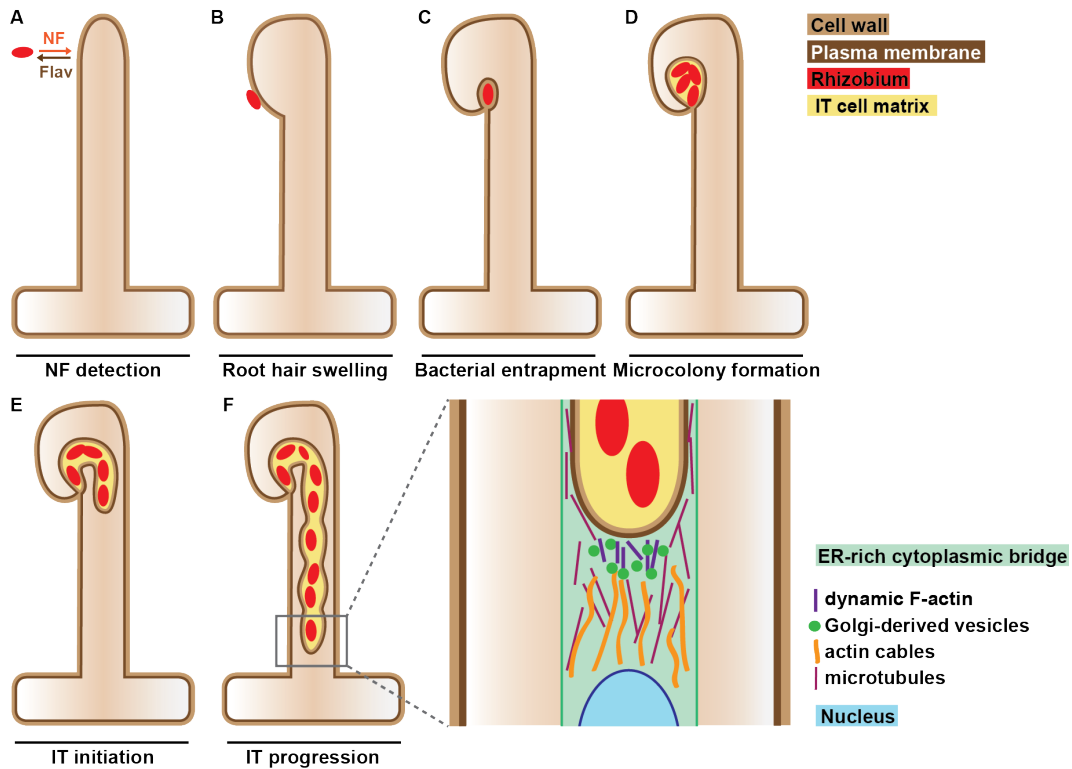


Figure 1 Scheme of the symbiotic, epidermal infection process. (A) Under nitrogen-limiting conditions, the plant secretes so called flavonoids (Flav), which attract rhizobia. Rhizobia secrete Nodulation-factors (NF) that are recognized by symbiotic receptor-like kinases, located in the PM of the root hairs. **(B)** Detection of NFs induces cellular responses in the root hair that include Ca^{2+} fluxes, cytoskeletal rearrangements, and cell wall modifications. These result in root hair swelling. **(C)** Reorientation of root hair tip growth leads to root hair curling and entrapment of a rhizobium in a three dimensional structure. This occurs within 1.5 hours after first symbiotic signaling. **(D)** A pause of 10-20 hours, in which rhizobia continue dividing to form a microcolony, precedes the initiation of an infection thread (IT). **(E)** After the pause, the IT begins to grow by inward directed polar tip growth. **(F)** The IT elongates in alternating periods of rapid expansion, and subsequent pauses, during which the dividing bacteria catch up with the IT-tip. The boxed inset is a magnification of (F), which emphasizes that rhizobia are surrounded by a plant-produced IT-cell wall and the plant's PM. During IT-initiation and -progression, directed vesicle trafficking, active remodeling of the cytoskeleton, and precise nucleus positioning are vital and tightly controlled. Model drawn according to (Fournier et al., 2008; Oldroyd et al., 2011).

Proteins located in the nuclear membranes are believed to generate the calcium oscillations. Mutants of the calcium-gated potassium channels POLLUX (*L. japonicus*)/DMI1 (*M. truncatula*), and CASTOR (Ane et al., 2004; Riely et al., 2007; Charpentier et al., 2008; Capoen et al., 2011), and of the nucleoporins, NUP85, NUP133, and NENA (Kanamori et al., 2006; Saito et al., 2007;

Groth et al., 2010) do not produce regular calcium spiking signatures. The true calcium channel has not been identified, yet.

At the future site of infection in the root hair cell, a ‘pre-infection thread’ (PIT) structure is formed. Similar to the PPA in the mycorrhizal symbiosis, the PIT is formed by active nucleus relocation, cytoskeletal rearrangements and endoplasmic reticulum alignment to the site of NF detection (Van Brussel et al., 1992b; Fournier et al., 2008). The PIT directs the growth of the IT, which is filled with actively dividing rhizobia towards the root cortex where the IT branches out (Fournier et al., 2008).

Cytoskeletal Rearrangements During the Infection

NF-detection induces root hair swelling, and curling, the initiation-, and polar progression of ITs, which coincide with, and are dependent on, continuous cytoskeletal rearrangements in the plant (Cárdenas et al., 1998; Timmers et al., 1999; Esseling et al., 2003; Gage, 2004; Timmers, 2008; Oldroyd et al., 2011). Many mutants identified emphasize the necessity of a dynamic actin cytoskeleton. ITs of *L. japonicus nap1* (Nck-ASSOCIATED PROTEIN 1) and *pir1* (121F-SPECIFIC P53 INDUCIBLE RNA) mutants are strongly reduced in number, arrested within the root hairs and severely deformed into inflated sac-like structures (Yokota et al., 2009). NAP1 and PIR1 are components of a large complex that regulates actin polymerization (Ibarra et al., 2005). *Lotus* mutants of *arpc1* (ACTIN-RELATED PROTEIN COMPONENT 1) show defects in trichomes, and root hair elongation, and are also impaired in symbiotic root hair curling, and IT-initiation (Hossain et al., 2012). The ‘REQUIRED FOR INFECTION THREAD’ locus (*RIT*) encodes for the *Medicago* orthologue of *NAP1*. ITs of *rit-1* mutants frequently abort in the epidermis or outer cortex as swollen structures. This indicates that NAP1/RIT1 is required for directing filamentous actin reorganization in such a manner that supports polar growth of ITs (Yokota et al., 2009; Miyahara et al., 2010). Another *Lotus* mutant, *crinkle*, displays an altered actin cytoskeleton and is blocked during IT-progression (Tansengco et al., 2003; Tansengco et al., 2004). Remarkably, it appears that legumes have adapted proteins from the SCAR/WAVE actin regulatory complex by gene duplication to function specifically in RNS (Qiu et al., 2015). *SCAR-NODULATION* (*SCARN*) is induced in a *NIN*-dependent manner, highlighting the importance, and specificity of symbiosis induced actin remodeling. While early actin rearrangements occur unimpaired in response to rhizobia, the ITs do not progress further than the microcolony stage (Qiu et al., 2015). Potentially, *SCARN* is only required for later actin rearrangements, during elongation of the ITs.

CERBERUS (*Lotus*)/LUMPY INFECTIONS (LIN, *Medicago*), an E3 ubiquitin ligase is also required for the progression of ITs. The mutant *cerberus* entraps bacteria in root hair curls, however IT-formation and penetration into root hairs is strongly impaired (Kiss et al., 2009; Yano

et al., 2009). CERBERUS/LIN is required, but not essential, for development of nodule primordia (Kiss et al., 2009; Yano et al., 2009).

Nodule Organogenesis

Concomitant with IT-production, previously dormant cortical cells begin to divide and create a nodule primordium. It is within this maturing nodule where nitrogen-fixing bacteria are finally released from ITs, differentiate into bacteroids and live in organelle-like structures termed symbiosomes. These symbiosomes are surrounded by a plant-PM-derived specialized membrane (Whitehead et al., 1998), in which the nitrogenase-enzyme complex of the bacteria is protected by an oxygen-diffusion barrier, ensuring the anoxic environment needed for the fixation of atmospheric nitrogen (Tjepkema and Yocum, 1974; Hunt et al., 1987; Macfall et al., 1992; Wycoff et al., 1998). At the symbiosome membrane the bacteria trade with the plant ammonium for sugars (Whitehead et al., 1998).

Although bacterial infection and nodule organogenesis are jointly tuned in spatial and timely manner, the latter can also be induced in axenic environments (i.e. in the absence of NFs or rhizobia), and, therefore, this is a process genetically decoupled from IT formation.

As an essential component of RNS, a nuclear-localized CALCIUM- AND CALMODULIN-DEPENDENT KINASE (CCaMK, *L. japonicus*) has been identified. CCaMK, or DOESN'T MAKE INFECTIONS 3 (DMI3, *M. truncatula*), is required for the decoding of the calcium-spiking signal that occurs after NF perception (Levy et al., 2004; Mitra et al., 2004). DMI3/CCaMK's activity is strictly controlled by antagonistic effects of Ca^{2+} or calmodulin binding to the protein and, under RNS-specific conditions, results in the induction of cortical cell division and activation of symbiosis specific genes (Levy et al., 2004; Mitra et al., 2004; Miller et al., 2013). Mutant variants of CCaMK that either lack the auto-inhibitory domain (i.e. consisting of only the kinase domain) (Gleason et al., 2006) or are mutated at a single nucleotide position in the kinase domain (*L. japonicus* CCaMK, *spontaneous nodule formation 1 (snf1)* allele T265I, or T265D) induce the formation of empty nodules in the absence of symbiotic stimuli (Tirichine et al., 2006b; Tirichine et al., 2006a; Hayashi et al., 2010).

In the nucleus, Interacting Protein of DMI3 (IPD3, *M. truncatula*)/CYCLOPS (*L. japonicus*) interacts with and is phosphorylated by DMI3/CCaMK (Messinese et al., 2007; Horvath et al., 2011; Singh et al., 2014). CYCLOPS/DMI3 is a transcriptional activator, that after activation initiates the expression of nodule organogenesis and infection genes (Singh et al., 2014). *Cyclops/dmi3* plants do not form ITs but only nodule primordia and no mature nodules in symbiotic conditions (Messinese et al., 2007; Yano et al., 2008).

Several proteins have been identified specific for RNS that act downstream of the CCaMK-CYCLOPS complex. The putative transcription factors encoded by *NODULE INCEPTION (NIN)*

(Schauser et al., 1999), *NODULATION SIGNALING PATHWAY 1 (NSP1)* and *NSP2* (Heckmann et al., 2006), *ERF REQUIRED FOR NODULATION 1 (ERN1)* (Middleton et al., 2007; Cerri et al., 2012), *NF-YAI* (Combier et al., 2006; Soyano et al., 2013), and *SIN1 (SCL13 INVOLVED IN NODULATION 1)* (Battaglia et al., 2014) all induce genes required for RNS (Mitra et al., 2004; Hogslund et al., 2009; Madsen et al., 2010).

Separation of the Infection- from the Nodulation-Process

The *snfl* mutant provides a powerful genetic background to clarify the components, which are specifically required for the formation of ITs and/or for nodule organogenesis in *L. japonicus*. By crossing the *snfl* allele with other symbiotic mutants and analyzing their responses to NF and rhizobia, it was found that two parallel pathways exist that facilitate the formation of ITs and nodule organogenesis (Madsen et al., 2010).

According to this model, SYMRK, NUP133, NUP85, CASTOR and POLLUX are not required for IT formation in the *snfl* background; their mutants in the *snfl* background still form ITs. NFR1 and NFR5, however, are essential for IT formation, while their polar progression is dependent on NAP1, PIR1 and CERBERUS. Autoactive CCaMK, which induces spontaneous nodulation, was not able to restore IT formation in *cyclops-3* mutants, which suggests that CYCLOPS, a downstream target of CCaMK, is required for cross-signaling from the CCaMK-controlled organogenic pathway to the infection pathway (Madsen et al., 2010). Interestingly, calcium spiking itself seems not sufficient for initiating ITs because *snfl* does not induce IT formation in the absence of the receptors NFR1 and NFR5. Calcium spiking may therefore be a signal to induce organogenesis; the initial rapid NF induced calcium-flux at the root hair tips the signal for IT formation (Madsen et al., 2010).

1.3 Symbiotic Signaling at the Plasma Membrane During RNS

1.3.1 The Role of the Receptor-like Kinases

The first mutant that was identified to be completely unresponsive to NF or rhizobial inoculation was *nfp* (Ben Amor et al., 2003). Unlike other nodulation negative (*Nod*⁻) mutants, *nfp-1* does not display rapid calcium flux, root hair swelling or branching, no calcium spiking, no induction of early nodulin genes. Consequently, no root hair curling, and ITs are formed (Ben Amor et al., 2003). *NFP* encodes for an unusual kinase dead LysM RLK, that is constitutively expressed in the root zone that is susceptible for NF responses. In the presence of the symbiont *S. meliloti*, *NFP* is expressed not only at infection sites of root hairs, but also in cortical cells throughout nodule

Introduction

primordium formation in *M. truncatula* (Arrighi et al., 2006). The complete lack of *nfp-1* responding to symbiotic cues, but the ability to undergo AM symbiosis (Ben Amor et al., 2003), places NFP at the very beginning of RNS-specific signaling, most likely by directly binding NFs (Mulder et al., 2006). However, when *NFP*'s transcript is knocked down through RNAi, these plants form malformed sac-like ITs, which indicates that NFP may also be involved in IT growth (Arrighi et al., 2006).

LYK3 of *M. truncatula* is essential for the establishment of RNS. RNAi knockdown of *LYK3* transcript resulted in a nodule negative (Nod⁻) phenotype when inoculated with *S. meliloti* (Limpens et al., 2003). However, unlike *nfp-1*, the early responses of calcium spiking, root hair curling and bacterial entrapment still occur in *LYK3*-silenced roots. In these, the infection process frequently stops at the microcolony stage with aborted, tube- or sac-like ITs (Limpens et al., 2003). EMS mutagenesis of *M. truncatula* resulted in the identification of the 'HAIR CURLING' (*HCL*) gene. Three mutant alleles, *hcl-1*, *hcl-2* and *hcl-3*, were isolated. Their root hairs show calcium spiking and undergo extensive deformations upon detection of *Sinorhizobium meliloti*, but plants are unable to form ITs or nodules (Catoira et al., 2001). These, and one additional mutant *HCL* allele, *hcl-4* (Smit et al., 2007), have been shown to encode the RLK LYK3 (Limpens et al., 2003). Unlike the other *hcl* mutants, *hcl-4* can efficiently entrap bacteria; however, the resulting ITs are impaired in their polar growth and form severely impaired, bloated structures (Smit et al., 2007). Kinase dead variants of LYK3 have been shown to lose the ability to complement the non-nodulating phenotype of the *hcl-1* mutant, demonstrating that kinase activity is essential for the symbiotic signaling function of this RLK (Klaus-Heisen et al., 2011).

However, because only *nfp-1* and *nfp-2* (Arrighi et al., 2006) mutants are completely unresponsive to NF, it is proposed that NFP is primarily required for NF sensitivity ('signaling receptor') (Ardourel et al., 1994; Mulder et al., 2006), whereas LYK3, as a so-called 'entry receptor', is required during the rhizobial infection process in *Medicago truncatula* (Smit et al., 2007).

In *Lotus*, NFR1 and NFR5 function as the first NF perceivers. NFR1 is the orthologue to LYK3. *Nfr1* mutants are unable to form nodules, and their root hairs are completely unresponsive to NFs or inoculation with their symbiont *Mesorhizobium loti*. No root hairs deformation or curling occurs in the *nfr1* mutants analyzed (Schauser et al., 1998; Szczyglowski et al., 1998; Radutoiu et al., 2003). Isolated *nfr5* mutants, orthologous to NFP, completely phenocopy *nfr1* mutants, as they are incapable of forming nodules and do not respond to purified NF or *M. loti* (Madsen et al., 2003).

The co-expression of NFR1 and NFR5 in *M. truncatula* resulted in a host-range extension of the plant, that now responded to the recognition of *M. loti* or *Rhizobium leguminosarum* bv. *viciae* strain DZL, symbionts of *L. japonicus*, by developing indeterminate, but nonfunctional nodules.

However, the single expression of NFR1 or NFR5 in *Medicago* did not result in nodulation after inoculation. In these plants, minor root hair reorientation was observed for the LjNFR1 expressing roots, while the NFR5 expression roots showed root hair curling and entrapment of *M. loti* or *R. leguminosarum* DLZ strains (Radutoiu et al., 2007). Therefore, it is hypothesized that the presence of both RLKs is needed for correct NF recognition and signaling, possibly as a heterodimeric/multimeric receptor complex (Radutoiu et al., 2003; Madsen et al., 2011; Moling et al., 2014).

In vitro, NFR1 and NFR5 directly bind NFs via their extracellular LysM domains providing more evidence of them being the NF receptors (Broghammer et al., 2012). NFR1, as well as LYK3, contain an active kinase domain with auto-phosphorylation activity, and it is possible that NF-binding to the LysM domain activates the intracellular kinase activity to transduce intracellular signaling. NFR1/LYK3 has been shown to trans-phosphorylate NFR5/NFP *in vitro*. The kinase activity is also the cause of a hypersensitive cell death response when NFR1/LYK3 is co-expressed with NFR5/NFP in *Nicotiana benthamiana* leaf epidermal cells (Madsen et al., 2011; Pietraszewska-Bogiel et al., 2013). This suggests that the symbiotic receptors must be tightly regulated by a yet unknown mechanism. NFR5/NFP itself is not a functional kinase (Arrighi et al., 2006; Klaus-Heisen et al., 2011; Madsen et al., 2011).

Downstream of the LysM-type RLK, another receptor is essential for RNS signaling. DOESN'T MAKE INFECTIONS 2 of *M. truncatula* (DMI2; NODULATION RECEPTOR KINASE 'NORK' from *Medicago sativa*; SYMRK, *L. japonicus*) is a Leucine-rich-repeats-containing RLKs (Endre et al., 2002b; Endre et al., 2002a; Stracke et al., 2002). Upon contact with NFs, *dmi2* mutants show calcium influx and root hair swelling; however, they are incapable to elicit calcium spiking and early nodulin gene expression (Catoira et al., 2000; Endre et al., 2002a). *Lotus symrk* mutants react to NF with strong root hair deformations, but bacteria cannot be entrapped and no ITs are formed (Stracke et al., 2002). Unlike the LysM-RLK mutants described above, *dmi2/symrk* mutants are also incapable of establishing AM symbiosis, making this RLK the most upstream *common-symbiosis* gene (Endre et al., 2002a; Stracke et al., 2002). Therefore, initial NF perception is independent of DMI2/SYMRK, but this RLK is required for the transduction of the signal, possibly by acting as a co-receptor with the LysM receptors.

1.3.2 Downstream Targets of the Receptor-like Kinases

How the signal is then transduced from the PM to the nuclear localized proteins is not yet fully known, but RLK-interacting proteins that could play a role in this process have been identified. PLANT U-BOX E3 UBIQUITIN LIGASE FAMILY PROTEIN (PUB1) interacts with LYK3 at the PM (Mbengue et al., 2010). PUB1 is directly phosphorylated by LYK3. RNAi of *PUB1* led to

Introduction

more nodules formed; overexpression of PUB1 reduced the nodule number after inoculation. This revealed a role for PUB1 in the negative control of nodulation in a LYK3-dependent process (Mbengue et al., 2010). SYMRK INTERACTION PROTEIN 2 (SIP2) in *L. japonicus* is a MAP Kinase Kinase (MAPKK) that interacts with the intracellular region of SYMRK *in planta* (Chen et al., 2012). Silencing *SIP2* reduced IT-formation and the number of nodules formed after *M. loti* inoculation and suggests that a MAPK signaling network downstream of SYMRK may be involved in relaying the signal from the PM to the nucleus (Chen et al., 2012).

The enzyme 3-HYDROXY-3-METHYLGLUTARYL COA REDUCTASE 1 (HMGR1) interacts with DMI2 (Kevei et al., 2007). HMGR1 catalyzes the reaction of a mevalonate precursor into mevalonate. Interestingly, the silencing of *HMGR1* by RNAi, or pharmacological inhibition of HMGR1 enzymatic activity, led to fewer nodules formed, which suggested that direct products of the mevalonate pathway act as second messengers that transduce the signals from the PM to the nuclear localized proteins. ITs were rarely formed in these plants (Kevei et al., 2007). Calcium spiking can be directly induced by the external application of mevalonate to *M. truncatula* roots (Venkateshwaran et al., 2015). The responses of the symbiotic mutants, *nfp*, *dmi1*, *dmi2* and *dmi3*, to externally applied mevalonate demonstrated that HMGR1 induces the expression of early nodulation genes downstream of the receptor DMI2, and upstream of the nuclear membrane localized DMI3 (CCaMK), thus providing evidence of mevalonate (or its metabolic derivatives) acting as messengers that link symbiotic signaling at the PM to the nucleus (Venkateshwaran et al., 2015).

1.3.3 Symbiotic Flotillins

At the PM, RNS-specific flotillins have been identified. Flotillins are PM-resident scaffold proteins and in mammalian cells are implicated in membrane shaping and in clathrin- and caveolin- independent endocytosis pathways within pathogenesis responses (Glebov et al., 2006; Babuke and Tikkanen, 2007; Langhorst et al., 2008).

In a reverse genetics approach a gene family with seven *M. truncatula* FLOTILLIN-LIKE (FLOTs) members was identified. Two of these displayed a RNS specific function (Haney and Long, 2010). The expression of *FLOT2* and *FLOT4* was up-regulated after inoculation with *S. meliloti*, and their expression pattern correlated with the process on rhizobial infection. *FLOT2* and *FLOT4* localize to the PM of root hairs, the place where the symbiotic receptors are also present (Haney and Long, 2010). Their precise localization in the PM will be described in their own chapter (see 1.6). With the use of stable RNA-induced gene silencing lines of *FLOT2* or *FLOT4*, it was shown that these are required for nodulation; *FLOT2*-silenced plants produced fewer nitrogen fixing nodules, or even were nodulation minus. When *FLOT4* was silenced the

plants also produced less functional nodules. 30% fewer total infection threads in *FLOT2*-silenced roots compared to wildtype plants infer that this flotillin is required for IT formation. A significant 20% reduction of ITs was also measured in plants reduced of the *FLOT4* transcript. From the ITs that formed, the vast majority aborted or collapsed prematurely in the root hairs only in *FLOT4*-silenced plants, and in these, bacterial release was reduced more than 3-fold. Silencing of *FLOT2* only leads to the described reduction of IT-number. No premature abortion of IT growth or impairment of bacterial release was detected in *FLOT2*:RNAi lines (Haney and Long, 2010). These data strongly suggest a function during the initiation of IT formation for *FLOT2* and *FLOT4*; however, *FLOT4* is also required for the progression of ITs through root hair and cortical cells.

1.3.4 Symbiotic Remorin

A remorin protein, *M. truncatula* SYMBIOTIC REMORIN 1 (MtSYMREM1), is an important part of the RNS-specific infection process (Lefebvre et al., 2010). Remorins are plant-specific proteins, most of which can be characterized as having an non-conserved, intrinsically disordered N-terminal region and a coiled-coil containing C-terminal region (Raffaele et al., 2007; Marin and Ott, 2012). The remorin SYMREM1 exists only in legumes. *SYMREM1* is inactive under non-symbiotic conditions, but, upon contact with *S. meliloti* or purified NF, it is highly up-regulated within 4 days or 24 hours, respectively. RNA interference of *SYMREM1* resulted in 36% fewer total nodules two weeks post inoculation (wpi) with the symbiont. At 6 wpi, a third of the plants did not form any nodules compared to 7% in control plants. Although a 3-fold increase in total ITs was observed in *SYMREM1* silenced plants, a high degree of IT-branching and -arrest in sac-like structures during the early stages of infection pointed towards an infection-related function of SYMREM1 (Lefebvre et al., 2010).

In RNAi silenced plants, as well as in a TNT1-insertion knock out *symrem1* mutant, the nodules that formed were smaller and stunted compared to regular nodules (Lefebvre et al., 2010). Furthermore, similar to *FLOT4*-silenced roots, bacterial release from ITs into the symbiosomes of nodules was highly impaired in *symrem1*.

Immunogold labeling and fluorescence microscopy showed SYMREM1 localize to the PM. At the PM, Bimolecular Fluorescence complementation (BiFC) and yeast-2-hybrid assays revealed SYMREM1 specifically interacts with the symbiotic RLKs LYK3, NFP and DMI2 (Lefebvre et al., 2010). Also, the *L. japonicus* SYMREM1 homolog, through its conserved C-terminal region, directly binds to NFR1, NFR5 and SYMRK. Fluorescence Lifetime Imaging Microscopy based on Foerster Resonance Energy-Transfer (FLIM-FRET) experiments revealed the interaction occurs between the conserved C-terminal region of LjSYMREM1 and NFR1 in *Nicotiana*

benthamiana (Tóth et al., 2012). Noteworthy, LjSYMREM1 was phosphorylated in its unstructured N-terminal region by SYMRK and NFR1 *in vitro* (Marin and Ott, 2012; Tóth et al., 2012).

Thus, SYMREM1 is a symbiotic-RLKs-binding protein, which most likely is involved in the regulation or maintenance of symbiotic signaling during the progression of the IT.

1.4 Plasma Membrane Compartmentalization

The PM separates the cell interior from the outside. The first signaling events for the establishment of RNS, described above, occur at the PM. In plants, the PM consists of a glycolipid double layer to which proteins are bound by various mechanisms and motifs. In order to specifically transduce signals across the membrane, it has to be highly organized in a spatial manner.

1.4.1 The Fluid Mosaic Model

The classic view on the PM was shaped by the ‘fluid mosaic’ model, which stated that the phospholipid bilayer forms a two-dimensional solvent in which the lipids and proteins undergo continuous and unconfined lateral diffusion along the entire membrane (Singer and Nicolson, 1972). Proteins residing in the PM, termed integral proteins, were generally thought to spread out in random manner over the whole area of the PM, and, in short range some protein-protein interactions would have a minor impact on membrane structure. Peripheral proteins were described as being only loosely attached to the PM and therefore insignificant for membrane structure (Singer and Nicolson, 1972).

At the time, immunostaining and electron microscopic techniques to visualize integral proteins in various mammalian membranes supported the assumption that proteins spread out randomly in the membrane (Lee and Feldman, 1964; Green, 1967; Nicolson et al., 1971b; Nicolson et al., 1971a). Virus induced fusion of two different cell types showed that within 40 minutes the proteins were equally distributed (termed ‘mosaicism’) along the entire PM of the heterokaryon in a temperature dependent process in line with a free diffusion model (Frye and Edidin, 1970).

However, the presence and impact that membrane resident and associated proteins play in shaping the membrane had been vastly underestimated. In red blood cells, transmembrane proteins occupy nearly a quarter of the PM area (Engelman, 1969; Guidotti, 1972; Dupuy and Engelman, 2008). In the membranes of synaptic vesicles, it has been found that transmembrane proteins cover more than 25% of the surface area (Takamori et al., 2006). Additionally, substantially more non-

transmembrane proteins bind to the synaptic vesicle and make the lipid surface of the membrane 'hardly visible' (Takamori et al., 2006). Genomic analyses have estimated that up to 30% of the genome encodes for transmembrane proteins, with a positive correlation between the size of the genome and the number of membrane proteins encoded (Wallin and von Heijne, 1998; Kihara and Kanehisa, 2000; Schwacke et al., 2003; Almen et al., 2009). Also, the extreme high number of different lipid species contributes to a more complex membrane environment than initially proposed (van Meer et al., 2008). It quickly became apparent that the fluid-mosaic model needed several adjustments.

1.4.2 The Picket Fence Model

Now it is clear that membranes are not at all simply two-dimensional fluids, in which lipids and proteins are in constant motion. Some lipids and proteins do diffuse freely, but the dynamic behavior of the majority of analyzed membrane proteins is far more complex (Jacobson et al., 1995; Sheets et al., 1995; Simson et al., 1995). A three-tiered mesoscale-domain architecture of the plasma membrane has been proposed, and this model currently most closely describes the architecture of membranes (Kusumi and Suzuki, 2005; Kusumi et al., 2012a).

According to this model, the entire membrane is partitioned into mesoscale compartments of 40-300 nm diameters due to direct and indirect interactions of a membrane skeleton immediately underlying the membrane (the 'fence'). This fence interacts predominantly, but not exclusively, with transmembrane (TM) proteins. The places of interaction with the TM proteins form the immobile posts or 'pickets' to the fence. This is the most basic and, therefore, first tier of compartmentalization of the membrane, where the pickets function as diffusion barriers for membrane proteins, by causing steric hindrance and hydrodynamic friction-like effects. The first tier thus defines so-called 'meso-scale membrane domains' (MDs) in the PM (Kusumi et al., 2012a).

Evidence in support of the picket fence model is provided by single particle tracking and fluorescence recovery after photo-bleaching (FRAP) analysis of membrane resident molecules. In mouse erythrocyte cells, the integral PM protein 'BAND 3', showed 50 times higher diffusion rates in mutant cells that were lacking the functional spectrin network (Sheetz et al., 1980). Furthermore, BAND 3 interacts with the spectrin meshwork directly beneath the PM, and the place of this interaction coincided with the observed immobile fraction of BAND 3 leading to the proposal of a 'membrane skeleton fence model' (Tsuji and Ohnishi, 1986; Tsuji et al., 1988; Sako and Kusumi, 1994; Sheetz, 1983; Saxton, 1989). A direct involvement of the cytoskeleton fences was further supported by the observation that transmembrane-domain-containing receptors and

Introduction

GPI-anchored receptors, which were moved across the cell surface using laser optical tweezers, usually encountered barriers after a distance of 1.7 or 0.6 μm (Edidin et al., 1991).

Building on the data on BAND 3 proteins, single particle tracking analysis of this protein confirmed that one third of the BAND 3 population does not show macroscopic diffusion (and thus was linked to the spectrin mesh); the major population showed free diffusion within certain specified compartments, then suddenly ‘jumped’ into a neighboring area, within which the proteins again were unrestricted in their diffusion kinetics. When the intracellular domain of band 3 was removed, no immobile BAND 3 population was observed (Tomishige and Kusumi, 1999). Single particle tracking performed on several other membrane proteins confirmed the existence of a confined area of free diffusion. These proteins display sudden jumps, termed ‘hop diffusion’, to adjacent compartments that are defined and regulated by dynamic rearrangements of the membrane skeleton creating diffusion windows (Kusumi et al., 1993; Jacobson et al., 1995; Kusumi and Suzuki, 2005; Suzuki et al., 2005).

The cytoskeleton diffusion barriers have been shown to reduce the mobility of proteins by a factor of 5-50 (Kusumi et al., 2012a). Phospholipids also show restrained diffusion (by a factor of 5-100) and hop diffusion dynamics, which can also be explained using the picket-fence model (Saxton, 1990; Bussell et al., 1995b, a; Fujiwara et al., 2002; Murase et al., 2004). Importantly, the membrane skeleton has been shown to cover almost the entire cytoplasmic surface of the PM and is predominantly made up of actin filaments and actin-associated proteins (Morone et al., 2006; Morone et al., 2008). Therefore, it can be considered the rule and not the exception that long-range diffusion of transmembrane-proteins or lipid-anchored proteins is strongly restricted and regulated by dynamic changes or fluctuations of the membrane skeleton.

Within these first tier compartments, the PM is further structured into co-existing second tier domains (described in the following chapter), and third tier dynamic oligomeric protein complexes (Kusumi et al., 2012a; Kusumi et al., 2012b).

1.4.3 Membrane Rafts

The second tier corresponds to the postulated so-called ‘lipid rafts’ (Simons and Ikonen, 1997). Often unequal partitioning of lipids in the PM was observed and this phenomena was called ‘clusters of lipids’, (rigid) ‘quasi-crystalline membrane regions’ surrounded by ‘liquid crystalline regions’ or, ‘liquid ordered domains’ (Lee et al., 1974; Wunderlich et al., 1975; Wunderlich et al., 1978; Karnovsky et al., 1982; Ipsen et al., 1987). These observations were summarized in a ‘lipid raft hypothesis’ that described the existence of small (2-20 nm) and short-lived structures that are enriched with (glyco-) sphingolipids and cholesterol in the PM and are held together primarily by lipid-lipid acyl chain interactions (van Meer and Simons, 1988; Brown and Rose, 1992; Simons

and Ikonen, 1997; Simons and Vaz, 2004). The clustering of such lipid rafts was believed to create a unique environment in the PM for the subsequent attachment and recruitment of specific proteins with an affinity to this membrane lipid environment (e.g. GPI-anchored proteins are considered ‘raftophilic’) thereby creating ‘raft domains’ (Brown and Rose, 1992; Hancock, 2006; Ikonen, 2008). Proteins, that do not have this affinity, would not occur in lipid rafts.

The current definition of lipid rafts, now more commonly called ‘membrane rafts’, describes them to be small, highly dynamic and multifaceted domains enriched with sterols and sphingolipids with the presumed function of compartmentalizing cellular signaling processes (Pike, 2006). Protein-protein interactions and protein-lipid interactions then further stabilize the rafts to form larger clusters of platforms (Pike, 2006, 2009), which correspond to the mesoscale MDs.

For a while it was thought that the biochemical isolation of detergent (Triton-X-100) insoluble membrane fractions (DIMs), allowed the isolation of functional lipid rafts and the proteins residing within them (Brown and Rose, 1992; Schroeder et al., 1994; Brown and London, 1998; Zhang et al., 1998; Niv et al., 2002; Foster et al., 2003; Bae et al., 2004; Sprenger et al., 2004; MacLellan et al., 2005). A substantial number of proteins involved in signaling processes have been identified by this method (Pike, 2009). However, it has been shown that this method does not reliably isolate membrane rafts and is prone to result in substantial artifacts. It is now considered to primarily determine solubility of proteins and not necessarily constituents of membrane rafts (Foster et al., 2003; Munro, 2003; Schuck et al., 2003; Shogomori and Brown, 2003; Zurzolo et al., 2003; Kierszniowska et al., 2009; Simons and Gerl, 2010; Tanner et al., 2011; Malinsky et al., 2013).

Direct observation of lipid rafts has been less frequent; but with the development of more sophisticated microscopic methods, the presence and dynamics of putative membrane rafts can now be monitored. Laurdan is an environmentally sensitive fluorescent probe, which shows a 50-nm blue shift when the lipid environment is ordered and a red shift of the emission spectrum when the membrane environment is disordered (Parasassi et al., 1997; Bagatolli et al., 2003). By combining 2-photon excitation of Laurdan-labeled living cells with immunofluorescence microscopy, it was shown that liquid ordered domains were strongly enriched at filopodia, or, more general, at places of membrane protrusion (Gaus et al., 2003). CAVEOLIN-1, CAVEOLIN-2 and FLOTILLIN-1 and other proteins co-localized with these membrane rafts (Gaus et al., 2003). Flotillins have been frequently detected to localize in membrane rafts (although microscopically they would be termed microdomains), and have often been identified in DIM fractions, making them one of the most established membrane raft markers (Bickel et al., 1997; Lang et al., 1998; Stuermer et al., 2001; Frick et al., 2007; Solis et al., 2007; Bach and Bramkamp, 2013, 2015; Bramkamp and Lopez, 2015). Flotillins can also connect with the

Introduction

membrane cytoskeleton, providing a plausible link between membrane rafts and the first tier of membrane compartmentalization (Langhorst et al., 2007).

Stimulated emission depletion (STED) nanoscopy was able to monitor the movement of single molecules in living cells and confirmed that sphingolipids and GPI-anchored proteins were trapped in cholesterol-enriched complexes in the PM (Eggeling et al., 2009). Cholesterol depletion reduced the observed trapping of the molecules. This was seen as another piece of evidence confirming the existence of membrane rafts *in vivo* (Eggeling et al., 2009). Single particle tracking of other GPI-anchored protein (GM1) further supported the existence of membrane rafts *in vivo* (Chang and Rosenthal, 2012). Although these observations may be attributed to membrane rafts, they could still be explained by other mechanisms, e.g. the picket-fence model.

The concept of the existence of membrane rafts is still under discussion, but mostly argues with the precise definition of what rafts are, and not the occurrence of signaling domains (Munro, 2003; Shaw, 2006; Jacobson et al., 2007).

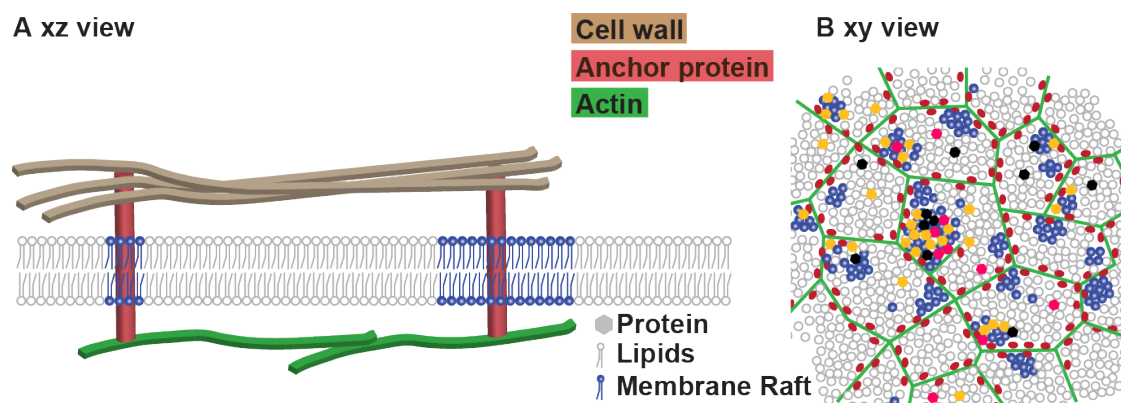


Figure 2 Simplified model of plasma membrane compartmentalization. (A) Side view illustrating the bilayer of lipids creating the general PM structure. Actin filaments directly underneath the PM form the membrane skeleton ('the fence') that is anchored, directly and indirectly, to the PM by proteins ('the pickets'). This structure creates a diffusion barrier for lipids and proteins and defines the first tier, the mesoscale compartments, of the proposed three-tiered architecture of the PM. The compartments create restrictions for the diffusion of dynamic nanoscale sterol, sphingolipid-enriched membrane rafts and proteins. Similarly, the cell wall (i.e. extracellular matrix) is an extrinsic factor that directly impacts the dynamics of proteins in the PM. **(B)** Top view (without the cell wall). A membrane skeleton defines mesoscale compartments. Within these compartments, membrane rafts can diffuse freely, but encounter restrictions along actin filaments and actin anchoring proteins. Lipids and proteins diffuse within compartments, and only 'hop' into neighboring compartments if dynamic membrane-skeleton rearrangements open diffusion windows ('hop diffusion'). The mesoscale compartments condense the area for protein-protein interactions, enhance the recruitment of proteins into membrane rafts, and support the clustering of proteins and rafts into mesoscale microdomains. All components of this model are not drawn to scale, and their abundance is highly underrepresented.

It is clear, however, that the PM is compartmentalized further than the first tier (mesoscale MD) and that this is most likely due to the simultaneous presence of liquid-ordered membrane regions,

as well as protein-protein and protein-lipid interactions with the actin cytoskeleton at the PM (Kusumi et al., 2011). Theoretically, membrane rafts are trapped in the compartments defined by the membrane skeleton. The protruding amino acids from the transmembrane domains of the ‘pickets’ are structurally incompatible with the bulky and rigid sterol backbone of cholesterol (the major lipid in membrane rafts), and therefore the compartment boundary is considered to be very raft-unfriendly. Raft growth, leading to MD formation, and hop-diffusion dynamics would thus be limited, suppressed or controlled by the compartment boundaries created by TM proteins and the actin cytoskeleton (Kusumi et al., 2012b).

1.4.4 The Plasma Membrane - Cell Wall Continuum

In living plants, the high turgor pressure within the cells presses the PM closely against the cell wall (Proseus and Boyer, 2005). During synthesis of the cell wall, it is physically anchored to the PM through cellulose fibrils and interactions with PM resident proteins (Baluska et al., 2003). Captivatingly, the localization, arrangements in microdomains, orientation, and mobility of cellulose synthase (CesA) complexes (CSC) in the PM, all are parameters directly influenced by both the actin and microtubule cytoskeleton (Lerouxel et al., 2006; Paredez et al., 2006; Geisler et al., 2008; Gutierrez et al., 2009; Watanabe et al., 2015). Perturbing either microtubules, or actin filaments and then monitoring CesA mobility, and localization, demonstrated that the global organization, and distribution of CesA complexes in the PM was dependent on the actin cytoskeleton, but the fine-tuning of their positioning is regulated by dynamic microtubule cytoskeleton components (Gutierrez et al., 2009). In *Arabidopsis actin* mutants the cellulose content of the cell wall is significantly reduced, unevenly distributed, and cell walls with irregular thickness are produced (Sampathkumar et al., 2011). Interestingly, sterol synthesis mutants are defective in cellulose biosynthesis, a dependency of CesA localization in MDs on membrane rafts, therefore, is theoretically possible (Schrick et al., 2012). This shows that cytoskeleton-, as well as membrane structures, influence the production and structure of cell walls. Aside from cellulose, the cell wall is made up of many other compounds, such as hemicellulose, pectins, lignins and proteins (Kohorn, 2000).

Inversely, evidence exists that emphasizes the effect the cell wall has on PM-compartmentalization. The localization of PIN2, an auxin transporter involved in cell polarity determination, depends on the cell wall (Wisniewska et al., 2006), and PIN2 loses its specific polar localization in the cell-wall synthesis (CesA3) mutant, *repp3* (Feraru et al., 2011). In *Arabidopsis*, one of the first proteins identified to label MD in the PM inward rectifying potassium channel KAT1 (Schachtman et al., 1992). When expressed heterologously in *Nicotiana* leaves, KAT1 localized to the PM in randomly distributed immobile MDs (Sutter et al., 2006).

Introduction

Interestingly, only in guard cells of *Vicia faba*, KAT1:GFP-labeled MDs arranged in a radially striped pattern (Homann et al., 2007). The radial pattern was independent of cytoskeletal structures, co-localized with a Calcofluor-white stained cell wall, and disappeared after osmotically disconnecting the PM from the cell wall (Homann et al., 2007). It appears the cell wall has a strong impact on dynamics of PM-resident proteins. The first direct evidence for this was discovered with *Arabidopsis thaliana* formin1 (AtFH1), a nucleator of actin filaments that locates to the PM (Michelot et al., 2006), with a extracellular domain protruding towards the cell wall (Deeks et al., 2002). AtFH1 directly binds the cell wall, and FRAP experiments (with truncated versions, or after plasmolysis) revealed that this connection was directly responsible for the immobile behavior of AtFH1 (Martiniere et al., 2011).

Thus, the cell wall impacts localization and behavior of PM-resident proteins. In analogy to the ‘picket-fence model’ where a membrane-cytoskeleton influences the PM from the inside by connecting with PM-resident proteins, it is suggested that a universal cell-wall meshwork similarly influences PM-proteins from the outside (Martiniere et al., 2012). Many proteins have been identified that protrude towards the cell wall, directly bind to cell-wall-components, or bind to cell wall-associated proteins (Steinwand and Kieber, 2010; Martiniere et al., 2011; Liu et al., 2015a; Liu et al., 2015b). Because of the highly dynamic nature of the cell wall (Wolf et al., 2012), and its re-modeling is regulated by the cytoskeleton, all three factors - the cell wall, the PM and the cytoskeleton – are now considered to orchestrate the compartmentalization of proteins in the PM. They work together in an interdependent ‘cell wall- PM –membrane-skeleton continuum’ (McKenna et al., 2014; Liu et al., 2015a; Liu et al., 2015b).

1.5 Microdomains in the Plant’s Plasma Membrane

By now, there have been several proteins identified that form specific domains in the PM of plants (Konrad and Ott, 2015). However, compared to the great number of hypothesized PM resident proteins (Schwacke et al., 2003), evidence for MD-formation and the biological necessity and their functions is still limited. For some examples, a picture is emerging that emphasizes the importance of specific membrane localization of proteins. In the following, due to the difficulty of clearly distinguishing between membrane rafts and MD, proteins that were found to label the PM distinctly and not uniformly will be termed proteins that label ‘mesoscale microdomains’ (MDs).

1.5.1 The Casparian Strip Domain

In *Arabidopsis thaliana*, the so-called casparian strip protects the vascular system from the uncontrolled influx of solutes and toxins (Nagahashi et al., 1974). The strip is formed by the local thickening of the transverse cell wall of the endodermis and consists primarily of lignin (Zeier et al., 1999; Naseer et al., 2012). Although it was first described in 1865, it was not until 2011 when the proteins responsible, the ‘CASPARIAN STRIP DOMAIN PROTEINS’ (CASPs), were identified (Roppolo et al., 2011). Fluorescently tagged CASPs localized to a specific area in the PM; the exact place where the casparian strip is later formed (Roppolo et al., 2011). CASP1:GFP in particular was shown to first localize uniformly in the PM of endodermal cells, then to re-locate in an endocytosis-driven process into punctate form at the PM. The localization of these MDs were described as a ‘string-of-pearls’, until, finally, these CASP1:GFP MDs accumulate in a continuous band. Along this precise band, the casparian strip domain (CSD) predetermines where the casparian strip will be formed (Roppolo et al., 2011). Based on this, it was shown that in the CSD, CASP1 specifically co-localized with the peroxidase PER64, involved in assembling the lignin polymerization machine, throughout its dynamic re-localization process (Lee et al., 2013).

In the PM, CASP proteins can be described as PM-localized MDs with the purpose of localizing peroxidases and other cell-wall-modifying enzymes to the correct subcellular location in the PM. Therefore, they have the function of specific scaffold proteins (Roppolo et al., 2011; Lee et al., 2013). What makes this even more interesting is that the CASPs themselves appear to be dependent on other proteins (SCHENGEN 3 (SGN3)/GASSHO1 (GSO1)) for their correct targeting into the uninterrupted CSD. Prior to the formation of the CSD, the RLK SGN3 localizes into a broad band at the PM. Even though CASPs still localize to the PM in the *sgn3* deletion mutant, SGN3 is necessary for CASPs to correctly localize into the typical string-of-pearls and the continuous ring of MDs for CSD formation. *Sgn3* mutants do not properly form the casparian strip diffusion barrier (Pfister et al., 2014). Thus, in this pathway, MDs appear to play a vital role.

1.5.2 Microdomains in Plant Development

At the core of the development of plants and their adaptation to the environment lies a directional flow of the hormone auxin (Berleth and Sachs, 2001; Sauer et al., 2006; Teale et al., 2006; Leyser, 2011). For example, embryogenesis (Hamann et al., 2002; Friml et al., 2003) and organ development (Benkova et al., 2003; Heisler et al., 2005) are regulated by polar auxin gradients. This flow does not rely on localized synthesis of auxin itself, but rather on the polar localization of several auxin transporters. The most well known are the PIN-FORMED proteins, auxin efflux transporters that direct the hormone to the place of its function. They are asymmetrical, but each found on their own specifically localized in polar apical, basal or lateral domains to the PM,

depending on cell type and developmental context. Some locate specifically to the ER (reviewed in (Grunewald and Friml, 2010)).

Their combined patterns of localization direct the flow of auxin towards distinct parts of the cell and results in the determination of the main apical-basal plant axis (Galweiler et al., 1998; Friml et al., 2003; Blilou et al., 2005; Petrasek et al., 2006; Wisniewska et al., 2006; Vieten et al., 2007; Rahman et al., 2010). Manipulation of the PINs polar MD-localization leads to changes of the auxin gradient and, subsequently, impacts auxin-related responses and plant development (Friml et al., 2004; Michniewicz et al., 2007; Huang et al., 2010; Zhang et al., 2010). Under specific developmental or environmental signals, PINs dynamically re-locate to modify the auxin flow and enforce a suitable plant response (Friml et al., 2002; Benkova et al., 2003; Friml et al., 2003; Heisler et al., 2005). Curiously, PINs are secreted to the PM in a nonpolar manner, and polarity is then generated, upon stimuli, by endocytosis and polar re-secretion processes (Dhonukshe et al., 2008; Geldner, 2009).

The dynamic, polar, re-localization has been shown to be dependent on secondary modifications. Phosphorylation by the kinases WAG1, WAG2, PID (PINOID) and D6PK (D6 PROTEIN KINASE), which themselves specifically localize into polar domains in the PM, directly impacts the dynamics of PIN proteins (Friml et al., 2004; Kleine-Vehn et al., 2009; Dhonukshe et al., 2010; Huang et al., 2010; Li et al., 2011; Willige et al., 2013; Barbosa and Schwechheimer, 2014; Zourelidou et al., 2014). Furthermore, PIN2, which is involved in root gravitropism, only locates into its proper polar domain in a cholesterol-dependent composition of the PM (Willemsen et al., 2003; Men et al., 2008).

PIN proteins and their interactors are prime examples of the necessity of the proteins to localize into specific and highly regulated polar domains in order to function.

1.5.3 Microdomains in Plant-Biotic Interactions

The potato (*Solanum tuberosum*) remorin 1.3 (StREM1.3) attaches to the cytosolic side of the PM in typical MDs (Raffaele et al., 2009b). Sterol depletion with methyl- β -cyclodextrin (m β CD) changed the clustered MD-localization of StREM1.3 into a more homogenous labeling of the PM, indicating that StREM1.3-labeled MDs are dependent on the sterol content of its membrane environment. In *N. benthamiana* leaf epidermal cells, YFP:StREM1.3 forms specific mesoscale MDs and co-localizes with a plasmodesmata (PD) marker. When StREM1.3 was transgenically overexpressed in *Solanum lycopersicum* (tomato), the propagation of the potato virus X (PVX) was significantly reduced in areas where the remorin was present (Raffaele et al., 2009b). A model was proposed in which StREM1.3 reduced virus propagation by directly binding to a viral movement protein, TRIPLE GENE BLOCK PROTEIN 1 (TGBp1). By StREM1.3 binding to

TGBp1, the virus no longer can open PD, thereby blocking the infection into neighboring cells (Raffaele et al., 2009b; Perraki et al., 2014). Thus, specific MD-localization in PD is key for the biological function of StREM1.3.

During the interaction of *N. benthamiana* with the oomycete pathogen *Phytophthora infestans*, the fungus produces specialized infection structures, named haustoria inside the host. These likely enable the pathogen to deliver virulence proteins to the plants (Garnica et al., 2014; Petre and Kamoun, 2014). A host-derived specialized membrane, the extrahaustorial membrane (EHM) continuous with the PM, surrounds these haustoria. The EHM is highly specialized, and mechanisms exist that entirely exclude certain proteins from this membrane (Koh et al., 2005; Lu et al., 2012). Vice versa, proteins that accumulate in the EHM have also been identified (e.g. RPW8.2 (Wang et al., 2009)). Curiously, the remorin REM1.3 is present in the EHM (Lu et al., 2012) where it labels distinct MDs (Bozkurt et al., 2014). Silencing of *REM1.3* reduced-, and forced overexpression enhanced, the virulence of *P. infestans*, implicating REM1.3-labeled MDs in promoting virulence of this oomycete (Bozkurt et al., 2014).

1.5.4 Remorins as Markers for Plant Microdomains

Remorin proteins are the most established MD-markers in plants (Raffaele et al., 2009b; Lefebvre et al., 2010; Tóth et al., 2012; Demir et al., 2013; Gui et al., 2014; Jarsch et al., 2014). Unlike receptor proteins, remorins do not contain a transmembrane domain but attach to the cytosolic side of the inner leaflet of the PM through S-acylation of a C-terminal anchor sequence (REM_{Ca}) and through protein-protein interactions (Perraki et al., 2012; Konrad et al., 2014). Typical for remorins is their canonical structure. They usually consist of a variable N-terminal region and a highly-conserved C-terminal region (Raffaele et al., 2007). The C-terminal region contains a coiled-coiled domain that is believed to be the driving force in the frequently observed oligomerization of remorins (Raffaele et al., 2007; Marin et al., 2012; Tóth et al., 2012; Jarsch et al., 2014).

Remorins have been implicated in many diverse biological processes, which may be explained by their high sequence diversity and intrinsically disordered regions (Raffaele et al., 2007; Marin and Ott, 2012; Marin et al., 2012). The Remorin SYMREM1 is needed for rhizobial infection during RNS (Lefebvre et al., 2010; Tóth et al., 2012). REM1.3 impairs virus propagation through plasmodesmata (PD) (Raffaele et al., 2009b; Perraki et al., 2012) and promotes *P. infestans* propagation (Bozkurt et al., 2014). Another PD-localized remorin, GRAIN SETTING DEFECT 1 (GSD1) from *Oryza sativa*, is involved in grain filling of rice. In PD, GSD1 co-localizes with ACTIN1 and the PD CALLOSE BINDING PROTEIN 1 and reduces PD conductance (Gui et al., 2014). The mulberry (*Morus indica*) remorin MiREM awards tolerance to drought and salinity to

seedlings of *Arabidopsis* when transgenically overexpressed. Therefore, MiREM is implicated in osmotic sensing (Checker and Khurana, 2013). Two other remorins (StREM1.3 and AtREM1.2) were shown to co-localize in MDs when expressed in heterologously in *Nicotiana* leaf epidermal cells (Demir et al., 2013). These Remorins were used as co-localization markers for proteins involved in abscisic-acid-induced ion channel activation. Importantly, for the function of the ion channel MD-localization was essential (Demir et al., 2013).

In *Arabidopsis thaliana*, it was shown for the first time that the plant's PM is subdivided into many co-existing MDs (Jarsch et al., 2014). The *Arabidopsis* genome encodes for 16 remorins. Fluorophore-tagged versions of these and four other membrane proteins (including a flotillin) label the PM of *Arabidopsis* and *N. benthamiana* in manifold manner. Interestingly, all fusion-proteins were strongly compartmentalized in the PM of both plant systems; most of the markers used localized into specific immobile punctate MDs. From two remorins, the MDs aligned as filamentous structures (Jarsch et al., 2014). Interestingly, closely related (i.e. more similar) remorins usually were more alike in the features of the MDs they labeled (Jarsch et al., 2014). Two remorins belonging to group 1, did not label any MDs in root-, or leaf epidermal cells, however, they formed strong punctate MD specifically in hypocotyl cells. The forming of these MDs may, therefore, be dependent on a specific tissue composition, developmental cues or stages of the cell (Jarsch et al., 2014).

Co-expressing 45 different remorin-pairs revealed that these MD-markers displayed specific behaviors. Some remorins co-localized (strongly), some excluded each other (strongly) and some were distributed randomly in the PM (Jarsch et al., 2014). Extensive quantitative measurements on MD shape, size, density, area and mobility gave rise to the first MD-marker atlas of the plant's PM. By now, it is clear that the PM is a complex organelle, and the extensive compartmentalization of proteins into specific MDs is the rule and not the exception (Spira et al., 2012; Jarsch et al., 2014).

1.6 Root Nodule Symbiosis Specific Microdomains

Several signaling components that are required early during the establishment of RNS have been shown to form punctate MDs.

Immunogold-labeling and electron microscopy of 10-day-old *M. truncatula* nodules showed that SYMREM1 occurred in distinct patches in the PM of nodular infection threads (Lefebvre et al., 2010). Also in *Lotus*, LjSYMREM1 localized into the symbiosome membrane and was present in remnants of nodular infection threads (Tóth et al., 2012). The constitutive expression of an YFP:SYMREM1 fusion construct labeled immobile punctate MDs in the PM of transgenic

Medicago roots (Konrad et al., 2014). The sterol-depleting agent, methyl- β -cyclodextrin destabilized these MDs, suggesting MD-labeling of SYMREM1 could be dependent on the lipid composition of the membrane (Konrad et al., 2014). Truncation experiments revealed that the C-terminal region of SYMREM1 alone (SYMREM1_C) also forms MDs in the PM of *Medicago* roots. An S-acylation at the C-terminal end of the protein assists in PM attachment but is not essential for the localization into specific MDs (Konrad et al., 2014). Interestingly, YFP:SYMREM1 and YFP:SYMREM1_C clearly formed MDs in the heterologous system *Saccharomyces cerevisiae* (Konrad et al., 2014).

The flotillins, FLOT2 and FLOT4, required early for the rhizobial infection process of *Medicago*, also label distinct MDs (Haney and Long, 2010). Genomic FLOT2 and FLOT4 GFP fusions localize into explicit MDs that co-localize with the membrane marker FM4-64. Importantly, FLOT4:GFP clearly labels MDs when expressed under its native 2 kilobase promoter (Haney and Long, 2010). Both flotillins labeled MDs that were evenly distributed in the PM of root hairs, but after inoculation with *S. meliloti*, FLOT4:GFP accumulated in polar fashion at root hair tips. FLOT2:GFP-labeled MDs remained evenly distributed after inoculation (Haney and Long, 2010). In epidermal cells, MDs labeled with FLOT2:GFP are polarly localized before and after inoculation, while FLOT4:GFP puncta show no polarity in these cells (Haney and Long, 2010). During infection, only FLOT4, and not FLOT2, was shown to localize to membranes of ITs of root hair cells and maturing nodules (Haney and Long, 2010).

LYK3 locates to the PM in *Nicotiana* leaf epidermal cells but there, curiously, labels the PM homogeneously (Lefebvre et al., 2010; Mbengue et al., 2010; Klaus-Heisen et al., 2011). A GFP tagged version of LYK3 localized in distinct MDs in root hairs of a stable transgenic *M. truncatula* line. In this line, *hcl-1* was complemented with a pLYK3:gLYK3:GFP construct (*hcl-1 compl.*), and LYK3:GFP-labeled MDs accumulated in the PM of root hair cells with a rising gradient towards the root hair tip, similar to FLOT4:GFP (Haney and Long, 2010; Haney et al., 2011). A minor fraction of LYK3:GFP was presumed to be located in membrane-tethered vesicles (Haney et al., 2011). After rhizobial inoculation, LYK3:GFP was detected along the membrane of ITs. In absence of Nod factor (NF)-producing rhizobia, the LYK3:GFP-labeled MDs were mobile. Curiously, these became immobilized in a NF-dependent manner after rhizobial inoculation. NF-deficient rhizobia were not able to induce the lateral arrest of these MDs (Haney et al., 2011).

In co-localization studies averaged over time, FLOT4- and LYK3-labeled MDs, under non-symbiotic conditions, displayed distinct dynamic behavior independent from each other. Interestingly, after contact with *S. meliloti*, the LYK3-labeled MD became laterally arrested and co-localized greatly with the FLOT4 puncta (Haney et al., 2011). The highest degree of co-localization was detected in root hairs that had reinitiated tip growth, i.e. root hairs that were

Introduction

actively responding to the symbiotic signals. The density of FLOT4-labeled MD in root hairs was reduced in *hcl-1* plants, and restored in the *hcl-1 compl.*, indicating a dependency of these MDs on the presence of wildtype LYK3.

LYK3 may also localize into MDs in two specific layers of *Medicago nodules* (Moling et al., 2014). It is possible that the specific accumulation in MDs in two defined cell layers is essential to precisely integrate and regulate the formation of a symbiotic interface for the perception of NFs. Furthermore, FLIM-FRET analysis pointed towards an interaction between LYK3 and NFP, which are thought to form heteromeric complexes *in vivo* (Moling et al., 2014).

2 Aim of This Study

It is widely recognized that proteins localize to the plasma membrane in microdomains, which are thought to be important for condensing relevant signaling components into the same spatial area. Remorins are a protein family that presents unique microdomain patterns; however, only for a few remorins a phenotype suggests a function. So far, SYMREM1 is the only remorin that can be precisely placed into a specific signaling pathway. The structures required for SYMREM1's MD-localization have not been found.

In this work we aimed to identify how SYMREM1-labeled MDs are formed in the PM and what components are required for their formation in the homologous system *Medicago truncatula*. Due to *SYMREM1* being exclusively expressed during RNS, we hypothesized that SYMREM1 may be spatially connected with other RNS-specific, PM-resident proteins in a symbiosis-specific MD, and tested this assumption in a heterologous overexpression system, *Nicotiana benthamiana*.

In a methodical project, Fluorescence Lifetime Imaging Microscopy (FLIM) based on Foerster Resonance Energy Transfer (FRET) microscopy was established as a tool to identify protein-protein interactions *in planta*. Furthermore, we aimed to apply FLIM, to pinpoint precise places of interactions *in planta*.

3 Results

3.1 FLIM-FRET Microscopy as a Tool to Identify Microdomains

During the process of fluorescence, the time a fluorophore exists in its excited state before returning to the ground state by emitting photons is termed fluorescence lifetime (τ). Relaxation can alternatively occur by ‘fluorescence resonance energy transfer’ (FRET). It describes the non-radiative transfer of energy stored in an excited ‘donor’-fluorophore to a non-excited ‘acceptor’-fluorophore. Prerequisite for this process is that the emission spectrum of the donor overlaps with the excitation spectrum of the acceptor. FRET only occurs if the two molecules are in very close proximity (< 10 nm) and, thus, can be used to determine if physical interactions occur between two molecules or proteins of interest.

The processes of donor fluorescence and FRET are competing and during fluorescence lifetime imaging microscopy (FLIM) only the relaxing photons from the donor molecules are observed. Energy transferred to the acceptor fluorophore is not detected due to its longer wavelength. Therefore, FRET shortens the donor lifetime τ , which can be measured by constructing a histogram of detected fluorescence events (i.e. timed photon counting). If the donor lifetime without FRET is known (as a reference), one can quantify the extent to which FRET occurs. Therefore, using a pulsed multi-photon laser for excitation, FLIM allows the determination of the fluorescence lifetime (τ) of a donor fluorophore in a time-resolved manner.

3.1.1 LjSYMREM1 Interacts with NFR1 in Microdomains

In previous experiments, an interaction between *Lotus japonicus* SYMREM1 and the symbiotic receptors NFR1 was found. This was based on Bimolecular Fluorescence Complementation analysis (BiFC/split YFP) in *Nicotiana benthamiana* and split-ubiquitin yeast-2-hybrid assays in *Saccharomyces cerevisiae* (Tóth et al., 2012).

In FLIM-FRET experiments with NFR1:Cerulean (donor) and LjSYMREM1:mOrange (acceptor) co-expressed in *Nicotiana* leaves we confirmed the interactions (Tóth et al., 2012). The NFR1:Cerulean fusion protein expressed without any potential interactors displayed a fluorescence lifetime of $\tau = 2.18$ ns (SE= 0.013; n= 35 cells) at the plasma membrane. This fusion construct was co-expressed with the freely diffusing acceptor fluorophore mOrange and no

significant reduction in the average lifetime of the cerulean fluorophore was detectable ($\tau = 2.16$ ns; SE= 0.014; n= 19; p= 0.221). A strong reduction was detected in the presence of either the SYMREM1:mOrange fusion protein (LjSYMREM1; $\tau = 1.99$ ns; SE= 0.022; FRET efficiency 8.8%; n= 40; p= $1.32E^{-10}$) or the conserved C-terminal region of SYMREM1 (LjSYMREM1_C; $\tau = 1.97$ ns; SE= 0.021; FRET efficiency 9.6%; n= 38; p= $1.47E^{-10}$). Furthermore, even though the lifetime of NFR1:Cerulean decreased slightly but still significantly in the presence of the N-terminal region of SYMREM1 (LjSYMREM1_N; $\tau = 2.09$; SE= 0.019; FRET efficiency 4.1%; n= 36; p= 0.0001), these data confirmed that the stable interaction of LjSYMREM1 with NFR1 is primarily formed through residues in the C-terminal region. The N-terminal region alone does not display strong interaction ability with NFR1 (Tóth et al., 2012).

Bimolecular Fluorescence Complementation (BiFC) experiments between NFR1 and SYMREM1 showed interactions that occurred only in specific MDs, even though the proteins were evenly present throughout the whole PM surface (Tóth et al., 2012). However, this method has been criticized for resulting in artifacts, due to the irreversible nature of fluorophore complementation (Kodama and Hu, 2012). Therefore, we asked ourselves if we could apply FLIM-FRET microscopy to determine whether this interaction truly is restricted to specific areas of the PM.

For this, the lifetime of the donor-fluorophore cerulean was visualized as a false color-coded image, giving a visual output of Cerulean-lifetimes within the PM, superimposed over the visible light image. The range for the false color-code was chosen in such a way to emphasize regions in the PM that have significantly lower values than the average lifetime measured for NFR1:Cerulean alone (2.16 ns). Therefore, the false color-code was set to display as follows: 1.5 - 1.999 ns (blue), 2.000 - 2.149 ns (green) and 2.15 – 2.8 ns (red). With these settings, we aimed at depicting ‘hot spots’ of protein-protein interactions, i.e. microdomains.

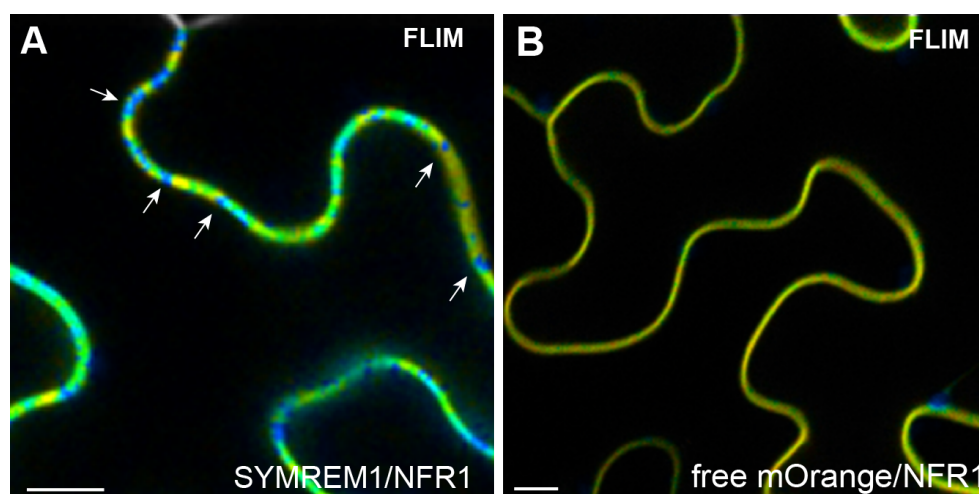


Figure 3 FLIM-FRET reveals interaction between SYMREM1 and NFR1 in precise areas of the plasma membrane. Fluorescence lifetime of NFR1:Cerulean in *Nicotiana benthamiana* leaf epidermal cells. The lifetime is displayed in a false color-code with these ranges: 1.5 - 1.999 ns (blue), 2.000 - 2.149 ns (green) and 2.15 – 2.8 ns (red). **(A)** NFR1:Cerulean was co-expressed

Results

with SYMREM1:mOrange. Arrows point to the distinct blue areas with reduced fluorescence lifetime. The interaction is occurring in specific locations in the PM. **(B)** NFR1:Cerulean co-expressed with free mOrange. No areas with significantly reduced lifetimes are visible, except for one blue area in the lower right corner. This could be a single auto-fluorescent chloroplast. No interaction is occurring. Scale bars indicate 10 μm .

Clearly defined regions of reduced fluorescence lifetime of the donor NFR1:Cerulean in the presence of the SYMREM1:mOrange were visible (blue). This indicated interaction hotspots between NFR1 and SYMREM1 occurred in specific membrane MDs (Figure 3A), even though NFR1:Cerulean clearly was present along the whole surface of the PM (green). This pattern was not observed when NFR1:Cerulean was co-expressed with a free mOrange fluorophore (Figure 3B). No specific areas in the PM with a reduced donor lifetime were detected. This is in line with the lifetimes and FRET efficiencies obtained for these two combinations.

Therefore, FLIM-FRET not only is a tool to successfully detect interactions *in planta*, but also was suitable to determine that interactions between SYMREM1 and NFR1 occurring in MDs in the PM.

3.1.2 MtSYMREM1 SLiM Mutants Interact with LYK3

Remorins display regions with so-called intrinsic disorder (ID) (Marin and Ott, 2012; Marin et al., 2012; Marin and Ott, 2014). Under physiological conditions, intrinsically disordered regions are unstructured but possess the ability to undergo folding (disorder-to order transition) when binding to an interacting protein, or after being secondarily modified, e.g. phosphorylation (Iakoucheva et al., 2004). Intrinsically disordered (regions of) provide variable, but simultaneously highly specific interaction sites for low affinity binding to partners, and as such are implicated in playing important roles during signaling processes (Wright and Dyson, 1999; Dunker and Obradovic, 2001; Dyson and Wright, 2005) and plant-pathogen interactions (Marin and Ott, 2014). Within ID-regions, so-called Molecular Recognition Features (MoRFs), or Short Linear Motifs (SLiMs) exist, which are short segments of 3-30 amino acid length. Depending on the binding of interacting proteins, these SLiMs undergo disorder-to-order transition and can have an impact on a diverse set of functions, which include, secondary modifications, subcellular localization, controlling the stability of interactions, or influencing the context-dependent activity of proteins (Oldfield et al., 2005; Mohan et al., 2006; Neduva and Russell, 2006; Vacic et al., 2007; Dinkel et al., 2014; Van Roey et al., 2014).

In collaboration with Dr. Macarena Marín (LMU) SLiM mutants of MtSYMREM1 were tested for their relevance on the interaction with LYK3 in *Nicotiana*. For this, three predicted SLiMs (amino acids 10-12; 27-31; and 90-94) were deleted from the coding sequence of MtSYMREM1 and the mutants termed MtSYMREM1 Δ 1, Δ 2, Δ 3, respectively. FLIM-FRET experiments

were performed with the FRET pair GFP (fused to LYK3) and mCherry (fused to the N-terminal beginning of the SYMREM1 constructs).

LYK3:GFP expressed alone resulted in a fluorescence lifetime τ of 2.59 ns (SE= 0.007, n= 10 cells). Co-expressing mCherry:SYMREM1 significantly reduced the lifetime τ to 2.52 ns (SE= 0.007, n= 13, $p= 6.48E^{-06}$, FRET efficiency 2.5%), confirming an interaction is occurring. In presence of the C-terminal region (mCherry:MtSYMREM1_C) the fluorescence lifetime of LYK3:GFP strongly decreased ($\tau= 2.37$ ns, SE= 0.022, n= 13, $p= 2.66E^{-08}$, FRET efficiency 8.6%). Although these data deviate to those obtained between LjSYMREM1:mOrange and NFR1:Cerulean (see 3.1.1) the overall tendencies are the same: SYMREM1 and SYMREM1_C interact with LYK3.

LYK3:GFP co-expressed with MtSYMREM1_Δ1 resulted in a donor Lifetime of 2.42 ns (SE= 0.009, n= 13, $p= 9.91E^{-12}$, FRET efficiency 6.3 %). MtSYMREM1_Δ2 reduced the lifetime to 2.36 ns (SE= 0.02, n= 14, $p= 2.48E^{-09}$, FRET efficiency 8.7%), and MtSYMREM1_Δ3 to 2.40 ns (SE= 0.023, n= 12, $p= 6.59E^{-07}$, FRET efficiency 7.4%). All three SLiM mutants and the C-terminal region of MtSYMREM1 interacted more strongly with LYK3 than the full length wildtype SYMREM1 protein. This would suggest that the N-terminal region as a whole, as well as the individual SLiMs have a negative regulatory function during the interaction with LYK3. However, due to the only mild reduction of LYK3:GFP τ upon the co-expression of wildtype mCherry:MtSYMREM1 (FRET efficiency 2.5%) compared to the interaction between LjSYMREM1 and NFR1 (FRET efficiency 8.8%), it was, unfortunately, not possible to deduce a direct functional relevance of the SLiMs from these data.

3.1.3 FLIM-FRET in *Arabidopsis thaliana*

After having established that the FLIM-FRET methods was applicable to detect interactions in specific, small MDs at the PM (Figure 3) we wanted to test if we could apply our settings to proteins in their native context. For this, in collaboration with Prof. Dr. Kay Schneitz (Plant Developmental Biology, TUM), we investigated the *Arabidopsis* proteins STRUBBELIG (SUB) and QUIRKY (QKY) in their native context.

SUB is a leucine-rich repeat transmembrane receptor-like kinase that localizes to the PM and is involved in tissue morphogenesis of many plant organs. SUB is required for inter-cell-layer signaling in processes that include the determination of the shape of flowers, height and shape of the stem, leaf shape and root hair patterning (Chevalier et al., 2005; Kwak et al., 2005; Fulton et al., 2009). *Sub-1* mutants exhibit, e.g. aberrant cell shapes, leaf twisting and disturbed cell division planes in floral meristems (Chevalier et al., 2005).

Results

QKY was found in a forward genetics screen, in which a mutant identified, *qky-8*, phenocopied the *sub-1* mutant on both the morphological and cellular levels (Fulton et al., 2009). QKY is a transmembrane domain-containing protein that localizes to the PM in plasmodesmata, and this localization is essential for QKY to function (Fulton et al., 2009; Trehin et al., 2013; Vaddepalli et al., 2014). SUB and QKY interact in the heterologous system *Saccharomyces cerevisiae* (Trehin et al., 2013).

To investigate if this interaction also occurs *in planta*, FLIM-FRET was performed with 7-day-old seedlings of stably transformed *Arabidopsis* lines. The control line only expressed gSUB:eGFP from its native promoter. The second line analyzed co-expressed gSUB:eGFP with a mCherry:QKY overexpression construct driven by the polyUbiquitin promoter. These marker constructs localize to the PM, are biologically functional and able to complement the *sub-1* or *qky-8* mutant phenotypes (Vaddepalli et al., 2014). Both proteins appeared to also accumulate in plasmodesmata (PD) (Vaddepalli et al., 2014).

First, in plants that only express SUB:eGFP from its native promoter, the mean fluorescence lifetime value was determined along the entire PM of root epidermal cells. The average τ value was 2263.6 ps (SE= 9.1 ps; n= 41). When mCherry:QKY was co-expressed, an overall τ value of 2243.3 ps (SE= 6.8 ps; n= 42) was measured. Therefore, no significant reduction in fluorescence lifetime of SUB:eGFP was detected (Student's's t-test, p= 0.04). This suggested that no interaction occurs between these proteins.

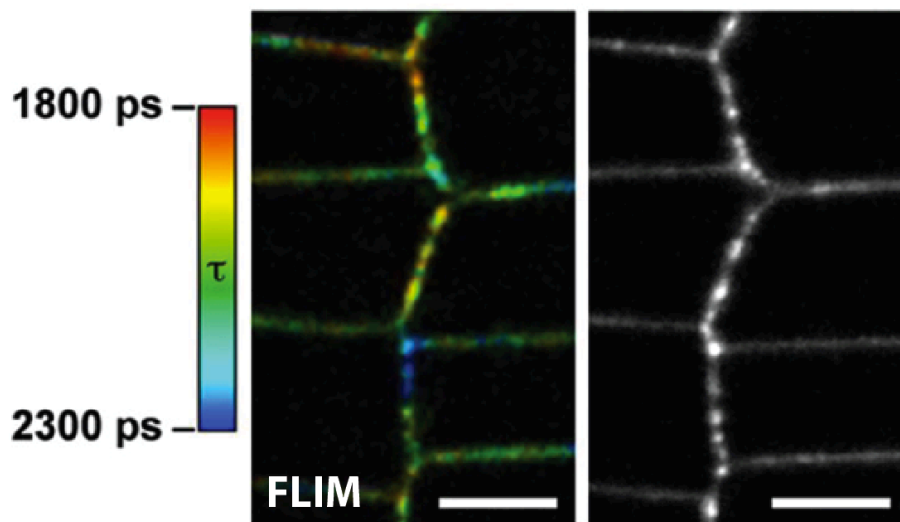


Figure 4 FLIM-FRET in *Arabidopsis thaliana* reveals plasmodesmata-localized interaction between SUB and QKY. *Arabidopsis thaliana* stably transformed with pSUB::gSUB:eGFP and pUbi::QKY:mCherry. The fluorescence lifetime τ of SUB:eGFP in root cells from 7 day old seedlings was measured by FLIM-FRET microscopy. The false color-code depicting τ ranges from 1800 ps (red) to 2300 ps (blue). The color code reveals reduced donor lifetimes in a subpopulation of the plasmodesmata. The image to the right is a grey scale image of SUB:eGFP of the identical area. Scale bars indicate 5 μ m.

However, upon inspection of the corresponding FLIM- and confocal microscopy images, a non-uniform reduction in the fluorescence lifetime appeared to occur and was restricted to specific areas. These spots co-localized with the brighter regions labeled by SUB:eGFP, and therefore they likely represent PD (Vaddepalli et al., 2014).

Within these precise areas the lifetime of SUB:eGFP was re-analyzed. A τ value of 2123.8 ps (SE= 6.05 ps; n= 205) indicated that in PD the τ of SUB:eGFP alone was significantly reduced in comparison with the overall fluorescence lifetime (2263.6 ps; $p= 6.8E^{-20}$). This is not unusual, because the lifetime of a fluorophore is strongly dependent on its cellular environment (Nakabayashi et al., 2008; van Manen et al., 2008). Importantly, in the presence of mCherry:QKY, the lifetime τ of SUB:eGFP in PD was reduced to 2075.5 ps (SE= 4.98 ps; n= 210). This is a statistically significant reduction when compared to the lifetimes in PD of SUB:eGFP alone ($p= 7.9E^{-10}$).

These data indicated that SUB:eGFP and mCherry:QKY interact only in a subpopulation of PD in *Arabidopsis* epidermal root cells, and FLIM-FRET analysis was successfully applied in a native, low-expressing context. These data have been published (Vaddepalli et al., 2014).

3.2 Identification of Components Required for SYMREM1-labeled Microdomains

3.2.1 SYMREM1-labeled Microdomains are Actin Dependent

To test for the requirements of SYMREM1 localization, an YFP:SYMREM1 fusion protein was ectopically expressed from the polyubiquitin promoter in WT *Medicago truncatula* ecotype A17 transgenic roots and imaged using confocal-laser scanning microscopy. Here, YFP:SYMREM1 localized in distinct and stationary microdomains (MDs) (Figure 6A) as had been published for SYMREM1 (Lefebvre et al., 2010; Konrad et al., 2014).

SYMREM1 attaches from the cytosol to the inner leaflet of the plasma membrane (PM), and according to the picket-fence model its localization could be influenced by the plant cytoskeleton. To ascertain whether this was the case, the YFP:SYMREM1 expressing roots were treated with cytoskeletal disruptors.

First, pharmacological disruption of the microtubule-, and actin cytoskeleton, were verified to establish the conditions in which the cytoskeleton was most effectively destabilized. For this, the coding sequence from the microtubule binding domain of the mammalian MICROTUBULE ASSOCIATED PROTEIN 4 (MAP4) (Marc et al., 1998) and the 17 amino acid long actin binding peptide Lifeact were cloned in Golden Gate compatible manner (Binder et al., 2014) and N-

Results

terminally fused to YFP. These constructs were transformed into and expressed under the polyubiquitin promoter in transgenic *M. truncatula* roots. YFP:MAP4 clearly bound to microtubules (Figure 5A), and these were efficiently disrupted when treated with oryzalin, a microtubule-destabilizing reagent (Figure 5B). Accordingly, YFP:Lifeact successfully labeled actin filaments (Figure 5C), and these were mostly, but not completely, depolymerized when the sample was incubated with cytochalasin D, an inhibitor of actin polymerization that leads to the collapse of actin filaments (Figure 5D).

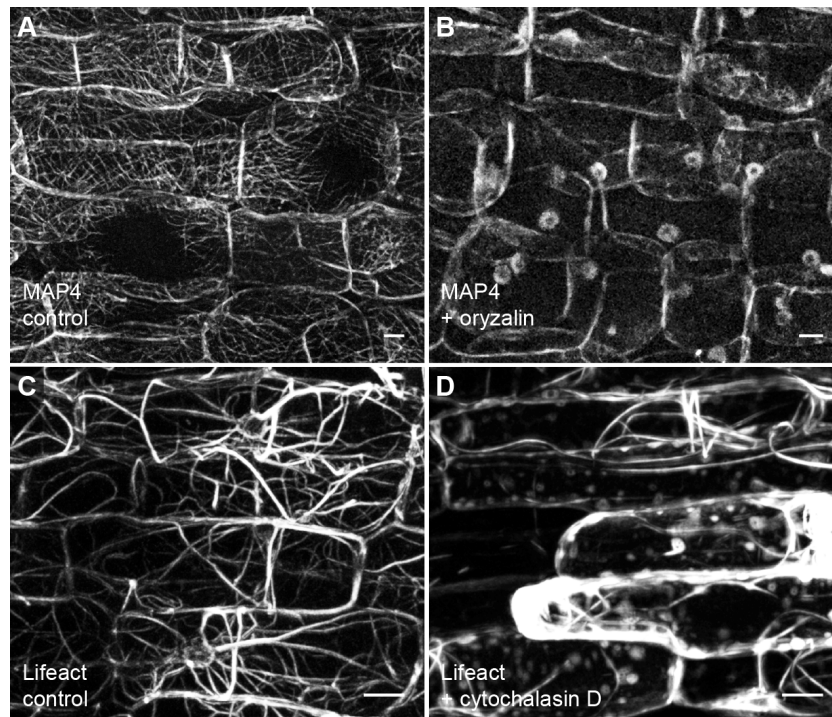


Figure 5 Depolymerisation of microtubules and actin filaments in *Medicago truncatula* A17 roots. (A) The expression of an YFP:MAP4 fusion protein labeled the MT network. **(B)** Upon incubation with oryzalin the MT network was depolymerized. **(C)** The actin network was labeled by the YFP:Lifeact construct and destabilized to a large degree, but not fully, through the application of cytochalasin D **(D)**. Scale bars indicate 10 μm.

In roots that were treated with oryzalin, YFP:SYMREM1-labeled MDs remained stable even after MT disruption (Figure 6B). This suggests the microtubule cytoskeleton is not a significant factor in the formation or stabilization of SYMREM1-labeled MDs. The incubation of transgenic roots in cytochalasin D, however, resulted in a clear decrease in the number of SYMREM1-labeled MDs (Figure 6C). This indicated a dependency of these MDs on an intact actin cytoskeleton.

To monitor this qualitative observation precisely, the images were analyzed quantitatively. Individual YFP:SYMREM1-expressing cells were segmented into foreground and background signals so that only the MDs remained visible (see Figure 29 in methods). Then, MDs were counted making use of the plugin ‘analyze particles’ of the image processing program, ImageJ. No further discrimination on additional features, e.g. MD surface area or shape was taken into

account in this study. On average, YFP:SYMREM1 labeled MDs at a density of 0.057 domains/ μm^2 (Figure 6A, standard error (SE)= 0.0051; n= 47) when it was ectopically overexpressed in *M. truncatula* A17 and incubated in water with an equal amount of solvent. The destabilization of the MTs with oryzalin resulted in an average density of SYMREM1-labeled MD of 0.062 domains/ μm^2 (SE= 0.0058; p= 0.54; n= 17). This increase did not differ significantly from the control value (0.057 domains/ μm^2 ; SE= 0.0051; n= 47).

After the destabilization of the actin filaments with cytochalasin D, a more than 3-fold decrease of SYMREM1-labeled MDs with a domain-density of 0.018 domains/ μm^2 (SE= 0.0012; p= 4.74E⁻¹⁰; n= 77) was measured, thereby confirming the qualitative observation statistically.

These data indicate that MDs labeled with YFP:SYMREM1 are not influenced by microtubules but are stabilized by the presence of the actin cytoskeleton.

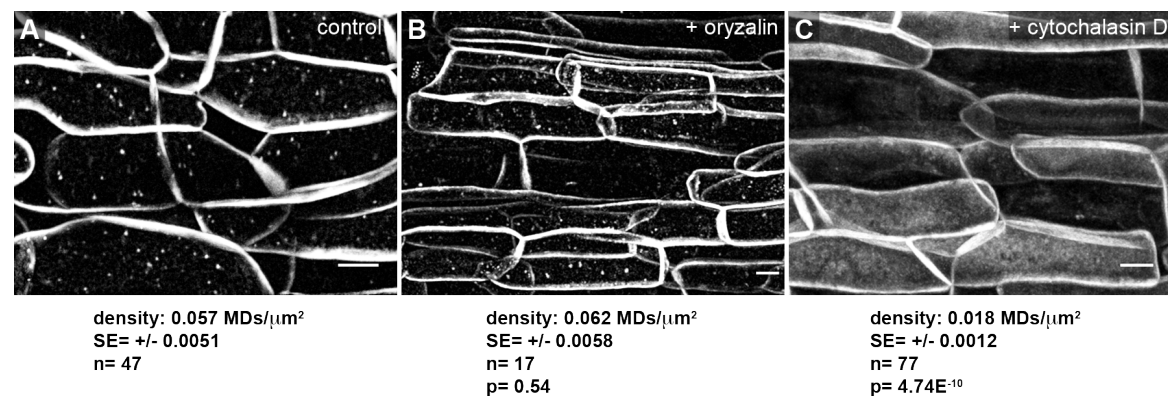


Figure 6 SYMREM1-labeled microdomains are dependent on the actin cytoskeleton. The YFP:SYMREM1 fusion protein was ectopically expressed under the polyubiquitin promoter in transgenic *Medicago truncatula* WT A17 roots and imaged using confocal-laser scanning microscopy. **(A)** YFP:SYMREM1 labels distinct membrane microdomains (MDs) in control roots. **(B)** Treatment with the microtubule destabilizing drug oryzalin did not change YFP:SYMREM1 localization significantly. **(C)** Disruption of the actin cytoskeleton through the application of cytochalasin D abolishes MD targeting of the protein. Below each panel the results of the MD-quantification are placed. SE= standard error; p-value= confidence interval obtained from a Student's t-test. Scale bars indicate 10 μm .

3.2.2 SYMREM1 Domains Co-localize with Actin Filaments

Because SYMREM1-labeled MDs disappeared after actin disruption, we tested whether they would also localize closely with actin filaments. Therefore, the potential co-localization of these MDs with the actin cytoskeleton was analyzed. For this, a Golden Gate Level 3 co-expression vector was assembled, which encoded for both a mCherry:SYMREM1 and a Cerulean:Lifect fusion construct. *Medicago* A17 roots were transformed via *Agrobacterium rhizogenes* (strain ARqua1)-mediated hairy root transformation and screened for the presence of the fluorophores. In roots that co-expressed both proteins, mCherry:SYMREM1 localized into MDs, as expected (Figure 7B, H). Cerulean:Lifect efficiently labeled actin cytoskeleton filaments (Figure 7A, C, E,

Results

G). In most cases, the mCherry:SYMREM1 MDs appeared to associate closely with Cerulean:Lifect-labeled actin filaments, not only in root hairs, but also in epidermal cells (Figure 7).

To support this observation, the images were analyzed statistically. The Pearson correlation coefficient, which measures the linear dependency between two datasets, was calculated for the signals of mCherry:SYMREM1 and Cerulean:Lifect. The values of this coefficient ranges from -1 to +1. A value of -1 indicates complete exclusion (absolute negative correlation), and a value of +1 corresponds to total co-localization (absolute positive correlation). A value of 0 signifies complete randomness between the dataset, thus, no correlation. In biological samples, values above 0 could indicate positive correlation, and below 0 negative correlation, however, randomized simulations must be performed in order to examine the outcome (Manders et al., 1992; Bolte and Cordelieres, 2006).

For samples that co-expressed Cerulean:Lifect and mCherry:SYMREM1, quantitative pixel-based co-localization analysis resulted in a Pearson correlation coefficient of $R_r = 0.287$ ($SE = 0.022$; $n = 10$) which strongly indicated a positive correlation between the SYMREM1 labeled MDs and the Lifect-labeled actin cytoskeleton. To verify this observation statistically, or to determine whether this correlation appeared randomly, a 'Costes' randomization' procedure was applied to all images analyzed. One channel (here mCherry:SYMREM1) was randomized 200 times into images with randomly distributed blocks with the size of 10x10 pixels (see Figure 28 in methods section). Then, the artificially generated images were matched to the corresponding original second channel (here Cerulean:Lifect) as before. If the randomized images were to correlate to the same degree (or even higher) with the seconds channel (Cerulean:Lifect), the randomized $rd R_r$ would not differ much from the original R_r (or would not be close to 0).

In the case for mCherry:SYMREM1 and Cerulean:Lifect, however, this procedure resulted in a random Pearson correlation coefficient of ' $rd R_r$ ' = 0.001 ($SE = 0.0009$; $n = 10$; $p = 3.76E^{-07}$), which is significantly lower than the original value and indicates complete randomness in this dataset.

This demonstrated that the observed co-localization of mCherry:SYMREM1-labeled MDs and Cerulean:Lifect did not appear by chance and corroborated the results obtained by pharmacological actin disruption. SYMREM1-labeled MDs are, therefore, dependent on the actin cytoskeleton.

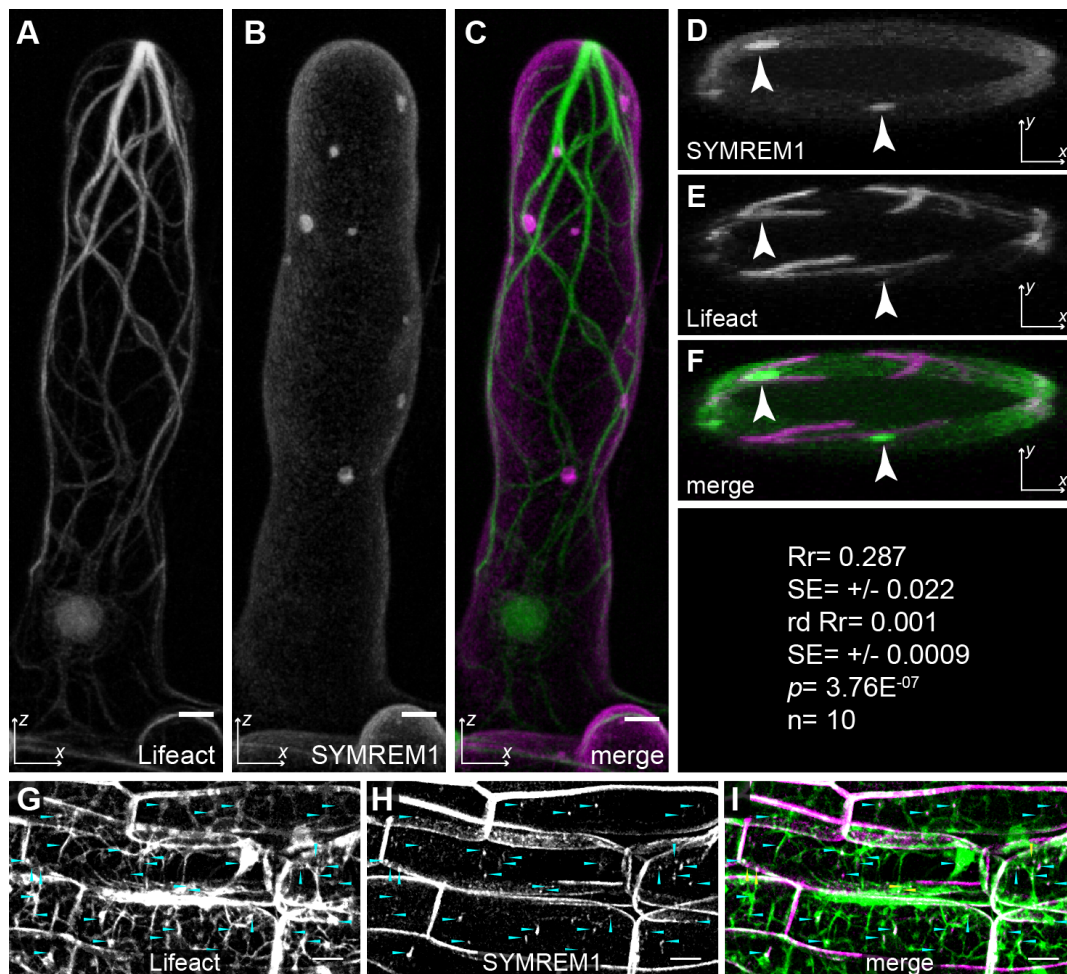


Figure 7 SYMREM1-labeled microdomains co-localize with actin filaments. Cerulean:Lifect and mCherry:SYMREM1 were cloned in tandem and co-expressed from the same T-DNA in transgenic *Medicago truncatula* A17 roots. Actin (**A**) and SYMREM1-labeled MDs (**B**) were visualized in the same root hair and co-localized (**C**). An optical cross-section of the same root hair revealed that SYMREM1-labeled MDs were stretched along the x-axis (arrowheads; **D**) and actin filaments (**E**) leading to a significant co-localization (**F**). In WT A17 root epidermal cells, Cerulean:Lifect (**G**) also associated with mCherry:SYMREM1-labeled MDs (**H**). Arrows highlight a selection of MDs that points to the same position in (**G**), (**H**) and (**I**). In the merged image (**I**), the closeness of SYMREM1-labeled MDs to the actin cytoskeleton becomes evident. Quantitative image analysis was performed on all samples as indicated by the numbers given below panel (**F**). Rr= Pearson correlation coefficient; rd Rr= Pearson correlation coefficient obtained after Costes' randomization was applied. The respective standard errors (SE) are provided below the Pearson values. p-value= confidence interval obtained from a Student's t-test comparing Rr and rd Rr. Scale bars indicate 5 μ m in (A), (B) and (C), 10 μ m in (G), (H) and (I).

3.3 SYMREM1 mis-localizes in the LYK3 Mutant Allele *hcl-1*

After a dependency of SYMREM1-labeled MDs on the actin cytoskeleton was established, the question arose whether these MDs are dependent on additional factors. SYMREM1 interacts with several other proteins. Among these are the symbiotic Receptor-like kinases (RLKs) NFP, LYK3

Results

and DMI2 (Lefebvre et al., 2010). An interaction with these PM-localized proteins could just as well play a role in the recruitment of SYMREM1 into MDs.

Therefore, the YFP:SYMREM1 construct was transformed into the respective *M. truncatula* RLKs mutants, and the expression of the fusion protein in transgenic roots was monitored. No qualitative difference in the formation of YFP:SYMREM1-labeled MDs in root hair cells was visible (Figure 8); YFP:SYMREM1 localized into distinct MDs in wildtype A17 (Figure 8A), as well as in the RLK-mutants, *nfp-2*, *dmi2-1*, *hcl-4* and *hcl-1* (Figure 8B-E). Also, the *hcl-1 compl.* line (*hcl-1* mutant complemented stably with a proLYK3::LYK3:HASt construct) shows clear labeling of MDs by YFP:SYMREM1 (Figure 8F).

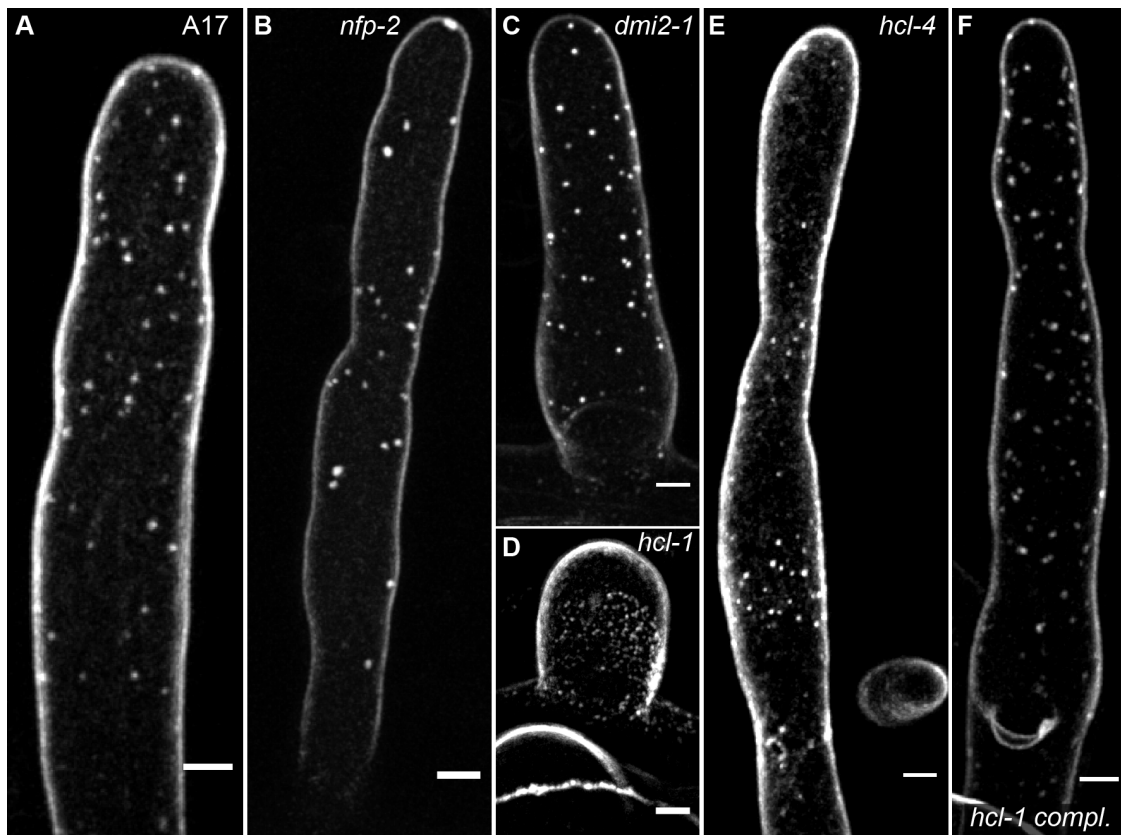


Figure 8 YFP:SYMREM1 localizes into microdomains in root hairs of *Medicago truncatula* RLKs mutants. An YFP:SYMREM1 fusion protein was ectopically expressed under the polyubiquitin promoter in different genetic backgrounds of transgenic *Medicago* roots and imaged using confocal-laser scanning microscopy. YFP:SYMREM1-labeled MDs are clearly visible in (A) WT A17, (B) *nfp-2*, (C) *dmi2-1*, (D) *hcl-1*, (E) *hcl-4* and (F) *hcl-1 compl.*. Root hairs of *hcl-1* were short and rounded (D). Scale bars indicate 5 μ m.

This indicated that a single interaction with the RLKs is not necessary for SYMREM1 to localize into MDs. To confirm this observation, YFP:SYMREM1's localization was additionally analyzed in different cell types. Epidermal and outer cortical cells of transformed roots that were expressing the YFP:SYMREM1 construct were inspected in more detail.

As expected, the YFP:SYMREM1 protein localized into clearly visible MDs in *nfp-2*, *dmi2-1*, and *hcl-4* (Figure 9B, C, D) and closely resembled the phenotype of YFP:SYMREM1 expressed in wildtype A17 root cells (Figure 9A). In contrast, YFP:SYMREM1 localized in a completely different and unexpected manner in the *hcl-1* mutant (Figure 9E). *Hcl-1* is a LYK3 mutant allele, which carries a glycine to glutamate mutation in the conserved GxGxxG motif in the ATP binding region of the kinase domain (Smit et al., 2007) and causes the LYK3 receptor to be catalytically inactive (kinase dead) (Klaus-Heisen et al., 2011).

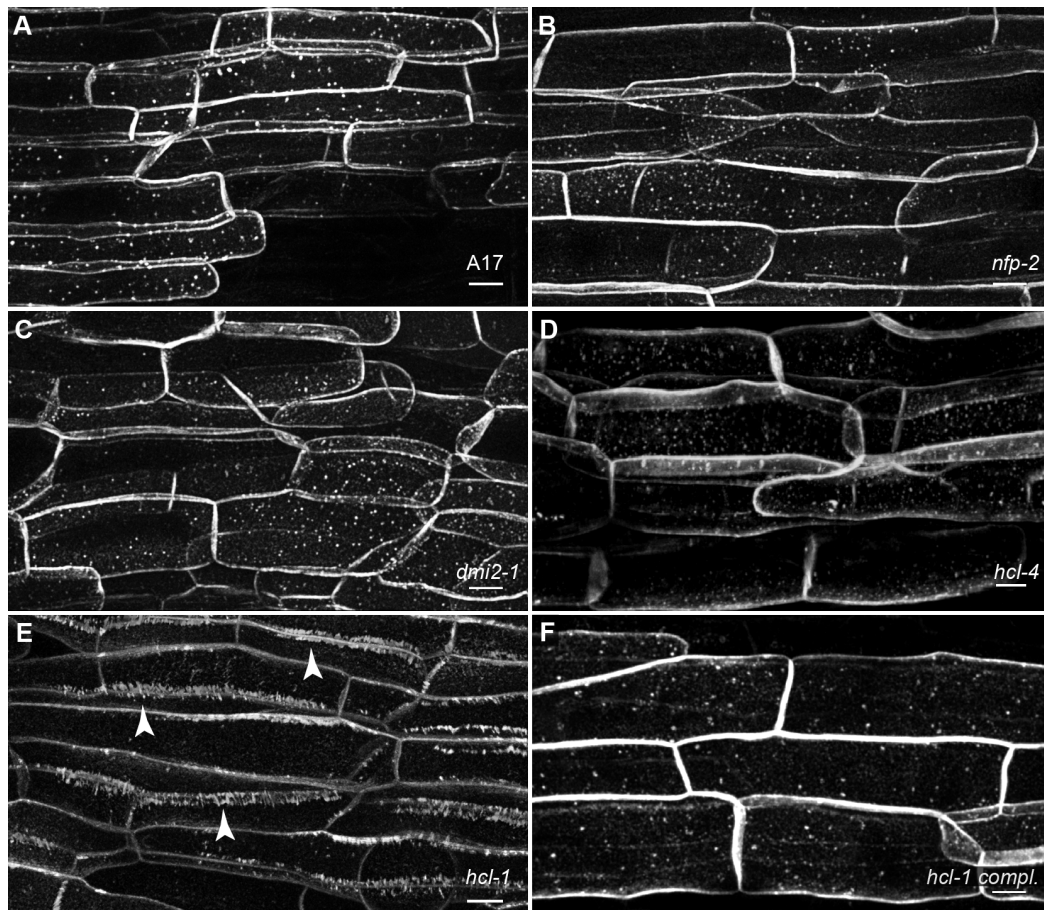


Figure 9 Patterns of SYMREM1-labelled MDs are altered in the *hcl-1* mutant allele. An YFP:SYMREM1 fusion protein was expressed in different genetic backgrounds of *Medicago truncatula* roots. (A) YFP:SYMREM1 clearly labeled MDs in A17. No qualitative differences were observed when this construct was expressed in the receptor mutant backgrounds *nfp-2* (B), *dmi2-1* (C), and *hcl-4* (D). In contrast, SYMREM1-labeled MD patterns were strongly altered in the *hcl-1* mutant (E; arrowheads). Wildtype-like patterns were restored in *hcl-1 compl.* (F). Scale bars indicate 10 μ m.

In epidermal and outer cortical cells of the LYK3 mutant *hcl-1*, MDs labeled by YFP:SYMREM1 clearly formed. However, these did not distribute over the whole PM but localized into short, almost parallel arrays of spike-like patterns (see arrowheads in Figure 9E). This abnormal pattern was not observed in *hcl-4* (Figure 9D), a splice site mutant allele that reduces wildtype *LYK3* transcript by 92% (i.e. 8% WT-transcript remains) (Smit et al., 2007). Here, YFP:SYMREM1 labeled MDs normally. Their frequency was counted (as previously done), and they occurred at a

Results

density of 0.0634 domains/ μm^2 (SE= 0.0052; n= 30). Although this value was slightly higher than the density measured in wildtype A17 cells (0.057 domains/ μm^2 ; SE= 0.0051; Figure 6), the MD-densities were not significantly different between these two genetic backgrounds (Student's t-test; $p= 0.376$).

In the *hcl-1 comp.* line, YFP:SYMREM1 attached to the PM in wildtype-like manner (Figure 9F); no aberrant SYMREM1 localization was observed. This suggested *hcl-1* is the causative mutation for the unusual localization of SYMREM1.

3.4 The Actin Cytoskeleton is Altered in *Medicago truncatula hcl-1*

SYMREM1 localized in an unusual manner in *hcl-1*, and its labeling of MDs was dependent on the actin cytoskeleton. Therefore, we wondered if the actin cytoskeleton in *hcl-1* was directly responsible for this.

Medicago truncatula A17, *hcl-4* and *hcl-1 compl.* do not display any evident developmental defects, when grown on plates containing standard Fahraeus-medium. The roots develop normally and the root hairs display tip growth and elongate (Figure 10A, D, E). The kinase dead LYK3 mutant allele *hcl-1*, however, displays a strong root hair growth defect. Not a single root hair was elongates; instead they remain short, round, and appeared balloon-like (Figure 10B, C). Short root hairs of *hcl-1* had been described before (Haney et al., 2011), even though originally this phenotype had not been observed (Catoira et al., 2001).

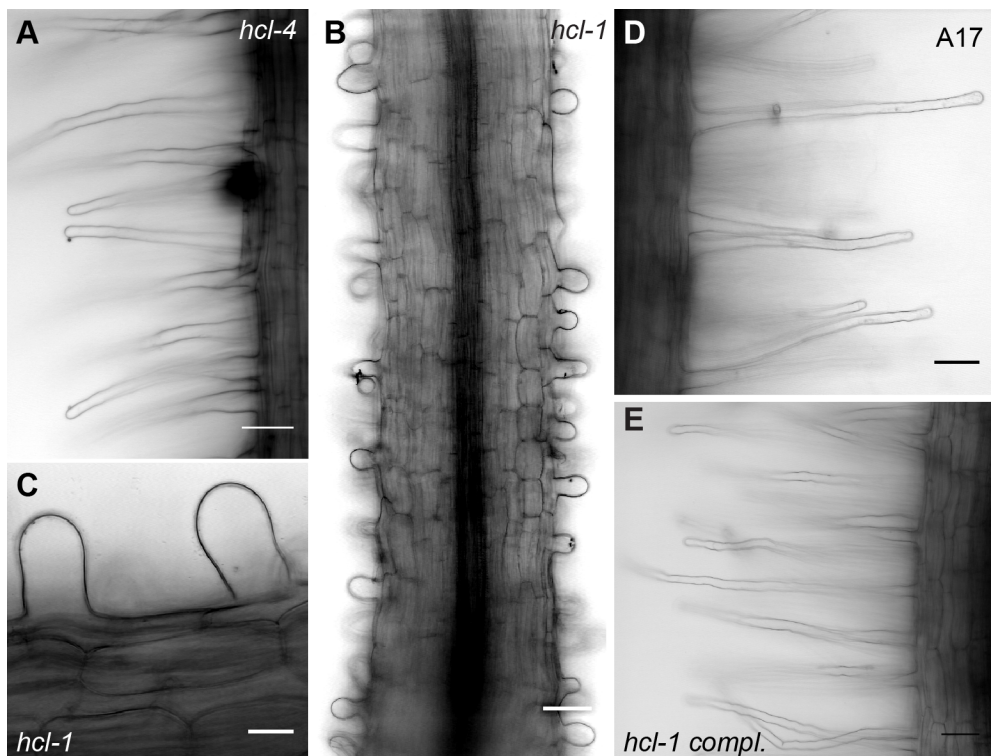


Figure 10 The *Medicago truncatula* LYK3 mutant *hcl-1* shows a strong root hair elongation defect. Untransformed *Medicago* plants were grown on plates containing Fahraeus medium pH6.0 and root hairs of 5 days old seedlings were imaged. The wildtype A17 root hairs (**D**) function as a reference for comparison. Root hairs of the mutant *hcl-1* never elongated and were of round balloon-like appearance (**C**) throughout the root (**B**). In contrast, *hcl-4* showed normally elongated root hairs (**A**), as did the complemented line *hcl-1 compl.* (**E**). Scale bars indicate 10 μm .

Root hair growth is a process that strongly depends on the polymerization of actin for the targeted delivery of cargo to the tip (Baluska et al., 2000; Carol and Dolan, 2002); therefore, it was possible that *hcl-1* harbors an actin cytoskeleton defect.

To address this, the YFP:Lifeact fusion construct was transformed into and expressed in the *Medicago* A17, *hcl-1* and *hcl-1 compl.* backgrounds. Confocal microscopy revealed that YFP:Lifeact efficiently labeled actin filaments in transgenic root cells (Figure 11). The appearance of the actin cytoskeleton in A17 and *hcl-1* was examined first. In wildtype A17 root cells, the actin was predominantly arranged in direction of the cell elongation axis (Figure 11A). In *hcl-1*, the actin cytoskeleton was transversally turned in relation to the cell elongation axis (Figure 11B), revealing a clear disparity of the Lifeact-labeled cytoskeleton between these two backgrounds (compare Figure A to B). The actin cytoskeleton in the root hairs also differed strongly between *hcl-1* and the A17 or *hcl-1 compl.* lines. YFP:Lifeact labeled thicker strands in the shorter, balloon-like *hcl-1* root hairs (Figure 11C) than in A17 (inset, Figure 11A). In A17, finer and more diffuse actin structures are present, especially towards the root hair tip. The Lifeact-labeled signal in root hairs of *hcl-1 compl.* also was finer and more diffuse than in *hcl-1* towards the tip. (Figure 11C, D).

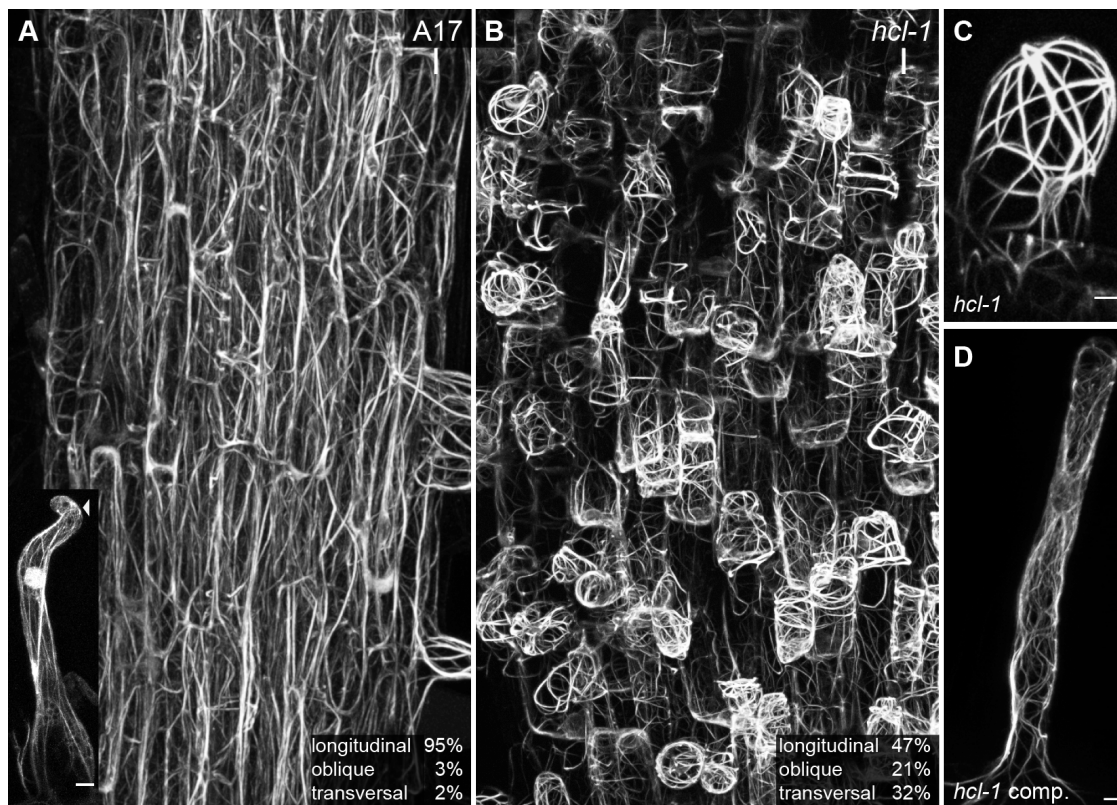


Figure 11 Transgenic roots of *hcl-1* show a strongly altered actin pattern. YFP:Lifect was expressed in wildtype A17 (A), *hcl-1* (B), and *hcl-1 compl.* roots (D) to visualize actin filaments. The orientation of actin strands relative to the root growth axis was scored in root epidermal cells and grouped into longitudinal (0-30°), oblique (30-60°) and transversal (60-90°) classes relative to the cell elongation axis. (A) In A17, YFP:Lifect-labeled filaments run mostly parallel to the cell elongation axis. In root hairs, thick actin bundles in the base and become finer filaments (F-actin) extending towards the tip. There, F-actin becomes randomized into more diffuse signals at the root hair tip (arrowhead points toward globular actin, G-actin), typical for tip growing root hairs. (B) *Hcl-1* actin appears more bundled and changed in its relative orientation. (C) *Hcl-1* root hairs have thick bundles of actin. Finer filaments were not observed (n= 12). (D) In *hcl-1 compl.* the Lifect signal labels filaments that more closely resemble WT root hairs. Scale bars indicate 10 μ m in (A) and (B), 5 μ m in (C) and (D).

To corroborate this observation statistically, the actin orientation was measured by scoring transects of epidermal root cells expressing YFP:Lifect along the initial 1 cm from the root tip (of roots of 3-4 cm length). The overall actin orientation of individual cells in *hcl-1* and A17 (n= 198) was analyzed and categorized into 3 relative orientation classes: longitudinal, in which the average filament orientation was 0°-30° relative to the cell elongation axis, oblique (30°-60° relative to the axis) and transversal (60°-90° relative to the axis).

In A17 roots, the overall relative orientation of the Lifect-labeled actin filaments was classified longitudinal in 95% of the cells (Figure 12A). In *hcl-1*, the actin strands were more diverse: in 47% of the cells, the relative actin orientation classified longitudinal, in 21% they were assigned to the oblique class and 32% of the cells classified transversally (Figure 12B).

This confirmed, that transgenic *hcl-1* roots showed a prominent actin defect, and the abnormal (YFP:) SYMREM1-localization may, therefore, be a consequence of cytoskeletal rearrangements.

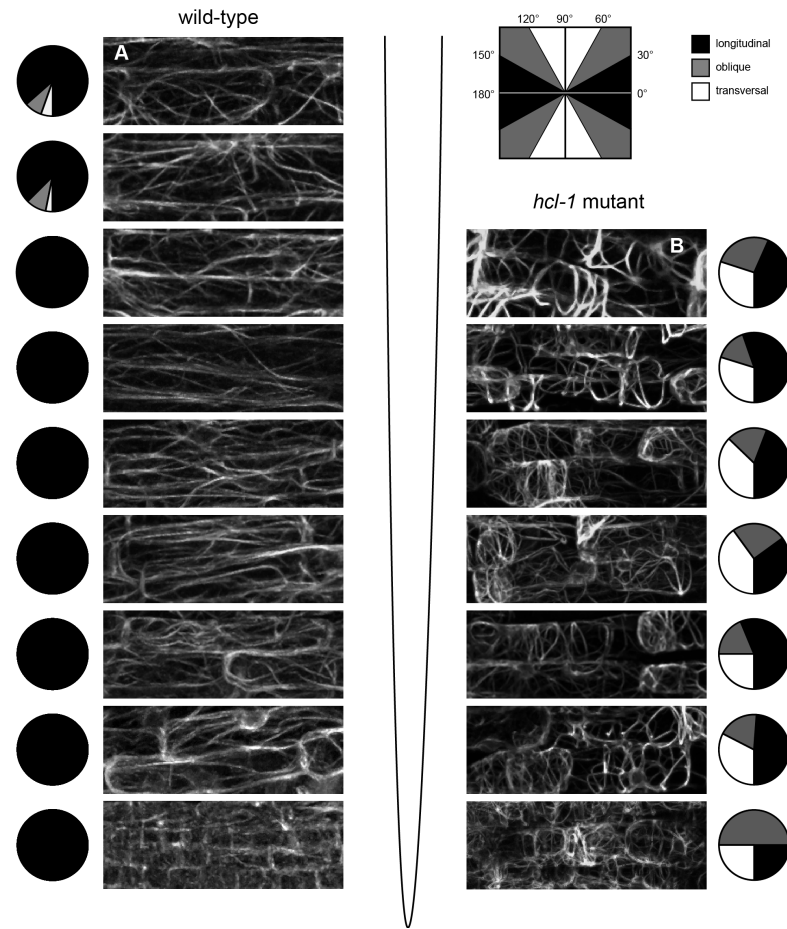


Figure 12 Actin patterns are altered throughout *hcl-1* roots. Expressing the YFP tagged Lifeact peptide in wildtype (A) and *hcl-1* mutant roots (B) revealed an altered actin pattern in the mutant along the lower 1 cm of the root. As in Figure 11, the actin orientation was categorized relative to the root growth axis and average values of each category are displayed as pie charts. Longitudinal, oblique and transversal patterns are represented by black, grey and white coloration, respectively. 198 cells were analyzed in each genotype.

To test this, the co-expression vector that encodes both, mCherry:SYMREM1 and Cerulean:Lifeact was transformed into *M. truncatula hcl-1* roots and imaged with CSLM. In epidermal and cortical cells that were expressing this construct, mCherry:SYMREM1 localized into the same spike-like arrangement as seen with YFP:SYMREM1 in *hcl-1* (Compare Figure 9E and Figure 13B). The abnormal localization, therefore, cannot be attributed to the YFP-fluorophore tag itself. Interestingly, SYMREM1 appeared to align along the actin filaments that were efficiently labeled with Cerulean:Lifeact (Figure 13). This observation was measured and revealed a Pearson correlation coefficient of $R_r = 0.351$ ($SE = 0.095$). Compared to the randomized value of $rd R_r = 0.051$ ($SE = 0.009$; $p = 1.40E^{-11}$; $n = 19$), this confirmed in *hcl-1* the actin cytoskeleton and SYMREM1, do show positive correlation (i.e. co-localized). This, again, supported the notion that SYMREM1 mis-localized due to an altered actin cytoskeleton in this mutant.

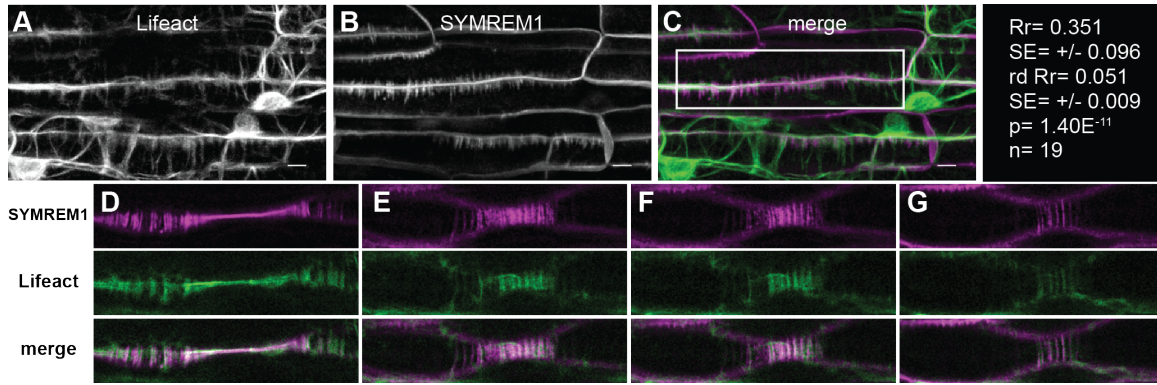


Figure 13 SYMREM1 and Lifeact co-localize in *hcl-1*. The co-expression of Cerulean:Lifeact (A) and mCherry:SYMREM1 (B) in the *hcl-1* mutant resulted in a significant co-localization (C). (A) – (C) Maximum projection of 8 slices taken with 0.5 μ m increments. In the panels (D) – (G) individual slices of the boxed region in (C) are shown to emphasize the occurring mis-localization of mCherry:SYMREM1 and the similarity with Cerulean:Lifeact. Quantitative image analysis revealed a $R_r = 0.351$. Statistics are provided to the right of figure (C). R_r = Pearson correlation coefficient; rd R_r = Pearson correlation coefficient obtained after Costes' randomization was applied to the Cerulean:Lifeact image. The respective standard errors (SE) are provided below the Pearson values. p-value = confidence interval obtained from a Student's t-test comparing R_r and rd R_r . Scale bars indicate 5 μ m.

3.5 SYMREM1 Localization is Dependent on FLOT4 in the Homologous *Medicago truncatula* Root System

3.5.1 SYMREM1 and FLOT4 Co-localize in *Medicago truncatula*

Another root nodule symbiosis related protein, FLOT4, localizes in an unusual manner in *hcl-1* (Haney and Long, 2010; Haney et al., 2011). A 50% decrease in FLOT4:GFP puncta (MDs) density was specifically measured in root hair cells of only the *hcl-1* background and not for the other mutant lines tested (*hcl-2*, *nfp1-2*, *dmi2-4* and the wildtype-like *hcl-1 compl.* line). Therefore, the question arose whether FLOT4, like SYMREM1, also incorrectly localizes, not only in root hair cells but also in root epidermal and outer cortical cells of *hcl-1*.

In transgenic *hcl-1 compl.* roots, FLOT4:mCherry labeled specific MDs in root epidermal cells, as well as root hairs (Figure 14A, B, C). However, when this construct was expressed in *hcl-1*, FLOT4:mCherry also labeled MDs in spike-like arrangements (Figure 14E) in addition to punctate MDs (Figure 14D, E). This pattern strongly resembled SYMREM1 and the actin cytoskeleton in *hcl-1*, providing evidence of a possible link between FLOT4 and SYMREM1 in the homologous system (Figure 13).

To test this more thoroughly, a Level 3 co-expression vector was cloned, which allowed FLOT4:mCherry and YFP:SYMREM1 to be simultaneously expressed under the control of polyubiquitin promoters. Indeed, in transgenic *hcl-1* roots, both fusion proteins followed very

similar transversal spike-like patterns (Figure 14F, G, H), similar to YFP:SYMREM1 alone (see Figure 9E). These proteins may, therefore, label the same MDs in the PM.

This tandem YFP:SYMREM1/FLOT4:mCherry construct was then transformed and co-expressed in in the *hcl-1 compl.* background. As described above, this line has elongated root hairs and behaves like wildtype plants when inoculated with rhizobia (Figure 10) (Haney et al., 2011). Therefore, a regular wildtype-like localization of both proteins was expected.

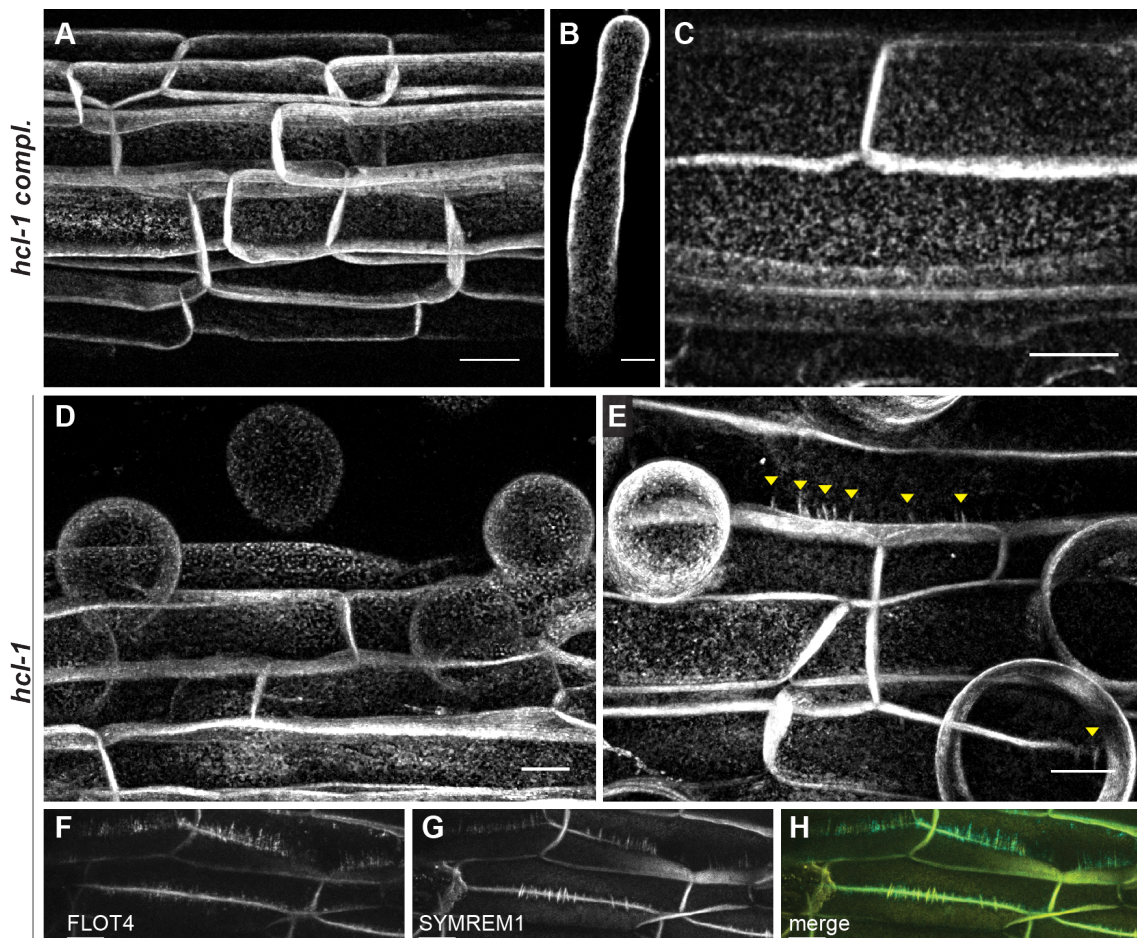


Figure 14 FLOT4 localization in transgenic *Medicago truncatula* root cells. *Medicago hcl-1 compl.* and *hcl-1* root cells transformed with a FLOT4:mCherry overexpression, or a FLOT4:mCherry + YFP:SYMREM1 co-overexpression construct. FLOT4:mcherry localized into distinct puncta in the plasma membrane of cortical and epidermal cells in the *hcl-1 compl.* line (A) - (C). In *hcl-1*, FLOT4:mCherry forms puncta in root hair cells, epidermal and cortical cell layers (D). In addition, only in the *hcl-1* mutant, the FLOT4:mCherry protein mis-localized in spikes-like structures, shown by green arrows in (E). (G) The co-expression of FLOT4:mCherry (F) and YFP:SYMREM1 as a tandem construct from the same T-DNA in *hcl-1* roots revealed that both proteins followed the altered actin pattern described in Figure 13. Scale bars indicate 10 μ m.

In these roots, YFP:SYMREM1 and FLOT4:mCherry each localized into MDs in root cells of the epidermis and outer cortex (Figure 15A, B). Indeed, the signal of the fusion proteins overlapped (Figure 15D, E, F). This observation was quantified as described before. The highly positive Pearson correlation coefficient of $Rr = 0.344$ ($SE = 0.027$; $n = 16$), differed significantly to the randomized value $rd Rr = 0.043$ ($SE = 0.008$; $p = 5.78E^{-09}$, $n = 16$). Even though the co-localization

Results

is not perfect, these data demonstrate that YFP:SYMREM1 and FLOT4:mCherry co-localize to a high degree and can occur in spatially the same MDs. As the number of YFP:SYMREM1-labeled MDs qualitatively seemed to be elevated in the presence of the FLOT4:mCherry overexpression construct (compare Figure 9A, F to Figure 15A), the SYMREM1-labeled MD density was also quantified in these cells.

An almost 5-fold increase in YFP:SYMREM1-labeled MDs ($0.395 \text{ domains}/\mu\text{m}^2$; SE= 0.0581) was measured, in comparison to the *hcl-1 compl.* line that was expressing YFP:SYMREM1 alone (see next chapter; $0.077 \text{ domains}/\mu\text{m}^2$; SE= 0.0099; n= 23). A 7-fold increase was measured in comparison to the SYMREM1-labeled MD-density in A17 (Figure 6A; $0.057 \text{ domains}/\mu\text{m}^2$; SE= 0.0051). This indicated that FLOT4 could be a decisive factor for the recruitment and localization of SYMREM1 into distinct MDs.

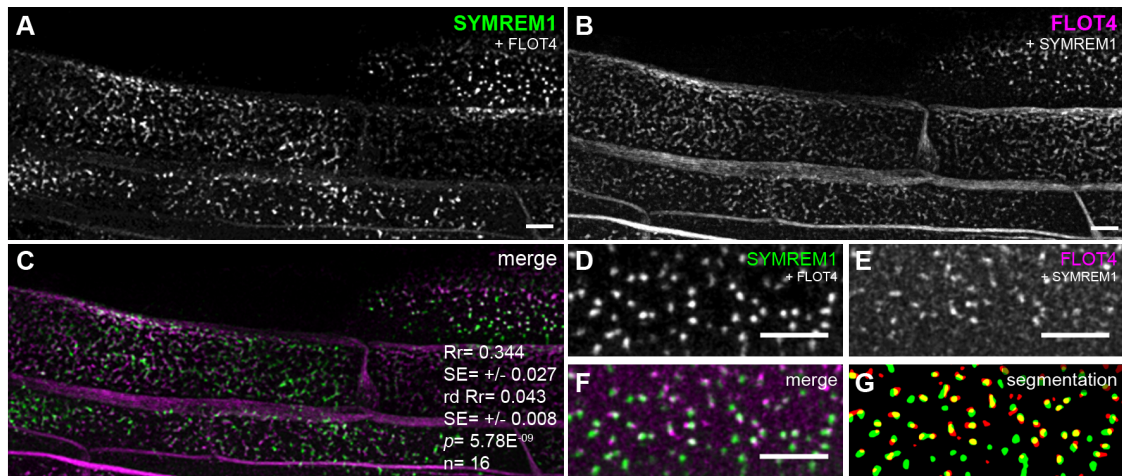


Figure 15 FLOT4 is an essential building block of SYMREM1-labelled microdomains. (A) YFP:SYMREM1 and (B) FLOT4:mCherry co-localize (C) in transgenic *Medicago truncatula* root epidermal cells when expressed simultaneously in the *hcl-1 compl.* background. Quantitative co-localization data are provided in panel C. Rr= Pearson correlation coefficient; rd Rr= Pearson correlation coefficient obtained after image randomization of the Cerulean:Lifeact image. The respective standard errors (SE) are provided below the Pearson values. p= confidence interval obtained from a Student's t-test comparing Rr and rd Rr. (D) Close-up of YFP:SYMREM1- and (E) FLOT4:Cherry-labeled MDs at the plasma membrane surface. (F) A merged image of both channels and (G) a segmented image better illustrate co-localization between the two proteins. Scale bars indicate 5 μm .

3.5.2 SYMREM1 and FLOT4 Promoters are Active at the Same Time

The increase in SYMREM1-labeled MDs in the presence of an FLOT4 overexpression construct indicates that FLOT4 may be a prerequisite for the localization into MDs. Even though *FLOT4* is strongly induced by the inoculation with *Sinorhizobium meliloti*, it is still constitutively expressed in *M. truncatula* roots (Haney and Long, 2010) and, thus FLOT4 is always present at the PM.

The symbiotic RLK LYK3 is actively recruited into FLOT4-labeled MDs, and this process coincides timely with the induction of *SYMREM1* expression upon contact with *S. meliloti* (Lefebvre et al., 2010; Haney et al., 2011). *SYMREM1* is activated, at the latest, 4 days post inoculation and most highly in nodules: however, direct Nod factor application leads to an even faster gene induction even within a few hours (Lefebvre et al., 2010).

To confirm that the *SYMREM1* promoter is active, not just in a required timely manner but also spatially in the epidermis, the place of activity for the *FLOT4* and *LYK3* promoters, two reporter constructs were created to analyze *SYMREM1* and *FLOT4* promoter activity. For the *SYMREM1* native promoter, the 643 base pairs preceding the *SYMREM1* gene were chosen. For the *FLOT4* promoter, the published 2-kilobase fragment directly upstream of the *FLOT4* gene was cloned (Haney and Long, 2010). As reporters, a nuclear localization signal was linked C-terminally with a double GFP encoding sequence (NLS-2xGFP) and fused to the promoters. Both constructs additionally carried a constitutively expressed pNOS::NEOMYCIN-PHOSPHOTRANSFERASE II (NEO_R) sequence on the T-DNA cassette, which conferred resistance of transgenic roots to kanamycin.

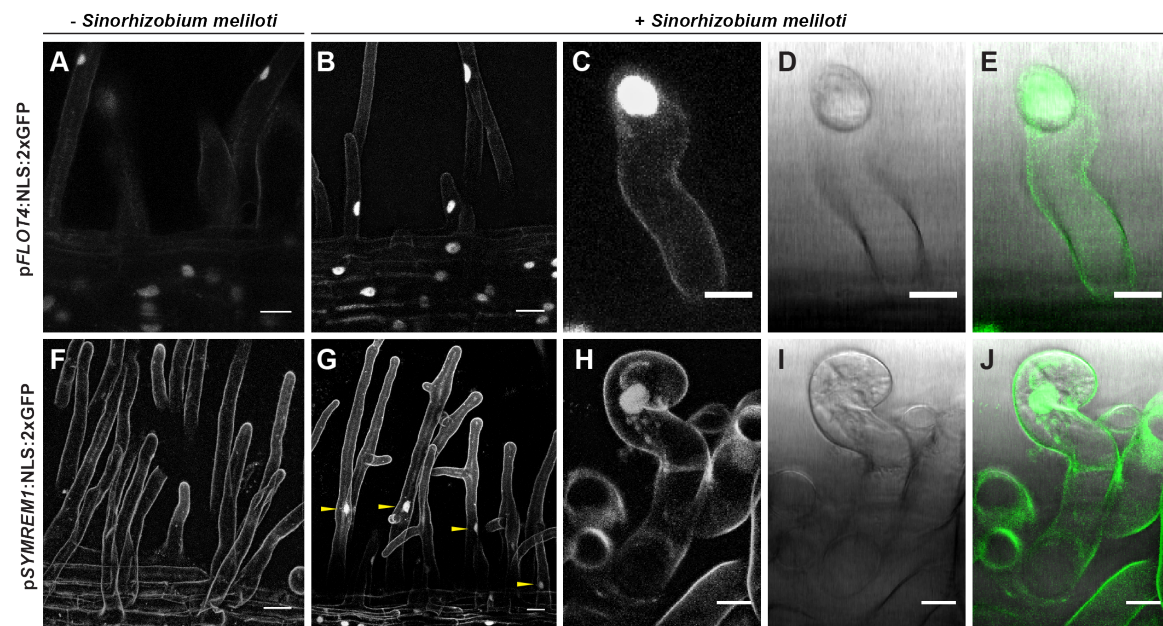


Figure 16 The *SYMREM1* and *FLOT4* promoters are active in the epidermis. Transgenic *Medicago truncatula* A17 roots, transformed with native promoter reporter constructs. *pFLOT4::NLS:2xGFP* (A) – (E) and *pSYMREM1::NLS:2xGFP* (F) – (J) constructs were grown under selective conditions to reduce the growth of non-transgenic roots. 4 weeks post transformation, the roots were spot-inoculated with *Sinorhizobium meliloti* and the promoter activity was analyzed 4 days post inoculation. (A) The *FLOT4* promoter is constitutively active under non-symbiotic conditions, and is strongly up regulated 4 dpi (B), shown by a strong increase in GFP fluorescence in the nuclei. (C) – (E) In root hairs that show typical root hair curling fluorescent nuclei were clearly visible. (F) The *pSYMREM1::NLS:2xGFP* construct is inactive in non-inoculated roots, as expected, and induced, however to a lower degree than the *FLOT4* promoter, in roots treated with *S. meliloti* (G). GFP accumulated in the nuclei of root hair cells that curled upon inoculation (H) – (J). Scale bars indicate 50 μ m in (A, B) and (F, G) and 20 μ m in (C-E) and (H-J).

Results

Medicago A17 transgenic roots were produced via *Agrobacterium rhizogenes* mediated transformation, grown under selective conditions and inoculated with *Sinorhizobium meliloti*. Activity of the promoter-reporter constructs was analyzed 4 days post inoculation.

As expected, the *FLOT4* promoter was active even under non-symbiotic conditions, which was visible by the moderate accumulation of GFP fluorescence in the nuclei of epidermal root hair cells (Figure 16A). Upon inoculation, the GFP fluorescence increased markedly, indicating increased promoter activity (Figure 16B-E), which is in line with published data (Haney and Long, 2010). The *SYMREM1* promoter was inactive in non-symbiotic conditions, evident by the lack of reporter construct expression in transgenic roots (Figure 16). After rhizobial inoculation, root hair deformations were visible and nuclear-localized GFP was detectable (Figure 16G). The signal intensity, however, was much lower than reporter construct expressed under *pFLOT4*. Therefore, the microscope settings had to be adjusted, accordingly. The stronger, auto-fluorescent background signal detected in these roots was a result of these adjustments (compare Figure 16A with F). Interestingly, 4 dpi, individual root hair cells, which had formed the typical curl for the entrapment of rhizobia, clearly accumulated GFP in the nuclei (Figure 16H, I, J). These data confirmed the *SYMREM1* and *FLOT4* promoters are active, not only in a fitting timely manner, but also spatially in the epidermis.

3.5.3 SYMREM1 Microdomains are Reduced upon RNAi of *FLOT4*

The increased SYMREM1-labeled MD-density in the presence of a *FLOT4* overexpression construct indicates that *FLOT4* is, indeed, necessary for SYMREM1's ability to localize into MDs.

A *FLOT4* RNA interference (RNAi) construct was used to further test this possibility genetically in the homologous *M. truncatula* system.

The *FLOT4*:RNAi construct chosen targeted 100 base pairs of the 3' UTR from the *FLOT4* transcript and has been shown to efficiently silence *FLOT4* in *Medicago* roots (Haney and Long, 2010). Therefore, the identical sequence was cloned into a Golden Gate Level 3 silencing vector that additionally encodes for pUbi::YFP:SYMREM1 and was transformed into *M. truncatula*.

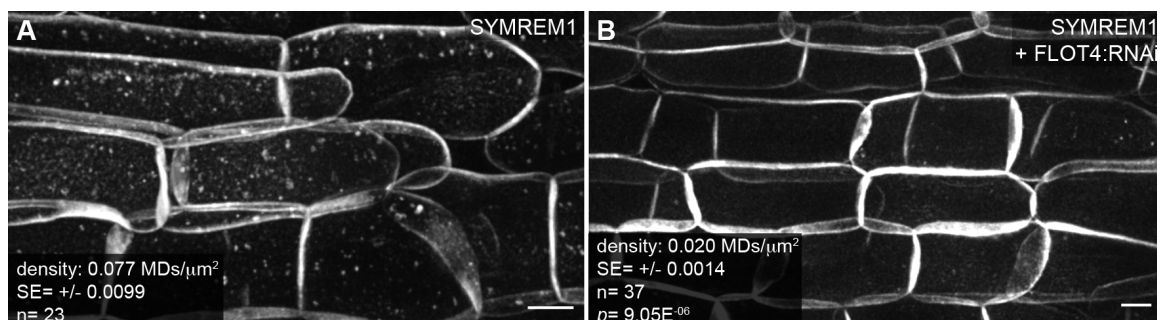


Figure 17 Microdomain-labeling by SYMREM1 is FLOT4-dependent. YFP:SYMREM1 labels MDs in transformed *Medicago truncatula hcl-1 compl.* root epidermal cells (**A**); their density was greatly reduced upon co-expression with the FLOT4:RNAi construct (**B**). p-value= confidence interval obtained from a Student's t-test comparing roots expressing endogenous *FLOT4* (as in A) and those where *FLOT4* was silenced (as in B). Scale bars indicate 10 μm .

First, YFP:SYMREM1 was expressed alone in the *hcl-1 compl.* line. In this situation, YFP:SYMREM1 clearly labeled MDs that appeared in a frequency of 0.077 domains/ μm^2 (SE= 0.0099; n= 23; Figure 17A).

If FLOT4 truly plays a role in SYMREM1's ability to label MDs, then the co-expression of the FLOT4:RNAi construct with YFP:SYMREM1 should lead to a reduction of SYMREM1-labeled MDs. Indeed, significantly fewer MDs were found in roots co-expressing the FLOT4 silencing construct (0.02 domains/ μm^2 , SE= 0.0014; p= 9.05E⁻⁰⁶; n= 37). Importantly, YFP:SYMREM1 still clearly located at the PM, which was indicated by the peripheral localization of the protein and complete absence of any detectable cytosolic signal (Figure 17B).

This supported the assumption that FLOT4 plays an important role in the accumulation of SYMREM1 into distinct MDs, and FLOT4 is not needed for SYMREM1 localization to the PM *per se*.

3.6 Artificial Assembly of a Root- and Symbiosis- Specific Microdomain

SYMREM1, FLOT4 and LYK3 all share some features: They are exclusively expressed in legume roots and/or nodules, the place where rhizobia infect the plant; and they are all PM-resident proteins that occur in MDs. (Haney and Long, 2010; Lefebvre et al., 2010; Haney et al., 2011; Tóth et al., 2012; Moling et al., 2014). SYMREM1 interacts with LYK3 (Lefebvre et al., 2010), and FLOT4 co-localizes with LYK3 in a Nod factor dependent manner, but only after rhizobial inoculation (Haney et al., 2011). SYMREM1 and FLOT4 co-localize in MDs in *Medicago truncatula* A17 transgenic roots (and in spike-like patterns in *hcl-1*). Additionally, SYMREM1's localization in MDs appears to be dependent on FLOT4, as the experiment silencing *FLOT4* demonstrated.

If these MDs do serve as so-called hubs for specific signaling pathways, it could be that all three components, SYMREM1, FLOT4 and LYK3 may be targeted to the same symbiosis-related microdomain (symMD). Therefore, we tested, whether consecutive addition of each of these proteins was sufficient to artificially reconstitute such a MD in the heterologous *Nicotiana benthamiana* leaf expression system.

3.6.1 FLOT4 induces SYMREM1 Compartmentalization in *Nicotiana benthamiana*

A striking difference between the homologous *Medicago* roots, where SYMREM1 forms MDs and the heterologous *Nicotiana* system was observed. The transformation of *Nicotiana* leaves with YFP:SYMREM1 in the presence of the silencing suppressor P19 (Koncz et al., 1989; Voinnet et al., 2003) did not lead to the formation of YFP:SYMREM1-labeled MDs. Instead, the protein usually attached to the PM uniformly. The YFP:SYMREM1 signal was only absent from defined tracks and round spots (Figure 18A). These signal-negative tracks were hypothesized to represent microtubules; and co-expressing a mCherry:MAP4 fusion construct with YFP:SYMREM1 showed microtubules clearly localized into these tracks (Figure 19).

The PM was labeled slightly more distinctly by the expression of FLOT4:mCherry alone (Figure 18B). LYK3:GFP alone appeared less homogeneously distributed in the PM. However, no clear MDs were visible (Figure 18C) in the single expression conditions. There were, as was the case for YFP:SYMREM1, also defined spots and lines visible in which these two proteins did not locate.

As in *Medicago* (Figure 6B), microtubules may act only as a more broad, or general organizer at the PM and are not the driving force for SYMREM1 localization. Curiously, *Nicotiana* leaf epidermal cells lack a, or possibly several, components for the specific accumulation of YFP:SYMREM1 into MDs.

The simultaneous expression of the tandem YFP:SYMREM1 and FLOT4:mCherry construct from the same Level 3 expression vector changed the localization of both proteins in *N. benthamiana*. Although the FLOT4:mCherry protein now appeared to be more compartmentalized in the PM, the basic pattern remained similar to that observed in leaf epidermal cells expressing only FLOT4; and the fusion protein still labeled the PM except for black spots and tracks (compare Figure 18E with B).

YFP:SYMREM1, however, accumulated in specific highly-compartmentalized areas in the PM; the tracks and spots that previously were absent of YFP:SYMREM1 now were signal positive (compare Figure 18D with A). A merged image of both channels emphasized the unexpected compartmentalization that occurred when these proteins were co-expressed; and the signals excluded each other (Figure 18F).

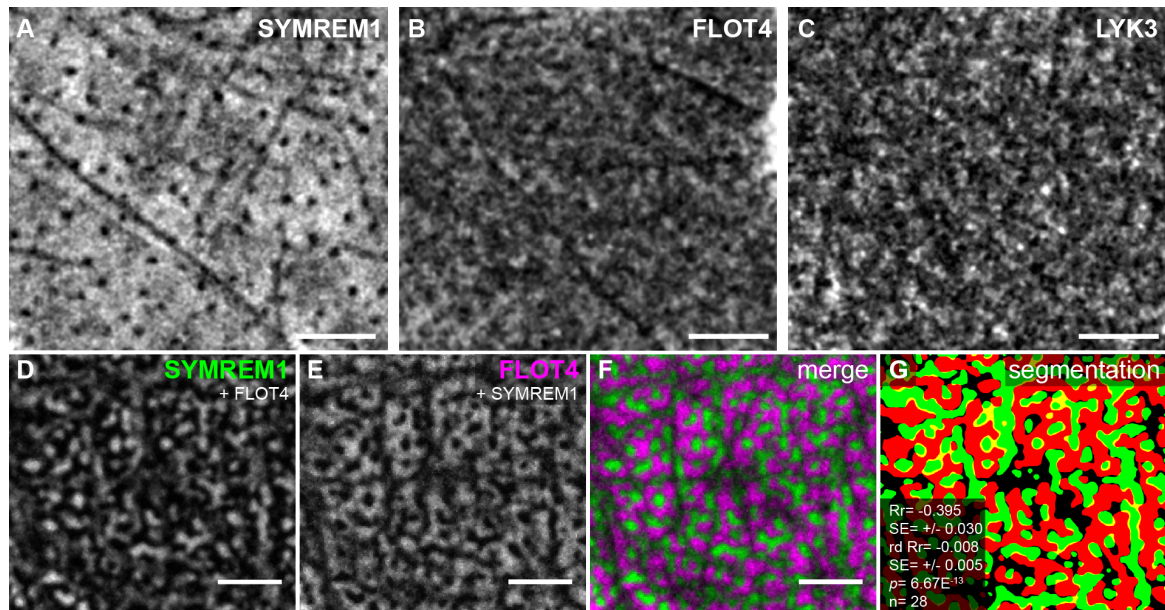
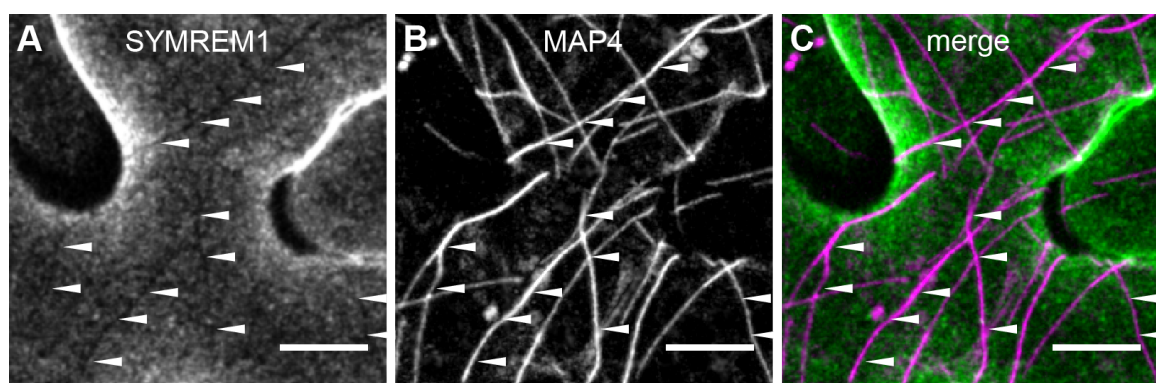


Figure 18 SYMREM1 and FLOT4 exclude each other locally in *Nicotiana benthamiana*. *Nicotiana* leaf epidermal cells individually expressing the legume-specific proteins YFP:SYMREM1, FLOT4:mCherry, or LYK3:GFP reveal almost no MDs being labeled. (A) SYMREM1 is not compartmentalized. FLOT4 (B) and LYK3 (C) show a low degree of protein compartmentalization. The co-expression of YFP:SYMREM1 and FLOT4:mCherry induced strong compartmentalization of SYMREM1 (D) and also of FLOT4 (E). Overlaying the signals from both channels (F) and image segmentation (G) not only revealed a lack of co-localization, but even more so, strong exclusion of both proteins. The respective standard errors (SE) are provided below the Pearson values. $p =$ confidence interval obtained from a Student's t-test comparing Rr and rd Rr. Scale bars indicate 5 μm .

This observation was substantiated by quantitative data based on pixel-based correlation analysis. Although both proteins remained in close vicinity, they clearly failed to co-localize, as shown by a strongly negative Pearson correlation coefficient of $Rr = -0.395$ ($SE = 0.030$; $rd Rr = -0.008$; $rd SE = 0.005$; $p = 6.67E^{-13}$; $n = 28$). Both channels were segmented into binary masks, which emphasized the observed effect (YFP:SYMREM1 is depicted in green and FLOT4:mCherry in red (Figure 18G)).

This pattern contrasts strongly with the localization observed in the homologous *Medicago* root system, in which both proteins occurred in distinct MDs and co-localized to a great degree ($Rr = 0.344$; compare Figure 15A-G with Figure 18D-G).



Results

Figure 19 Microtubules tracks exclude SYMREM1. In *Nicotiana benthamiana*, the co-expression of YFP:SYMREM1 and mCherry:MAP4 revealed SYMREM1 attached to the plasma membrane homogenously, except for signal negative tracks (examples marked with white arrowheads **(A)**). MCherry:MAP4 labeled microtubules efficiently **(B)** and these microtubules coincide with the places where SYMREM1 was not present **(C)**. Arrowheads mark the same coordinates in all three images. Scale bars indicate 10 μ m.

In order to determine whether the observed compartmentalization of YFP:SYMREM1 in *Nicotiana* is the specific consequence of the presence of FLOT4, several control experiments were performed. First, YFP:SYMREM1 was co-expressed with either a pUBI::FLOT4:HA or a p35s::LYK3:HA construct. No change in SYMREM1's localization was seen in cells co-transformed with LYK3:HA (Figure 20B) in comparison to cells expressing YFP:SYMREM1 alone (Figure 20A). In leaves co-transformed with the FLOT4:HA, the YFP:SYMREM1 signal was comparably compartmentalized as observed for YFP:SYMREM1 and FLOT4:mCherry (compare Figure 15D, E, F with Figure 20C). Immunological detection of the HA epitope tag confirmed the p35s::LYK3:HA and pUbi::FLOT4:HA constructs to be functional (Figure 20). This indicates that FLOT4 (and not LYK3) is the driving force for SYMREM1 to compartmentalize.

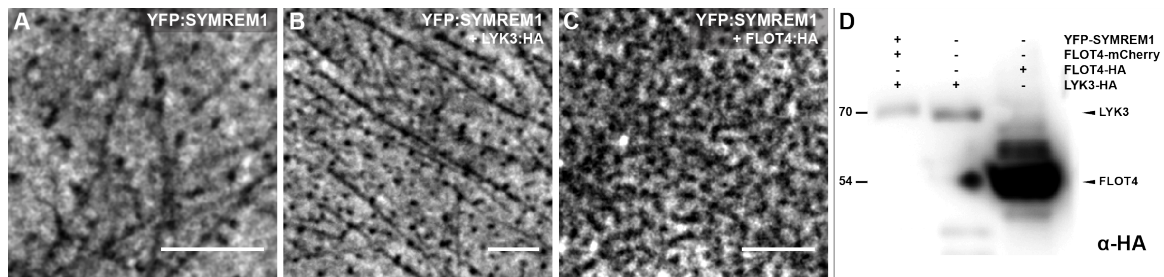


Figure 20 YFP:SYMREM1 is compartmentalized by FLOT4 and not by LYK3. Transient expression of constructs in leaf epidermal cells of *Nicotiana benthamiana*. **(A)** YFP:SYMREM1 alone labels the PM uniformly. **(B)** The co-expression of a LYK3:HA construct had no effect on YFP:SYMREM1 compartmentalization in the PM. **(C)** When FLOT4:HA is co-expressed with YFP:SYMREM1, SYMREM1 is compartmentalized. Total protein extract of transformed *Nicotiana* leaves. Immunological detection with α -HA antibody to target the hemagglutinin epitope fused to LYK3 and FLOT4. LYK3:HA and FLOT4:HA are detected in lanes 2 and 3. In lane 1, LYK3:HA is detected from the experiment described in Figure 24. Scale bars indicate 5 μ m.

In line with this, the induced compartmentalization of YFP:SYMREM1 in *Nicotiana* was revertible upon the additional expression of a FLOT4:RNAi construct without the silencing suppressor P19. Because the FLOT4:mCherry construct used did not encode for any 3'UTR sequence, a new silencing construct was cloned to facilitate silencing in *Nicotiana*. The last 114 base pairs of the *FLOT4* gene, immediately upstream of the 3'UTR, were additionally added to the 5' end of the RNAi construct used in *M. truncatula*. This new FLOT4:RNAi construct was then co-expressed with YFP:SYMREM1.

First, the co-expression of YFP:SYMREM1 and FLOT4:mCherry without P19 led to, as previously seen, to a strong compartmentalization of the SYMREM1 and FLOT4 signals (Figure

21A, B). When the silencing construct was co-transformed on the same vector backbone, no FLOT4:mCherry fluorescence was detectable with the identical microscope settings. This confirmed the functionality of the silencing construct (Figure 21E). In these cells, YFP:SYMREM1 again labeled the PM homogenously, except for the signal negative spots and tracks, as seen before (compare Figure 21D to A).

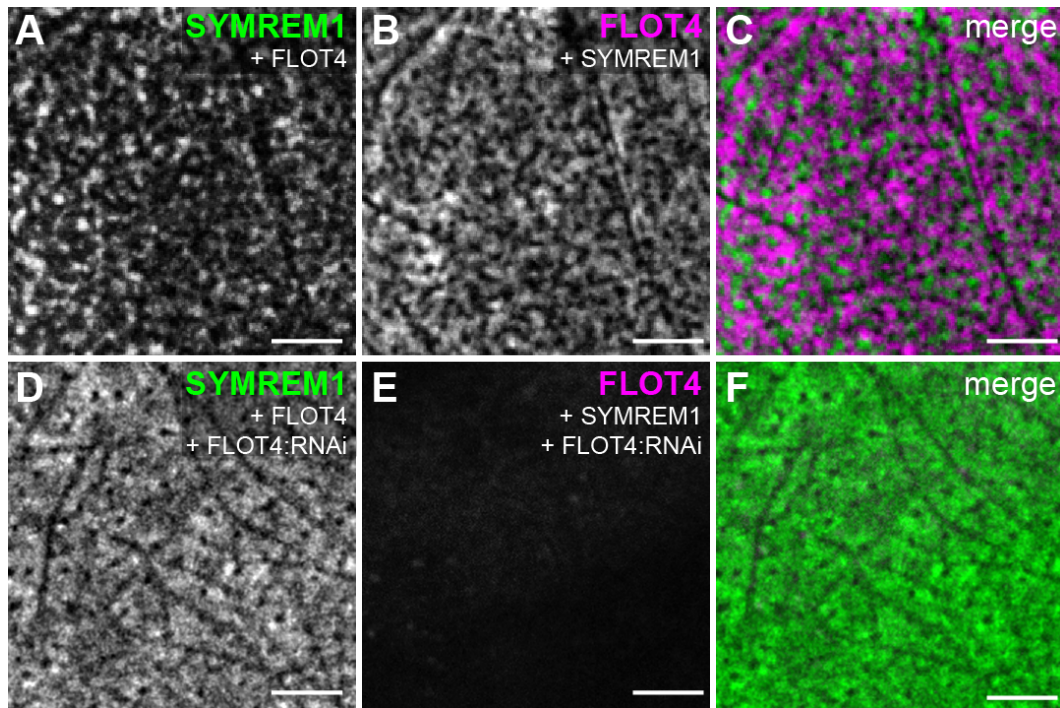


Figure 21 Compartmentalization of SYMREM1 in leaf epidermal cells is FLOT4 dependent. The co-expression of YFP:SYMREM1 (A) and FLOT4:mCherry (B) in *Nicotiana benthamiana* without the silencing suppressor P19 in leaf epidermal cells results in compartmentalization of both proteins, although they do not co-localize (C). Additional expression of the FLOT4:RNAi construct results in a loss of FLOT4:mCherry fluorescence (E) and reverted the localization of YFP:SYMREM1 back to a more homogenous distribution (D). The silencing experiment was reproduced in 3 different plants with the identical result. Scale bars indicate 5 μ m.

This indicated that FLOT4:mCherry is a major facilitator of YFP:SYMREM1 compartmentalization in *Nicotiana* and corroborates the observations made in the homologous *Medicago* system (see Figure 17). To further rule out that this exclusion was not the result of unexpected behavior of overexpressing two fluorophores in *Nicotiana* leaves, the following experiments were performed.

YFP:SYMREM1 was co-expressed with mCherry:SYMREM1, a combination in which neither of the SYMREM1 fusion proteins was expected to compartmentalize if the fluorophores were irrelevant for compartmentalization; they are identical proteins, simply attached to two different fluorophores. As expected, they did not compartmentalize and even strongly co-localized. Quantitative measurements resulted in a highly positive Pearson correlation coefficient value of $R_r = 0.820$ (SE=0.017; rd $R_r = 0.120$; rd SE= 0.064; $p = 4.16E^{-09}$; $n = 17$; Figure 22E, F). A value

Results

this high is in the typical range of identical proteins that are fused to two different fluorophores and co-expressed in biological samples (Spira et al., 2012; Jarsch et al., 2014). YFP:SYMREM1 and mCherry:SYMREM1 co-localize in the PM of the cells analyzed, and, therefore, the fluorophores have no immediate effect on SYMREM1 and FLOT4 localization behavior.

To substantiate that FLOT4 induces the strong compartmentalization of SYMREM1 specifically, FLOT4:mCherry was also co-expressed with FLOT2:GFP. *FLOT2* is strongly up-regulated upon rhizobial inoculation and the FLOT2, like FLOT4, also located into MDs in *Medicago*. The silencing of *FLOT2* transcripts via RNAi led to fewer total nodules formed, and less infection threads (ITs) were initiated (but those that are initiated progress normally). This is a striking difference to *FLOT4*-silenced roots, where ITs continuously abort prematurely (Haney and Long, 2010).

FLOT2:GFP alone labeled the PM mostly uniformly in *Nicotiana* (Figure 22C), similar to FLOT4:mCherry (Figure 18B; Figure 21B; Figure 22B). When both proteins were expressed in the cell simultaneously, no obvious compartmentalization was observed (Figure 22H, I). The signals of both channels overlapped strongly with a highly positive $R_r = 0.552$ ($SE = 0.033$; rd $R_r = 0.136$; rd $SE = 0.027$; $p = 1.06E^{-09}$; $n = 19$; Figure 22J). The lack of any visible change in the localization of FLOT2:GFP in this combination emphasized the specific role FLOT4 plays in causing SYMREM1 to compartmentalize in *Nicotiana*.

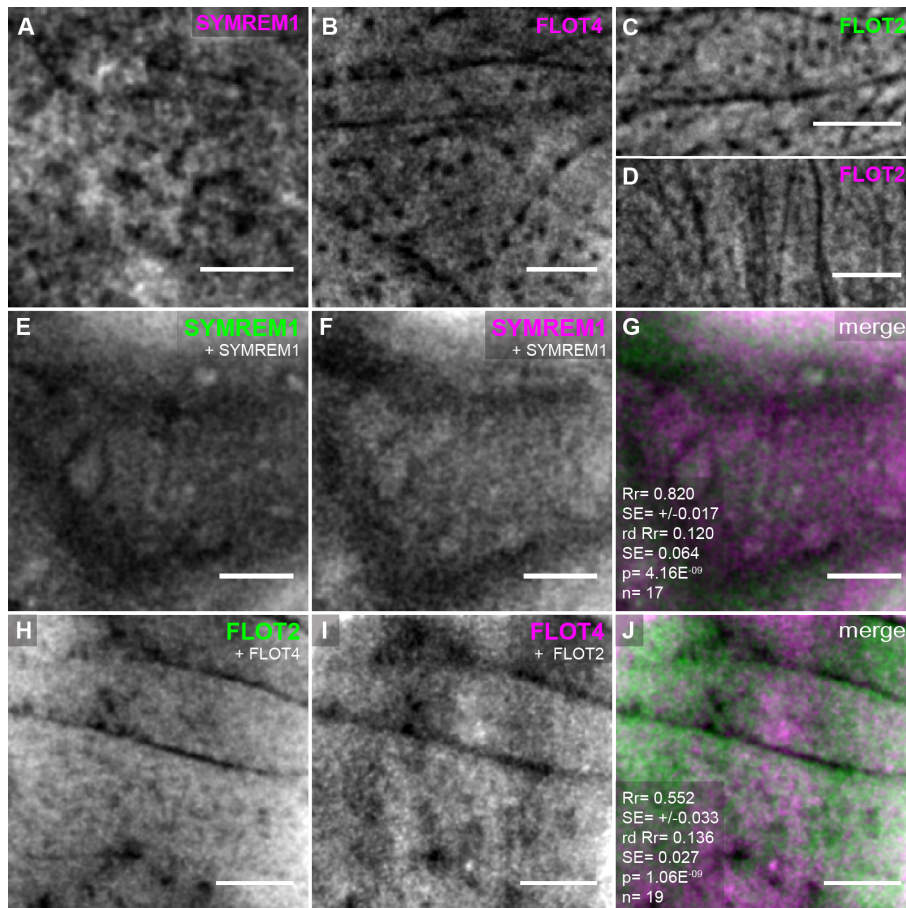


Figure 22 Controls for FLOT4-mCherry induced compartmentalization in *Nicotiana benthamiana*. (A) MCherry:SYMREM1 labeled the plasma membrane smoothly except for dark puncta and tracks. (B) FLOT4:mCherry labeled the PM mostly homogenously. (C) FLOT2:GFP and (D) FLOT2:mCherry also labeled the PM uniformly. (E) – (G) The co-expression of YFP:SYMREM1 (E) with mCherry:SYMREM1 (F) resulted in no noticeable compartmentalization, but high co-localization. (H) – (J) The simultaneous expression of FLOT2:GFP (H) with FLOT4:mCherry (I) also gave no indication of compartmentalization of either protein, and revealed high co-localization. Quantitative data are provided in panels G and J. R_r = Pearson correlation coefficient; $rd R_r$ = Pearson correlation coefficient obtained after image randomization. The respective standard errors (SE) are provided below the Pearson values. p = confidence interval obtained from a Student's t-test comparing R_r and $rd R_r$. Scale bars indicate 5 μ m.

Next, it was tested if a non-symbiotic flotillin also influences SYMREM1 compartmentalization in *Nicotiana*. The *Arabidopsis thaliana* flotillin protein FLOT1a is involved in seedling development by functioning in a clathrin-independent endocytosis pathway. It also is a protein that localizes in MDs, although not exclusively in the PM (Li et al., 2012). Therefore, a p35s::FLOT1a:YFP construct was infiltrated alone, or co-infiltrated with pUbi::mCherry:SYMREM1, into *Nicotiana*.

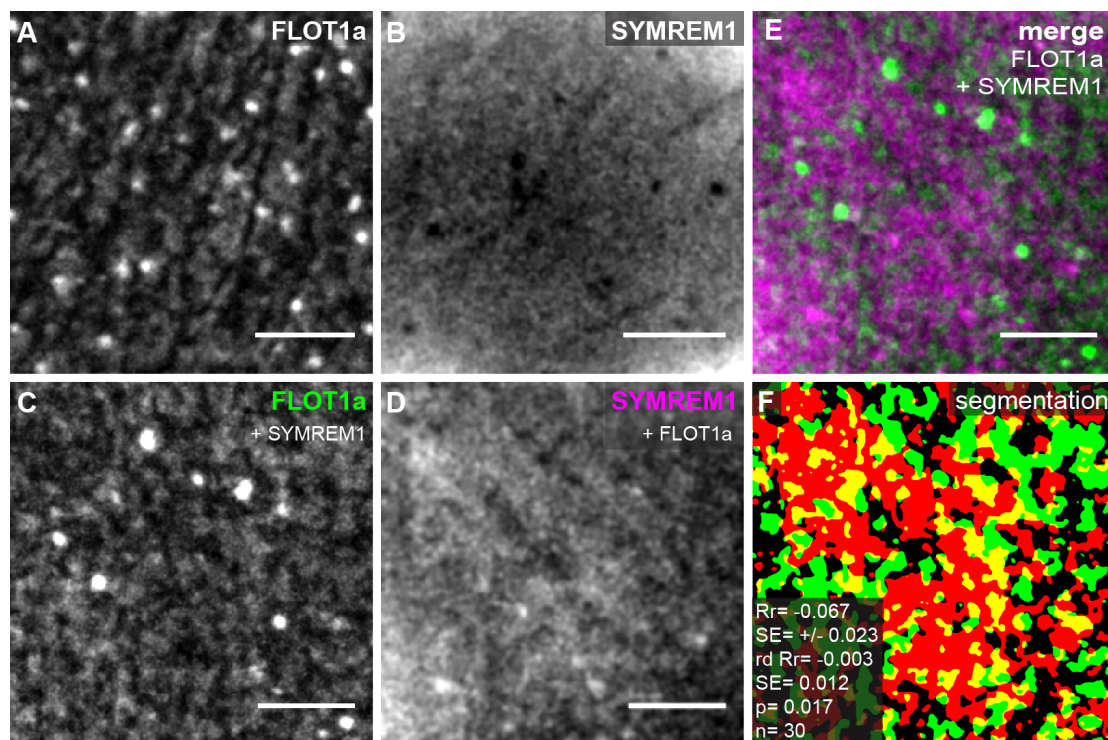


Figure 23 *Arabidopsis thaliana* Flotillin1a does not induce SYMREM1-compartmentalization in *Nicotiana benthamiana*. (A) FLOT1a:YFP forms clear MDs in the PMs of *Nicotiana* leaf epidermal cells. (B) MCherry:SYMREM1 distributes homogeneously. The co-expression of FLOT1a:YFP (C) with mCherry:SYMREM1 (D) results in an almost unchanged localization for both proteins. (E) The merged picture of both channels indicates random distribution of both signals to each other. (F) Image segmentation demonstrates almost random behavior and pixel based correlation analysis results in a R_r = -0.067. Quantitative data is provided in panel (F). R_r = Pearson correlation coefficient; $rd R_r$ = Pearson correlation coefficient obtained after image randomization. The respective standard errors (SE) are provided below the Pearson values. p = confidence interval obtained from a Student's t-test comparing R_r and $rd R_r$. Scale bars indicate 5 μ m.

Results

Already by itself, FLOT1a:YFP formed distinct MDs; mCherry:SYMREM1 attached to the PM homogeneously, as expected (Figure 23A, B). In cells that were co-expressing these two proteins, no obvious change in the localization of FLOT1a:YFP was visible (Figure 23C). MCherry:SYMREM1 showed a slight change in localization, where a few spots occurred in the PM (Figure 23D).

However, this change is less drastic than the one observed for SYMREM1 in the FLOT4/SYMREM1 co-expression situation. The mildly negative Pearson correlation coefficient and the randomization procedures support this ($R_r = -0.067$; $SE = 0.023$; $n = 30$; $rd R_r = -0.003$; $SE = 0.012$; $p = 0.017$). This value lies close to 0, and, therefore, indicates randomness between the two signals. These data confirm the unique effect the FLOT4 protein had on SYMREM1's compartmentalization in the PM.

3.6.2 LYK3 is Required for SYMREM1 and FLOT4 Localization Into Microdomains in *Nicotiana benthamiana*

When SYMREM1 is constitutively overexpressed in *hcl-1*, it mis-localizes in spike-like patterns (Figure 9, Figure 13). Also, FLOT4 displays mis-localization (Figure 14) and a reduced number of MDs in the *hcl-1* allele (Haney et al., 2011). Therefore, LYK3 might also play a role in SYMREM1's ability to form symbiotic MDs.

A Level 3 expression vector was created, in which pUbi::YFP:SYMREM1, pUbi::FLOT4:mCherry and LYK3 fused to the hemagglutinin tag (p35s::LYK3:HA) were encoded as a triple-tandem construct on a single T-DNA cassette. This vector was infiltrated into *N. benthamiana*. When all three proteins were co-expressed simultaneously, distinct YFP:SYMREM1- (Figure 24A) and FLOT4:mCherry-labeled MDs appeared (Figure 24B).

Quantitative image analysis showed that a strong co-localization occurred between these MDs ($R_r = 0.40$, $SE = 0.051$, $rd R_r = 0.017$, $rd SE = 0.017$; $p = 3.03E^{-06}$; $n = 17$; Figure 24C, D), supporting the possibility of the labeled MDs being identical. Western Blot analysis confirmed that the protein LYK3:HA was expressed in the samples analyzed (Western Blot lane 1, Figure 20).

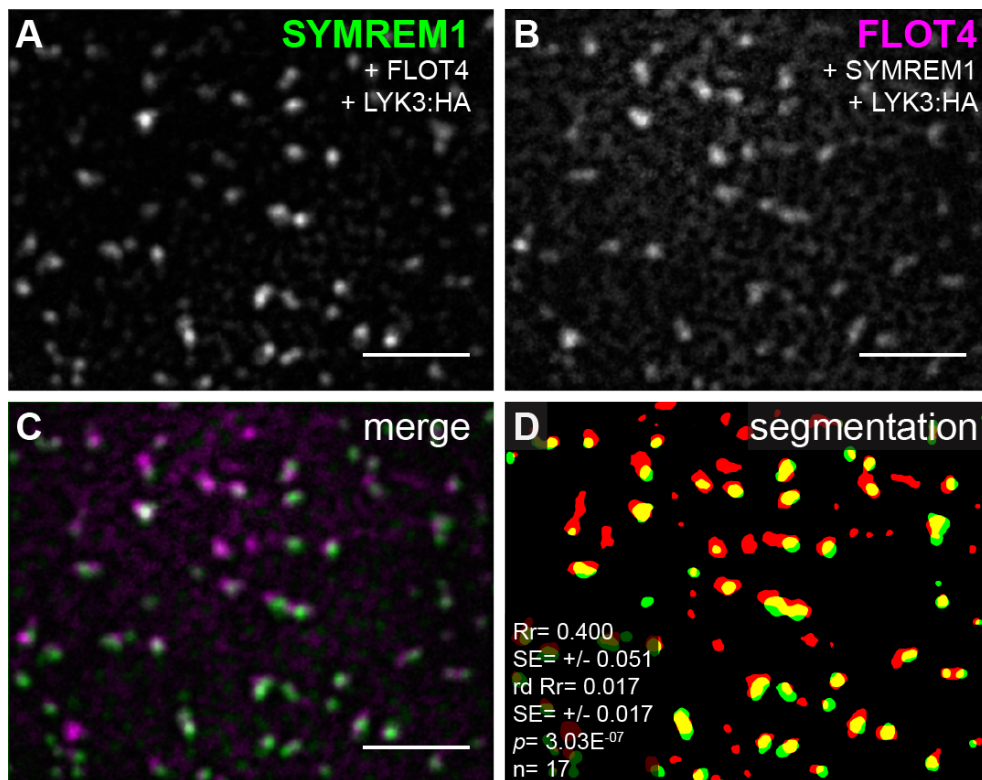


Figure 24 Artificial reconstitution of a symbiosis-related MD in *Nicotiana benthamiana*.

Nicotiana leaf epidermal cells expressing the legume-specific proteins YFP:SYMREM1, FLOT4:mCherry and LYK3:HA simultaneously. In this situation, YFP:SYMREM1 (A) and FLOT4:mCherry (B) formed distinct MDs that co-localized, which is evident in the merged image (C) and a segmented image (D). Quantitative pixel based co-localization analysis confirmed the positive correlation of the two MD signals. Quantitative data are provided in panel (D). Rr= Pearson correlation coefficient; rd Rr= Pearson correlation coefficient obtained after image randomization. The respective standard errors (SE) are provided below the Pearson values. p = confidence interval obtained from a Student's t-test comparing Rr and rd Rr. Scale bars indicate 5 μ m.

Therefore, for YFP:SYMREM1 and FLOT4:mCherry to co-localize in MDs, the presence of LYK3 seems to be essential in *N. benthamiana*. In a reciprocal manner, it is possible that SYMREM1 is needed for the recruitment of LYK3 into FLOT4-labeled MDs. This question was tackled by co-expressing the 3 proteins, SYMREM1, FLOT4 and LYK3, at the same time, but with different tags in the heterologous leaf expression system.

First, LYK3 was fused C-terminally to GFP (p35s::LYK3:GFP) and co-expressed with pUbi::FLOT4:mCherry. Under these conditions, LYK3:GFP and FLOT4:mCherry, although they appeared to be mildly compartmentalized in the PM (Figure 25A, B), failed to co-localize (Figure 25C). The signals of both channels were random to each other (Rr= 0.010, rd Rr= -0.002, Figure 25D). Therefore, FLOT4 is not capable of recruiting LYK3 into a MD by itself. It must be noted, however, that the differences in signal intensities for both LYK3:GFP and FLOT4:mCherry in the PM were not sufficiently high enough for robust segmentation; therefore, the images provided in Figure 25A, B were subjected to a stronger background subtraction than usual. This, in part, accounts for the compartmentalization observed in this case.

Results

However, when HA-tagged SYMREM1 was co-expressed with FLOT4 and LYK3, a clear compartmentalization and even labeling of MD-structures by both LYK3:GFP and FLOT4:mCherry occurred (Figure 25E, F). The signals of the GFP and mCherry-tagged fusion proteins appeared to co-localize. Indeed, a high degree of co-localization was measured ($R_r=0.60$, $SE=0.046$; $rd\ R_r=0.021$; $rd\ SE=0.019$; $p=4.79E^{-08}$; Figure 25H).

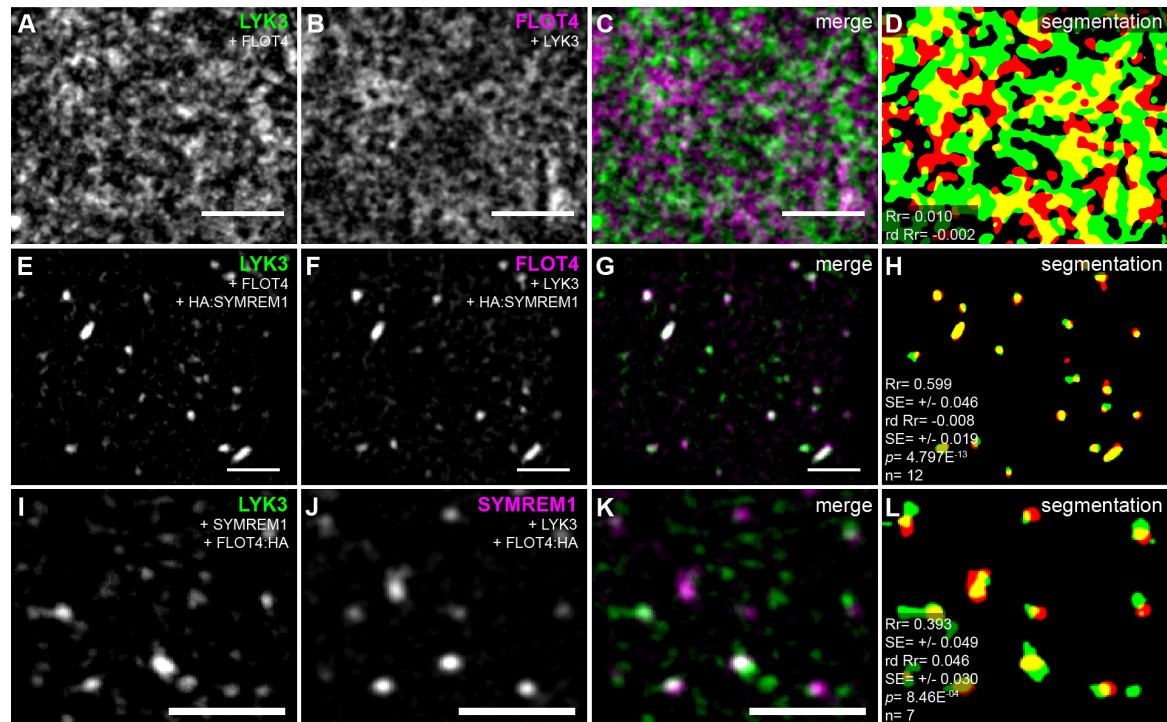


Figure 25 LYK3 is recruited into a symMD in a SYMREM1-dependent manner. Expression of LYK3, FLOT4 and SYMREM1 fusion-proteins in different combinations in *Nicotiana benthamiana* leaf epidermal cells. The simultaneous expression of LYK3:GFP (A) and FLOT4:mCherry (B) in the absence of SYMREM1 resulted in moderate compartmentalization of both proteins but random distribution (C, D). In contrast, the additional expression of HA:SYMREM1 with these proteins resulted in labeling of distinct MDs by LYK3:GFP (E) and FLOT4:mCherry (F) that co-localized under these conditions (G, H). Similar patterns were observed during co-expression of LYK3:GFP (I) and mCherry:SYMREM1 (J) in the presence of FLOT4:HA; the fluorophore-tagged proteins co-localized (K, L). Proteins fused to GFP are indicated in green, those fused to mCherry in magenta (C, G, K) or red (D, H, L). R_r = Pearson correlation coefficient; $rd\ R_r$ = Pearson correlation coefficient obtained after Costes' randomization was applied to the GFP channel image. The respective standard errors (SE) are provided below the Pearson values. p = confidence interval obtained from a Student's t-test comparing R_r and $rd\ R_r$. Scale bars indicate 5 μ m.

A clear restriction of the LYK3:GFP signal to distinct spots in the PM was observed in the presence of both, mCherry:SYMREM1 and FLOT4:HA (Figure 25I). In this combination, mCherry:SYMREM1 localized in clear, distinguishable MDs (Figure 25J) that co-localized strongly with LYK3:GFP ($R_r=0.39$, $SE=0.049$; $rd\ R_r=0.046$; $rd\ SE=0.030$; $p=8.46E^{-04}$). This co-localization was, however, slightly lower than that for LYK3:GFP with FLOT4:mCherry. These data strongly support the hypothesis that recruitment of LYK3 into FLOT4-labeled symMDs is dependent on SYMREM1.

The experiment was repeated with the other RNS-specific flotillin, FLOT2, in the place of FLOT4 to control whether the recruitment of these proteins into a symbiosis-related MD is specific to the three proteins tested.

FLOT2:mCherry and FLOT2:GFP were cloned and expressed in *Nicotiana*. On their own, both fusion proteins labeled the PM in a homogenous manner (Figure 22C, D). FLOT2:GFP did not change its localization when co-expressed with FLOT4:mCherry (see Figure 22H, I, J).

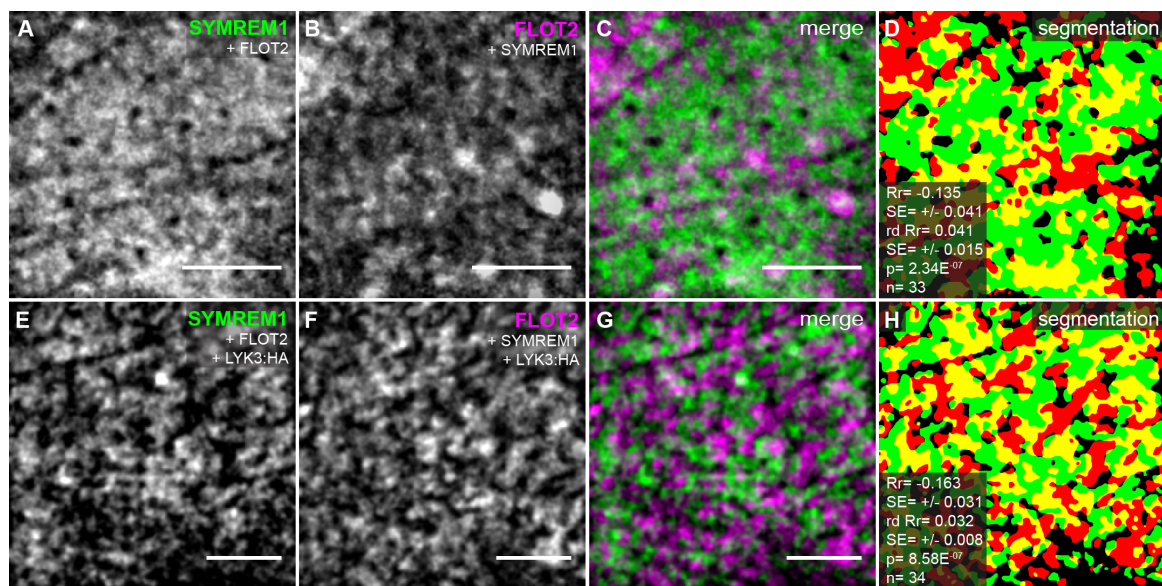


Figure 26 FLOT2 does not induce the formation of microdomains in *Nicotiana benthamiana*. The triple expression of FLOT2, SYMREM1 and LYK3:HA is not enough to induce compartmentalization or MD labeling in *Nicotiana*. When YFP:SYMREM1 (A) was co-expressed with FLOT2:mCherry (B), a compartmentalization of both proteins ensued. (C) A representative merged image revealed only a moderate exclusion of the signals from each other occurred, which was more noticeable after image segmentation and pixel based co-localization analysis (D). The addition of LYK3:HA to these two proteins did not change the localization of YFP:SYMREM1 (E) or FLOT2:mCherry (F). No clear co-localizing MDs were visible. A merged image of both channels is depicted in (G) and the segmented representation in shown in (H). Rr= Pearson correlation coefficient; rd Rr= Pearson correlation coefficient obtained after Costes' randomization was applied to the GFP channel image. The respective standard errors (SE) are provided below the Pearson values in (D) and (H). p= confidence interval obtained from a Student's t-test comparing Rr and rd Rr. Scale bars indicate 5 μ m.

A compartmentalization and exclusion were observed when YFP:SYMREM1 and FLOT2:mCherry were co-expressed simultaneously (Figure 26A, B, C). However, it appeared weaker than the combination YFP:SYMREM1 and FLOT4:mCherry (Figure 18D-G). Indeed, the Pearson correlation coefficient Rr= -0.135 (SE= 0.041, rd Rr= -0.041, rd SE= 0.015; p= 2.34E⁻⁰⁷; n= 33; Figure 26D) confirmed this assessment. This value showed that even though FLOT2 and SYMREM1 clearly have excluding tendencies, this value was 3 times less pronounced than the negative correlation between SYMREM1 and FLOT4 (Rr= -0.395; SE= 0.030).

Results

The additional infiltration of these two proteins with a p35s::LYK3:HA-encoding construct had only a minor impact on the compartmentalization of these proteins (Figure 26E-H). No clear structures (e.g. unique MDs) with overlapping signals appeared. YFP:SYMREM1 and FLOT2:mCherry did not co-localize. The opposite was the case, as the Pearson correlation coefficient decreased slightly to $R_r = -0.165$ ($SE = 0.031$; rd $R_r = 0.032$; rd $SE = 0.008$; $p = 8.85E^{-07}$; $n = 34$). This decrease was, however, not significant to the value obtained for FLOT2:mCherry and YFP:SYMREM1 co-expressed without LYK3:HA (t-test $p = 0.52$).

Therefore, the formation of a symMD in the heterologous *Nicotiana* system was specific for the presence of LYK3, FLOT4 and SYMREM1.

4 Discussion

Recent evidence suggests different MDs coexist in the PM of plants (Jarsch et al., 2014). The substantial amount of proteins identified to play a part in the establishment of RNS raises the question whether these signaling components in the PM are organized into identical MDs. A first hint was provided by the stimulus dependent co-localization of FLOT4 with LYK3 (Haney et al., 2011). Data from this project adds to the hypothesis of the existence of a symbiosis-specific population of MDs in the PM and suggests a mechanism for their assembly. In this work, we provide evidence that FLOT4, SYMREM1, LYK3, and the actin cytoskeleton coordinately form such a MD.

4.1 Stability of SYMREM1-labeled Microdomains

According to data presented in this project, SYMREM1-labeled MDs closely associate with actin filaments and are formed in an actin-dependent manner (, or their stability depends on an intact actin-cytoskeleton). While oryzalin treatment to destabilize microtubules did not significantly impact the density of YFP:SYMREM1-labeled MDs, they were strongly reduced upon disruption of the actin network by cytochalasin D (Figure 6). This would be in line with the suggested picket-fence-model for compartmentalization of the PM. In mammalian cells, it is clear that the actin based membrane skeleton actively regulates the diffusion dynamics of PM-resident proteins and lipids, and promotes clustering of proteins, or condensing of receptor-ligand complexes for signaling processes (Andrews et al., 2008; Jaqaman et al., 2011).

How pharmacological disruption of the membrane-skeleton precisely leads to the reduction of SYMREM1-labeled MDs cannot be explained with certainty, yet. The dependency on actin could have at least two explanations. First, SYMREM1 could directly interact with the cortical actin cytoskeleton, or second, SYMREM1 interacts, or associates, with other PM-resident components/structures that are dependent on actin. Interestingly, the remorin GSD1 from rice (*Oryza sativa*), which affects grain setting, co-localizes with the protein ACTIN1 (OsACT1) in plasmodesmata. Furthermore, BiFC, and co-immunoprecipitation (Co-IP) experiments showed

Discussion

that this remorin directly interacts with ACT1, and this interaction is required for GSD1 to function in the regulation of plasmodesmata conductance (Gui et al., 2014). Remarkable is, that truncations of GSD1 showed the interaction occurs specifically between ACT1 and the coiled-coil domain in the C-terminal region of GSD1 (Gui et al., 2015). So far, no evidence exists that SYMREM1 interacts with actin, and no known actin-binding motif can be predicted *in silico*. However, a coiled-coil domain is predicted to exist in the C-terminal region of all remorins with SYMREM1 being no exception (Raffaele et al., 2007). Because *Lotus* SYMREM1 interacts with the three RLKs, NFR5, NFR1 and SYMRK through residues in its promiscuous coiled-coil-domain containing C-terminal region (Tóth et al., 2012), it is conceivable that SYMREM1 could also directly interact with actin or actin binding proteins. This has not been investigated.

In previous work, SYMREM1-labeled MDs disappeared after methyl- β -cyclodextrin (M β CD)-treatment (Konrad et al., 2014). M β CD depletes sterols from membranes (Rodal et al., 1999), and, therefore, SYMREM1-labeled MDs also show a dependency on the sterol composition of the PM environment. This infers SYMREM1 is present in membrane rafts, which was proposed for other remorins (Raffaele et al., 2009b; Raffaele et al., 2009a; Perraki et al., 2012). This dual dependency of SYMREM1-labeled MDs stability on both the actin cytoskeleton, as well as on the sterol composition is not contradictory. Sterols induce tightly packed lipid-domains, and are thought to be a driving force in the formation of membrane rafts, which then recruit ‘raftophilic’ proteins into liquid ordered phases of the PM (Simons and Ikonen, 1997). These liquid ordered (rafts) and disordered phases (non rafts) in the PM of live mammalian cells are directly dependent on the presence of the actin membrane skeleton (Dinic et al., 2013). Here, monitoring the behavior of environmentally sensitive probes (Laurdan and di-4-ANEPPDHQ) upon treatment with latrunculin B, which inhibits polymerization of actin filaments, revealed a decrease of liquid ordered phases in the PM (Dinic et al., 2013). Cytochalasin D, which was used in our studies, also functions by inhibiting actin filament polymerization and could result in a more disordered PM environment, thereby reducing SYMREM1-labeled membrane rafts. Interestingly, incubation of live cells with jasplakinolide, a stabilizing agent of actin filaments, promotes the formation of liquid ordered phases in the PM (Dinic et al., 2013). It would be interesting to study whether an increase of SYMREM1-labeled MDs in *Medicago* roots occurs in presence of jasplakinolide.

Further studies emphasize the close link between the sterol composition of the PM, dynamics of membrane proteins, and the underlying actin cytoskeleton in mammalian cells (Ganguly and Chattopadhyay, 2010; Mueller et al., 2011). Importantly, M β CD-induced cholesterol depletion in the PM results in a less dynamic and unstable actin cytoskeleton with fewer connections formed between the actin network and the PM (Kwik et al., 2003; Chubinskiy-Nadezhdin et al., 2013). Similarly, pharmacologically reducing the amount of actin connections to the PM in live cells leads to a decrease of liquid ordered areas in the PM (Dinic et al., 2013). Corroborating this, the

inhibition of the actin nucleator complex ARP2/3, which reduces actin branching and attachments to the PM, enhances lipid diffusion dynamics in live cells (Andrade et al., 2015). Most interestingly, transmission electron microscopy in mammalian cells showed MDs are further subdivided into regions that are labeled by ‘raft’ and ‘non-raft’ constituents and are always heavily enriched in actin (, or actin binding proteins) (Lillemeier et al., 2006).

Several reports describe opposite effects cholesterol depletion has on membrane dynamics, depending on compound (concentration), and the depletion-method, or incubation-time used (Goodwin et al., 2005; Shvartsman et al., 2006; Zidovetzki and Levitan, 2007). However, fewer SYMREM1-labeled MDs after M β CD-treatment could either be explained by destabilization of membrane rafts before these would be able to associate into larger platforms, or due an effect M β CD treatment has on the actin cytoskeleton, which could impair the forming or stabilization of MDs. A hypothetical model exists that suggests the sites of PM-connection with the actin cytoskeleton (the pickets) act as MD-nucleation sites, where a raft-like lipid phase develops, which recruits and clusters raftophilic membrane (-associated) proteins by lipid-protein interactions (Gomez-Llobregat et al., 2013). This protein cluster disintegrates when the actin-PM connection is lost (Gomez-Llobregat et al., 2013). Other models propose a more active role of the actin cytoskeleton, which requires not only cortical actin mesh to define mesoscale compartments, but also very dynamic, short actin filaments, that actively condense proteins into nanoclusters and, subsequently, MDs (Chaudhuri et al., 2011; Gowrishankar et al., 2012). Nevertheless, a general model, in which SYMREM1 may be first present in small membrane rafts that then cluster to form larger structures, the mesoscale MDs seen, is in accordance with the proposed three-tiered membrane architecture (Kusumi et al., 2012a; Kusumi et al., 2012b), and reconciles the data SYMREM1-labeled MDs being influenced by both the actin membrane-skeleton (Figure 6, Figure7) and the cholesterol composition of the membrane (Konrad et al., 2014).

Evidence in support of this assumption exists also for other remorins. In a proteomic screen of detergent soluble and detergent insoluble membrane (DIM) fractions of *Arabidopsis*, after actin depolymerization, remorins were no longer observed in DIM fractions (Szymanski et al., 2015). Even though it is clear that this method does not allow the isolation of functional rafts (or MDs) (Tanner et al., 2011), this was consistent with the observation that MD-labeling of two other remorins (YFP fusions of AtREM1.3 and AtREM1.2) in *Arabidopsis* was reduced upon depolymerization of the actin cytoskeleton (but not after microtubule disruption) (Szymanski et al., 2015). This further indicates that some remorin-labeled MDs are dependent on the actin cytoskeleton and concurrently are membrane raft-associated. However, adding to a complex picture, two *Arabidopsis* remorins (At1g13920/At4g00670) have a unique localization pattern. When heterologously expressed in *Nicotiana*, these remorins labeled MDs that aligned as filamentous structures in the PM (Jarsch et al., 2014). For the remorin tested (At1g13920), these

MDs disappeared after microtubule destabilization and remained stable when actin was disrupted (Jarsch et al., 2014). This suggests that there may be different mechanisms of forming or maintaining stability of remorin-labeled MDs. For SYMREM1 the actin cytoskeleton is needed.

It would have been of great interest to investigate whether SYMREM1-labeled MDs are reduced in number, or mis-localize in actin mutants. Unfortunately, attempts in trying to generate YFP:SYMREM1-expressing transgenic roots in *Medicago (rit)*; (Miyahara et al., 2010), or *Lotus (nap1-1, pir1-1)*; (Yokota et al., 2009)) actin mutants were unsuccessful, because of strong pleiotropic growth defects these plants exhibited under our experimental conditions. In addition, if SYMREM1 serves as an anchoring point for actin, it would be of great value to investigate whether symbiotic actin dynamics are changed in the *symrem1* tobacco-retrotransposon (*Tnt1*) insertion knock out mutants (Noble Foundation identifiers NF3495, NF4432) (Lefebvre et al., 2010).

4.2 Flotillins Compartmentalize the Plasma Membrane

The PM is also organized into many small subdomains in bacteria (Bramkamp and Lopez, 2015). Bacterial flotillins are master regulators for this (Bach and Bramkamp, 2013). In *Bacillus subtilis*, the flotillins FloT and FloA label the PM in distinct MDs, where they co-localize and interact with many signaling proteins that are essential for several processes including biofilm production or sporulation (Donovan and Bramkamp, 2009; Lopez and Kolter, 2010; Bach and Bramkamp, 2013; Schneider et al., 2015).

Bacillus cells that do not express *FloT* and/or *FloA* show a severely disturbed PM-organization, where membrane lipids coalesce into larger areas and flotillin-labeled MDs are reduced in numbers (Bach and Bramkamp, 2013). Flotillins are, therefore, thought to organize, maintain, and sustain MD-formation, and separation of lipid domains in the PM of bacteria. This can be seen as a mechanism to separate certain proteins from each other (in MDs), to condense specific proteins into same MDs, or both at the same time (Bach and Bramkamp, 2013). Interestingly, FloT and FloA physically interact in MDs, however, they differentially distribute (or accumulate) within MDs, based on their unique expression pattern (Schneider et al., 2015). Importantly, each of these two flotillins recruits a different set of signaling proteins into MDs, resulting in functionally specialized MDs (Schneider et al., 2015). Also in other systems, flotillins (termed Reggie) recruit proteins into specific MDs (Babuke and Tikkanen, 2007; Otto and Nichols, 2011; Stuermer, 2011).

Evidence also exists in plants that show a dependency of a PM-localized RLK to label MDs in a flotillin-dependent manner. In *Arabidopsis*, co-localization of the brassinosteroid hormone

receptor BRI1 ('BRASSINOSTEROID INSENSITIVE 1') with the flotillin AtFLOT1 is increased in (mobile) MDs upon exogenous brassinosteroid application. Reducing *AtFLOT1* in a stable RNAi (artificial microRNA, amiRNA) line decreases BRI1-labeled MDs, consistent with flotillins being essential for PM-compartmentalization (Wang et al., 2015b). Moreover, disruption of BRI1-labeled MDs by M β CD-treatment strongly reduced the ability of BRI1 to phosphorylate target proteins, thereby demonstrating a biological significance of MDs functioning as organizing signaling-platforms *in vivo* (Wang et al., 2015b). Staining the PM of the amiRNAi *AtFLOT1* line showed a strong decrease in the uptake of filipin, a fluorescent histochemical marker for cholesterol, indicating that the downregulation of this flotillin decreases the order of the membrane compared to wildtype plants (Li et al., 2012). This was confirmed by the observation that the di-4-ANEPPDHQ-labeled PM also showed strongly reduced membrane order in the amiRNAi *FLOT1* line (Zhao et al., 2015). Thus, also in plants, evidence is accumulating that proposes flotillins are required for establishing membrane rafts in the PM, as well as being essential for MD formation.

In line with this, RNAi of *FLOT4* in *Medicago* significantly reduced the number of SYMREM1-labeled MDs, suggesting FLOT4 may function as a primary scaffold at the PM that assists in, or enables the recruitment of SYMREM1 into MDs. Whether an interaction occurs between SYMREM1 and FLOT4 has not been tested. However, based on the excluding localization of these two proteins in *Nicotiana* (Figure 18), a direct interaction seems unlikely or would only be achieved in the homologous system after symbiosis-induced modifications (e.g. phosphorylation). How silencing of *FLOT4* specifically affects SYMREM1 cannot be said with certainty, but a change in the general liquid ordered and disordered phases of the PM (Bach and Bramkamp, 2013; Zhao et al., 2015) or of the underlying cytoskeleton are possibilities.

Interestingly, FLOT4-labeled MDs are reduced more than 50% (Haney et al., 2011) and mis-localize (Figure 14) in *hcl-1*. The spike-like arrangement of SYMREM1-labeled MDs in *hcl-1* clearly followed the same orientation as the actin cytoskeleton (Figure 13), and FLOT4 also localized in spikes that co-localized with SYMREM1 (Figure 14). Thus, the FLOT4-labeled MDs in the PM may, indeed, be dependent on the actin-cytoskeleton. In mammalian cells, flotillins form direct contacts with the actin-based cytoskeleton underneath the PM and modulate actin dynamics (Neumann-Giesen et al., 2004; Liu et al., 2005; Langhorst et al., 2007; Neumann-Giesen et al., 2007; Ludwig et al., 2010). A link between flotillins and the actin cytoskeleton in *Medicago* seems, therefore, possible. Co-localization of actin markers with FLOT4, or pharmacological disruption of the actin cytoskeleton could reveal information on this aspect.

4.3 Cytoskeleton Defect in *hcl-1*

In this study, we observed an actin-cytoskeleton defect for transgenic roots of the *M. truncatula* *hcl-1* mutant allele expressing YFP-Lifeact, which may be the cause of SYMREM1 mislocalization. Under our experimental conditions, root hairs of *hcl-1* efficiently initiated but did not elongate (Figure 10), confirming the observations of a previous study (Haney et al., 2011). As tip growing cells, root hairs typically have an actin cytoskeleton that is organized as thick actin bundles running in parallel with the root hair shank that randomize into finer and diffuse structures in the apex of the tip (Baluska et al., 2000; Ketelaar et al., 2002; Ketelaar et al., 2003; Ketelaar, 2013). The fine actin filaments towards the elongating root hair tips are highly dynamic and believed to deliver cargo towards the growing tip. YFP:Lifeact did not label any fine actin filaments in transgenic *hcl-1* root hairs, instead we only observed thick bundles (Figure 11). Lifeact is a short 17 amino acid long peptide from the actin binding domain of ACTIN BINDING PROTEIN 140 (Abp140) that was described to not interfere with cellular functions or actin dynamics (Riedl et al., 2008; Era et al., 2009), and is used to label actin filaments and follow their dynamics in root hairs (Vidali et al., 2009). One report describes that a very high expression of Lifeact in the model system *Arabidopsis* reduces actin dynamics and induces actin bundling in root epidermal cells. Curiously, even then, this construct does not cause defects in the plant's development (van der Honing et al., 2011). The short, non-elongating root hairs in *hcl-1* are most likely a consequence of the disturbed actin network observed. Small, stunted root hair phenotypes are frequently observed in *actin* mutants and plants treated for a prolonged period with actin disrupting drugs (Baluska et al., 2000; Gilliland et al., 2002; Ringli et al., 2002; Diet et al., 2004; Kandasamy et al., 2009; Sampathkumar et al., 2011). Untransformed *hcl-1* plants show the same short root hair phenotype as transgenic YFP:Lifeact-expressing plants (Figure 10). Why inactivating the kinase domain of LYK3 results in an actin cytoskeleton defect cannot immediately be explained. However, because we observed (and measured) a specific change in the actin cytoskeleton in *Medicago hcl-1* in comparison to wildtype and *hcl1-compl* plants (which express WT LYK3), it appears as if this RLK is functionally connected to the actin cytoskeleton (or actin cytoskeleton modifiers).

Interestingly, the roots of a *Lotus symrk* mutant (line cac41.5 (Stracke et al., 2002)) also form shorter and swollen (and more branched) root hairs than WT plants under non-symbiotic conditions (Esseling et al., 2004). In Figure 8, the *dmi2-1* root hair is shorter, however, this was not investigated on a larger scale. Also, *Medicago dmi2-1* mutant's root hairs are more touch sensitive than WT roots (Esseling et al., 2004). Even though they respond to rhizobial inoculation by reinitiating tip growth and forming root hair curls, they cannot efficiently entrap bacteria. The

root hairs stop growing once the tip touches the shank (Esseling et al., 2003). It is possible that the actin cytoskeleton is also altered in *symrk/dmi2* mutants; however, this has not been tested yet.

In addition to the actin-defect we describe, the microtubule cytoskeleton in *hcl-1* is also impaired (Catoira et al., 2001). Microtubule-rearrangements in root hairs and polarization of microtubules in cortical cells, which are needed for the production of the pre-infection thread, usually coincide with rhizobial inoculation (Timmers et al., 1999; Timmers, 2008). The microtubule cytoskeleton in *hcl-1* does not show this reorganization upon symbiotic stimuli and remains unpolarized (Catoira et al., 2001). The changed actin cytoskeleton structure in *hcl-1* could be the result of a microtubule cytoskeleton defect, or vice versa. It is clear that strong codependences between actin and microtubules exist in plants (Petrasek and Schwarzerova, 2009). After actin destabilization with drugs, live cell microscopy in *Arabidopsis* revealed that newly produced actin filaments co-localize with, move along and re-organize dependent on the microtubules (Sampathkumar et al., 2011). Disrupting microtubules and actin simultaneously for a longer period and then removing the actin disruptor leads to disorganized and incomplete actin recovery. A similar experiment with removal of the microtubule depolymerizer (and in continued presence of the actin disruptor) results in a disorganized microtubule cytoskeleton, confirming a co-dependency of both cytoskeletons (Sampathkumar et al., 2011). Live cell microscopy in other model systems also reports links between actin and microtubule cytoskeleton (Preciado Lopez et al., 2014), and important roles of actin-microtubule cross-linking proteins (Schneider and Persson, 2015). Whether a connection between the microtubule cytoskeleton defect (Catoira et al., 2001) and the altered actin structure in *hcl-1* exists, is not known, yet.

The observed spike-like mis-localization of SYMREM1-labeled MDs was only investigated in non-symbiotic overexpression conditions, suggesting a more general actin defect independent of symbiotic stimuli (unlike the microtubule defect, which was only seen under symbiotic stimuli (Catoira et al., 2001)). Thus, LYK3 (and potentially other RLKs) could be needed to provide spatial cues for cytoskeleton-remodelers, and/or anchors. This could be achieved either by direct, and indirect, interactions with such proteins or through their activation by phosphorylation. A candidate could be the symbiosis specific *Medicago* GTPases ROP10 (discussed later; (Lei et al., 2015)). Another interesting aspect would be to investigate the localization of the fluorophore tagged kinase dead LYK3 mutant *HCL-1* protein; unfortunately, no null mutants exist for LYK3.

However, sterol synthesis mutants, cell wall mutants, and ethylene synthesis mutants also have short root hair phenotypes (Pitts et al., 1998; Souter et al., 2002; Jones et al., 2006). This could either be a direct result of the mutations, or it is possible that the mutations have an impact on the actin cytoskeleton, which then leads to root hair elongation defects. Links of these three components to cytoskeleton dependent processes exist in plants (Grebe et al., 2003; Plett et al., 2009; Panteris et al., 2013; Sampathkumar et al., 2014)

4.4 The Cell Wall and the Immobilization of LYK3

As introduced, the dynamics of proteins in the PM are synchronized by an interdependent ‘cell wall - PM – membrane-skeleton continuum’ (McKenna et al., 2014; Liu et al., 2015a; Liu et al., 2015b).

In contrast to mammalian cells, most MDs observed in the PM of plants are laterally relatively immobile (Sutter et al., 2006; Roppolo et al., 2011; Demir et al., 2013). This holds true especially for remorins, where of the 16 remorins tested, 14 were immobile (for at least 20 minutes); only two remorins displayed moderate lateral mobility (Jarsch et al., 2014). FLOT4-, and SYMREM1-labeled MDs are immobile in *Medicago* (Haney et al., 2011; Konrad et al., 2014). Fascinatingly, LYK3-labeled MDs are, by default, mobile and become static in symbiotically engaged root hairs (Haney et al., 2011).

The cell wall could play a role during this immobilization. A study nicely demonstrated the influence the cell wall has on lateral mobility of proteins in the PM, by constructing and testing a set of 13 artificial, membrane-targeting proteins in stable transgenic *Arabidopsis* plants. Eleven of these were immobile (Martiniere et al., 2012). Artificial proteins that projected into the outer phase of the PM, or into the extracellular space towards the cell wall, generally displayed a lower lateral mobility than proteins that did not have an extracellular domain. The lateral mobility (determined by FRAP measurements) of the proteins increased if the cell wall was detached from the PM by plasmolysis or removed by enzymatic treatment (Martiniere et al., 2012). The proteins that displayed the highest mobility either attached to the PM at the inner leaflet or did not contain extracellular domains. However, even those were influenced by the proximity of the cell wall, and can be considered relatively immobile in plants (Martiniere et al., 2012). Curiously, applying the cell-wall-synthesis blocking drug, isoxaben, for one hour significantly reduced the mobility of a PM-resident protein without an extracellular domain (Martiniere et al., 2012). The relatively short duration of the isoxaben treatment (1 hour) is unlikely to result in a dramatic cell-wall collapse but presumably changes the cell wall’s structure and dynamics. Therefore, it was suggested that cell-wall synthesis not only passively enforces restrictions on proteins by its sheer presence, but also, at the same time, actively impacts protein-mobility in the PM. During cell-wall synthesis, the cell wall forms tight connections with the PM (Giddings et al., 1980; Mueller and Brown, 1980; Carpita, 2011). When cell-wall synthesis is stopped (but the cell wall is still present), the proteins become arrested (Martiniere et al., 2012). Evidence exists that suggests the cell wall may play a role in remorin-labeled MDs.

Two *Arabidopsis* remorins label MDs only in hypocotyl cells of 5 days old seedlings. These remorins attached to the PM uniformly in other cell types (Jarsch et al., 2014). Hypocotyl cells are rapidly expanding cells, which coincide with massive cell wall remodeling (Refregier et al.,

2004). Thus, for these two *Arabidopsis* remorins, the cell wall may be imperative for MD-stabilization or formation.

The remorin REM1.3 labels MDs in the PM (Raffaele et al., 2009b; Demir et al., 2013; Jarsch et al., 2014). In stable, transgenic *Arabidopsis* plants, a direct influence the cell wall has on (*Solanum tuberosum*, potato) eGFP:StREM1.3-labeled MDs was discovered. FRAP-experiments on mesophyll cells, and on cell-wall free protoplasts from mesophyll cells, revealed distinct recovery-profiles of the MDs. In mesophyll cells, the MD-signals did not recover after 2 minutes confirming a low mobility of StREM1.3. Curiously, in protoplasts the remorin still efficiently labeled MDs, demonstrating that MD-labeling of StREM1.3 itself is not dependent on the presence of the cell wall. However, within these MDs the REM1.3-population was significantly more mobile in protoplasts compared to mesophyll cells. Therefore, REM1.3-labeled MDs themselves are formed independent of the cell wall, but (some) proteins within MDs are stabilized by cell-wall influences (Blachutzik et al., 2015). This is particularly striking, because remorins attach to the cytosolic side of the PM without any protrusions into the transmembrane or extracellular space. This raises intriguing possibilities on how LYK3-labeled MDs become immobilized.

The immobilization of LYK3 appears to be ligand induced, because it requires detection of NF and potentially the presence of a second rhizobial signal (Haney et al., 2011). Another possibility would be, that precise localized concentrations of NF-secretion by rhizobia are required that cannot be mimicked by external application. According to the co-localization data on LYK3, FLOT4, and SYMREM1 gathered in *Nicotiana* (Figure 15, Figure 24, Figure 25), and the timing of LYK3 immobilization during RNS (Haney et al., 2011), we hypothesize that the detection of NF leads to the induction of *SYMREM1*, which is needed for the arrest of LYK3-mobility in *Medicago*.

The mechanism underlying this immobilization is unknown, but could be based on at least two processes: First, because SYMREM1 is immobile in the PM (anchored by the actin cytoskeleton, and/or to FLOT4), the interaction between SYMREM1 and LYK3 transiently stops the movements of LYK3. Then, LYK3 phosphorylates the remorin. *In vitro* data exist, which show LjSYMREM1 is phosphorylated by the *Lotus japonicus* RLKs NFR1 and SYMRK in the N-terminal region (Tóth et al., 2012). Binding to LYK3 and becoming phosphorylated could promote SYMREM1 oligomerization and/or induced folding of the intrinsically disordered N-terminal region, creating new docking sites for additional proteins that could play a pivotal role in the immobilization of LYK3 (e.g. by further connections to the actin cytoskeleton). *In vitro*-folding of the disordered N-terminal region of AtREM1.3, under buffer-conditions that mimic protein-protein interactions, support such a possibility (Marin et al., 2012). In addition, the N-terminal region of AtREM1.3 was shown to be required for homo-oligomerization and for

Discussion

interactions with other proteins (Marin et al., 2012). Thus, the immobilization of LYK3 would predominantly be determined from influences the actin cytoskeleton asserts on the PM.

A second mechanism would involve active remodeling of the cell wall. Strong immobilization of LYK3 was observed 24 hours after rhizobial infection only in responding root hairs, with the highest co-localization of LYK3 and FLOT4 occurring at the tips of the root hairs (Haney et al., 2011). There, the symbiotic root hair swellings, deformations, and curling, as well as later IT-initiation, coincide with massive cell wall remodeling. By 24 hours, the cell wall of root hairs has undergone/is undergoing modifications, localized degradation, reinforcement, and/or structural rearrangements to prime the root hair for growth alterations (Ridge and Rolfe, 1985; van Spronsen et al., 1994; Gage, 2004; Xie et al., 2012; Rich et al., 2014). Thus, these processes may limit the mobility of LYK3, in analogy to the influence the cell wall has on confining PM-resident proteins, especially those which contain extracellular domains (Martiniere et al., 2012). Thus, the immobilization of LYK3 could also be the result of cell-wall induced altered dynamics of proteins residing within MDs (Blachutzik et al., 2015).

A combination of both mechanisms is also possible. Here, a protein residing in the symbiotic MDs, possibly SYMREM1, would recruit cell wall modifying enzymes into the MDs during root hair curling, IT initiation and polar growth. Thereby, these MDs would be simultaneously supported by the actin cytoskeleton, and their mobility actively regulated by cell wall modifying processes. Cell wall degrading enzymes implicated in RNS will be discussed in chapter 4.6.4.

A nice system to study LYK3-mobility would be in the *symrem1* mutant background. It would be interesting to analyze the dynamics of LYK3 in these mutants, and investigate if lateral mobility of LYK3-labeled MDs is changed upon rhizobial inoculation compared to WT plants. Unfortunately, despite several attempts, LYK3:GFP was not detectable in *Medicago* roots with the confocal microscope system available. LYK3 may be regulated by a posttranslational mechanism to keep receptor levels low, which makes microscopic detection difficult (Moling et al., 2014). Alternatively, when better microscopic systems enable the detection of LYK3, it would also be possible to produce transgenic roots in the (available) stable *Medicago* pLYK3::LYK3:GFP background. Transiently expressing FLOT4:mCherry in this line, the degree of co-localization with LYK3 is expected to be small. Co-transformation of (an inducible) HA:SYMREM1 construct then would result in stronger co-localization of LYK3/FLOT4. This would strongly indicate SYMREM1 is directly involved in the immobilization of LYK3.

4.5 A Model for Microdomain-Assembly

While the *LYK3* and *FLOT4*-promoters are active prior to contact with the symbiont (Limpens et al., 2005; Mbengue et al., 2010; Haney et al., 2011), the *SYMREM1*-promoter is activated only under symbiotic conditions (Figure 16, (Lefebvre et al., 2010; Tóth et al., 2012)). Data presented here on the *SYMREM1*-promoter indicates that *LYK3*, *FLOT4*, and *SYMREM1* are expressed timely, and spatially, in similar manner during RNS. The mobile *LYK3*-containing MDs become arrested in a NF-dependent manner and then co-localize with *FLOT4*-labeled MDs (Haney et al., 2011). In the heterologous overexpression system (*Nicotiana benthamiana*, *Saccharomyces cerevisiae*), *SYMREM1* interacts with *LYK3* and NFP in MDs (Lefebvre et al., 2010; Tóth et al., 2012; Jarsch et al., 2014).

Based on the data presented in this thesis and in previously published work, we propose a hypothetical model for the formation of RNS, pathway specific, MD (Figure 27).

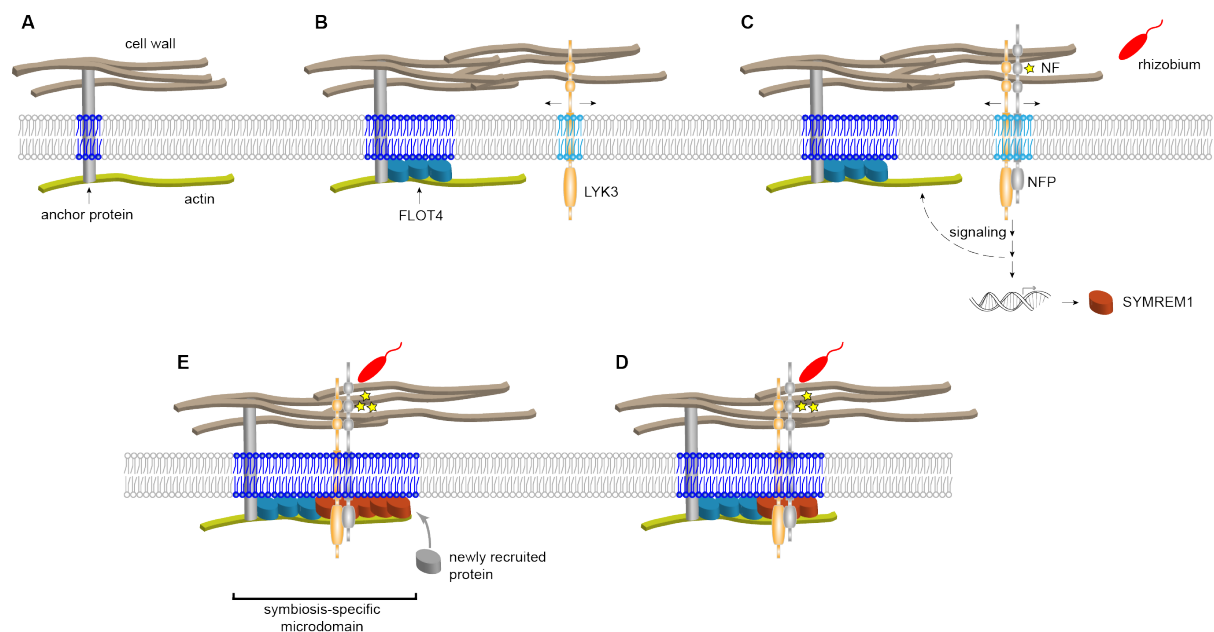


Figure 27 Model depicting steps in microdomain assembly during Root Nodule Symbiosis.

(A) The cell wall forms a continuum with the plasma membrane and the membrane-skeleton. **(B)** *FLOT4* (turquoise) forms immobile MDs in the PM that are associated with the cytoskeleton and creates a specific lipids environment (blue). The receptor *LYK3* (orange, and, potentially, *NFP* (grey)) is present in mobile MDs in the PM. **(C)** Upon rhizobial stimuli detected by *NFP* (possibly also in MDs) and *LYK3*, symbiotic signaling leads to the production of *SYMREM1* (red) and more *FLOT4*. **(D)** *SYMREM1* and *LYK3* are recruited to the *FLOT4*-labeled MDs in a mutually dependent manner. *LYK3* and *NFP* are immobilized in MDs **(E)** and *SYMREM1* is phosphorylated by *LYK3*, potentially leading to oligomerization of the remorin, and enlargement of the MD. More symbiosis specific proteins are recruited to the MDs. (Model drawn and provided by Prof. Dr. Thomas Ott)

The membrane-skeleton is connected with the PM, and the cell wall is in close contact with the PM, which compartmentalizes the PM (Figure 27A). Constitutively present, FLOT4 (turquoise) creates a specific lipid environment in the PM and forms MDs in an actin-dependent manner (Figure 27B). In the presence of rhizobia, the mobile receptor LYK3, and NFP, detect Nod factors to induce symbiotic signaling, resulting in the expression of *SYMREM1* (Figure 27C). NFP and LYK3 have been shown to form homo- and hetero-oligomers in *Medicago* (Moling et al., 2014). *SYMREM1*, initially binds to the PM through S-acylation (Konrad et al., 2014), then immediately is recruited to the FLOT4-labeled MD in co-dependence with LYK3 (and NFP) (Figure 27D). This leads to the immobilization of LYK3. Now, the three symbiotic proteins co-localize in a specialized symbiosis-related MD. FLOT4 and *SYMREM1* do not contain enzymatic activity themselves, and therefore function as scaffold proteins. Upon their phosphorylation or oligomerization, they create more docking sites or a new lipid environment for the recruitment of additional proteins (grey) that are crucial for rhizobial infection (Figure 27E). *In vitro*, the N-terminal region of *SYMREM1* is phosphorylated by NFR1 (*Medicago* LYK3), which is hypothesized to serve in a regulatory way during protein-protein interactions (Marin and Ott, 2012; Tóth et al., 2012).

4.6 Hypothesis on the Biological Meaning of Root Nodule Symbiosis Specific Microdomains

The phenotypes of *LYK3*, *FLOT4* and *SYMREM1* mutant and/or RNAi silenced plants, suggest a role for these during the infection process (Catoira et al., 2001; Limpens et al., 2003; Smit et al., 2007; Haney and Long, 2010; Lefebvre et al., 2010; Haney et al., 2011; Klaus-Heisen et al., 2011; Tóth et al., 2012). Fascinatingly, LYK3 and FLOT4 label MDs not only in root hairs but also on IT-membranes when expressed from their native promoters, strongly suggesting a biological relevance of these MDs (Haney et al., 2011). The initiation of ITs, and their progression, requires extensive cell-wall modifications such as degradation, peroxide-induced hardening, and production. Calcium fluxes, cytoskeletal rearrangements that target vesicle trafficking to the PM, and a high amount of membrane production are also important. All these processes depend on continuous, localized signaling between rhizobia and the plant (Oldroyd et al., 2011).

Furthermore, the IT progresses intermittently, during which rapidly growing phases are interrupted by paused events, during which the rhizobia catch up with the IT-tip. The pauses are thought to provide the plant with time to monitor symbiotic signaling at the PM of the IT (Fournier et al., 2008). Oscillatory growth, episodes of rapid elongation followed by slowly growing periods, is also a common mechanism during the polarized extension of pollen tubes and

root hairs, which requires targeted vesicle trafficking for the deposition of cell wall and membrane material (Holdaway-Clarke et al., 1997; Monshausen et al., 2007; Monshausen et al., 2008; Ketelaar, 2013). Moreover, gradients of Ca^{2+} , the pH (e.g. at the cell wall), and reactive oxygen species (ROS) act in concert, and need to be recognized to sustain these growth oscillations (Cardenas, 2009). It is likely that similar components to those involved in the growth of root hairs (or pollen tubes) are also involved in the symbiotic infection process.

Therefore, we hypothesize that the MDs containing LYK3, FLOT4, and SYMREM1 act as signaling hubs in the PM during rhizobial infection, by recruiting, condensing, or regulating. The symbiotic RLKs themselves may be present in MDs as receptor complexes (Riely et al., 2013; Antolin-Llovera et al., 2014; Moling et al., 2014). Based on the cytoskeleton defect the LYK3 mutant-allele, *hcl-1*, displays ((Catoira et al., 2001) and Figure 11, Figure 12) and the vast amount of dynamic cytoskeletal rearrangements occurring during the infection process, prominent candidates to be regulated or associated in these MDs could be cytoskeleton remodelers. Cell wall modifying enzymes and exocytosis proteins are also possible candidates. Examples of such proteins have been identified as important components of RNS and will be described more thoroughly in the following chapters.

4.6.1 GTPases

In mammalian cells and epithelia of *Drosophila melanogaster*, GTPases are the most common regulators of cytoskeletal reorganization (Kaibuchi et al., 1999; Schoeck and Perrimon, 2002) and cycle from the cytosol to specific sites at the membrane ('focal adhesions') after extracellular stimulation. There, they activate their effectors to induce changes in cytoskeleton structure and dynamics (Fukata and Kaibuchi, 2001; Geiger et al., 2001).

The small GTPase ROP10 (RHO OF PLANT 10) of *Medicago truncatula* localizes at the PM of root hair tips (Lei et al., 2015). Also in plants, small GTPases function as molecular switches and are vital in many processes such as establishing cell polarity (and membrane polarity, e.g. during polarized root hair growth), polar vesicular trafficking (endo/exocytosis), cell-wall-integrity, and cytoskeletal rearrangements (Li et al., 2001; Gu et al., 2003; Gu et al., 2004; Yang and Fu, 2007; Craddock et al., 2012; Nagawa et al., 2012; Oda and Fukuda, 2012; Yang and Lavagi, 2012). During the RNS infection process, ROP10 is localized to the PM precisely at infection sites, and is necessary for proper root hair curling and the initiation of ITs. De-regulated, heterologous expression of ROP10 in transgenic *Medicago* roots induced a disordered structure of the actin cytoskeleton. Additionally, in yeast-2-hybrid-, and BiFC-assays, ROP10 interacted with the symbiotic NF-receptor NFP (Lei et al., 2015). Thus, ROP10 (, and potentially other small

Discussion

GTPases,) links symbiosis-specific actin dynamics to the PM. This possibly depends on the MD-localization of the symbiotic RLKs, which in turn depends on FLOT4 or SYMREM1.

Similarly, *Lotus* ROP6 is induced under symbiotic conditions, and interacts with NFR5 in the heterologous yeast and tobacco systems (Ke et al., 2012). Moreover, NFR5 and ROP6 co-localize. ROP6 is vital for the progression of ITs through the epidermis and was likewise suggested to link symbiotic signaling with arranging the actin cytoskeleton (Ke et al., 2012). A role in clathrin-mediated endocytosis during IT-progression was also hypothesized (Wang et al., 2015a). In common bean (*Phaseolus vulgaris*), silencing the small GTPase *Rab2A*, which localizes to root hair tips, leads to a short root hair-phenotype, and the inability of the plant to initiate root hair deformations and ITs in response to the symbiont *Rhizobium etli* (Blanco et al., 2009).

Another promising candidate could be the GTPase DYNAMIN 2B (DRP2B, Accession Medtr4g030140), which was differentially phosphorylated upon rhizobial inoculation in *Medicago* (Rose et al., 2012). Dynamins can be recruited to precise locations at the PM by protein and lipid interactions, and are involved membrane-deformation and -scission events (Praefcke and McMahon, 2004). Dynamins directly influence cytoskeletal dynamics of mammalian cells (Gonzalez-Jamett et al., 2013; Morlot and Roux, 2013). In *Arabidopsis*, DRP2B localizes directly underneath the PM of root hair tips, where it oligomerizes (Taylor, 2011). Along with DRP2A, DRP2B is essential for clathrin-mediated endocytosis at the PM (Fujimoto et al., 2008; Fujimoto et al., 2010; Huang et al., 2015). Intriguingly, DRP2B also plays a role in ligand-induced endocytosis of the plant flagellin receptor FLS2 (Flagellin Sensing 2) (Smith et al., 2014).

Endocytosis of cell-surface receptors (or other proteins) may be a way to fine-tune, or temporarily terminate, signaling at the PM. During plant immunity responses towards pathogens, such a mechanism presumably exists and is associated with the formation of MDs (Geldner and Robatzek, 2008; Hao et al., 2014). In *Arabidopsis*, AMMONIUM UPTAKE TRANSPORTER (AMT1;3) dynamically locates in the PM in unique MDs; under high ammonium stress, these puncta cluster into bigger structures, which are then internalized. This may be a way to regulate the uptake of too much ammonium, which is toxic to the cell (Wang et al., 2013). A similar role for DRP2B, involved in negatively regulating signaling during IT-initiation, and progression, is conceptually possible, and endocytosis could take place in/at a symbiotic MD.

4.6.2 E3 Ubiquitin Ligases

If endocytosis plays a prominent role during the infection process remains to be determined, however, E3 ubiquitin ligases, which target symbiotic receptors, have been identified. Ubiquitination is a common mechanism to label membrane proteins to enter the endocytic

pathway for subsequent lysosomal/vacuolar degradation (Hicke, 1997; Bonifacino and Weissman, 1998; Scita and Di Fiore, 2010). It also is implicated in non-proteolytic processes such as vesicle trafficking or activation of signaling pathways (Ikeda and Dikic, 2008; Komander, 2009; Yang et al., 2010). Plant immune receptors are regulated by ubiquitination and ligand-induced endocytosis to attenuate signaling (Robatzek et al., 2006; Gohre et al., 2008; Gimenez-Ibanez et al., 2009; Lu et al., 2011; Furlan et al., 2012). Interestingly, six hours after NF application LYK3:GFP localizes to mobile internal vesicles, however, LYK3 is also present at the IT-membrane throughout the infection (Haney et al., 2011).

PUB1 (PLANT U-BOX PROTEIN 1) of *Medicago truncatula*, is induced by Nod factors, and directly interacts with (and is phosphorylated by) the kinase domain of LYK3 (Mbengue et al., 2010). It acts as a negative regulator of infection and nodulation. Because no indications were found that the PUB1 activity targets LYK3, it was hypothesized that LYK3 activates PUB1 to then target other symbiotic proteins for internalization at the PM (Mbengue et al., 2010). Since LYK3 is immobilized in MD, PUB1 itself, or its targets, may also be present in MDs.

In *Lotus japonicus*, the E3 ubiquitin ligase SINA (SEVEN IN ABSENTIA) interacts with the receptor SYMRK. Co-expressing both, in the heterologous tobacco system, leads to a dramatic reduction of SYMRK levels at the PM, and SYMRK appears as punctate structures in the cytosol. Strikingly, prior to the hypothesized internalization and degradation of SYMRK, SINA and SYMRK co-localize in specific MDs at the PM in tobacco (Den Herder et al., 2012). Other E3 ubiquitin ligases involved in RNS have been identified (Kiss et al., 2009; Yano et al., 2009). These data point towards an involvement of endocytosis-related proteins in MDs during RNS. SYMRK-INTERACTING E3 UBIQUITIN LIGASE (SIE3) directly binds to, and ubiquitinates, SYMRK. However, SIE3 is a positive regulator of RNS (Yuan et al., 2012) suggesting a role different to endocytosis of SYMRK for the attenuation of signaling.

4.6.3 Proteins Required for Exocytosis

For symbiosome formation in the nodule, bacterial release from nodular infection threads requires exocytosis (Catalano et al., 2007; Ivanov et al., 2012). Exocytosis is a secretory process, during which vesicles fuse with the membrane, facilitated by SNARE proteins (SOLUBLE N-ETHYLMALIMIDE SENSITIVE FACTOR ATTACHMENT PROTEIN RECEPTOR). A vesicle-SNARE (vSNARE) usually binds to three target-SNAREs (tSNARE), where a ‘zipper-like process’ is believed to enforce vesicle fusion (Lang and Jahn, 2008). In *Medicago truncatula*, the two vSNARE proteins, VAMP72d and VAMP72e (VESICLE-ASSOCIATED MEMBRANE PROTEINS), are vital for symbiosome formation during RNS. They are also required for AM-symbiosis (Ivanov et al., 2012). These proteins localize to sites of bacterial release and on the

symbiosome membrane in nodules. Silencing *MtVAMP72d*, and *MtVAMP72d*, impairs the release of bacteria from nodular infection threads (Ivanov et al., 2012). Interestingly, live cell imaging of constitutively expressed GFP:*MtVAMP721e* revealed this protein localizes to the tip of growing root hairs during early stages of symbiosis (Fournier et al., 2015). Upon rhizobial inoculation, GFP:*MtVAMP721e* accumulates at the PM of the infection chamber in the curled root hairs. Intriguingly, this process was dependent on the RNS-specific gene *NODULE INCEPTION (NIN)*, demonstrating that the accumulation in the infection pocket is part of a specific symbiotic program (and not the result of constitutive overexpression) (Fournier et al., 2015). This emphasizes the requirement of targeting vesicles (with their cargo, e.g. membranes, extracellular material etc.) to the place where the IT will be formed. MDs could very well serve as anchor points in the PM, where the vesicles will fuse.

4.6.4 Cell-wall-degrading Enzymes

Possible cargo of vesicles could be enzymes for the degrading of cell wall material. The *Lotus* NODULATION PECTATE LYASE (*LjNPL*) degrades pectin, a prominent component of the cell wall. Mutants form very few functional nodules; most infections are arrested at the microcolony stage in curled root hairs, and proper ITs are only rarely formed (Xie et al., 2012). Another cell-wall degrading enzyme *Medicago sativa* POLYGALATURONASE 3 (*PG3*), encoded by the plant, is specifically expressed under symbiotic conditions (Munoz et al., 1998; Rodriguez-Llorente et al., 2003). Cell-wall-degradation, -synthesis, or -remodeling, are compulsory for root hair curling, IT-initiation, and -progression. The degrading of the cell wall occurs locally, and again it is possible that MDs serve as hubs for these enzymes, ensuring proper positioning. *SYMREM1* or the symbiotic Flotillins (*FLOT4*, *FLOT2*) may recruit these proteins into MDs, or assist in their targeted delivery. In addition to plant-derived cell-wall degraders, rhizobia also produce such enzymes (Mateos et al., 1992; Robledo et al., 2008), thereby loosening the cell wall from the outside. Symbiotic MDs may form at these locations, with receptors monitoring the walls integrity.

4.6.5 Exopolysaccharides Receptors

In addition to Nod factors, rhizobia produce lipopolysaccharides, cyclic beta-glycan (D'Antuono et al., 2005), and exopolysaccharides (EPS) that are recognized by the plant and important for infection (Leigh et al., 1985; Cangelosi et al., 1987; Leigh et al., 1987; Gonzalez et al., 1996; Jones et al., 2008; Downie, 2010). IT-initiation and –elongation, in *Lotus japonicus*, is diminished in the presence of rhizobia producing incompatible or mis-structured EPS (Kelly et al., 2013). Plants continuously monitor EPS during the infection process as a means to distinguishing

beneficial bacteria from other endophytes (or pathogens). This serves as a mechanism for the plant to either support, or block infection (Zgadzaaj et al., 2015). Only recently, The EXOPOLYSACCHARIDE RECEPTOR 3 (EPR3) was identified, that directly recognizes EPS in *Lotus japonicus*. After NF-detection, EPR3 is expressed in root hairs and the epidermis (Kawaharada et al., 2015). It would be interesting to see if EPR3 resides in MDs, or interacts with other symbiotic receptors, the symbiotic flotillins, or SYMREM1.

4.6.6 DMI2/ SYMRK and Its Interactors

Another potential protein localizing to/ interacting with components of symbiosis-specific MDs could be the symbiotic receptor DMI2/SYMRK (Endre et al., 2002a; Stracke et al., 2002). SYMRK is known to interact with NFR1 and NFR5 *in vivo*, and constitutive overexpression of these receptors individually induces spontaneous nodule organogenesis (Antolin-Llovera et al., 2014; Ried et al., 2014). Interestingly, only overexpression of SYMRK simultaneously activates RNS and AM-specific responses (Ried et al., 2014), two processes that are usually tightly separated, confirming an active signaling role for SYMRK in both symbiotic programs. Thus, SYMRK is placed at the beginning of the junction for RNS or AM-specific signaling (Ried et al., 2014). SYMRK function appears to be regulated by a complex mechanism that involves (tissue- and species- independent) constitutive cleavage of an extracellular malectin-like domain (resulting in SYMRK- Δ MLD) that makes the cleaved receptor less stable, but enhances its interaction with NFR5 (Antolin-Llovera et al., 2014). How this precisely integrates into RNS specific signaling is not known, yet. However, it was hypothesized that SYMRK may have both a positive signaling role (induces nodule organogenesis), while SYMRK- Δ MLD negatively regulates signaling at the PM by associating with NFR5 prior to internalization and degradation (Antolin-Llovera et al., 2014; Ried et al., 2014). A hyper infection thread phenotype when overexpressing a SYMRK variant lacking the whole extracellular domain emphasizes the need for tight regulation (Antolin-Llovera et al., 2014). It would be interesting to investigate if SYMRK/DMI2 signaling (transiently) occurs in MDs and could provide a clue as to how specificity of the symbiotic programs (RNS vs. AM) is achieved. SYMRK/DMI2 is known to interact with the RNS specific MD-marker SYMREM1 (Lefebvre et al., 2010; Tóth et al., 2012). One hint is provided by a stable pDMI2::DMI2:GFP expressing *Medicago* line, in which DMI2:GFP localizes into clear punctate MDs in the PM of root hairs (Riely et al., 2013). After external NF application, a sharp increase in DMI2:GFP containing cytosolic vesicles was observed (Riely et al., 2013), suggesting MDs and endocytosis of this symbiotic receptor indeed play a role .

Discussion

Furthermore, the kinase activity of the SYMRK-interacting MAP Kinase Kinase SIP2, which may be involved in transmitting PM-resident signaling to the nucleus, is negatively regulated by SYMRK (Chen et al., 2012). SIP2, like SYMRK/DMI2, localizes to the PM (Capoen et al., 2005; Limpens et al., 2005; Chen et al., 2012). It would be interesting if a more detailed investigation on the subcellular localization of SIP2, and its signaling targets, would reveal transient associations to symbiotic MDs.

The DMI2-interacting enzyme HMGR1 (3-HYDROXY-3-METHYLGLUTARYL COA REDUCTASE 1) is also a possible candidate. Localization studies have only been performed in *Arabidopsis* protoplasts, where HMGR1 was present in the membranes of what were presumed to be endoplasmic reticulum-derived vesicles. Where this protein would localize in the homologous system has not been shown yet. It was hypothesized that upon symbiotic stimuli, HMGR1, located in the membrane of vesicles (with the catalytic domain protruding into the cytosol), would interact with DMI2, upon which the vesicles would fuse with the PM. This would result in the creation of a specific MD at the PM (Kevei et al., 2007). That the product of HMGR1 enzymatic activity, mevalonate, relays the signal from the PM to the nuclear envelope to elicit symbiotic spiking has recently been demonstrated (Venkateshwaran et al., 2015).

4.6.7 NADPH Oxidases

Additionally, NADPH oxidases RBOH (RESPIRATORY BURST OXIDASE HOMOLOGS), which produce reactive oxygen species (ROS) are possible candidates that could be present in a symbiosis related MD. The common bean (*Phaseolus vulgaris*) RbohB localizes to the PM of root hair tips, (similar to FLOT4 and LYK3 (Haney et al., 2011)). In *RbohB* RNAi silenced plants, the ITs do not advance past the outer epidermal cell layer (i.e. they arrest within root hairs) (Montiel et al., 2012). *Medicago* RBOHs are also implicated in root nodule symbiosis (Marino et al., 2011), where they could be involved in the polar directing of ITs. ROS, as signaling molecules, have an impact on the actin cytoskeleton to direct vesicular trafficking, the rigidity of the cell wall, and the activation of Ca²⁺ channels (that induce a calcium flux) during the polar development of root hairs (Foreman et al., 2003; Monshausen et al., 2007; Ishida et al., 2008; Takeda et al., 2008; Cardenas, 2009). In RNS, similar roles for RBOHs are conceivable and MDs could serve as targets for these enzymes.

Several other candidates that could play a role during the infection process were identified to be differentially phosphorylated, and/or upregulated upon NF-detection/rhizobial inoculation (Rose et al., 2012; Breakspear et al., 2014). These include an actin-nucleating gene *ABIL1* (ABL-INTERACTOR-LIKE 1), a sugar transporter (*SWEET13*), a sucrose synthase (*SUCS1*), other RLKs (e.g. *LYK10*, LYK-related receptors *LYRs*) and a subtilase (Breakspear et al., 2014).

4.7 Outlook

The (co-) localization studies performed in this work are based on transiently transgenic systems that are constitutively overexpressing the constructs analyzed. It would be of great interest (and importance) to investigate the precise localization of SYMREM1, FLOT4 and LYK3 under lower expression conditions. Unfortunately, in experiments in which these proteins were expressed from native promoters, the fluorescent signal intensities were not detectable with the confocal microscope available. In the previous publication, the observations of FLOT4 and LYK3 localizing on infection thread membranes in their native context were only possible with spinning disk confocal microscopy (and a better detection camera) (Haney et al., 2011). More advanced microscopic methods, e.g. Total Internal Reflection Fluorescence Microscopy (TIRF), or Photoactivated Localization Microscopy (PALM) will have to be applied in order to investigate symbiotic MDs in low expressing (native) situations.

The prolonged activation of signaling by NFP/NFR5 with LYK3/NFR1 triggers defense like responses in nodules (Moling et al., 2014), or a hypersensitive cell death in *Nicotiana* (Madsen et al., 2011; Pietraszewska-Bogiel et al., 2013). Likewise, the receptors will be activated, and different proteins will be associated with symbiotic MDs, only transiently. The composition of the symbiotic MDs will vary at different stages of the progressing infection, to efficiently modulate the signaling required for successful infection. A live cell imaging setup would be greatly beneficial to screen these events precisely during the different stages. The initiation, and progression, of the IT has been very well observed by such a method (Fournier et al., 2008; Fournier et al., 2015). However, this approach would be limited by the necessity of fluorophore-tagged proteins of interest, and therefore is most efficient for the targeted verification, or identification, of individual symbiotic players.

A biochemically complementary approach to this could be the establishment of a BioID (biotin identification) protocol (Roux et al., 2012; Roux et al., 2013). Although not tested in plants yet, this method is a proximity-based assay that relies on the enzyme ‘biotin ligase’ (BirA*) that is fused to a protein of interest, and expressed *in vivo*. Neighboring proteins, even those that only transiently or weakly interact with the tagged protein, become biotinylated. Marked proteins can then be identified by immunodetection, or mass spectrometry. By fusing BirA* to SYMREM1, or FLOT4, one could identify and confirm potential MD-associated proteins biochemically, on a larger scale than microscopic methods would allow.

5 Methods

5.1 Cultivation Methods

5.1.1 Bacterial Growth Conditions

The *Escherichia coli* strains, DH5 α and TOP10, were grown at a constant temperature of 37°C. Liquid cultures were shaken at 200 rounds per minute (rpm). As culture medium, LB medium, containing the appropriate antibiotics, was used. The *Agrobacterium tumefaciens* strains GV3101, AGL1 and Arqua1 were grown at 28°C for 2-3 days in or on selective LB medium.

The *Sinorhizobium meliloti lacZ* and *S. m.* DsRED strains were grown in or on TY-Medium supplemented with 6 mM CaCl₂ and 15 μ M tetracycline and incubated at 28°C. Liquid cultures were also shaken at 200 rpm.

5.1.2 Rhizobial Inoculation of *Medicago truncatula*

A *Sinorhizobium meliloti* DsRED 60% glycerol stock culture was struck on TY-Medium supplemented with 6 mM CaCl₂ and tetracycline (15 μ g/ml) and incubated at 28 °C overnight. A 20 ml overnight culture was inoculated and grown overnight at 28°C, 200 rpm. Cells were harvested by centrifugation at 4000 rpm for 5 min and washed twice with water. Plants were spot-inoculated with rhizobia at a final O.D._{600nm} of 0.005 and analyzed 4 dpi.

5.1.3 *Nicotiana benthamiana* Growth Conditions

Prior to infiltration, *N. benthamiana* plants for were grown 4 weeks in a walk in growth chamber set at 24°C in long day conditions (16 h light/8 h darkness).

5.1.4 *Medicago truncatula* Growth Conditions

Medicago truncatula plants were grown on square plates in Sanyo incubation chambers under repetitive periods of 16 h light and 8 h darkness. The first week temperature was 20°C, then for weeks 2-3 the temperature was raised to 24°C. For seed production, seedlings were grown in dirt

supplied with Osmocote fertilizer in the greenhouse for 5 months under long day conditions (16 h day/8 h darkness). Prior to seed harvest the plants were dried for 1 week.

5.2 Transformation Methods

5.2.1 Transformation of *Escherichia coli*

Chemically competent *E. coli* cells frozen at -80°C in 20% glycerol were thawed on ice prior to the addition of 15 ng plasmid DNA (or 3 µl of an cut-ligation reaction). The reaction was incubated on ice for 30 minutes. A 30 s heat shock of 42°C was applied and the cells placed back on ice, briefly. After the addition of 250 µl of LB medium, an incubation period of 1 h at 37°C 200 rpm ensued. Cells were then plated on the appropriate media. Successful transformation was verified by colony PCR.

5.2.2 Transformation of *Agrobacterium* Strains

Electro-competent *Agrobacterium tumefaciens* (strains AG11 or GV3101) cells were stored as 50 µl aliquots at -80°C in 20% glycerol. For transformation, cells were thawed on ice, ~15 ng plasmid DNA were added and the mixture was transferred into a precooled electroporation cuvette. The settings were: Voltage 1.25 V, current: 25/25/125 F (Farad) and the Ohmic resistance was 200 Ω. After the pulse of current, 200 µl of LB media were added and the cells were incubated at 28°C at 200 rpm for a minimum of 1.5 h. 20 µl of the culture was plated onto selective LB plates. Successful transformation was verified by colony PCR.

5.2.3 Transient Transformation of *Nicotiana benthamiana* Leaves

Nicotiana benthamiana leaf infiltration was performed as previously described (Tóth et al., 2012; Jarsch et al., 2014). *Agrobacterium tumefaciens* GV3101 or Ag11 were infiltrated at a final OD_{600nm} of 0.4 for p35S::LYK3-GFP and 0.005 for pUbi::HA:SYMREM1. Level 2 single expression vectors and Level 3 co-expression vectors obtained by Golden Gate cloning (Binder et al., 2014) were infiltrated with a final OD 600nm of 0.1 in presence of the silencing suppressor P19 (Koncz et al., 1989). The infiltration with the FLOT4:RNAi silencing construct, as well as the respective controls, were performed without P19. Microscopy was performed 2 and 3 days post infiltration. To obtain full PM localization of LYK3 and minimize possible interference with the still trafficking protein fraction, microscopy involving LYK3:GFP or LYK3:HA constructs was conducted three days after leaf infiltration.

5.2.4 Sterilization and Germination of *Medicago truncatula* Seeds

Seeds were treated with 98 % sulfuric acid for 10 min, or until brown spots appeared on the seed coat, then the sulfuric acid was removed and the seeds washed 6 times with a large volume of sterile distilled water. Then, a bleach solution (1.2 % Sodiumhypochloride, 0.1 % SDS in water) was applied for 1 min, and then removed. Again, the seeds were rinsed with large volumes of water 6 times, and then placed on a water agar plate. The plate was sealed with parafilm, an air hole was punctured into the seal, and the plate wrapped in aluminum foil. The seeds were placed upside down at 4°C for 3 days, and then germinated, still upside down, at 24°C for 24 h in darkness.

5.2.5 Transient Transformation of *Medicago truncatula*

M. truncatula hairy root transformation was performed as previously described, with slight modifications using the *Agrobacterium rhizogenes* strain ARQUA1 (Boisson-Dernier et al., 2001; Konrad et al., 2014). Sterilized seeds were vernalized for 3 days at 4°C, then germinated overnight at 24°C. Seedlings were cut above the root radicle with a blade and the plant's wound was dipped into the *Agrobacterium* culture grown for two days on selective LB-plates. The seedlings were placed along a line on Fahrhaeus (FP) medium plates (Boisson-Dernier et al., 2001) with p.H. 6.0 supplemented with 1 mM NH₄NO₃. The plants were grown at 20°C (sometimes 22°C) for the first week, then transferred weekly onto new plates and grown at 24°C. All plants that were transformed with a fluorescent construct were screened by the detection of fluorescence 3-4 weeks post transformation. The pFLOT4::NLS:2xGFP and pSYMREM1::NLS:2xGFP transformed plants were grown under selective pressure on FP medium supplemented with 25 µg/ml Kanamycin. Prior to rhizobial inoculation the plants were starved of nitrogen of 5 days.

5.3 Confocal Microscopy

For microscopic analysis, leaf discs of 5 mm width were punched out from *N. benthamiana*, or transgenic *M. truncatula* roots were cut with a scalpel and mounted on glass slides and imaged directly in water. Confocal laser scanning microscopy was performed on a Leica TCS SP5 confocal microscope equipped with 63x and 20x HCX PL APO water immersion lenses (Leica Microsystems, Mannheim, Germany). GFP was excited with the Argon laser (AR) line at 488 nm and the emission detected at 500-550 nm. YFP was excited with the 514nm AR laser line and detected at 520–555 nm. mCherry was excited using the Diode Pumped Solid State (DPSS) laser at 561 nm and emission was detected between 575-630 nm. Excitation of Cerulean was performed

at 860 nm with a picosecond rate Ti:Sapphire (Mai Tai) multi-photon laser pulsing at 80 MHz, and emission was detected at 470-530 nm. Samples that were co-expressing two fluorophores were imaged in sequential mode between frames. Images were taken with a Leica DFC350FX digital camera. During stack acquisition, slices were usually taken, at 0.5 μm increments. 3 line and 2 frame averages were used mostly during image acquisition.

5.4 FLIM-FRET Microscopy

5.4.1 Interaction Between SYMREM1 and NFR1/LYK3

The *L. japonicus* SYMREM1 (region) constructs, as well as the NFR1 constructs were cloned into the pAMPAT::35S vector series by LR reactions, thereby fusing the fluorophores Cerulean or mOrange to their C-terminus. The *M. truncatula* SYMREM1 constructs, under the p35s promoter, were N-terminally fused to mCherry through Golden Gate cloning. P35s::LYK3:GFP was cloned with the Golden Gate procedure.

To confirm expression in *N. benthamiana*, fluorescence was first detected by CSLM as described above. A HCX PL APO 20.0x 0,70 IMM UV water-immersion objective lens was used for imaging cells during FLIM measurements. In the LASAF software, the pixel format 256x256 was chosen, and the pinhole set at 9.89. MP laser settings were set at 12.5 % gain, 12.5 % offset and the MP laser at 1.

The predefined setup, 256_256_80mhz-256tch, was selected in the SPCM data acquisition software. Then, the donor fluorophore was excited by a Ti:Sapphire (Mai Tai) picosecond-pulse multi-photon laser set at 810 nm for Cerulean (or 900 nm for GFP), pulsing at 80 MHz. Photons were collected for 5 min in 64 cycles (≈ 5 s/cycle).

Only selected, magnified areas of the cells were subjected to FLIM analysis, which was performed with SPCImage software version 2.8 (Becker & Hickl). Several regions of interest (ROIs) were chosen per lifetime image, each time choosing the brightest (or nearly brightest) pixel as reference to calculate the instrument response function. To reduce the signal to noise ratio, pixels were binned mostly by the factor 3-4, and in a few cases, if necessary up to a factor of 6. A threshold value of 20 was implemented. The components were chosen to yield a X^2 fit closest to 1.0 (most often in the range of 0.97-1.07). Finally, the fluorescence decay matrix was calculated, yielding a value for Cerulean or GFP lifetime. Data were statistically analyzed using Student's's t-test ($p < 0.01$).

5.4.2 Interaction Between Strubbelig and Quirky

Settings for FRET-FLIM analysis and measurements were adapted from above. FLIM was performed using a Leica SP5 confocal microscope with an integrated ~100 femtosecond pulse-Ti:Sapphire laser (Mai Tai) with a 80 MHz pulse rate, for multi-photon excitation and a fast FLIM photomultiplier (Becker & Hickl, Berlin, Germany). Two-photon excitation of the donor fluorophore eGFP (pSUB::gSUB:eGFP) was done at 900 nm and fluorescence detected between 500-580 nm. Time-correlated, spectral-photon counting was performed for a maximum of 5 min and 64 scanning cycles with a spatial resolution of 256x256 pixels. Fluorophore lifetimes at the plasma membranes were determined using SPCImage software version 2.80 (Becker & Hickl) and with image-adapted settings. A total of 40 images from a minimum of 12 independent roots were acquired and evaluated. For PD-confined lifetime analysis, five individual spots were analyzed per image, resulting in over 200 measurements per genotype. Data were statistically analyzed using Student's t-test.

5.5 Image Processing

5.5.1 Co-localization Analysis

Image analysis was performed with the open source ImageJ/(Fiji) software (Schindelin et al., 2012). For illustration, images were background subtracted according to the rolling ball algorithm, filtered with a Mean filter pixel radius of 1 and then maximum z-projected ('create stack'). Contrast was enhanced for visualization in figures but not for quantification. Pixel based co-localizations to determine Pearson Correlation Coefficient values were performed using the Fiji Plugins 'Squassh' (Rizk et al., 2014) and 'JACoP' (Bolte and Cordelieres, 2006). Image segmentation was performed with 'Squassh'. Randomization was performed with the automatic Costes' Randomization method in 'JACoP', in which one channel was clustered into blocks of 10x10 pixel. These were then randomly distributed in one channel and correlated to the original image of the other channel. This was performed 200 times for each image. The randomized correlation coefficient r_d was then compared to the original R_r . Additionally, randomization was also performed on maximum z-projections via horizontal flip of one channel as described previously (Jarsch et al., 2014).

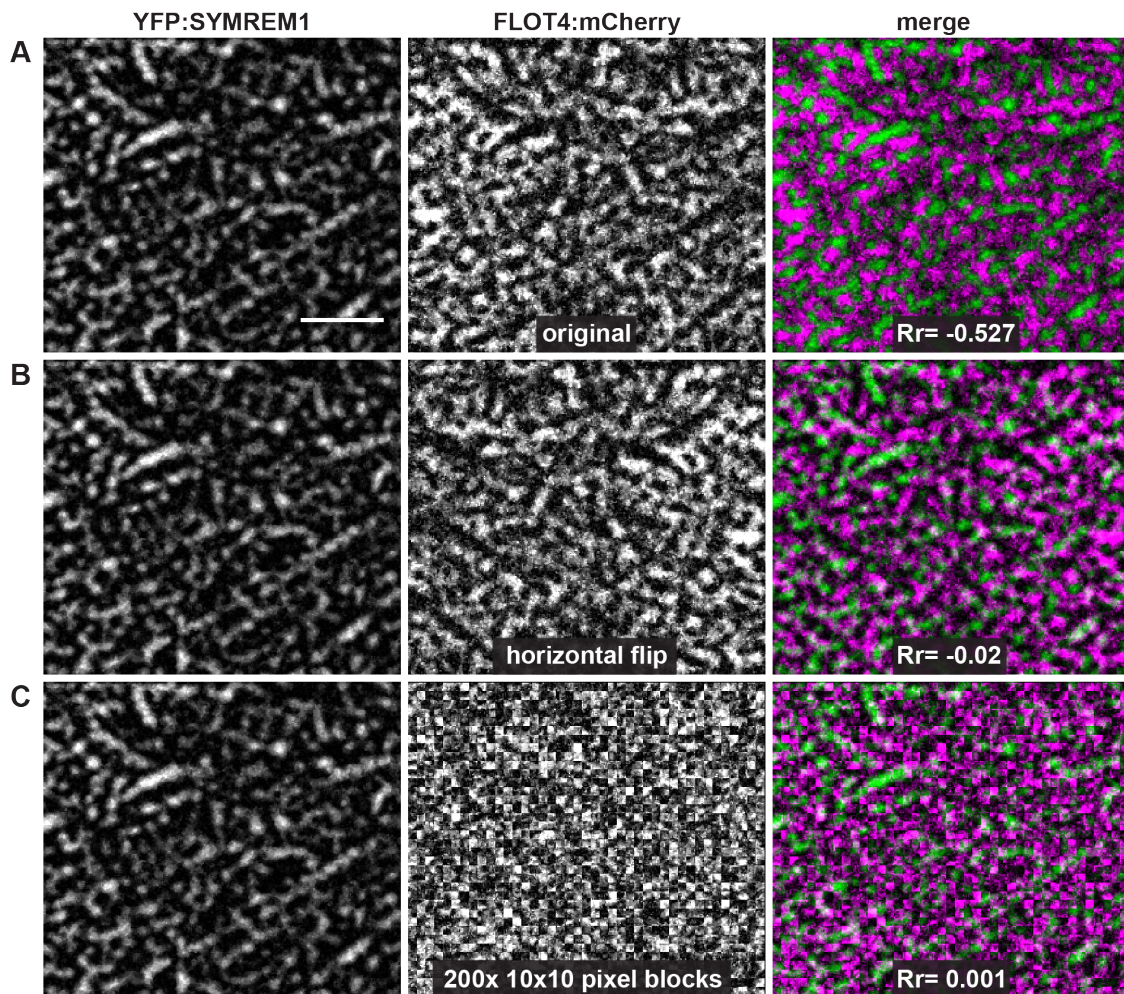


Figure 28 The procedure of co-localization analysis and verification by randomization.

Measuring the correlation coefficient, here shown with the example of a *Nicotiana benthamiana* leaf cell that is expressing YFP:SYMREM1 and FLOT4:mCherry. **(A)** YFP:SYMREM1 and FLOT4:mCherry images were background subtracted to reduce noise. The Pearson correlation coefficient R_r was measured with the FIJI/Image plugins JACoP and Squassh. Here, an exclusion was detected, shown by the highly negative $R_r = -0.527$. For the verification of co-localization two randomization procedures were performed. **(B)** The FLOT4:mCherry channel was horizontally flipped and then merged onto the original YFP:SYMREM1 image. Then, JACoP and Squassh were applied accordingly. This led to a $R_r = -0.02$ indicating random distribution between the channels. **(C)** The Costes' randomization procedure arranged the FLOT4:mCherry channel into random blocks of 10x10 pixels. This was performed 200 times. These 200 images were individually and automatically merged with the YFP:SYMREM1 channel and the correlation coefficient was measured each time. Here, the value of $R_r = 0.001$ demonstrates complete randomness. The scale bar in the top left image indicates 10 μm .

5.5.2 Domain Counting

YFP:SYMREM1, LYK3:GFP or FLOT4:mCherry domain images were segmented to differentiate background from domains. For this, the background was subtracted with the rolling ball algorithm with a radius corresponding to the largest structure of interest. In essence, the largest domain was encircled, and its dimension was used for the radius. A mean blur with radius 1 was then applied, and the slices of the region of interest or cell (usually $n= 5-12$ slices, with distances of mostly $0.5 \mu\text{m}$) maximum projected along the z-axis. One additional background subtraction step was performed. The threshold was determined automatically with the use of the ‘automatic threshold’ plugin in Fiji. The best threshold was applied to the images and the result saved as a binary mask. The ‘create selection’ tool was used to mark the outlines in the binary mask that were overlaid onto the original image to verify proper image segmentation. Domains were then counted with the ‘particle analyzer’ tool in Fiji.

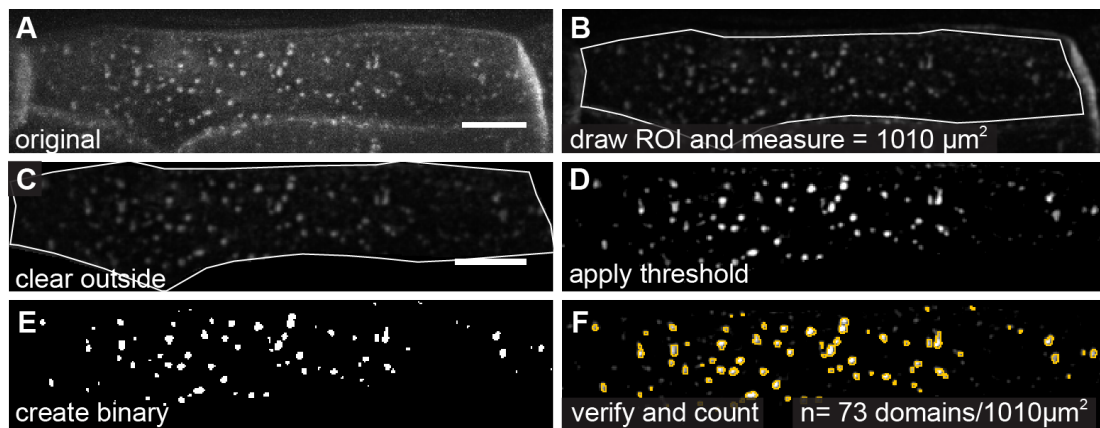


Figure 29 The steps for domain counting. Step by step processing of an image for domain counting, here shown for a root cell of *Medicago truncatula hcl-4* transformed with YFP:SYMREM1 (A) Representative image of an unprocessed maximum projection ($z= 6$ slices with $0.5 \mu\text{m}$ increments) of a single cell. Typical microdomains were detectable. (B) The same image after the subtraction of background signal with the rolling ball method. A Gaussian filter with radius 1 was applied. A region of interest (ROI) was drawn and the surface area measured. (C) The outside of the ROI was removed. (D) The image was adjusted for brightness and a threshold applied automatically to reduce the presence of leftover background pixels. (E) A binary mask was created showing the domains (white) and background (black). (F) With the create selection tool, the outlines of the MDs were drawn and applied onto the figure in (C) to verify proper image segmentation. Domains were then counted with the particle analyzer tool in Fiji/ImageJ. Scale bars indicate $10 \mu\text{m}$.

5.5.3 Determination of Actin Orientation

The orientation of the actin cytoskeleton was analyzed in Fiji using the open source plugin ‘Fibril Tool’ (Boudaoud et al., 2014). For this, regions of interest were drawn manually around single cells of a maximum z-projected stack (usually 3-5 slices of $0.5 \mu\text{m}$ depth), and then analyzed individually. During microscopy, the produced images of the root cells were aligned horizontally with the cell-elongation axis by the use of the ‘rotate’ knob of the control panel of the Leica

Application Suite. If this was not immediately possible, the images were rotated accordingly in FIJI, prior to analysis.

5.6 Cytoskeleton Disruption

A 1mM oryzalin (SIGMA-ALDRICH) stock solution in DMSO and a 10 mM cytochalasin D (SIGMA ALDRICH) stock solution in DMSO were prepared. *Medicago truncatula* root samples of 1 cm length were incubated in final concentrations of 10 μ M oryzalin or 10 μ M cytochalasin D for 12 hours in water. The control samples were incubated in water with the equal amount of solvent for the same amount of time.

5.7 Molecular Biology Methods

5.7.1 PCRs

Standard colony PCRs, to verify correctly transformed clones, were performed in 20 μ l reactions with Taq polymerase, according to general recommendations from the New England Biolabs protocol. The elongation time was calculated from the length of the template and the speed of the polymerase (30 s/1000 base pairs). The initial denaturing temperature used was 94°C, the elongation temperature was set to 72°C.

For the amplification of DNA fragments meant for cloning, the Phusion High Fidelity or the OneTaq DNA polymerases (NEB) were used according to New England Biolabs recommendations. The annealing temperatures were set at 2°C below the melting temperature of the primers. The initial denaturing step was performed at 98°C for 30 sec.

5.7.2 Cloning

The coding sequence of *Medicago truncatula* SYMREM1 (GenBank accession JQ061257) was recombined into the Gateway compatible pUBi::YFP:GW:HYG vector (Konrad et al., 2014) via classic LR-reaction. All other constructs were cloned as Golden Gate compatible constructs. Bpi and BsaI restriction sites were removed from: MtSYMREM1, LYK3 (GenBank accession AY372406), MAP4 (GenBank accession: M72414) cDNA templates, as well as the genomic FLOT4 (GenBank accession: GU224281) and FLOT2 (GenBank accession: GU224279) and the pSYMREM1 promoter sequence. The 2 kilobase promoter sequence of FLOT4 was synthesized by GenScript with Golden Gate compatible (A-B) BpiI/BsaI overhangs in the pUC-AMP vector.

Methods

A double stranded Lifeact template, with flanking BsaI restriction sites, was generated by primer annealing and directly inserted into pUC-Bpi via blunt end StuI (NEB) cut-ligation for subsequent Golden Gate cloning. Double-stranded sequences for the FLOT4:RNAi constructs with flanking BsaI sites were also cloned via blunt-end StuI cut-ligation into pUC-Bpi. The RNAi silencing vectors were assembled as previously described (Binder et al., 2014). Level 2 single expression and Level 3 double and triple expression vectors for microscopy were assembled in a Golden Gate compatible fashion (Binder et al., 2014).

Gateway-compatible entry vectors for FLIM-FRET analysis of LjSYMREM1/NFR1 and the destination vectors for expression in *Nicotiana* were created via TOPO cloning or BP reaction according to recommended protocols (Thermo Fisher Scientific). The FLIM-FRET constructs of LjSYMREM1 and NFR1 are described in (Tóth et al., 2012),

5.7.3 Western Blot

Nicotiana benthamiana leaf disks were harvested 3 dpi and shock-frozen with liquid nitrogen. Proteins were extracted by grinding 3 leaf disks (5 mm diameter) in lysis buffer (150 mM NaCl, 10 mM TrisHCl pH 7.5, 1% Triton-X-100, 1 mM EDTA, 2 mM DTT, Pefabloc, protease inhibitor cocktail). Samples were then spun down at 14000x g at 4°C and pellets were discarded. The samples were diluted with 5x SDS-sample buffer and denatured at 70°C for 5 min. Samples were loaded onto 10% polyacrylamide SDS- polyacrylamide gels and transferred onto a nitrocellulose membrane with the 'Trans-Blot Turbo Transfer System' (BIO RAD) using the 'STANDARD SD' protocol (30 min, 1.0 A, 25 V constant). For blocking and antibody incubation, the SNAP i.d. 2.0 protein detection system was used. The membrane was blocked with 3% milk in 1xTBS-Tween (0.1%) and incubated with the anti-HA-antibody that was directly conjugated with horseradish peroxidase (dilution 1:3000, Roche). Detection of proteins was performed with the SuperSignal™ West Pico Chemiluminescent Substrate (Pierce).

5.7.4 Constructs Used/Generated in This Study

LEVEL 0	Vector	Purpose
LYK3 part1	1593 pUC-AMP	Subcloning
LYK3 part2	104 pUC-AMP	Subcloning
LYK3 part 3	261 pUC-AMP	Subcloning
gFLOT4 part 1	144 pUC-AMP	Subcloning
gFLOT4 part 2	105 pUC-AMP	Subcloning
gFLOT4 part 3	2087 pUC-AMP	Subcloning
gFLOT2 part1	pUC-AMP	Subcloning
gFLOT2 part2	pUC-AMP	Subcloning
MAP4 part1	346 pUC-AMP	Subcloning
MAP4 part2	820 pUC-AMP	Subcloning
MAP4 part3	188 pUC-AMP	Subcloning
LEVEL 1	Vector	Purpose
LYK3 cDNA	B-C pUC-Bpi	For cloning in Level 2
MtSYMREM1 cDNA	C-D pUC-Bpi	For cloning (cloned by C. Popp, LMU)
MtSYMREM1 _c	C-D pUC-Bpi	For cloning (Dr. M. Marin, LMU)
MtSYMREM1Δ1	C-D pUC-Bpi	For cloning (M. Marin)
MtSYMREM1Δ2	C-D pUC-Bpi	For cloning (M. Marin)
MtSYMREM1Δ3	C-D pUC-Bpi	For cloning (M. Marin)
Lifeact	C-D pUC-Bpi	For cloning
MAP4	C-D pUC-Bpi	For cloning
FLOT4 genomic	C-D pUC-Bpi	For cloning
FLOT2 genomic	C-D pUC-Bpi	For cloning
pSYMREM1 643bp	A-B pUC-Bpi	For cloning (C. Popp)
pFLOT4 2000bp	A-B pUC-AMP	For cloning
FLOT4:RNAi	C-D pUC-AMP	For cloning
FLOT4:RNAiLong	C-D pUC-AMP	For cloning
LEVEL 2	Vector	Purpose
pUbi::YFP:MtSYMREM1	L2cF1-2	Cloning into Level 3
pUbi::YFP:MtSYMREM1	L2βF1-2	Nicotiana expression
pUbi::YFP:MtSYMREM1	L2R3-4	<i>Nicotiana/ Medicago</i> expression
pUbi::mCherry:MtSYMREM1	L2βR3-4	<i>Nicotiana</i> expression; cloning into L3
p35s::mCherry:MtSYMREM1 _c	L2	<i>Nicotiana</i> expression, (M. Marin)
p35s::mCherry:MtSYMREM1Δ1		<i>Nicotiana</i> expression, (M. Marin)
p35s::mCherry:MtSYMREM1Δ2		<i>Nicotiana</i> expression, (M. Marin)
p35s::mCherry:MtSYMREM1Δ3		<i>Nicotiana</i> expression, (M. Marin)
pUbi::HA:MtSYMREM1	L2F5-6	<i>Nicotiana</i> expression; Cloning into L3
pUbi::YFP:Lifeact	L2F1-2	<i>Nicotiana</i> expression; Cloning into L3
pUbi::Cerulean:Lifeact	L2βR3-4	Cloning into L3
pUbi::YFP:MAP4	L2Xpre2S	<i>Medicago</i> expression; Cloning into L3
pUbi::mCherry:MAP4	L2Xpre2S	<i>Nicotiana</i> expression
p35s::LYK3:GFP	L2βF1-2	<i>Nicotiana</i> expression; Cloning into L3
P35s::LYK3:HA	L2βF5-6	<i>Nicotiana</i> expression; Cloning into L3
pUbi::FLOT4:HA	L2βF5-6	<i>Nicotiana</i> expression; Cloning into L3
pUbi::FLOT4:mCherry	L2βR3-4	<i>Nicotiana/ Medicago</i> expression; Cloning into L3 (S. Konrad, LMU)
pUbi::FLOT2:GFP	L2βR3-4	<i>Nicotiana</i> expression, Cloning into L3
pUbi::FLOT2:mCherry	L2βR3-4	<i>Nicotiana</i> expression, cloning into L3

Methods

pSYMREM1:NLS:2xGFP_NEO _R	L2βF1-2	<i>Medicago</i> expression; Cloning into L3
pFLOT4:NLS:2xGFP_NEO _R	L2βF1-2	<i>Medicago</i> expression; Cloning into L3
pUbi::FLOT4:RNAi	L2βRNAI F1-2	Cloning into Level 3
pUbi::FLOT4:RNAilong	L2βRNAI F1-2	Cloning into Level 3
LEVEL3	Vector	Purpose
pUbi::YFP:MtSYMREM1 + pUbi::FLOT4:mCherry	L3βfin	<i>Nicotiana/ Medicago</i> expression
pUbi::YFP:MtSYMREM1 + pUbi::FLOT4:mCherry + p35s::LYK3:HA	L3βfin	<i>Nicotiana</i> expression
pUbi::Cerulean:Lifeact + pUbi::mCherry:MtSYMREM1	L3βfin	<i>Medicago</i> expression
p35s::LYK3GFP + pUbi::mCherry:MtSYMREM1	L3βfin	<i>Nicotiana</i> expression
p35s::LYK3GFP +pUbi::FLOT4:mCherry	L3βfin	<i>Nicotiana</i> expression
pUbi::FLOT4:RNAi + pUbi::FLOT4:mCherry	L3βfin	<i>Nicotiana</i> expression
pUbi::FLOT4:RNAi + pUbi::YFP:MtSYMREM1	L3βfin	<i>Medicago</i> expression
pUbi::FLOT4:RNAilong + pUbi::YFP:MtSYMREM1	L3βfin	<i>Nicotiana</i> expression
pUbi::mCherry:SYMREM1 + pUbi::FLOT2:GFP	L3βfin	<i>Nicotiana</i> expression
Other constructs	Vector	Purpose
pUbi::YFP:MtSYMREM1	pUbi:GW:Hyg pCAMBIA	<i>Medicago</i> transformation
p35s::FLOT1a:YFP	p35s:GW:YFP pAM-PAT	<i>Nicotiana</i> expression (S. Konrad)
p35s::LjSYMREM1:mOrange	p35s::GW:mOrange pAM-PAT	<i>Nicotiana</i> expression
p35s::LjSYMREM1N:mOrange	p35s::GW:mOrange pAM-PAT	<i>Nicotiana</i> expression
p35s::LjSYMREM1C:mOrange	p35s::GW:mOrange pAM-PAT	<i>Nicotiana</i> expression
p35s::GW:mOrange	pAM-PAT	<i>Nicotiana</i> expression
p35s::NFR1:Cerulean	p35s::GW:Cerulean pAM-PAT	<i>Nicotiana</i> expression
LjSYMREM1	pENTR/D-TOPO	For Gateway cloning (Katalin Toth, LMU)

5.7.5 Primer Used in This Study

Name	Sequence 5'-3'
Lifeact_Bsa1_FW	ATGGTCTCACACCGGTGTCGCAGATTTGATCAAGAAA TTCGAAAGCATCTCAAAGGAAGAAAAGGTGAGACCAT
Lifeact_Bsa1_Rev	ATGGTCTCACCTTTTCTTCCTTTGAGATGCTTTTCAAT TTCTTGATCAAATCTGCGACACCGGTGTGAGACCAT
MAP4_ESP3Lmut_inFW	ATGAAGACCAGGGACGTGAAGCCAAAGCCAATTACAG
MAP4_ESP3Lmut_InRev	ATGAAGACCGTCCCTGGCAGGTAGGGTGGAA
MAP4_BSA1mut_InFW	ATGAAGACAAGGTGTCCTCCAAGTGTGGGTCCAAA
MAP4_BSA1mut-InRev	ATGAAGACGACACCTTGGATATGTCCACTTTCTTGTTCT T
MAP4_BpiBsa1_OutFW	ATGAAGACTTTACGGGTCTCACACCTCCCGGCAAGAA GAAGCAAAGGCT
MAP4_BpiBsa1_OutRev	ATGAAGACTTCAGAGGTCTCACCTTGCACCTCCTGCA GGAAAGTGGC
FLOT2_out_FW	ATGAAGACTTTACGGGTCTCACACCAAATTTACCGG GTCGCGAAAGCATCAGA
FLOT2_out_Rev	ATGAAGACTTCAGAGGTCTCACCTTTCAAGAGCTTTTC TCAGATAAGG CTCCCAT
FLOT2_fw_364	[Phos]AATCACGTTAATGAACTCGTTCAA
FLOT2-Rev-364	GGAGTGTGATCATGAGGTGA
FLOT2_OutRev_noStop	ATGAAGACTTCAGAGGTCTCACCTTAGAGCTTTTCTCA GATAAGGCTCCCAT
FLOT2_Bbs1_in_FW	ATGAAGACCCGTGTTCACAATTGGTCCCTCGTGTGAC G
FLOT2_Bbs1_in_Rev	ATGAAGACGAACACGGCGGGGAGAACAAAAGGAAGT TTC
FLOT2_ESP3-InFW	ATGAAGACCAGAAACGAAGTTATTGCGATGCAGAGA G
FLOT2_ESP3_inRev	ATGAAGACCGTTTCTGCATCAATTTTTGCTGCATTCTG CAGCG
FLOT4_Out_FW	ATGAAGACTTTACGGGTCTCACACCTACAAGGTAGCA AAAGCATCACAATACCTTGT
FLOT4_Bbs1A_inRev	ATGAAGACGAACACGGAGTAGGATTGACCGGGTAGA ATCCAT
FLOT4_Bbs1A_inFW	ATGAAGACCCGTGTTGACCTCTCACCTGTAAATTACA CCTTTG
FLOT4_Bbs1B_inRev	ATGAAGACTAAATACAGCGGGGAGAACAAAAGGAAGT TTC
FLOT4_Bbs1B_inFW	ATGAAGACTGTATTTACTATCGGTCCTCGTGTGGATGA T
FLOT4_Out_REV	ATGAAGACTTCAGAGGTCTCACCTTATTCAAGTTTTTG TCAGGCAAGACTCCCATC
LYK3_Out_Rev	ATGAAGACTTCAGAGGTCTCACCTTTCTAGTTGACAAC AGATTTATGA GAGATTGATTTTCATATG
LYK3_Out_FW	ATGAAGACTTTACGGGTCTCACACCATGAATCTCAAAA ATGGATTACTATTGTTCAATTCTGTTTC

Methods

LYK3_1stsite-Rev	AAGAAGACTGTTTTTCAGGACAGCATTCTTTGCAGTAATAAG
LYK3_Part2_FW:	AAGAAGACCCAAAACAGGTGAATCTGTTGCAGAATCA AAGGGTCTTGACAATTGTTTGAAGAAGCACTTCATCG AATGGATCCTTTAGAAGGCCTGTCTTCTT
LYK3_Part2_Rev	AAGAAGACAGGCCTTCTAAAGGATCCATTTCGATGAAG TGCTTCTTCAAACAATTGTACAAGACCCTTTGATTCTG CAACAGATTCACCTGTTTTGGGTCTTCTT
LYK3_2nd_site_FW	AAGAAGACGAAGGCCTTCGAAAATTGGTGGATCCTAG GCTTAAAG
LYK3_FW_GG-B	ATGAAGACAATACGGGTCTCATCTGATGAATCTCAAAA ATGGATTACTATTGTTCACTTCTGTTTC
LYK3_Rev-GG_D	ATGAAGACTTCAGAGGTCTCACCTTTCTAGTTGACAAC AGATTTATGAGAGATTGATTTTCATATG
npFlot4_BbsBsa_FW	ATGAAGACTTTACGGGTCTCAGCGGTTCCCATGAACT TAACTCAATTG
npFlot4_BbsBsa-Rev	ATGAAGACTTAGACGGTCTCACAGACGTTGATTTTGT TTAATTTTTAAAAA
LjSR1Cterm_Topo_Fw+ATG	CACCATGTCAATTGATAGAGATGCTGTT
LjSYMREm1C_longFw_Topo	CACCTTGATAGAGATGCTGTTCTTGC
LjSYMREM1_N_Rev_noStop_s hort	AGTATTTATATTGTCTGTTTCAGCATCAAGAT
LjSYMREM1REM_Topo2R	AAAGCTGAAGTTGAAGCATGAC
LjSYMREM1Topo_1F	CACCATGGGAGAAGAAGAGACCAAAC
Bpil/Bsal SR1_F	ATGAAGACTTTACGGGTCTCACACCGAAGAATCGAAA AACAAAC
Bpil/Bsal SR1_R	ATGAAGACAACAGAGGTCTCACCTTACTGAAAAACCTT AAACCGC
Bpil/Bsal pMtSR1_F	ATGAAGACTTTACGGGTCTCAGCGGATTACGTTAGTTT ATATAAGGGG
Bpil/Bsal pMtSR1_R	ATGAAGACTTCAGAGGTCTCACAGAAATGTATTACTAG GGTTAC

6 References

- Al-Yahya'ei, M.N., Oehl, F., Vallino, M., Lumini, E., Redecker, D., Wiemken, A., and Bonfante, P.** (2011). Unique arbuscular mycorrhizal fungal communities uncovered in date palm plantations and surrounding desert habitats of Southern Arabia. *Mycorrhiza* **21**, 195-209.
- Almen, M.S., Nordstrom, K.J., Fredriksson, R., and Schioth, H.B.** (2009). Mapping the human membrane proteome: a majority of the human membrane proteins can be classified according to function and evolutionary origin. *BMC Biol* **7**, 50.
- Andrade, D.M., Clausen, M.P., Keller, J., Mueller, V., Wu, C., Bear, J.E., Hell, S.W., Lagerholm, B.C., and Eggeling, C.** (2015). Cortical actin networks induce spatio-temporal confinement of phospholipids in the plasma membrane--a minimally invasive investigation by STED-FCS. *Sci Rep* **5**, 11454.
- Andrews, N.L., Lidke, K.A., Pfeiffer, J.R., Burns, A.R., Wilson, B.S., Oliver, J.M., and Lidke, D.S.** (2008). Actin restricts FcepsilonRI diffusion and facilitates antigen-induced receptor immobilization. *Nat Cell Biol* **10**, 955-963.
- Ane, J.M., Kiss, G.B., Riely, B.K., Penmetsa, R.V., Oldroyd, G.E., Ayax, C., Levy, J., Debelle, F., Baek, J.M., Kalo, P., Rosenberg, C., Roe, B.A., Long, S.R., Denarie, J., and Cook, D.R.** (2004). *Medicago truncatula* DMI1 required for bacterial and fungal symbioses in legumes. *Science* **303**, 1364-1367.
- Antolin-Llovera, M., Ried, M.K., and Parniske, M.** (2014). Cleavage of the SYMBIOSIS RECEPTOR-LIKE KINASE Ectodomain Promotes Complex Formation with Nod Factor Receptor 5. *Curr Biol* **24**, 422-427.
- Ardourel, M., Demont, N., Debelle, F., Maillet, F., de Billy, F., Prome, J.C., Denarie, J., and Truchet, G.** (1994). *Rhizobium meliloti* lipooligosaccharide nodulation factors: different structural requirements for bacterial entry into target root hair cells and induction of plant symbiotic developmental responses. *Plant Cell* **6**, 1357-1374.
- Arrighi, J.F., Barre, A., Ben Amor, B., Bersoult, A., Soriano, L.C., Mirabella, R., de Carvalho-Niebel, F., Journet, E.P., Gherardi, M., Huguet, T., Geurts, R., Denarie, J., Rouge, P., and Gough, C.** (2006). The *Medicago truncatula* lysine motif-receptor-like kinase gene family includes NFP and new nodule-expressed genes. *Plant Physiology* **142**, 265-279.
- Babuke, T., and Tikkanen, R.** (2007). Dissecting the molecular function of reggie/flotillin proteins. *Eur J Cell Biol* **86**, 525-532.
- Bach, J.N., and Bramkamp, M.** (2013). Flotillins functionally organize the bacterial membrane. *Mol Microbiol* **88**, 1205-1217.
- Bach, J.N., and Bramkamp, M.** (2015). Dissecting the Molecular Properties of Prokaryotic Flotillins. *Plos One* **10**.

References

- Bae, T.J., Kim, M.S., Kim, J.W., Kim, B.W., Choo, H.J., Lee, J.W., Kim, K.B., Lee, C.S., Kim, J.H., Chang, S.Y., Kang, C.Y., Lee, S.W., and Ko, Y.G.** (2004). Lipid raft proteome reveals ATP synthase complex in the cell surface. *Proteomics* **4**, 3536-3548.
- Bagatolli, L.A., Sanchez, S.A., Hazlett, T., and Gratton, E.** (2003). Giant vesicles, Laurdan, and two-photon fluorescence microscopy: evidence of lipid lateral separation in bilayers. *Methods Enzymol* **360**, 481-500.
- Bago, B., Pfeffer, P.E., and Shachar-Hill, Y.** (2000). Carbon metabolism and transport in arbuscular mycorrhizas. *Plant Physiology* **124**, 949-957.
- Baluska, F., Samaj, J., Wojtaszek, P., Volkmann, D., and Menzel, D.** (2003). Cytoskeleton-plasma membrane-cell wall continuum in plants. Emerging links revisited. *Plant Physiol* **133**, 482-491.
- Baluska, F., Salaj, J., Mathur, J., Braun, M., Jasper, F., Samaj, J., Chua, N.H., Barlow, P.W., and Volkmann, D.** (2000). Root hair formation: F-actin-dependent tip growth is initiated by local assembly of profilin-supported F-actin meshworks accumulated within expansin-enriched bulges. *Dev Biol* **227**, 618-632.
- Barbosa, I.C., and Schwechheimer, C.** (2014). Dynamic control of auxin transport-dependent growth by AGCVIII protein kinases. *Curr Opin Plant Biol* **22**, 108-115.
- Battaglia, M., Ripodas, C., Clua, J., Baudin, M., Aguilar, O.M., Niebel, A., Zanetti, M.E., and Blanco, F.A.** (2014). A nuclear factor Y interacting protein of the GRAS family is required for nodule organogenesis, infection thread progression, and lateral root growth. *Plant Physiol* **164**, 1430-1442.
- Ben Amor, B., Shaw, S.L., Oldroyd, G.E.D., Maillet, F., Penmetsa, R.V., Cook, D., Long, S.R., Denarie, J., and Gough, C.** (2003). The NFP locus of *Medicago truncatula* controls an early step of Nod factor signal transduction upstream of a rapid calcium flux and root hair deformation. *Plant J* **34**, 495-506.
- Benkova, E., Michniewicz, M., Sauer, M., Teichmann, T., Seifertova, D., Jurgens, G., and Friml, J.** (2003). Local, efflux-dependent auxin gradients as a common module for plant organ formation. *Cell* **115**, 591-602.
- Berleth, T., and Sachs, T.** (2001). Plant morphogenesis: long-distance coordination and local patterning. *Curr Opin Plant Biol* **4**, 57-62.
- Bickel, P.E., Scherer, P.E., Schnitzer, J.E., Oh, P., Lisanti, M.P., and Lodish, H.F.** (1997). Flotillin and epidermal surface antigen define a new family of caveolae-associated integral membrane proteins. *J Biol Chem* **272**, 13793-13802.
- Binder, A., Lambert, J., Morbitzer, R., Popp, C., Ott, T., Lahaye, T., and Parniske, M.** (2014). A modular plasmid assembly kit for multigene expression, gene silencing and silencing rescue in plants. *PLoS One* **9**, e88218.
- Blachutzik, J., Kreuzer, I., Hedrich, R., and Harms, G.** (2015). Mobility of Group 1b Remorins in Membrane Nanodomains Differs Significantly between Mesophyll Cells and Protoplasts. *Journal of Plant Biochemistry and Physiology* **153**.
- Blanco, F.A., Meschini, E.P., Zanetti, M.E., and Aguilar, O.M.** (2009). A small GTPase of the Rab family is required for root hair formation and preinfection stages of the common bean-Rhizobium symbiotic association. *Plant Cell* **21**, 2797-2810.
- Blilou, I., Xu, J., Wildwater, M., Willemsen, V., Paponov, I., Friml, J., Heidstra, R., Aida, M., Palme, K., and Scheres, B.** (2005). The PIN auxin efflux facilitator network controls growth and patterning in *Arabidopsis* roots. *Nature* **433**, 39-44.

- Boisson-Dernier, A., Chabaud, M., Garcia, F., Becard, G., Rosenberg, C., and Barker, D.G.** (2001). *Agrobacterium rhizogenes*-transformed roots of *Medicago truncatula* for the study of nitrogen-fixing and endomycorrhizal symbiotic associations. *Mol Plant Microbe Interact* **14**, 695-700.
- Bolte, S., and Cordelières, F.P.** (2006). A guided tour into subcellular colocalization analysis in light microscopy. *J Microsc* **224**, 213-232.
- Bonifacino, J.S., and Weissman, A.M.** (1998). Ubiquitin and the control of protein fate in the secretory and endocytic pathways. *Annu Rev Cell Dev Biol* **14**, 19-57.
- Boudaoud, A., Burian, A., Borowska-Wykret, D., Uyttewaal, M., Wrzalik, R., Kwiatkowska, D., and Hamant, O.** (2014). FibrilTool, an ImageJ plug-in to quantify fibrillar structures in raw microscopy images. *Nat Protoc* **9**, 457-463.
- Bozkurt, T.O., Richardson, A., Dagdas, Y.F., Mongrand, S., Kamoun, S., and Raffaele, S.** (2014). The Plant Membrane-Associated REMORIN1.3 Accumulates in Discrete Perihyphal Domains and Enhances Susceptibility to *Phytophthora infestans*. *Plant Physiol* **165**, 1005-1018.
- Bramkamp, M., and Lopez, D.** (2015). Exploring the Existence of Lipid Rafts in Bacteria. *Microbiol Mol Biol R* **79**, 81-100.
- Breakspear, A., Liu, C., Roy, S., Stacey, N., Rogers, C., Trick, M., Morieri, G., Mysore, K.S., Wen, J., Oldroyd, G.E., Downie, J.A., and Murray, J.D.** (2014). The root hair "infectome" of *Medicago truncatula* uncovers changes in cell cycle genes and reveals a requirement for Auxin signaling in rhizobial infection. *Plant Cell* **26**, 4680-4701.
- Broghammer, A., Krusell, L., Blaise, M., Sauer, J., Sullivan, J.T., Maolanon, N., Vinther, M., Lorentzen, A., Madsen, E.B., Jensen, K.J., Roepstorff, P., Thirup, S., Ronson, C.W., Thygesen, M.B., and Stougaard, J.** (2012). Legume receptors perceive the rhizobial lipochitin oligosaccharide signal molecules by direct binding. *P Natl Acad Sci USA* **109**, 13859-13864.
- Brown, D.A., and Rose, J.K.** (1992). Sorting of GPI-anchored proteins to glycolipid-enriched membrane subdomains during transport to the apical cell surface. *Cell* **68**, 533-544.
- Brown, D.A., and London, E.** (1998). Functions of lipid rafts in biological membranes. *Annu Rev Cell Dev Biol* **14**, 111-136.
- Buist, G., Steen, A., Kok, J., and Kuipers, O.R.** (2008). LysM, a widely distributed protein motif for binding to (peptido)glycans. *Mol Microbiol* **68**, 838-847.
- Bunn, R., Lekberg, Y., and Zabinski, C.** (2009). Arbuscular mycorrhizal fungi ameliorate temperature stress in thermophilic plants. *Ecology* **90**, 1378-1388.
- Bussell, S.J., Koch, D.L., and Hammer, D.A.** (1995a). Effect of hydrodynamic interactions on the diffusion of integral membrane proteins: tracer diffusion in organelle and reconstituted membranes. *Biophys J* **68**, 1828-1835.
- Bussell, S.J., Koch, D.L., and Hammer, D.A.** (1995b). Effect of hydrodynamic interactions on the diffusion of integral membrane proteins: diffusion in plasma membranes. *Biophys J* **68**, 1836-1849.
- Cangelosi, G.A., Hung, L., Puvanesarajah, V., Stacey, G., Ozga, D.A., Leigh, J.A., and Nester, E.W.** (1987). Common loci for *Agrobacterium tumefaciens* and *Rhizobium meliloti* exopolysaccharide synthesis and their roles in plant interactions. *J Bacteriol* **169**, 2086-2091.
- Capoen, W., Goormachtig, S., De Rycke, R., Schroeyers, K., and Holsters, M.** (2005). SrSymRK, a plant receptor essential for symbiosome formation. *Proc Natl Acad Sci U S A* **102**, 10369-10374.

References

- Capoen, W., Sun, J., Wysham, D., Otegui, M.S., Venkateshwaran, M., Hirsch, S., Miwa, H., Downie, J.A., Morris, R.J., Ane, J.M., and Oldroyd, G.E.** (2011). Nuclear membranes control symbiotic calcium signaling of legumes. *Proc Natl Acad Sci U S A* **108**, 14348-14353.
- Cardenas, L.** (2009). New findings in the mechanisms regulating polar growth in root hair cells. *Plant Signal Behav* **4**, 4-8.
- Cárdenas, L., Vidalí, L., Domnguez, J., Prez, H., Snchez, F., Hepler, P.K., and Quinto, C.** (1998). Rearrangement of actin microfilaments in plant root hairs responding to rhizobium etli nodulation signals. *Plant Physiol* **116**, 871-877.
- Carol, R.J., and Dolan, L.** (2002). Building a hair: tip growth in *Arabidopsis thaliana* root hairs. *Philos Trans R Soc Lond B Biol Sci* **357**, 815-821.
- Carpita, N.C.** (2011). Update on mechanisms of plant cell wall biosynthesis: how plants make cellulose and other (1->4)-beta-D-glycans. *Plant Physiol* **155**, 171-184.
- Catalano, C.M., Czymbek, K.J., Gann, J.G., and Sherrier, D.J.** (2007). *Medicago truncatula* syntaxin SYP132 defines the symbiosome membrane and infection droplet membrane in root nodules. *Planta* **225**, 541-550.
- Catoira, R., Timmers, A.C.J., Maillet, F., Galera, C., Penmetsa, R.V., Cook, D., Denarie, J., and Gough, C.** (2001). The HCL gene of *Medicago truncatula* controls Rhizobium-induced root hair curling. *Development* **128**, 1507-1518.
- Catoira, R., Galera, C., de Billy, F., Penmetsa, R.V., Journet, E.P., Maillet, F., Rosenberg, C., Cook, D., Gough, C., and Denarie, J.** (2000). Four genes of *Medicago truncatula* controlling components of a nod factor transduction pathway. *Plant Cell* **12**, 1647-1666.
- Cerri, M.R., Frances, L., Laloum, T., Auriac, M.C., Niebel, A., Oldroyd, G.E., Barker, D.G., Fournier, J., and de Carvalho-Niebel, F.** (2012). *Medicago truncatula* ERN transcription factors: regulatory interplay with NSP1/NSP2 GRAS factors and expression dynamics throughout rhizobial infection. *Plant Physiol* **160**, 2155-2172.
- Chang, J.C., and Rosenthal, S.J.** (2012). Visualization of lipid raft membrane compartmentalization in living RN46A neuronal cells using single quantum dot tracking. *ACS Chem Neurosci* **3**, 737-743.
- Charpentier, M., Bredemeier, R., Wanner, G., Takeda, N., Schleiff, E., and Parniske, M.** (2008). Lotus japonicus CASTOR and POLLUX Are Ion Channels Essential for Perinuclear Calcium Spiking in Legume Root Endosymbiosis. *Plant Cell* **20**, 3467-3479.
- Chaudhuri, A., Bhattacharya, B., Gowrishankar, K., Mayor, S., and Rao, M.** (2011). Spatiotemporal regulation of chemical reactions by active cytoskeletal remodeling. *Proc Natl Acad Sci U S A* **108**, 14825-14830.
- Checker, V.G., and Khurana, P.** (2013). Molecular and functional characterization of mulberry EST encoding remorin (MiREM) involved in abiotic stress. *Plant Cell Rep* **32**, 1729-1741.
- Chen, T., Zhu, H., Ke, D., Cai, K., Wang, C., Gou, H., Hong, Z., and Zhang, Z.** (2012). A MAP kinase kinase interacts with SymRK and regulates nodule organogenesis in *Lotus japonicus*. *Plant Cell* **24**, 823-838.
- Chevalier, D., Batoux, M., Fulton, L., Pfister, K., Yadav, R.K., Schellenberg, M., and Schneitz, K.** (2005). STRUBBELIG defines a receptor kinase-mediated signaling pathway regulating organ development in *Arabidopsis*. *Proc Natl Acad Sci U S A* **102**, 9074-9079.
- Chubinskiy-Nadezhdin, V.I., Efremova, T.N., Khaitlina, S.Y., and Morachevskaya, E.A.** (2013). Functional impact of cholesterol sequestration on actin cytoskeleton in normal and transformed fibroblasts. *Cell Biol Int* **37**, 617-623.

- Combiér, J.P., Frugier, F., de Billy, F., Boualem, A., El-Yahyaoui, F., Moreau, S., Vernie, T., Ott, T., Gamas, P., Crespi, M., and Niebel, A.** (2006). MtHAP2-1 is a key transcriptional regulator of symbiotic nodule development regulated by microRNA169 in *Medicago truncatula*. *Genes Dev* **20**, 3084-3088.
- Coronado, C., Zuanazzi, J.A.S., Sallaud, C., Quirion, J.C., Esnault, R., Husson, H.P., Kondorosi, A., and Ratet, P.** (1995). Alfalfa Root Flavonoid Production Is Nitrogen Regulated. *Plant Physiology* **108**, 533-542.
- Craddock, C., Lavagi, I., and Yang, Z.B.** (2012). New insights into Rho signaling from plant ROP/Rac GTPases. *Trends Cell Biol* **22**, 492-501.
- D'Antuono, A.L., Casabuono, A., Couto, A., Ugalde, R.A., and Lepek, V.C.** (2005). Nodule development induced by *Mesorhizobium loti* mutant strains affected in polysaccharide synthesis. *Mol Plant Microbe In* **18**, 446-457.
- Deeks, M.J., Hussey, P.J., and Davies, B.** (2002). Formins: intermediates in signal-transduction cascades that affect cytoskeletal reorganization. *Trends Plant Sci* **7**, 492-498.
- Demir, F., Horntrich, C., Blachutzyk, J.O., Scherzer, S., Reinders, Y., Kierszniowska, S., Schulze, W.X., Harms, G.S., Hedrich, R., Geiger, D., and Kreuzer, I.** (2013). Arabidopsis nanodomain-delimited ABA signaling pathway regulates the anion channel SLAH3. *P Natl Acad Sci USA* **110**, 8296-8301.
- Den Herder, G., Yoshida, S., Antolin-Llovera, M., Ried, M.K., and Parniske, M.** (2012). Lotus japonicus E3 ligase SEVEN IN ABSENTIA4 destabilizes the symbiosis receptor-like kinase SYMRK and negatively regulates rhizobial infection. *Plant Cell* **24**, 1691-1707.
- Denarie, J., Debelle, F., and Prome, J.C.** (1996). Rhizobium lipo-chitoooligosaccharide nodulation factors: Signaling molecules mediating recognition and morphogenesis. *Annu Rev Biochem* **65**, 503-535.
- Dhonukshe, P., Huang, F., Galvan-Ampudia, C.S., Mahonen, A.P., Kleine-Vehn, J., Xu, J., Quint, A., Prasad, K., Friml, J., Scheres, B., and Offringa, R.** (2010). Plasma membrane-bound AGC3 kinases phosphorylate PIN auxin carriers at TPRXS(N/S) motifs to direct apical PIN recycling. *Development* **137**, 3245-3255.
- Dhonukshe, P., Tanaka, H., Goh, T., Ebine, K., Mahonen, A.P., Prasad, K., Blilou, I., Geldner, N., Xu, J., Uemura, T., Chory, J., Ueda, T., Nakano, A., Scheres, B., and Friml, J.** (2008). Generation of cell polarity in plants links endocytosis, auxin distribution and cell fate decisions. *Nature* **456**, 962-966.
- Diet, A., Brunner, S., and Ringli, C.** (2004). The *enl* mutants enhance the *lrx1* root hair mutant phenotype of *Arabidopsis thaliana*. *Plant Cell Physiol* **45**, 734-741.
- Dinic, J., Ashrafzadeh, P., and Parmryd, I.** (2013). Actin filaments attachment at the plasma membrane in live cells cause the formation of ordered lipid domains. *Bba-Biomembranes* **1828**, 1102-1111.
- Dinkel, H., Van Roey, K., Michael, S., Davey, N.E., Weatheritt, R.J., Born, D., Speck, T., Kruger, D., Grebnev, G., Kuban, M., Strumillo, M., Uyar, B., Budd, A., Altenberg, B., Seiler, M., Chemes, L.B., Glavina, J., Sanchez, I.E., Diella, F., and Gibson, T.J.** (2014). The eukaryotic linear motif resource ELM: 10 years and counting. *Nucleic Acids Res* **42**, D259-266.
- Donovan, C., and Bramkamp, M.** (2009). Characterization and subcellular localization of a bacterial flotillin homologue. *Microbiology* **155**, 1786-1799.
- Downie, J.A.** (2010). The roles of extracellular proteins, polysaccharides and signals in the interactions of rhizobia with legume roots. *Fems Microbiol Rev* **34**, 150-170.

References

- Dunker, A.K., and Obradovic, Z.** (2001). The protein trinity--linking function and disorder. *Nat Biotechnol* **19**, 805-806.
- Dupuy, A.D., and Engelman, D.M.** (2008). Protein area occupancy at the center of the red blood cell membrane. *Proc Natl Acad Sci U S A* **105**, 2848-2852.
- Dyson, H.J., and Wright, P.E.** (2005). Intrinsically unstructured proteins and their functions. *Nat Rev Mol Cell Biol* **6**, 197-208.
- Eddidin, M., Kuo, S.C., and Sheetz, M.P.** (1991). Lateral movements of membrane glycoproteins restricted by dynamic cytoplasmic barriers. *Science* **254**, 1379-1382.
- Eggeling, C., Ringemann, C., Medda, R., Schwarzmann, G., Sandhoff, K., Polyakova, S., Belov, V.N., Hein, B., von Middendorff, C., Schonle, A., and Hell, S.W.** (2009). Direct observation of the nanoscale dynamics of membrane lipids in a living cell. *Nature* **457**, 1159-1162.
- Ehrhardt, D.W., Wais, R., and Long, S.R.** (1996). Calcium spiking in plant root hairs responding to *Rhizobium* nodulation signals. *Cell* **85**, 673-681.
- Endre, G., Kereszt, A., Kevei, Z., Mihacea, S., Kalo, P., and Kiss, G.B.** (2002a). A receptor kinase gene regulating symbiotic nodule development. *Nature* **417**, 962-966.
- Endre, G., Kalo, P., Kevei, Z., Kiss, P., Mihacea, S., Szakal, B., Kereszt, A., and Kiss, G.B.** (2002b). Genetic mapping of the non-nodulation phenotype of the mutant MN-1008 in tetraploid alfalfa (*Medicago sativa*). *Mol Genet Genomics* **266**, 1012-1019.
- Engelman, D.M.** (1969). Surface area per lipid molecule in the intact membrane of the human red cell. *Nature* **223**, 1279-1280.
- Era, A., Tominaga, M., Ebine, K., Awai, C., Saito, C., Ishizaki, K., Yamato, K.T., Kohchi, T., Nakano, A., and Ueda, T.** (2009). Application of Lifeact reveals F-actin dynamics in *Arabidopsis thaliana* and the liverwort, *Marchantia polymorpha*. *Plant Cell Physiol* **50**, 1041-1048.
- Esseling, J.J., Lhuissier, F.G.P., and Emons, A.M.C.** (2003). Nod factor-induced root hair curling: Continuous polar growth towards the point of nod factor application. *Plant Physiology* **132**, 1982-1988.
- Esseling, J.J., Lhuissier, F.G., and Emons, A.M.** (2004). A nonsymbiotic root hair tip growth phenotype in NORK-mutated legumes: implications for nodulation factor-induced signaling and formation of a multifaceted root hair pocket for bacteria. *Plant Cell* **16**, 933-944.
- Feraru, E., Feraru, M.I., Kleine-Vehn, J., Martiniere, A., Mouille, G., Vanneste, S., Vernhettes, S., Runions, J., and Friml, J.** (2011). PIN polarity maintenance by the cell wall in *Arabidopsis*. *Curr Biol* **21**, 338-343.
- Foley, J.A., DeFries, R., Asner, G.P., Barford, C., Bonan, G., Carpenter, S.R., Chapin, F.S., Coe, M.T., Daily, G.C., Gibbs, H.K., Helkowski, J.H., Holloway, T., Howard, E.A., Kucharik, C.J., Monfreda, C., Patz, J.A., Prentice, I.C., Ramankutty, N., and Snyder, P.K.** (2005). Global consequences of land use. *Science* **309**, 570-574.
- Foley, J.A., Ramankutty, N., Brauman, K.A., Cassidy, E.S., Gerber, J.S., Johnston, M., Mueller, N.D., O'Connell, C., Ray, D.K., West, P.C., Balzer, C., Bennett, E.M., Carpenter, S.R., Hill, J., Monfreda, C., Polasky, S., Rockstrom, J., Sheehan, J., Siebert, S., Tilman, D., and Zaks, D.P.M.** (2011). Solutions for a cultivated planet. *Nature* **478**, 337-342.
- Foreman, J., Demidchik, V., Bothwell, J.H., Mylona, P., Miedema, H., Torres, M.A., Linstead, P., Costa, S., Brownlee, C., Jones, J.D., Davies, J.M., and Dolan, L.** (2003). Reactive oxygen species produced by NADPH oxidase regulate plant cell growth. *Nature* **422**, 442-446.

- Foster, L.J., De Hoog, C.L., and Mann, M.** (2003). Unbiased quantitative proteomics of lipid rafts reveals high specificity for signaling factors. *Proc Natl Acad Sci U S A* **100**, 5813-5818.
- Fournier, J., Timmers, A.C.J., Sieberer, B.J., Jauneau, A., Chabaud, M., and Barker, D.G.** (2008). Mechanism of Infection Thread Elongation in Root Hairs of *Medicago truncatula* and Dynamic Interplay with Associated Rhizobial Colonization. *Plant Physiology* **148**, 1985-1995.
- Fournier, J., Teillet, A., Chabaud, M., Ivanov, S., Genre, A., Limpens, E., de Carvalho-Niebel, F., and Barker, D.G.** (2015). Remodeling of the Infection Chamber before Infection Thread Formation Reveals a Two-Step Mechanism for Rhizobial Entry into the Host Legume Root Hair. *Plant Physiology* **167**, 1233-1242.
- Frick, M., Bright, N.A., Riento, K., Bray, A., Merrified, C., and Nichols, B.J.** (2007). Coassembly of flotillins induces formation of membrane microdomains, membrane curvature, and vesicle budding. *Curr Biol* **17**, 1151-1156.
- Friml, J., Wisniewska, J., Benkova, E., Mendgen, K., and Palme, K.** (2002). Lateral relocation of auxin efflux regulator PIN3 mediates tropism in *Arabidopsis*. *Nature* **415**, 806-809.
- Friml, J., Vieten, A., Sauer, M., Weijers, D., Schwarz, H., Hamann, T., Offringa, R., and Jurgens, G.** (2003). Efflux-dependent auxin gradients establish the apical-basal axis of *Arabidopsis*. *Nature* **426**, 147-153.
- Friml, J., Yang, X., Michniewicz, M., Weijers, D., Quint, A., Tietz, O., Benjamins, R., Ouwerkerk, P.B., Ljung, K., Sandberg, G., Hooykaas, P.J., Palme, K., and Offringa, R.** (2004). A PINOID-dependent binary switch in apical-basal PIN polar targeting directs auxin efflux. *Science* **306**, 862-865.
- Frye, L.D., and Edidin, M.** (1970). The rapid intermixing of cell surface antigens after formation of mouse-human heterokaryons. *J Cell Sci* **7**, 319-335.
- Fujimoto, M., Arimura, S., Nakazono, M., and Tsutsumi, N.** (2008). *Arabidopsis* dynamin-related protein DRP2B is co-localized with DRP1A on the leading edge of the forming cell plate. *Plant Cell Rep* **27**, 1581-1586.
- Fujimoto, M., Arimura, S., Ueda, T., Takanashi, H., Hayashi, Y., Nakano, A., and Tsutsumi, N.** (2010). *Arabidopsis* dynamin-related proteins DRP2B and DRP1A participate together in clathrin-coated vesicle formation during endocytosis. *Proc Natl Acad Sci U S A* **107**, 6094-6099.
- Fujiwara, T., Ritchie, K., Murakoshi, H., Jacobson, K., and Kusumi, A.** (2002). Phospholipids undergo hop diffusion in compartmentalized cell membrane. *J Cell Biol* **157**, 1071-1081.
- Fukata, M., and Kaibuchi, K.** (2001). Rho-family GTPases in cadherin-mediated cell-cell adhesion. *Nat Rev Mol Cell Biol* **2**, 887-897.
- Fulton, L., Batoux, M., Vaddepalli, P., Yadav, R.K., Busch, W., Andersen, S.U., Jeong, S., Lohmann, J.U., and Schneitz, K.** (2009). DETORQUEO, QUIRKY, and ZERZAUST represent novel components involved in organ development mediated by the receptor-like kinase STRUBBELIG in *Arabidopsis thaliana*. *Plos Genet* **5**, e1000355.
- Furlan, G., Klinkenberg, J., and Trujillo, M.** (2012). Regulation of plant immune receptors by ubiquitination. *Front Plant Sci* **3**, 238.
- Gage, D.J.** (2004). Infection and invasion of roots by symbiotic, nitrogen-fixing rhizobia during nodulation of temperate legumes. *Microbiol Mol Biol R* **68**, 280-+.
- Galweiler, L., Guan, C., Muller, A., Wisman, E., Mendgen, K., Yephremov, A., and Palme, K.** (1998). Regulation of polar auxin transport by AtPIN1 in *Arabidopsis* vascular tissue. *Science* **282**, 2226-2230.

References

- Ganguly, S., and Chattopadhyay, A.** (2010). Cholesterol depletion mimics the effect of cytoskeletal destabilization on membrane dynamics of the serotonin1A receptor: A zFCS study. *Biophys J* **99**, 1397-1407.
- Garnica, D.P., Nemri, A., Upadhyaya, N.M., Rathjen, J.P., and Dodds, P.N.** (2014). The ins and outs of rust haustoria. *Plos Pathog* **10**, e1004329.
- Gaus, K., Gratton, E., Kable, E.P., Jones, A.S., Gelissen, I., Kritharides, L., and Jessup, W.** (2003). Visualizing lipid structure and raft domains in living cells with two-photon microscopy. *Proc Natl Acad Sci U S A* **100**, 15554-15559.
- Geiger, B., Bershadsky, A., Pankov, R., and Yamada, K.M.** (2001). Transmembrane crosstalk between the extracellular matrix--cytoskeleton crosstalk. *Nat Rev Mol Cell Biol* **2**, 793-805.
- Geisler, D.A., Sampathkumar, A., Mutwil, M., and Persson, S.** (2008). Laying down the bricks: logistic aspects of cell wall biosynthesis. *Curr Opin Plant Biol* **11**, 647-652.
- Geldner, N.** (2009). Cell polarity in plants: a PARspective on PINs. *Curr Opin Plant Biol* **12**, 42-48.
- Geldner, N., and Robatzek, S.** (2008). Plant receptors go endosomal: a moving view on signal transduction. *Plant Physiol* **147**, 1565-1574.
- Genre, A., Chabaud, M., Timmers, T., Bonfante, P., and Barker, D.G.** (2005). Arbuscular mycorrhizal fungi elicit a novel intracellular apparatus in *Medicago truncatula* root epidermal cells before infection. *Plant Cell* **17**, 3489-3499.
- Genre, A., Chabaud, M., Faccio, A., Barker, D.G., and Bonfante, P.** (2008). Prepenetration apparatus assembly precedes and predicts the colonization patterns of arbuscular mycorrhizal fungi within the root cortex of both *Medicago truncatula* and *Daucus carota*. *Plant Cell* **20**, 1407-1420.
- Gerland, P., Raftery, A.E., Sevcikova, H., Li, N., Gu, D.A., Spoorenberg, T., Alkema, L., Fosdick, B.K., Chunn, J., Lalic, N., Bay, G., Buettner, T., Heilig, G.K., and Wilmoth, J.** (2014). World population stabilization unlikely this century. *Science* **346**, 234-237.
- Giddings, T.H., Jr., Brower, D.L., and Staehelin, L.A.** (1980). Visualization of particle complexes in the plasma membrane of *Micrasterias denticulata* associated with the formation of cellulose fibrils in primary and secondary cell walls. *J Cell Biol* **84**, 327-339.
- Gilliland, L.U., Kandasamy, M.K., Pawloski, L.C., and Meagher, R.B.** (2002). Both vegetative and reproductive actin isoforms complement the stunted root hair phenotype of the *Arabidopsis* act2-1 mutation. *Plant Physiol* **130**, 2199-2209.
- Gimenez-Ibanez, S., Hann, D.R., Ntoukakis, V., Petutschnig, E., Lipka, V., and Rathjen, J.P.** (2009). AvrPtoB targets the LysM receptor kinase CERK1 to promote bacterial virulence on plants. *Curr Biol* **19**, 423-429.
- Gleason, C., Chaudhuri, S., Yang, T.B., Munoz, A., Poovaiah, B.W., and Oldroyd, G.E.D.** (2006). Nodulation independent of rhizobia induced by a calcium-activated kinase lacking autoinhibition. *Nature* **441**, 1149-1152.
- Glebov, O.O., Bright, N.A., and Nichols, B.J.** (2006). Flotillin-1 defines a clathrin-independent endocytic pathway in mammalian cells. *Nat Cell Biol* **8**, 46-54.
- Gohre, V., Spallek, T., Haweker, H., Mersmann, S., Mentzel, T., Boller, T., de Torres, M., Mansfield, J.W., and Robatzek, S.** (2008). Plant pattern-recognition receptor FLS2 is directed for degradation by the bacterial ubiquitin ligase AvrPtoB. *Curr Biol* **18**, 1824-1832.
- Gomez-Llobregat, J., Buceta, J., and Reigada, R.** (2013). Interplay of cytoskeletal activity and lipid phase stability in dynamic protein recruitment and clustering. *Sci Rep* **3**, 2608.

- Gonzalez, J.E., York, G.M., and Walker, G.C.** (1996). Rhizobium meliloti exopolysaccharides: synthesis and symbiotic function. *Gene* **179**, 141-146.
- Gonzalez-Jamett, A.M., Momboisse, F., Haro-Acuna, V., Bevilacqua, J.A., Caviedes, P., and Cardenas, A.M.** (2013). Dynamin-2 function and dysfunction along the secretory pathway. *Front Endocrinol (Lausanne)* **4**, 126.
- Goodwin, J.S., Drake, K.R., Remmert, C.L., and Kenworthy, A.K.** (2005). Ras diffusion is sensitive to plasma membrane viscosity. *Biophys J* **89**, 1398-1410.
- Gowrishankar, K., Ghosh, S., Saha, S., C, R., Mayor, S., and Rao, M.** (2012). Active remodeling of cortical actin regulates spatiotemporal organization of cell surface molecules. *Cell* **149**, 1353-1367.
- Grebe, M., Xu, J., Mobius, W., Ueda, T., Nakano, A., Geuze, H.J., Rook, M.B., and Scheres, B.** (2003). Arabidopsis sterol endocytosis involves actin-mediated trafficking via ARA6-positive early endosomes. *Curr Biol* **13**, 1378-1387.
- Green, F.A.** (1967). Erythrocyte membrane sulfhydryl groups and Rh antigen activity. *Immunochemistry* **4**, 247-257.
- Groth, M., Takeda, N., Perry, J., Uchida, H., Draxl, S., Brachmann, A., Sato, S., Tabata, S., Kawaguchi, M., Wang, T.L., and Parniske, M.** (2010). NENA, a Lotus japonicus Homolog of Sec13, Is Required for Rhizodermal Infection by Arbuscular Mycorrhiza Fungi and Rhizobia but Dispensable for Cortical Endosymbiotic Development. *Plant Cell* **22**, 2509-2526.
- Grunewald, W., and Friml, J.** (2010). The march of the PINs: developmental plasticity by dynamic polar targeting in plant cells. *Embo J* **29**, 2700-2714.
- Gu, Y., Wang, Z., and Yang, Z.** (2004). ROP/RAC GTPase: an old new master regulator for plant signaling. *Curr Opin Plant Biol* **7**, 527-536.
- Gu, Y., Vernoud, V., Fu, Y., and Yang, Z.** (2003). ROP GTPase regulation of pollen tube growth through the dynamics of tip-localized F-actin. *J Exp Bot* **54**, 93-101.
- Gui, J., Liu, C., Shen, J., and Li, L.** (2014). Grain setting defect1, encoding a remorin protein, affects the grain setting in rice through regulating plasmodesmatal conductance. *Plant Physiol* **166**, 1463-1478.
- Gui, J., Zheng, S., Shen, J., and Li, L.** (2015). Grain setting defect1 (GSD1) function in rice depends on S-acylation and interacts with actin 1 (OsACT1) at its C-terminal. *Front Plant Sci* **6**, 804.
- Guidotti, G.** (1972). Membrane proteins. *Annu Rev Biochem* **41**, 731-752.
- Gust, A.A., Willmann, R., Desaki, Y., Grabherr, H.M., and Nurnberger, T.** (2012). Plant LysM proteins: modules mediating symbiosis and immunity. *Trends Plant Sci* **17**, 495-502.
- Gutierrez, R., Lindeboom, J.J., Paredes, A.R., Emons, A.M.C., and Ehrhardt, D.W.** (2009). Arabidopsis cortical microtubules position cellulose synthase delivery to the plasma membrane and interact with cellulose synthase trafficking compartments. *Nat Cell Biol* **11**, 797-U743.
- Hamann, T., Benkova, E., Baurle, I., Kientz, M., and Jurgens, G.** (2002). The Arabidopsis BODENLOS gene encodes an auxin response protein inhibiting MONOPTEROS-mediated embryo patterning. *Genes Dev* **16**, 1610-1615.
- Hancock, J.F.** (2006). Lipid rafts: contentious only from simplistic standpoints. *Nat Rev Mol Cell Biol* **7**, 456-462.

References

- Haney, C.H., and Long, S.R.** (2010). Plant flotillins are required for infection by nitrogen-fixing bacteria. *PNAS* **107**, 478-483.
- Haney, C.H., Riely, B.K., Tricoli, D.M., Cook, D.R., Ehrhardt, D.W., and Long, S.R.** (2011). Symbiotic Rhizobia Bacteria Trigger a Change in Localization and Dynamics of the *Medicago truncatula* Receptor Kinase LYK3. *Plant Cell* **23**, 2774-2787.
- Hao, H., Fan, L., Chen, T., Li, R., Li, X., He, Q., Botella, M.A., and Lin, J.** (2014). Clathrin and Membrane Microdomains Cooperatively Regulate RbohD Dynamics and Activity in *Arabidopsis*. *Plant Cell* **26**, 1729-1745.
- Hayashi, T., Banba, M., Shimoda, Y., Kouchi, H., Hayashi, M., and Imaizumi-Anraku, H.** (2010). A dominant function of CCaMK in intracellular accommodation of bacterial and fungal endosymbionts. *Plant J* **63**, 141-154.
- Heckmann, A.B., Lombardo, F., Miwa, H., Perry, J.A., Bunnell, S., Parniske, M., Wang, T.L., and Downie, J.A.** (2006). *Lotus japonicus* nodulation requires two GRAS domain regulators, one of which is functionally conserved in a non-legume. *Plant Physiol* **142**, 1739-1750.
- Heidstra, R., Geurts, R., Franssen, H., Spaink, H.P., Van Kammen, A., and Bisseling, T.** (1994). Root Hair Deformation Activity of Nodulation Factors and Their Fate on *Vicia sativa*. *Plant Physiol* **105**, 787-797.
- Heisler, M.G., Ohno, C., Das, P., Sieber, P., Reddy, G.V., Long, J.A., and Meyerowitz, E.M.** (2005). Patterns of auxin transport and gene expression during primordium development revealed by live imaging of the *Arabidopsis* inflorescence meristem. *Curr Biol* **15**, 1899-1911.
- Hicke, L.** (1997). Ubiquitin-dependent internalization and down-regulation of plasma membrane proteins. *FASEB J* **11**, 1215-1226.
- Hogslund, N., Radutoiu, S., Krusell, L., Voroshilova, V., Hannah, M.A., Goffard, N., Sanchez, D.H., Lippold, F., Ott, T., Sato, S., Tabata, S., Liboriussen, P., Lohmann, G.V., Schauser, L., Weiller, G.F., Udvardi, M.K., and Stougaard, J.** (2009). Dissection of symbiosis and organ development by integrated transcriptome analysis of *lotus japonicus* mutant and wild-type plants. *PLoS One* **4**, e6556.
- Holdaway-Clarke, T.L., Feijo, J.A., Hackett, G.R., Kunkel, J.G., and Hepler, P.K.** (1997). Pollen Tube Growth and the Intracellular Cytosolic Calcium Gradient Oscillate in Phase while Extracellular Calcium Influx Is Delayed. *Plant Cell* **9**, 1999-2010.
- Homann, U., Meckel, T., Hewing, J., Hutt, M.T., and Hurst, A.C.** (2007). Distinct fluorescent pattern of KAT1::GFP in the plasma membrane of *Vicia faba* guard cells. *Eur J Cell Biol* **86**, 489-500.
- Horvath, B., Yeun, L.H., Domonkos, A., Halasz, G., Gobbato, E., Ayaydin, F., Miro, K., Hirsch, S., Sun, J., Tadege, M., Ratet, P., Mysore, K.S., Ane, J.M., Oldroyd, G.E., and Kalo, P.** (2011). *Medicago truncatula* IPD3 is a member of the common symbiotic signaling pathway required for rhizobial and mycorrhizal symbioses. *Mol Plant Microbe Interact* **24**, 1345-1358.
- Hossain, M.S., Liao, J., James, E.K., Sato, S., Tabata, S., Jurkiewicz, A., Madsen, L.H., Stougaard, J., Ross, L., and Szczyglowski, K.** (2012). *Lotus japonicus* ARPC1 is required for rhizobial infection. *Plant Physiol* **160**, 917-928.
- Huang, F., Zago, M.K., Abas, L., van Marion, A., Galvan-Ampudia, C.S., and Offringa, R.** (2010). Phosphorylation of conserved PIN motifs directs *Arabidopsis* PIN1 polarity and auxin transport. *Plant Cell* **22**, 1129-1142.
- Huang, J., Fujimoto, M., Fujiwara, M., Fukao, Y., Arimura, S., and Tsutsumi, N.** (2015). *Arabidopsis* dynamin-related proteins, DRP2A and DRP2B, function coordinately in post-Golgi trafficking. *Biochem Biophys Res Commun* **456**, 238-244.

- Hunt, S., King, B.J., Canvin, D.T., and Layzell, D.B.** (1987). Steady and nonsteady state gas exchange characteristics of soybean nodules in relation to the oxygen diffusion barrier. *Plant Physiol* **84**, 164-172.
- Iakoucheva, L.M., Radivojac, P., Brown, C.J., O'Connor, T.R., Sikes, J.G., Obradovic, Z., and Dunker, A.K.** (2004). The importance of intrinsic disorder for protein phosphorylation. *Nucleic Acids Res* **32**, 1037-1049.
- Ibarra, N., Pollitt, A., and Insall, R.H.** (2005). Regulation of actin assembly by SCAR/WAVE proteins. *Biochem Soc Trans* **33**, 1243-1246.
- Iizasa, E., Mitsutomi, M., and Nagano, Y.** (2010). Direct binding of a plant LysM receptor-like kinase, LysM RLK1/CERK1, to chitin in vitro. *J Biol Chem* **285**, 2996-3004.
- Ikeda, F., and Dikic, I.** (2008). Atypical ubiquitin chains: new molecular signals. 'Protein Modifications: Beyond the Usual Suspects' review series. *EMBO Rep* **9**, 536-542.
- Ikonen, E.** (2008). Cellular cholesterol trafficking and compartmentalization. *Nat Rev Mol Cell Biol* **9**, 125-138.
- Ipsen, J.H., Karlstrom, G., Mouritsen, O.G., Wennerstrom, H., and Zuckermann, M.J.** (1987). Phase equilibria in the phosphatidylcholine-cholesterol system. *Biochim Biophys Acta* **905**, 162-172.
- Ishida, T., Kurata, T., Okada, K., and Wada, T.** (2008). A genetic regulatory network in the development of trichomes and root hairs. *Annu Rev Plant Biol* **59**, 365-386.
- Ivanov, S., Fedorova, E.E., Limpens, E., De Mita, S., Genre, A., Bonfante, P., and Bisseling, T.** (2012). Rhizobium-legume symbiosis shares an exocytotic pathway required for arbuscule formation. *Proc Natl Acad Sci U S A* **109**, 8316-8321.
- Jacobson, K., Sheets, E.D., and Simson, R.** (1995). Revisiting the fluid mosaic model of membranes. *Science* **268**, 1441-1442.
- Jacobson, K., Mouritsen, O.G., and Anderson, R.G.** (2007). Lipid rafts: at a crossroad between cell biology and physics. *Nat Cell Biol* **9**, 7-14.
- Jaqaman, K., Kuwata, H., Touret, N., Collins, R., Trimble, W.S., Danuser, G., and Grinstein, S.** (2011). Cytoskeletal control of CD36 diffusion promotes its receptor and signaling function. *Cell* **146**, 593-606.
- Jarsch, I.K., Konrad, S.S.A., Stratil, T.F., Urbanus, S.L., Szymanski, W., Braun, P., Braun, K.H., and Ott, T.** (2014). Plasma Membranes Are Subcompartmentalized into a Plethora of Coexisting and Diverse Microdomains in Arabidopsis and Nicotiana benthamiana. *Plant Cell* **26**, 1698-1711.
- Jones, K.M., Sharopova, N., Lohar, D.P., Zhang, J.Q., VandenBosch, K.A., and Walker, G.C.** (2008). Differential response of the plant *Medicago truncatula* to its symbiont *Sinorhizobium meliloti* or an exopolysaccharide-deficient mutant. *Proc Natl Acad Sci U S A* **105**, 704-709.
- Jones, M.A., Raymond, M.J., and Smirnov, N.** (2006). Analysis of the root-hair morphogenesis transcriptome reveals the molecular identity of six genes with roles in root-hair development in Arabidopsis. *Plant J* **45**, 83-100.
- Juszczuk, I.M., Wiktorowska, A., Malusa, E., and Rychter, A.M.** (2004). Changes in the concentration of phenolic compounds and exudation induced by phosphate deficiency in bean plants (*Phaseolus vulgaris* L.). *Plant Soil* **267**, 41-49.
- Kaibuchi, K., Kuroda, S., and Amano, M.** (1999). Regulation of the cytoskeleton and cell adhesion by the Rho family GTPases in mammalian cells. *Annu Rev Biochem* **68**, 459-486.

References

- Kaku, H., Nishizawa, Y., Ishii-Minami, N., Akimoto-Tomiyama, C., Dohmae, N., Takio, K., Minami, E., and Shibuya, N.** (2006). Plant cells recognize chitin fragments for defense signaling through a plasma membrane receptor. *Proc Natl Acad Sci U S A* **103**, 11086-11091.
- Kanamori, N., Madsen, L.H., Radutoiu, S., Frantescu, M., Quistgaard, E.M.H., Miwa, H., Downie, J.A., James, E.K., Felle, H.H., Haaning, L.L., Jensen, T.H., Sato, S., Nakamura, Y., Tabata, S., Sandal, N., and Stougaard, J.** (2006). A nucleoporin is required for induction of Ca²⁺ spiking in legume nodule development and essential for rhizobial and fungal symbiosis. *P Natl Acad Sci USA* **103**, 359-364.
- Kandasamy, M.K., McKinney, E.C., and Meagher, R.B.** (2009). A single vegetative actin isoform overexpressed under the control of multiple regulatory sequences is sufficient for normal *Arabidopsis* development. *Plant Cell* **21**, 701-718.
- Karnovsky, M.J., Kleinfeld, A.M., Hoover, R.L., and Klausner, R.D.** (1982). The concept of lipid domains in membranes. *J Cell Biol* **94**, 1-6.
- Kawaharada, Y., Kelly, S., Nielsen, M.W., Hjuler, C.T., Gysel, K., Muszynski, A., Carlson, R.W., Thygesen, M.B., Sandal, N., Asmussen, M.H., Vinther, M., Andersen, S.U., Krusell, L., Thirup, S., Jensen, K.J., Ronson, C.W., Blaise, M., Radutoiu, S., and Stougaard, J.** (2015). Receptor-mediated exopolysaccharide perception controls bacterial infection. *Nature* **523**, 308-312.
- Ke, D., Fang, Q., Chen, C., Zhu, H., Chen, T., Chang, X., Yuan, S., Kang, H., Ma, L., Hong, Z., and Zhang, Z.** (2012). The small GTPase ROP6 interacts with NFR5 and is involved in nodule formation in *Lotus japonicus*. *Plant Physiol* **159**, 131-143.
- Kelly, S.J., Muszynski, A., Kawaharada, Y., Hubber, A.M., Sullivan, J.T., Sandal, N., Carlson, R.W., Stougaard, J., and Ronson, C.W.** (2013). Conditional Requirement for Exopolysaccharide in the Mesorhizobium-Lotus Symbiosis. *Mol Plant Microbe In* **26**, 319-329.
- Ketelaar, T.** (2013). The actin cytoskeleton in root hairs: all is fine at the tip. *Curr Opin Plant Biol* **16**, 749-756.
- Ketelaar, T., de Ruijter, N.C., and Emons, A.M.** (2003). Unstable F-actin specifies the area and microtubule direction of cell expansion in *Arabidopsis* root hairs. *Plant Cell* **15**, 285-292.
- Ketelaar, T., Faivre-Moskalenko, C., Esseling, J.J., de Ruijter, N.C., Grierson, C.S., Dogterom, M., and Emons, A.M.** (2002). Positioning of nuclei in *Arabidopsis* root hairs: an actin-regulated process of tip growth. *Plant Cell* **14**, 2941-2955.
- Kevei, Z., Lounnon, G., Mergaert, P., Horvath, G.V., Kereszt, A., Jayaraman, D., Zaman, N., Marcel, F., Regulski, K., Kiss, G.B., Kondorosi, A., Endre, G., Kondorosi, E., and Ane, J.M.** (2007). 3-hydroxy-3-methylglutaryl coenzyme a reductase 1 interacts with NORK and is crucial for nodulation in *Medicago truncatula*. *Plant Cell* **19**, 3974-3989.
- Kierszniowska, S., Seiwert, B., and Schulze, W.X.** (2009). Definition of *Arabidopsis* Sterol-rich Membrane Microdomains by Differential Treatment with Methyl-beta-cyclodextrin and Quantitative Proteomics. *Mol Cell Proteomics* **8**, 612-623.
- Kihara, D., and Kanehisa, M.** (2000). Tandem clusters of membrane proteins in complete genome sequences. *Genome Res* **10**, 731-743.
- Kiss, E., Olah, B., Kalo, P., Morales, M., Heckmann, A.B., Borbola, A., Lozsa, A., Kontar, K., Middleton, P., Downie, J.A., Oldroyd, G.E., and Endre, G.** (2009). LIN, a novel type of U-box/WD40 protein, controls early infection by rhizobia in legumes. *Plant Physiol* **151**, 1239-1249.
- Klaus-Heisen, D., Nurisso, A., Pietraszewska-Bogiel, A., Mbengue, M., Camut, S., Timmers, T., Pichereaux, C., Rossignol, M., Gadella, T.W.J., Imberty, A., Lefebvre, B., and Cullimore,**

- J.V. (2011). Structure-Function Similarities between a Plant Receptor-like Kinase and the Human Interleukin-1 Receptor-associated Kinase-4. *Journal of Biological Chemistry* **286**, 11202-11210.
- Kleine-Vehn, J., Huang, F., Naramoto, S., Zhang, J., Michniewicz, M., Offringa, R., and Friml, J.** (2009). PIN auxin efflux carrier polarity is regulated by PINOID kinase-mediated recruitment into GNOM-independent trafficking in Arabidopsis. *Plant Cell* **21**, 3839-3849.
- Kodama, Y., and Hu, C.D.** (2012). Bimolecular fluorescence complementation (BiFC): a 5-year update and future perspectives. *Biotechniques* **53**, 285-298.
- Koh, S., Andre, A., Edwards, H., Ehrhardt, D., and Somerville, S.** (2005). Arabidopsis thaliana subcellular responses to compatible Erysiphe cichoracearum infections. *Plant J* **44**, 516-529.
- Kohorn, B.D.** (2000). Plasma membrane-cell wall contacts. *Plant Physiol* **124**, 31-38.
- Komander, D.** (2009). The emerging complexity of protein ubiquitination. *Biochem Soc Trans* **37**, 937-953.
- Koncz, C., Martini, N., Mayerhofer, R., Koncz-Kalman, Z., Korber, H., Redei, G.P., and Schell, J.** (1989). High-frequency T-DNA-mediated gene tagging in plants. *Proc Natl Acad Sci U S A* **86**, 8467-8471.
- Konrad, S.S., and Ott, T.** (2015). Molecular principles of membrane microdomain targeting in plants. *Trends Plant Sci.*
- Konrad, S.S.A., Popp, C., Stratil, T.F., Jarsch, I.K., Thallmair, V., Folgmann, J., Marin, M., and Ott, T.** (2014). S-acylation anchors remorin proteins to the plasma membrane but does not primarily determine their localization in membrane microdomains. *New Phytol* **203**, 758-769.
- Kusumi, A., and Suzuki, K.** (2005). Toward understanding the dynamics of membrane-raft-based molecular interactions. *Biochim Biophys Acta* **1746**, 234-251.
- Kusumi, A., Sako, Y., and Yamamoto, M.** (1993). Confined lateral diffusion of membrane receptors as studied by single particle tracking (nanovid microscopy). Effects of calcium-induced differentiation in cultured epithelial cells. *Biophys J* **65**, 2021-2040.
- Kusumi, A., Suzuki, K.G., Kasai, R.S., Ritchie, K., and Fujiwara, T.K.** (2011). Hierarchical mesoscale domain organization of the plasma membrane. *Trends Biochem Sci* **36**, 604-615.
- Kusumi, A., Fujiwara, T.K., Chadda, R., Xie, M., Tsunoyama, T.A., Kalay, Z., Kasai, R.S., and Suzuki, K.G.N.** (2012a). Dynamic Organizing Principles of the Plasma Membrane that Regulate Signal Transduction: Commemorating the Fortieth Anniversary of Singer and Nicolson's Fluid-Mosaic Model. *Annu Rev Cell Dev Bi* **28**, 215-250.
- Kusumi, A., Fujiwara, T.K., Morone, N., Yoshida, K.J., Chadda, R., Xie, M., Kasai, R.S., and Suzuki, K.G.** (2012b). Membrane mechanisms for signal transduction: the coupling of the meso-scale raft domains to membrane-skeleton-induced compartments and dynamic protein complexes. *Semin Cell Dev Biol* **23**, 126-144.
- Kwak, S.H., Shen, R., and Schiefelbein, J.** (2005). Positional signaling mediated by a receptor-like kinase in Arabidopsis. *Science* **307**, 1111-1113.
- Kwik, J., Boyle, S., Fooksman, D., Margolis, L., Sheetz, M.P., and Edidin, M.** (2003). Membrane cholesterol, lateral mobility, and the phosphatidylinositol 4,5-bisphosphate-dependent organization of cell actin. *Proc Natl Acad Sci U S A* **100**, 13964-13969.
- Lang, D.M., Lommel, S., Jung, M., Ankerhold, R., Petrausch, B., Laessing, U., Wiechers, M.F., Plattner, H., and Stuermer, C.A.** (1998). Identification of reggie-1 and reggie-2 as

References

- plasmamembrane-associated proteins which cocluster with activated GPI-anchored cell adhesion molecules in non-caveolar micropatches in neurons. *J Neurobiol* **37**, 502-523.
- Lang, T., and Jahn, R.** (2008). Core proteins of the secretory machinery. *Handb Exp Pharmacol*, 107-127.
- Langhorst, M.F., Solis, G.P., Hannbeck, S., Plattner, H., and Stuermer, C.A.O.** (2007). Linking membrane microdomains to the cytoskeleton: Regulation of the lateral mobility of reggie-1/flotillin-2 by interaction with actin. *Febs Lett* **581**, 4697-4703.
- Langhorst, M.F., Jaeger, F.A., Mueller, S., Sven Hartmann, L., Luxenhofer, G., and Stuermer, C.A.** (2008). Reggie/flotillins regulate cytoskeletal remodeling during neuronal differentiation via CAP/ponsin and Rho GTPases. *Eur J Cell Biol* **87**, 921-931.
- Lee, A.G., Birdsall, N.J., Metcalfe, J.C., Toon, P.A., and Warren, G.B.** (1974). Clusters in lipid bilayers and the interpretation of thermal effects in biological membranes. *Biochemistry-U S* **13**, 3699-3705.
- Lee, R.E., and Feldman, J.D.** (1964). Visualization of Antigenic Sites of Human Erythrocytes with Ferritin-Antibody Conjugates. *J Cell Biol* **23**, 396-401.
- Lee, Y., Rubio, M.C., Alassimone, J., and Geldner, N.** (2013). A mechanism for localized lignin deposition in the endodermis. *Cell* **153**, 402-412.
- Lefebvre, B., Timmers, T., Mbengue, M., Moreau, S., Herve, C., Tóth, K., Bittencourt-Silvestre, J., Klaus, D., Deslandes, L., Godiard, L., Murray, J.D., Udvardi, M.K., Raffaele, S., Mongrand, S., Cullimore, J., Gamas, P., Niebel, A., and Ott, T.** (2010). A remorin protein interacts with symbiotic receptors and regulates bacterial infection. *Proc Natl Acad Sci U S A* **107**, 2343-2348.
- Lei, M.J., Wang, Q., Li, X., Chen, A., Luo, L., Xie, Y., Li, G., Luo, D., Mysore, K.S., Wen, J., Xie, Z.P., Staehelin, C., and Wang, Y.Z.** (2015). The small GTPase ROP10 of *Medicago truncatula* is required for both tip growth of root hairs and nod factor-induced root hair deformation. *Plant Cell* **27**, 806-822.
- Leigh, J.A., Signer, E.R., and Walker, G.C.** (1985). Exopolysaccharide-deficient mutants of *Rhizobium meliloti* that form ineffective nodules. *Proc Natl Acad Sci U S A* **82**, 6231-6235.
- Leigh, J.A., Reed, J.W., Hanks, J.F., Hirsch, A.M., and Walker, G.C.** (1987). *Rhizobium meliloti* mutants that fail to succinylate their calcofluor-binding exopolysaccharide are defective in nodule invasion. *Cell* **51**, 579-587.
- Lerouxel, O., Cavalier, D.M., Liepman, A.H., and Keegstra, K.** (2006). Biosynthesis of plant cell wall polysaccharides - a complex process. *Curr Opin Plant Biol* **9**, 621-630.
- Levy, J., Bres, C., Geurts, R., Chalhoub, B., Kulikova, O., Duc, G., Journet, E.P., Ane, J.M., Lauber, E., Bisseling, T., Denarie, J., Rosenberg, C., and Debelle, F.** (2004). A putative Ca²⁺ and calmodulin-dependent protein kinase required for bacterial and fungal symbioses. *Science* **303**, 1361-1364.
- Leyser, O.** (2011). Auxin, self-organisation, and the colonial nature of plants. *Curr Biol* **21**, R331-337.
- Li, H., Shen, J.J., Zheng, Z.L., Lin, Y., and Yang, Z.** (2001). The Rop GTPase switch controls multiple developmental processes in *Arabidopsis*. *Plant Physiol* **126**, 670-684.
- Li, H., Lin, D., Dhonukshe, P., Nagawa, S., Chen, D., Friml, J., Scheres, B., Guo, H., and Yang, Z.** (2011). Phosphorylation switch modulates the interdigitated pattern of PIN1 localization and cell expansion in *Arabidopsis* leaf epidermis. *Cell Res* **21**, 970-978.
- Li, R.L., Liu, P., Wan, Y.L., Chen, T., Wang, Q.L., Mettbach, U., Baluska, F., Samaj, J., Fang, X.H., Lucas, W.J., and Lin, J.X.** (2012). A Membrane Microdomain-Associated Protein, *Arabidopsis*

- Flot1, Is Involved in a Clathrin-Independent Endocytic Pathway and Is Required for Seedling Development. *Plant Cell* **24**, 2105-2122.
- Lillemeier, B.F., Pfeiffer, J.R., Surviladze, Z., Wilson, B.S., and Davis, M.M.** (2006). Plasma membrane-associated proteins are clustered into islands attached to the cytoskeleton. *Proc Natl Acad Sci U S A* **103**, 18992-18997.
- Limpens, E., Franken, C., Smit, P., Willemse, J., Bisseling, T., and Geurts, R.** (2003). LysM domain receptor kinases regulating rhizobial Nod factor-induced infection. *Science* **302**, 630-633.
- Limpens, E., Mirabella, R., Fedorova, E., Franken, C., Franssen, H., Bisseling, T., and Geurts, R.** (2005). Formation of organelle-like N₂-fixing symbiosomes in legume root nodules is controlled by DMI2. *Proc Natl Acad Sci U S A* **102**, 10375-10380.
- Liu, J., Deyoung, S.M., Zhang, M., Dold, L.H., and Saltiel, A.R.** (2005). The stomatin/prohibitin/flotillin/HflK/C domain of flotillin-1 contains distinct sequences that direct plasma membrane localization and protein interactions in 3T3-L1 adipocytes. *J Biol Chem* **280**, 16125-16134.
- Liu, Z., Persson, S., and Sanchez-Rodriguez, C.** (2015a). At the border: the plasma membrane-cell wall continuum. *J Exp Bot* **66**, 1553-1563.
- Liu, Z., Persson, S., and Zhang, Y.** (2015b). The connection of cytoskeletal network with plasma membrane and the cell wall. *J Integr Plant Biol* **57**, 330-340.
- Lopez, D., and Kolter, R.** (2010). Functional microdomains in bacterial membranes. *Genes Dev* **24**, 1893-1902.
- Lu, D., Lin, W., Gao, X., Wu, S., Cheng, C., Avila, J., Heese, A., Devarenne, T.P., He, P., and Shan, L.** (2011). Direct ubiquitination of pattern recognition receptor FLS2 attenuates plant innate immunity. *Science* **332**, 1439-1442.
- Lu, Y.J., Schornack, S., Spallek, T., Geldner, N., Chory, J., Schellmann, S., Schumacher, K., Kamoun, S., and Robatzek, S.** (2012). Patterns of plant subcellular responses to successful oomycete infections reveal differences in host cell reprogramming and endocytic trafficking. *Cell Microbiol* **14**, 682-697.
- Ludwig, A., Otto, G.P., Riento, K., Hams, E., Fallon, P.G., and Nichols, B.J.** (2010). Flotillin microdomains interact with the cortical cytoskeleton to control uropod formation and neutrophil recruitment. *J Cell Biol* **191**, 771-781.
- Macfall, J.S., Pfeffer, P.E., Rolin, D.B., Macfall, J.R., and Johnson, G.A.** (1992). Observation of the Oxygen Diffusion Barrier in Soybean (*Glycine max*) Nodules with Magnetic Resonance Microscopy. *Plant Physiol* **100**, 1691-1697.
- MacLellan, D.L., Steen, H., Adam, R.M., Garlick, M., Zurakowski, D., Gygi, S.P., Freeman, M.R., and Solomon, K.R.** (2005). A quantitative proteomic analysis of growth factor-induced compositional changes in lipid rafts of human smooth muscle cells. *Proteomics* **5**, 4733-4742.
- Madsen, E.B., Madsen, L.H., Radutoiu, S., Olbryt, M., Rakwalska, M., Szczyglowski, K., Sato, S., Kaneko, T., Tabata, S., Sandal, N., and Stougaard, J.** (2003). A receptor kinase gene of the LysM type is involved in legume perception of rhizobial signals. *Nature* **425**, 637-640.
- Madsen, E.B., Antolin-Llovera, M., Grossmann, C., Ye, J.Y., Vieweg, S., Broghammer, A., Krusell, L., Radutoiu, S., Jensen, O.N., Stougaard, J., and Parniske, M.** (2011). Autophosphorylation is essential for the in vivo function of the *Lotus japonicus* Nod factor receptor 1 and receptor-mediated signalling in cooperation with Nod factor receptor 5. *Plant J* **65**, 404-417.

References

- Madsen, L.H., Tirichine, L., Jurkiewicz, A., Sullivan, J.T., Heckmann, A.B., Bek, A.S., Ronson, C.W., James, E.K., and Stougaard, J.** (2010). The molecular network governing nodule organogenesis and infection in the model legume *Lotus japonicus*. *Nature Communications* **1**.
- Maillet, F., Poinso, V., Andre, O., Puech-Pages, V., Haouy, A., Gueunier, M., Cromer, L., Giraudet, D., Formey, D., Niebel, A., Martinez, E.A., Driguez, H., Becard, G., and Denarie, J.** (2011). Fungal lipochitooligosaccharide symbiotic signals in arbuscular mycorrhiza. *Nature* **469**, 58-U1501.
- Malinsky, J., Opekarova, M., Grossmann, G., and Tanner, W.** (2013). Membrane Microdomains, Rafts, and Detergent-Resistant Membranes in Plants and Fungi. *Annu Rev Plant Biol* **64**, 501-529.
- Manders, E.M., Stap, J., Brakenhoff, G.J., van Driel, R., and Aten, J.A.** (1992). Dynamics of three-dimensional replication patterns during the S-phase, analysed by double labelling of DNA and confocal microscopy. *J Cell Sci* **103 (Pt 3)**, 857-862.
- Marc, J., Granger, C.L., Brincat, J., Fisher, D.D., Kao, T., McCubbin, A.G., and Cyr, R.J.** (1998). A GFP-MAP4 reporter gene for visualizing cortical microtubule rearrangements in living epidermal cells. *Plant Cell* **10**, 1927-1940.
- Marin, M., and Ott, T.** (2012). Phosphorylation of intrinsically disordered regions in remorin proteins. *Front Plant Sci* **3**, 86.
- Marin, M., and Ott, T.** (2014). Intrinsic disorder in plant proteins and phytopathogenic bacterial effectors. *Chem Rev* **114**, 6912-6932.
- Marin, M., Thallmair, V., and Ott, T.** (2012). The intrinsically disordered N-terminal region of AtREM1.3 remorin protein mediates protein-protein interactions. *J Biol Chem* **287**, 39982-39991.
- Marino, D., Andrio, E., Danchin, E.G., Oger, E., Gucciardo, S., Lambert, A., Puppo, A., and Pauly, N.** (2011). A *Medicago truncatula* NADPH oxidase is involved in symbiotic nodule functioning. *New Phytol* **189**, 580-592.
- Martiniere, A., Gayral, P., Hawes, C., and Runions, J.** (2011). Building bridges: formin1 of *Arabidopsis* forms a connection between the cell wall and the actin cytoskeleton. *Plant J* **66**, 354-365.
- Martiniere, A., Lavagi, I., Nageswaran, G., Rolfe, D.J., Maneta-Peyret, L., Luu, D.T., Botchway, S.W., Webb, S.E.D., Mongrand, S., Maurel, C., Martin-Fernandez, M.L., Kleine-Vehn, J., Friml, J., Moreau, P., and Runions, J.** (2012). Cell wall constrains lateral diffusion of plant plasma-membrane proteins. *P Natl Acad Sci USA* **109**, 12805-12810.
- Mateos, P.F., Jimenez-Zurdo, J.I., Chen, J., Squartini, A.S., Haack, S.K., Martinez-Molina, E., Hubbell, D.H., and Dazzo, F.B.** (1992). Cell-associated pectinolytic and cellulolytic enzymes in *Rhizobium leguminosarum* biovar *trifolii*. *Appl Environ Microbiol* **58**, 1816-1822.
- Mbengue, M., Camut, S., de Carvalho-Niebel, F., Deslandes, L., Froidure, S., Klaus-Heisen, D., Moreau, S., Rivas, S., Timmers, T., Herve, C., Cullimore, J., and Lefebvre, B.** (2010). The *Medicago truncatula* E3 Ubiquitin Ligase PUB1 Interacts with the LYK3 Symbiotic Receptor and Negatively Regulates Infection and Nodulation. *Plant Cell* **22**, 3474-3488.
- McKenna, J.F., Tolmie, A.F., and Runions, J.** (2014). Across the great divide: the plant cell surface continuum. *Curr Opin Plant Biol* **22**, 132-140.
- Men, S., Boutte, Y., Ikeda, Y., Li, X., Palme, K., Stierhof, Y.D., Hartmann, M.A., Moritz, T., and Grebe, M.** (2008). Sterol-dependent endocytosis mediates post-cytokinetic acquisition of PIN2 auxin efflux carrier polarity. *Nat Cell Biol* **10**, 237-244.
- Messinese, E., Mun, J.H., Yeun, L.H., Jayaraman, D., Rouge, P., Barre, A., Lougnon, G., Schornack, S., Bono, J.J., Cook, D.R., and Ane, J.M.** (2007). A novel nuclear protein interacts with the

- symbiotic DMI3 calcium- and calmodulin-dependent protein kinase of *Medicago truncatula*. *Mol Plant Microbe Interact* **20**, 912-921.
- Michelot, A., Derivery, E., Paterski-Boujemaa, R., Guerin, C., Huang, S., Parcy, F., Staiger, C.J., and Blanchoin, L.** (2006). A novel mechanism for the formation of actin-filament bundles by a nonprocessive formin. *Curr Biol* **16**, 1924-1930.
- Michniewicz, M., Zago, M.K., Abas, L., Weijers, D., Schweighofer, A., Meskiene, I., Heisler, M.G., Ohno, C., Zhang, J., Huang, F., Schwab, R., Weigel, D., Meyerowitz, E.M., Luschnig, C., Offringa, R., and Friml, J.** (2007). Antagonistic regulation of PIN phosphorylation by PP2A and PINOID directs auxin flux. *Cell* **130**, 1044-1056.
- Middleton, P.H., Jakab, J., Penmetsa, R.V., Starker, C.G., Doll, J., Kalo, P., Prabhu, R., Marsh, J.F., Mitra, R.M., Kereszt, A., Dudas, B., VandenBosch, K., Long, S.R., Cook, D.R., Kiss, G.B., and Oldroyd, G.E.** (2007). An ERF transcription factor in *Medicago truncatula* that is essential for Nod factor signal transduction. *Plant Cell* **19**, 1221-1234.
- Miller, J.B., Pratap, A., Miyahara, A., Zhou, L., Bornemann, S., Morris, R.J., and Oldroyd, G.E.D.** (2013). Calcium/Calmodulin-Dependent Protein Kinase Is Negatively and Positively Regulated by Calcium, Providing a Mechanism for Decoding Calcium Responses during Symbiosis Signaling. *Plant Cell* **25**, 5053-5066.
- Mitra, R.M., Gleason, C.A., Edwards, A., Hadfield, J., Downie, J.A., Oldroyd, G.E.D., and Long, S.R.** (2004). A Ca²⁺/calmodulin-dependent protein kinase required for symbiotic nodule development: Gene identification by transcript-based cloning. *Proc Natl Acad Sci USA* **101**, 4701-4705.
- Miwa, H., Sun, J., Oldroyd, G.E., and Downie, J.A.** (2006a). Analysis of Nod-factor-induced calcium signaling in root hairs of symbiotically defective mutants of *Lotus japonicus*. *Mol Plant Microbe Interact* **19**, 914-923.
- Miwa, H., Sun, J., Oldroyd, G.E., and Downie, J.A.** (2006b). Analysis of calcium spiking using aameleon calcium sensor reveals that nodulation gene expression is regulated by calcium spike number and the developmental status of the cell. *Plant J* **48**, 883-894.
- Miya, A., Albert, P., Shinya, T., Desaki, Y., Ichimura, K., Shirasu, K., Narusaka, Y., Kawakami, N., Kaku, H., and Shibuya, N.** (2007). CERK1, a LysM receptor kinase, is essential for chitin elicitor signaling in *Arabidopsis*. *Proc Natl Acad Sci U S A* **104**, 19613-19618.
- Miyahara, A., Richens, J., Starker, C., Morieri, G., Smith, L., Long, S., Downie, J.A., and Oldroyd, G.E.D.** (2010). Conservation in Function of a SCAR/WAVE Component During Infection Thread and Root Hair Growth in *Medicago truncatula*. *Mol Plant Microbe Interact* **23**, 1553-1562.
- Mohan, A., Oldfield, C.J., Radivojac, P., Vacic, V., Cortese, M.S., Dunker, A.K., and Uversky, V.N.** (2006). Analysis of molecular recognition features (MoRFs). *J Mol Biol* **362**, 1043-1059.
- Moling, S., Pietraszewska-Bogiel, A., Postma, M., Fedorova, E., Hink, M.A., Limpens, E., Gadella, T.W.J., and Bisseling, T.** (2014). Nod Factor Receptors Form Heteromeric Complexes and Are Essential for Intracellular Infection in *Medicago* Nodules. *Plant Cell* **26**, 4188-4199.
- Monshausen, G.B., Messerli, M.A., and Gilroy, S.** (2008). Imaging of the Yellow Cameleon 3.6 indicator reveals that elevations in cytosolic Ca²⁺ follow oscillating increases in growth in root hairs of *Arabidopsis*. *Plant Physiol* **147**, 1690-1698.
- Monshausen, G.B., Bibikova, T.N., Messerli, M.A., Shi, C., and Gilroy, S.** (2007). Oscillations in extracellular pH and reactive oxygen species modulate tip growth of *Arabidopsis* root hairs. *Proc Natl Acad Sci U S A* **104**, 20996-21001.
- Montiel, J., Nava, N., Cardenas, L., Sanchez-Lopez, R., Arthikala, M.K., Santana, O., Sanchez, F., and Quinto, C.** (2012). A *Phaseolus vulgaris* NADPH oxidase gene is required for root infection by *Rhizobia*. *Plant Cell Physiol* **53**, 1751-1767.

References

- Morlot, S., and Roux, A.** (2013). Mechanics of dynamin-mediated membrane fission. *Annu Rev Biophys* **42**, 629-649.
- Morone, N., Nakada, C., Umemura, Y., Usukura, J., and Kusumi, A.** (2008). Three-dimensional molecular architecture of the plasma-membrane-associated cytoskeleton as reconstructed by freeze-etch electron tomography. *Methods Cell Biol* **88**, 207-236.
- Morone, N., Fujiwara, T., Murase, K., Kasai, R.S., Ike, H., Yuasa, S., Usukura, J., and Kusumi, A.** (2006). Three-dimensional reconstruction of the membrane skeleton at the plasma membrane interface by electron tomography. *J Cell Biol* **174**, 851-862.
- Mueller, S.C., and Brown, R.M., Jr.** (1980). Evidence for an intramembrane component associated with a cellulose microfibril-synthesizing complex in higher plants. *J Cell Biol* **84**, 315-326.
- Mueller, V., Ringemann, C., Honigmann, A., Schwarzmann, G., Medda, R., Leutenegger, M., Polyakova, S., Belov, V.N., Hell, S.W., and Eggeling, C.** (2011). STED nanoscopy reveals molecular details of cholesterol- and cytoskeleton-modulated lipid interactions in living cells. *Biophys J* **101**, 1651-1660.
- Mulder, L., Lefebvre, B., Cullimore, J., and Imberty, A.** (2006). LysM domains of *Medicago truncatula* NFP protein involved in Nod factor perception. Glycosylation state, molecular modeling and docking of chitooligosaccharides and Nod factors. *Glycobiology* **16**, 801-809.
- Munoz, J.A., Coronado, C., Perez-Hormaeche, J., Kondorosi, A., Ratet, P., and Palomares, A.J.** (1998). MsPG3, a *Medicago sativa* polygalacturonase gene expressed during the alfalfa-*Rhizobium meliloti* interaction. *Proc Natl Acad Sci U S A* **95**, 9687-9692.
- Munro, S.** (2003). Lipid rafts: elusive or illusive? *Cell* **115**, 377-388.
- Murase, K., Fujiwara, T., Umemura, Y., Suzuki, K., Iino, R., Yamashita, H., Saito, M., Murakoshi, H., Ritchie, K., and Kusumi, A.** (2004). Ultrafine membrane compartments for molecular diffusion as revealed by single molecule techniques. *Biophys J* **86**, 4075-4093.
- Nagahashi, G., Thomson, W.W., and Leonard, R.T.** (1974). The casparian strip as a barrier to the movement of lanthanum in corn roots. *Science* **183**, 670-671.
- Nagawa, S., Xu, T., Lin, D., Dhonukshe, P., Zhang, X., Friml, J., Scheres, B., Fu, Y., and Yang, Z.** (2012). ROP GTPase-dependent actin microfilaments promote PIN1 polarization by localized inhibition of clathrin-dependent endocytosis. *Plos Biol* **10**, e1001299.
- Nakabayashi, T., Wang, H.P., Kinjo, M., and Ohta, N.** (2008). Application of fluorescence lifetime imaging of enhanced green fluorescent protein to intracellular pH measurements. *Photochem Photobiol Sci* **7**, 668-670.
- Nakagawa, T., Kaku, H., Shimoda, Y., Sugiyama, A., Shimamura, M., Takanashi, K., Yazaki, K., Aoki, T., Shibuya, N., and Kouchi, H.** (2011). From defense to symbiosis: limited alterations in the kinase domain of LysM receptor-like kinases are crucial for evolution of legume-*Rhizobium* symbiosis. *Plant J* **65**, 169-180.
- Naseer, S., Lee, Y., Lapierre, C., Franke, R., Nawrath, C., and Geldner, N.** (2012). Casparian strip diffusion barrier in *Arabidopsis* is made of a lignin polymer without suberin. *Proc Natl Acad Sci U S A* **109**, 10101-10106.
- Neduva, V., and Russell, R.B.** (2006). Peptides mediating interaction networks: new leads at last. *Curr Opin Biotechnol* **17**, 465-471.
- Neumann-Giesen, C., Fernow, I., Amaddii, M., and Tikkanen, R.** (2007). Role of EGF-induced tyrosine phosphorylation of reggie-1/flotillin-2 in cell spreading and signaling to the actin cytoskeleton. *J Cell Sci* **120**, 395-406.

- Neumann-Giesen, C., Falkenbach, B., Beicht, P., Claasen, S., Luers, G., Stuermer, C.A., Herzog, V., and Tikkanen, R.** (2004). Membrane and raft association of reggie-1/flotillin-2: role of myristoylation, palmitoylation and oligomerization and induction of filopodia by overexpression. *Biochem J* **378**, 509-518.
- Nicolson, G.L., Masouredis, S.P., and Singer, S.J.** (1971a). Quantitative two-dimensional ultrastructural distribution of Rh o (D) antigenic sites on human erythrocyte membranes. *Proc Natl Acad Sci U S A* **68**, 1416-1420.
- Nicolson, G.L., Hyman, R., and Singer, S.J.** (1971b). The two-dimensional topographic distribution of H-2 histocompatibility alloantigens on mouse red blood cell membranes. *J Cell Biol* **50**, 905-910.
- Niv, H., Gutman, O., Kloog, Y., and Henis, Y.I.** (2002). Activated K-Ras and H-Ras display different interactions with saturable nonraft sites at the surface of live cells. *J Cell Biol* **157**, 865-872.
- Oda, Y., and Fukuda, H.** (2012). Initiation of cell wall pattern by a Rho- and microtubule-driven symmetry breaking. *Science* **337**, 1333-1336.
- Oldfield, C.J., Cheng, Y., Cortese, M.S., Romero, P., Uversky, V.N., and Dunker, A.K.** (2005). Coupled folding and binding with alpha-helix-forming molecular recognition elements. *Biochemistry-Us* **44**, 12454-12470.
- Oldroyd, G.E., Murray, J.D., Poole, P.S., and Downie, J.A.** (2011). The rules of engagement in the legume-rhizobial symbiosis. *Annu Rev Genet* **45**, 119-144.
- Oldroyd, G.E.D.** (2013). Speak, friend, and enter: signalling systems that promote beneficial symbiotic associations in plants. *Nat Rev Microbiol* **11**, 252-263.
- Oldroyd, G.E.D., and Downie, J.A.** (2004). Calcium, kinases and nodulation signalling in legumes. *Nat Rev Mol Cell Bio* **5**, 566-576.
- Otto, G.P., and Nichols, B.J.** (2011). The roles of flotillin microdomains--endocytosis and beyond. *J Cell Sci* **124**, 3933-3940.
- Panteris, E., Adamakis, I.D., Daras, G., Hatzopoulos, P., and Rigas, S.** (2013). Differential responsiveness of cortical microtubule orientation to suppression of cell expansion among the developmental zones of Arabidopsis thaliana root apex. *PLoS One* **8**, e82442.
- Parasassi, T., Gratton, E., Yu, W.M., Wilson, P., and Levi, M.** (1997). Two-photon fluorescence microscopy of laurdan generalized polarization domains in model and natural membranes. *Biophys J* **72**, 2413-2429.
- Paredez, A.R., Somerville, C.R., and Ehrhardt, D.W.** (2006). Visualization of cellulose synthase demonstrates functional association with microtubules. *Science* **312**, 1491-1495.
- Parniske, M.** (2008). Arbuscular mycorrhiza: the mother of plant root endosymbioses. *Nat Rev Microbiol* **6**, 763-775.
- Peck, M.C., Fisher, R.F., and Long, S.R.** (2006). Diverse flavonoids stimulate NodD1 binding to nod gene promoters in Sinorhizobium meliloti. *J Bacteriol* **188**, 5417-5427.
- Perraki, A., Cacas, J.L., Crowet, J.M., Lins, L., Castroviejo, M., German-Retana, S., Mongrand, S., and Raffaele, S.** (2012). Plasma membrane localization of Solanum tuberosum remorin from group 1, homolog 3 is mediated by conformational changes in a novel C-terminal anchor and required for the restriction of potato virus X movement]. *Plant Physiol* **160**, 624-637.
- Perraki, A., Binaghi, M., Mecchia, M.A., Gronnier, J., German-Retana, S., Mongrand, S., Bayer, E., Zelada, A.M., and Germain, V.** (2014). StRemorin1.3 hampers Potato virus X TGBp1 ability to

References

- increase plasmodesmata permeability, but does not interfere with its silencing suppressor activity. *Febs Lett* **588**, 1699-1705.
- Petrasek, J., and Schwarzerova, K.** (2009). Actin and microtubule cytoskeleton interactions. *Curr Opin Plant Biol* **12**, 728-734.
- Petrasek, J., Mravec, J., Bouchard, R., Blakeslee, J.J., Abas, M., Seifertova, D., Wisniewska, J., Tadele, Z., Kubes, M., Covanova, M., Dhonukshe, P., Skupa, P., Benkova, E., Perry, L., Krecek, P., Lee, O.R., Fink, G.R., Geisler, M., Murphy, A.S., Luschnig, C., Zazimalova, E., and Friml, J.** (2006). PIN proteins perform a rate-limiting function in cellular auxin efflux. *Science* **312**, 914-918.
- Petre, B., and Kamoun, S.** (2014). How do filamentous pathogens deliver effector proteins into plant cells? *Plos Biol* **12**, e1001801.
- Petutschnig, E.K., Jones, A.M., Serazetdinova, L., Lipka, U., and Lipka, V.** (2010). The lysin motif receptor-like kinase (LysM-RLK) CERK1 is a major chitin-binding protein in *Arabidopsis thaliana* and subject to chitin-induced phosphorylation. *J Biol Chem* **285**, 28902-28911.
- Pfister, A., Barberon, M., Alassimone, J., Kalmbach, L., Lee, Y., Vermeer, J.E., Yamazaki, M., Li, G., Maurel, C., Takano, J., Kamiya, T., Salt, D.E., Roppolo, D., and Geldner, N.** (2014). A receptor-like kinase mutant with absent endodermal diffusion barrier displays selective nutrient homeostasis defects. *Elife* **3**, e03115.
- Pietraszewska-Bogiel, A., Lefebvre, B., Koini, M.A., Klaus-Heisen, D., Takken, F.L.W., Geurts, R., Cullimore, J.V., and Gadella, T.W.J.** (2013). Interaction of *Medicago truncatula* Lysin Motif Receptor-Like Kinases, NFP and LYK3, Produced in *Nicotiana benthamiana* Induces Defence-Like Responses. *Plos One* **8**.
- Pike, L.J.** (2006). Rafts defined: a report on the Keystone Symposium on Lipid Rafts and Cell Function. *J Lipid Res* **47**, 1597-1598.
- Pike, L.J.** (2009). The challenge of lipid rafts. *J Lipid Res* **50 Suppl**, S323-328.
- Pitts, R.J., Cernac, A., and Estelle, M.** (1998). Auxin and ethylene promote root hair elongation in *Arabidopsis*. *Plant J* **16**, 553-560.
- Plett, J.M., Mathur, J., and Regan, S.** (2009). Ethylene receptor ETR2 controls trichome branching by regulating microtubule assembly in *Arabidopsis thaliana*. *J Exp Bot* **60**, 3923-3933.
- Popp, C., and Ott, T.** (2011). Regulation of signal transduction and bacterial infection during root nodule symbiosis. *Curr Opin Plant Biol* **14**, 458-467.
- Power, A.G.** (2010). Ecosystem services and agriculture: tradeoffs and synergies. *Philos T R Soc B* **365**, 2959-2971.
- Praefcke, G.J., and McMahon, H.T.** (2004). The dynamin superfamily: universal membrane tubulation and fission molecules? *Nat Rev Mol Cell Biol* **5**, 133-147.
- Preciado Lopez, M., Huber, F., Grigoriev, I., Steinmetz, M.O., Akhmanova, A., Koenderink, G.H., and Dogterom, M.** (2014). Actin-microtubule coordination at growing microtubule ends. *Nat Commun* **5**, 4778.
- Proseus, T.E., and Boyer, J.S.** (2005). Turgor pressure moves polysaccharides into growing cell walls of *Chara corallina*. *Ann Bot* **95**, 967-979.
- Qiu, L., Lin, J.S., Xu, J., Sato, S., Parniske, M., Wang, T.L., Downie, J.A., and Xie, F.** (2015). SCARN a Novel Class of SCAR Protein That Is Required for Root-Hair Infection during Legume Nodulation. *Plos Genet* **11**, e1005623.

- Radutoiu, S., Madsen, L.H., Madsen, E.B., Jurkiewicz, A., Fukai, E., Quistgaard, E.M.H., Albrektsen, A.S., James, E.K., Thirup, S., and Stougaard, J.** (2007). LysM domains mediate lipochitin-oligosaccharide recognition and Nfr genes extend the symbiotic host range. *Embo J* **26**, 3923-3935.
- Radutoiu, S., Madsen, L.H., Madsen, E.B., Felle, H.H., Umehara, Y., Gronlund, M., Sato, S., Nakamura, Y., Tabata, S., Sandal, N., and Stougaard, J.** (2003). Plant recognition of symbiotic bacteria requires two LysM receptor-like kinases. *Nature* **425**, 585-592.
- Raffaele, S., Bayer, E., and Mongrand, S.** (2009a). Upregulation of the plant protein remorin correlates with dehiscence and cell maturation: a link with the maturation of plasmodesmata? *Plant Signal Behav* **4**, 915-919.
- Raffaele, S., Mongrand, S., Gamas, P., Niebel, A., and Ott, T.** (2007). Genome-wide annotation of remorins, a plant-specific protein family: evolutionary and functional perspectives. *Plant Physiol* **145**, 593-600.
- Raffaele, S., Bayer, E., Lafarge, D., Cluzet, S., German Retana, S., Boubekour, T., Leborgne-Castel, N., Carde, J.P., Lherminier, J., Noirot, E., Satiat-Jeunemaitre, B., Laroche-Traineau, J., Moreau, P., Ott, T., Maule, A.J., Reymond, P., Simon-Plas, F., Farmer, E.E., Bessoule, J.J., and Mongrand, S.** (2009b). Remorin, a solanaceae protein resident in membrane rafts and plasmodesmata, impairs potato virus X movement. *Plant Cell* **21**, 1541-1555.
- Rahman, A., Takahashi, M., Shibasaki, K., Wu, S., Inaba, T., Tsurumi, S., and Baskin, T.I.** (2010). Gravitropism of *Arabidopsis thaliana* roots requires the polarization of PIN2 toward the root tip in meristematic cortical cells. *Plant Cell* **22**, 1762-1776.
- Refregier, G., Pelletier, S., Jaillard, D., and Hofte, H.** (2004). Interaction between wall deposition and cell elongation in dark-grown hypocotyl cells in *Arabidopsis*. *Plant Physiol* **135**, 959-968.
- Rich, M.K., Schorderet, M., and Reinhardt, D.** (2014). The role of the cell wall compartment in mutualistic symbioses of plants. *Front Plant Sci* **5**, 238.
- Ridge, R.W., and Rolfe, B.G.** (1985). *Rhizobium* sp. Degradation of Legume Root Hair Cell Wall at the Site of Infection Thread Origin. *Appl Environ Microbiol* **50**, 717-720.
- Ried, M.K., Antolin-Llovera, M., and Parniske, M.** (2014). Spontaneous symbiotic reprogramming of plant roots triggered by receptor-like kinases. *Elife* **3**.
- Riedl, J., Crevenna, A.H., Kessenbrock, K., Yu, J.H., Neukirchen, D., Bista, M., Bradke, F., Jenne, D., Holak, T.A., Werb, Z., Sixt, M., and Wedlich-Soldner, R.** (2008). Lifeact: a versatile marker to visualize F-actin. *Nat Methods* **5**, 605-607.
- Riely, B.K., Lougnon, G., Ane, J.M., and Cook, D.R.** (2007). The symbiotic ion channel homolog DMI1 is localized in the nuclear membrane of *Medicago truncatula* roots. *Plant J* **49**, 208-216.
- Riely, B.K., Larrainzar, E., Haney, C.H., Mun, J.H., Gil-Quintana, E., Gonzalez, E.M., Yu, H.J., Tricoli, D., Ehrhardt, D.W., Long, S.R., and Cook, D.R.** (2013). Development of tools for the biochemical characterization of the symbiotic receptor-like kinase DMI2. *Mol Plant Microbe Interact* **26**, 216-226.
- Ringli, C., Baumberger, N., Diet, A., Frey, B., and Keller, B.** (2002). ACTIN2 is essential for bulge site selection and tip growth during root hair development of *Arabidopsis*. *Plant Physiol* **129**, 1464-1472.
- Rizk, A., Paul, G., Incardona, P., Bugarski, M., Mansouri, M., Niemann, A., Ziegler, U., Berger, P., and Sbalzarini, I.F.** (2014). Segmentation and quantification of subcellular structures in fluorescence microscopy images using Squassh. *Nat Protoc* **9**, 586-596.

References

- Robatzek, S., Chinchilla, D., and Boller, T.** (2006). Ligand-induced endocytosis of the pattern recognition receptor FLS2 in Arabidopsis. *Genes Dev* **20**, 537-542.
- Robledo, M., Jimenez-Zurdo, J.I., Velazquez, E., Trujillo, M.E., Zurdo-Pineiro, J.L., Ramirez-Bahena, M.H., Ramos, B., Diaz-Minguez, J.M., Dazzo, F., Martinez-Molina, E., and Mateos, P.F.** (2008). Rhizobium cellulase CelC2 is essential for primary symbiotic infection of legume host roots. *Proc Natl Acad Sci U S A* **105**, 7064-7069.
- Roche, P., Debelle, F., Maillet, F., Lerouge, P., Faucher, C., Truchet, G., Denarie, J., and Prome, J.C.** (1991). Molecular-Basis of Symbiotic Host Specificity in Rhizobium-Meliloti - Nodh and Nodpq Genes Encode the Sulfation of Lipo-Oligosaccharide Signals. *Cell* **67**, 1131-1143.
- Rockstrom, J., Steffen, W., Noone, K., Persson, A., Chapin, F.S., Lambin, E.F., Lenton, T.M., Scheffer, M., Folke, C., Schellnhuber, H.J., Nykvist, B., de Wit, C.A., Hughes, T., van der Leeuw, S., Rodhe, H., Sorlin, S., Snyder, P.K., Costanza, R., Svedin, U., Falkenmark, M., Karlberg, L., Corell, R.W., Fabry, V.J., Hansen, J., Walker, B., Liverman, D., Richardson, K., Crutzen, P., and Foley, J.A.** (2009). A safe operating space for humanity. *Nature* **461**, 472-475.
- Rodal, S.K., Skretting, G., Garred, O., Vilhardt, F., van Deurs, B., and Sandvig, K.** (1999). Extraction of cholesterol with methyl-beta-cyclodextrin perturbs formation of clathrin-coated endocytic vesicles. *Mol Biol Cell* **10**, 961-974.
- Rodriguez-Llorente, I.D., Perez-Hormaeche, J., Dary, M., Caviedes, M.A., Kondorosi, A., Ratet, P., and Palomares, A.J.** (2003). Expression of MsPG3-GFP fusions in Medicago truncatula hairy roots' reveals preferential tip localization of the protein in root hairs. *Eur J Biochem* **270**, 261-269.
- Roppolo, D., De Rybel, B., Denervaud Tendon, V., Pfister, A., Alassimone, J., Vermeer, J.E., Yamazaki, M., Stierhof, Y.D., Beeckman, T., and Geldner, N.** (2011). A novel protein family mediates Casparian strip formation in the endodermis. *Nature* **473**, 380-383.
- Rose, C.M., Venkateshwaran, M., Volkening, J.D., Grimsrud, P.A., Maeda, J., Bailey, D.J., Park, K., Howes-Podoll, M., den Os, D., Yeun, L.H., Westphall, M.S., Sussman, M.R., Ane, J.M., and Coon, J.J.** (2012). Rapid phosphoproteomic and transcriptomic changes in the rhizobia-legume symbiosis. *Mol Cell Proteomics* **11**, 724-744.
- Roux, K.J., Kim, D.I., and Burke, B.** (2013). BioID: a screen for protein-protein interactions. *Curr Protoc Protein Sci* **74**, Unit 19 23.
- Roux, K.J., Kim, D.I., Raida, M., and Burke, B.** (2012). A promiscuous biotin ligase fusion protein identifies proximal and interacting proteins in mammalian cells. *J Cell Biol* **196**, 801-810.
- Saito, K., Yoshikawa, M., Yano, K., Miwa, H., Uchida, H., Asamizu, E., Sato, S., Tabata, S., Imaizumi-Anraku, H., Umehara, Y., Kouchi, H., Murooka, Y., Szczyglowski, K., Downie, J.A., Parniske, M., Hayashi, M., and Kawaguchi, M.** (2007). NUCLEOPORIN85 is required for calcium spiking, fungal and bacterial symbioses, and seed production in Lotus japonicus. *Plant Cell* **19**, 610-624.
- Sako, Y., and Kusumi, A.** (1994). Compartmentalized structure of the plasma membrane for receptor movements as revealed by a nanometer-level motion analysis. *J Cell Biol* **125**, 1251-1264.
- Sampathkumar, A., Lindeboom, J.J., Debolt, S., Gutierrez, R., Ehrhardt, D.W., Ketelaar, T., and Persson, S.** (2011). Live Cell Imaging Reveals Structural Associations between the Actin and Microtubule Cytoskeleton in Arabidopsis. *Plant Cell* **23**, 2302-2313.
- Sampathkumar, A., Krupinski, P., Wightman, R., Milani, P., Berquand, A., Boudaoud, A., Hamant, O., Jonsson, H., and Meyerowitz, E.M.** (2014). Subcellular and supracellular mechanical stress prescribes cytoskeleton behavior in Arabidopsis cotyledon pavement cells. *Elife* **3**, e01967.

- Sauer, M., Balla, J., Luschnig, C., Wisniewska, J., Reinohl, V., Friml, J., and Benkova, E.** (2006). Canalization of auxin flow by Aux/IAA-ARF-dependent feedback regulation of PIN polarity. *Genes Dev* **20**, 2902-2911.
- Saxton, M.J.** (1989). The spectrin network as a barrier to lateral diffusion in erythrocytes. A percolation analysis. *Biophys J* **55**, 21-28.
- Saxton, M.J.** (1990). Lateral diffusion in a mixture of mobile and immobile particles. A Monte Carlo study. *Biophys J* **58**, 1303-1306.
- Schachtman, D.P., Schroeder, J.I., Lucas, W.J., Anderson, J.A., and Gaber, R.F.** (1992). Expression of an inward-rectifying potassium channel by the Arabidopsis KAT1 cDNA. *Science* **258**, 1654-1658.
- Schauser, L., Roussis, A., Stiller, J., and Stougaard, J.** (1999). A plant regulator controlling development of symbiotic root nodules. *Nature* **402**, 191-195.
- Schauser, L., Handberg, K., Sandal, N., Stiller, J., Thykjaer, T., Pajuelo, E., Nielsen, A., and Stougaard, J.** (1998). Symbiotic mutants deficient in nodule establishment identified after T-DNA transformation of *Lotus japonicus*. *Mol Gen Genet* **259**, 414-423.
- Schindelin, J., Arganda-Carreras, I., Frise, E., Kaynig, V., Longair, M., Pietzsch, T., Preibisch, S., Rueden, C., Saalfeld, S., Schmid, B., Tinevez, J.Y., White, D.J., Hartenstein, V., Eliceiri, K., Tomancak, P., and Cardona, A.** (2012). Fiji: an open-source platform for biological-image analysis. *Nat Methods* **9**, 676-682.
- Schneider, J., Klein, T., Mielich-Suss, B., Koch, G., Franke, C., Kuipers, O.P., Kovacs, A.T., Sauer, M., and Lopez, D.** (2015). Spatio-temporal remodeling of functional membrane microdomains organizes the signaling networks of a bacterium. *Plos Genet* **11**, e1005140.
- Schneider, R., and Persson, S.** (2015). Connecting two arrays: the emerging role of actin-microtubule cross-linking motor proteins. *Front Plant Sci* **6**, 415.
- Schoeck, F., and Perrimon, N.** (2002). Molecular mechanisms of epithelial morphogenesis. *Annu Rev Cell Dev Biol* **18**, 463-493.
- Schrick, K., Debolt, S., and Bulone, V.** (2012). Deciphering the molecular functions of sterols in cellulose biosynthesis. *Front Plant Sci* **3**, 84.
- Schroeder, R., London, E., and Brown, D.** (1994). Interactions between saturated acyl chains confer detergent resistance on lipids and glycosylphosphatidylinositol (GPI)-anchored proteins: GPI-anchored proteins in liposomes and cells show similar behavior. *Proc Natl Acad Sci U S A* **91**, 12130-12134.
- Schuck, S., Honsho, M., Ekroos, K., Shevchenko, A., and Simons, K.** (2003). Resistance of cell membranes to different detergents. *Proc Natl Acad Sci U S A* **100**, 5795-5800.
- Schwacke, R., Schneider, A., van der Graaff, E., Fischer, K., Catoni, E., Desimone, M., Frommer, W.B., Flugge, U.I., and Kunze, R.** (2003). ARAMEMNON, a novel database for Arabidopsis integral membrane proteins. *Plant Physiol* **131**, 16-26.
- Scita, G., and Di Fiore, P.P.** (2010). The endocytic matrix. *Nature* **463**, 464-473.
- Shaw, A.S.** (2006). Lipid rafts: now you see them, now you don't. *Nat Immunol* **7**, 1139-1142.
- Sheets, E.D., Simson, R., and Jacobson, K.** (1995). New insights into membrane dynamics from the analysis of cell surface interactions by physical methods. *Curr Opin Cell Biol* **7**, 707-714.

References

- Sheetz, M.P.** (1983). Membrane skeletal dynamics: role in modulation of red cell deformability, mobility of transmembrane proteins, and shape. *Semin Hematol* **20**, 175-188.
- Sheetz, M.P., Schindler, M., and Koppel, D.E.** (1980). Lateral mobility of integral membrane proteins is increased in spherocytic erythrocytes. *Nature* **285**, 510-511.
- Shogomori, H., and Brown, D.A.** (2003). Use of detergents to study membrane rafts: the good, the bad, and the ugly. *Biol Chem* **384**, 1259-1263.
- Shvartsman, D.E., Gutman, O., Tietz, A., and Henis, Y.I.** (2006). Cyclodextrins but not compactin inhibit the lateral diffusion of membrane proteins independent of cholesterol. *Traffic* **7**, 917-926.
- Simons, K., and Ikonen, E.** (1997). Functional rafts in cell membranes. *Nature* **387**, 569-572.
- Simons, K., and Vaz, W.L.** (2004). Model systems, lipid rafts, and cell membranes. *Annu Rev Biophys Biomol Struct* **33**, 269-295.
- Simons, K., and Gerl, M.J.** (2010). Revitalizing membrane rafts: new tools and insights. *Nat Rev Mol Cell Biol* **11**, 688-699.
- Simson, R., Sheets, E.D., and Jacobson, K.** (1995). Detection of temporary lateral confinement of membrane proteins using single-particle tracking analysis. *Biophys J* **69**, 989-993.
- Singer, S.J., and Nicolson, G.L.** (1972). The fluid mosaic model of the structure of cell membranes. *Science* **175**, 720-731.
- Singh, S., Katzer, K., Lambert, J., Cerri, M., and Parniske, M.** (2014). CYCLOPS, A DNA-Binding Transcriptional Activator, Orchestrates Symbiotic Root Nodule Development. *Cell Host Microbe* **15**, 139-152.
- Smit, P., Limpens, E., Geurts, R., Fedorova, E., Dolgikh, E., Gough, C., and Bisseling, T.** (2007). Medicago LYK3, an entry receptor in rhizobial nodulation factor signaling. *Plant Physiology* **145**, 183-191.
- Smith, J.M., Leslie, M.E., Robinson, S.J., Korasick, D.A., Zhang, T., Backues, S.K., Cornish, P.V., Koo, A.J., Bednarek, S.Y., and Heese, A.** (2014). Loss of *Arabidopsis thaliana* Dynamin-Related Protein 2B reveals separation of innate immune signaling pathways. *Plos Pathog* **10**, e1004578.
- Solis, G.P., Hoegg, M., Munderloh, C., Schrock, Y., Malaga-Trillo, E., Rivera-Milla, E., and Stuermer, C.A.** (2007). Reggie/flotillin proteins are organized into stable tetramers in membrane microdomains. *Biochem J* **403**, 313-322.
- Souter, M., Topping, J., Pullen, M., Friml, J., Palme, K., Hackett, R., Grierson, D., and Lindsey, K.** (2002). hydra Mutants of *Arabidopsis* are defective in sterol profiles and auxin and ethylene signaling. *Plant Cell* **14**, 1017-1031.
- Soyano, T., Kouchi, H., Hirota, A., and Hayashi, M.** (2013). NODULE INCEPTION Directly Targets NF-Y Subunit Genes to Regulate Essential Processes of Root Nodule Development in *Lotus japonicus*. *Plos Genet* **9**.
- Spira, F., Mueller, N.S., Beck, G., von Olshausen, P., Beig, J., and Wedlich-Soldner, R.** (2012). Patchwork organization of the yeast plasma membrane into numerous coexisting domains (vol 14, pg 640, 2012). *Nat Cell Biol* **14**, 890-890.
- Sprenger, R.R., Speijer, D., Back, J.W., De Koster, C.G., Pannekoek, H., and Horrevoets, A.J.** (2004). Comparative proteomics of human endothelial cell caveolae and rafts using two-dimensional gel electrophoresis and mass spectrometry. *Electrophoresis* **25**, 156-172.

- Steinwand, B.J., and Kieber, J.J.** (2010). The role of receptor-like kinases in regulating cell wall function. *Plant Physiol* **153**, 479-484.
- Stracke, S., Kistner, C., Yoshida, S., Mulder, L., Sato, S., Kaneko, T., Tabata, S., Sandal, N., Stougaard, J., Szczyglowski, K., and Parniske, M.** (2002). A plant receptor-like kinase required for both bacterial and fungal symbiosis. *Nature* **417**, 959-962.
- Stuermer, C.A.** (2011). Microdomain-forming proteins and the role of the reggies/flotillins during axon regeneration in zebrafish. *Biochim Biophys Acta* **1812**, 415-422.
- Stuermer, C.A., Lang, D.M., Kirsch, F., Wiechers, M., Deininger, S.O., and Plattner, H.** (2001). Glycosylphosphatidyl inositol-anchored proteins and fyn kinase assemble in noncaveolar plasma membrane microdomains defined by reggie-1 and -2. *Mol Biol Cell* **12**, 3031-3045.
- Sutter, J.U., Campanoni, P., Tyrrell, M., and Blatt, M.R.** (2006). Selective mobility and sensitivity to SNAREs is exhibited by the Arabidopsis KAT1 K⁺ channel at the plasma membrane. *Plant Cell* **18**, 935-954.
- Suzuki, K., Ritchie, K., Kajikawa, E., Fujiwara, T., and Kusumi, A.** (2005). Rapid hop diffusion of a G-protein-coupled receptor in the plasma membrane as revealed by single-molecule techniques. *Biophys J* **88**, 3659-3680.
- Szczyglowski, K., Shaw, R.S., Wopereis, J., Copeland, S., Hamburger, D., Kasiborski, B., Dazzo, F.B., and de Bruijn, F.J.** (1998). Nodule organogenesis and symbiotic mutants of the model legume *Lotus japonicus*. *Mol Plant Microbe In* **11**, 684-697.
- Szymanski, W.G., Zauber, H., Erban, A., Gorka, M., Wu, X.N., and Schulze, W.X.** (2015). Cytoskeletal Components Define Protein Location to Membrane Microdomains. *Mol Cell Proteomics* **14**, 2493-2509.
- Takamori, S., Holt, M., Stenius, K., Lemke, E.A., Gronborg, M., Riedel, D., Urlaub, H., Schenck, S., Brugger, B., Ringler, P., Muller, S.A., Rammner, B., Grater, F., Hub, J.S., De Groot, B.L., Mieskes, G., Moriyama, Y., Klingauf, J., Grubmuller, H., Heuser, J., Wieland, F., and Jahn, R.** (2006). Molecular anatomy of a trafficking organelle. *Cell* **127**, 831-846.
- Takeda, S., Gapper, C., Kaya, H., Bell, E., Kuchitsu, K., and Dolan, L.** (2008). Local positive feedback regulation determines cell shape in root hair cells. *Science* **319**, 1241-1244.
- Tanaka, K., Nguyen, C.T., Liang, Y., Cao, Y., and Stacey, G.** (2013). Role of LysM receptors in chitin-triggered plant innate immunity. *Plant Signal Behav* **8**, e22598.
- Tanner, W., Malinsky, J., and Opekarova, M.** (2011). In plant and animal cells, detergent-resistant membranes do not define functional membrane rafts. *Plant Cell* **23**, 1191-1193.
- Tansengco, M.L., Hayashi, M., Kawaguchi, M., Imaizumi-Anraku, H., and Murooka, Y.** (2003). crinkle, a novel symbiotic mutant that affects the infection thread growth and alters the root hair, trichome, and seed development in *Lotus japonicus*. *Plant Physiology* **131**, 1054-1063.
- Tansengco, M.L., Imaizumi-Anraku, H., Yoshikawa, M., Takagi, S., Kawaguchi, M., Hayashi, M., and Murooka, Y.** (2004). Pollen development and tube growth are affected in the symbiotic mutant of *Lotus japonicus*, crinkle. *Plant Cell Physiol* **45**, 511-520.
- Taylor, N.G.** (2011). A role for Arabidopsis dynamin related proteins DRP2A/B in endocytosis; DRP2 function is essential for plant growth. *Plant Mol Biol* **76**, 117-129.
- Teale, W.D., Paponov, I.A., and Palme, K.** (2006). Auxin in action: signalling, transport and the control of plant growth and development. *Nat Rev Mol Cell Biol* **7**, 847-859.

References

- Tilman, D., Fargione, J., Wolff, B., D'Antonio, C., Dobson, A., Howarth, R., Schindler, D., Schlesinger, W.H., Simberloff, D., and Swackhamer, D.** (2001). Forecasting agriculturally driven global environmental change. *Science* **292**, 281-284.
- Timmers, A.C.J.** (2008). The role of the plant cytoskeleton in the interaction between legumes and rhizobia. *J Microsc-Oxford* **231**, 247-256.
- Timmers, A.C.J., Auriac, M.C., and Truchet, G.** (1999). Refined analysis of early symbiotic steps of the Rhizobium-Medicago interaction in relationship with microtubular cytoskeleton rearrangements. *Development* **126**, 3617-3628.
- Tirichine, L., James, E.K., Sandal, N., and Stougaard, J.** (2006a). Spontaneous root-nodule formation in the model legume *Lotus japonicus*: A novel class of mutants nodulates in the absence of rhizobia. *Mol Plant Microbe In* **19**, 373-382.
- Tirichine, L., Imaizumi-Anraku, H., Yoshida, S., Murakami, Y., Madsen, L.H., Miwa, H., Nakagawa, T., Sandal, N., Albrektsen, A.S., Kawaguchi, M., Downie, A., Sato, S., Tabata, S., Kouchi, H., Parniske, M., Kawasaki, S., and Stougaard, J.** (2006b). Deregulation of a Ca²⁺/calmodulin-dependent kinase leads to spontaneous nodule development. *Nature* **441**, 1153-1156.
- Tjepkema, J.D., and Yocum, C.S.** (1974). Measurement of oxygen partial pressure within soybean nodules by oxygen microelectrodes. *Planta* **119**, 351-360.
- Tomishige, M., and Kusumi, A.** (1999). Compartmentalization of the erythrocyte membrane by the membrane skeleton: intercompartmental hop diffusion of band 3. *Mol Biol Cell* **10**, 2475-2479.
- Tóth, K., Stratil, T.F., Madsen, E.B., Ye, J., Popp, C., Antolin-Llovera, M., Grossmann, C., Jensen, O.N., Schussler, A., Parniske, M., and Ott, T.** (2012). Functional domain analysis of the Remorin protein LjSYMREM1 in *Lotus japonicus*. *PLoS One* **7**, e30817.
- Trehin, C., Schrempp, S., Chauvet, A., Berne-Dedieu, A., Thierry, A.M., Faure, J.E., Negrutiu, I., and Morel, P.** (2013). QUIRKY interacts with STRUBBELIG and PAL OF QUIRKY to regulate cell growth anisotropy during Arabidopsis gynoecium development. *Development* **140**, 4807-4817.
- Tsuji, A., and Ohnishi, S.** (1986). Restriction of the lateral motion of band 3 in the erythrocyte membrane by the cytoskeletal network: dependence on spectrin association state. *Biochemistry-U.S.* **25**, 6133-6139.
- Tsuji, A., Kawasaki, K., Ohnishi, S., Merkle, H., and Kusumi, A.** (1988). Regulation of band 3 mobilities in erythrocyte ghost membranes by protein association and cytoskeletal meshwork. *Biochemistry-U.S.* **27**, 7447-7452.
- Vacic, V., Oldfield, C.J., Mohan, A., Radivojac, P., Cortese, M.S., Uversky, V.N., and Dunker, A.K.** (2007). Characterization of molecular recognition features, MoRFs, and their binding partners. *J Proteome Res* **6**, 2351-2366.
- Vaddepalli, P., Herrmann, A., Fulton, L., Oelschner, M., Hillmer, S., Stratil, T.F., Fastner, A., Hammes, U.Z., Ott, T., Robinson, D.G., and Schneitz, K.** (2014). The C2-domain protein QUIRKY and the receptor-like kinase STRUBBELIG localize to plasmodesmata and mediate tissue morphogenesis in *Arabidopsis thaliana*. *Development* **141**, 4139-4148.
- van Brussel, A.A., Bakhuizen, R., van Spronsen, P.C., Spaink, H.P., Tak, T., Lugtenberg, B.J., and Kijne, J.W.** (1992a). Induction of pre-infection thread structures in the leguminous host plant by mitogenic lipo-oligosaccharides of Rhizobium. *Science* **257**, 70-72.
- Van Brussel, A.A.N., Bakhuizen, R., Vanspronsen, P.C., Spaink, H.P., Tak, T., Lugtenberg, B.J.J., and Kijne, J.W.** (1992b). Induction of Preinfection Thread Structures in the Leguminous Host Plant by Mitogenic Lipooligosaccharides of Rhizobium. *Science* **257**, 70-72.

- van der Honing, H.S., van Bezouwen, L.S., Emons, A.M., and Ketelaar, T.** (2011). High expression of Lifeact in *Arabidopsis thaliana* reduces dynamic reorganization of actin filaments but does not affect plant development. *Cytoskeleton (Hoboken)* **68**, 578-587.
- van Manen, H.J., Verkuijlen, P., Wittendorp, P., Subramaniam, V., van den Berg, T.K., Roos, D., and Otto, C.** (2008). Refractive index sensing of green fluorescent proteins in living cells using fluorescence lifetime imaging microscopy. *Biophys J* **94**, L67-69.
- van Meer, G., and Simons, K.** (1988). Lipid polarity and sorting in epithelial cells. *J Cell Biochem* **36**, 51-58.
- van Meer, G., Voelker, D.R., and Feigenson, G.W.** (2008). Membrane lipids: where they are and how they behave. *Nat Rev Mol Cell Biol* **9**, 112-124.
- Van Roey, K., Uyar, B., Weatheritt, R.J., Dinkel, H., Seiler, M., Budd, A., Gibson, T.J., and Davey, N.E.** (2014). Short linear motifs: ubiquitous and functionally diverse protein interaction modules directing cell regulation. *Chem Rev* **114**, 6733-6778.
- van Spronsen, P.C., Bakhuizen, R., van Brussel, A.A., and Kijne, J.W.** (1994). Cell wall degradation during infection thread formation by the root nodule bacterium *Rhizobium leguminosarum* is a two-step process. *Eur J Cell Biol* **64**, 88-94.
- Venkateshwaran, M., Jayaraman, D., Chabaud, M., Genre, A., Balloon, A.J., Maeda, J., Forshey, K., den Os, D., Kwiecien, N.W., Coon, J.J., Barker, D.G., and Ane, J.M.** (2015). A role for the mevalonate pathway in early plant symbiotic signaling. *Proc Natl Acad Sci U S A* **112**, 9781-9786.
- Vidali, L., Rounds, C.M., Hepler, P.K., and Bezanilla, M.** (2009). Lifeact-mEGFP reveals a dynamic apical F-actin network in tip growing plant cells. *PLoS One* **4**, e5744.
- Vieten, A., Sauer, M., Brewer, P.B., and Friml, J.** (2007). Molecular and cellular aspects of auxin-transport-mediated development. *Trends Plant Sci* **12**, 160-168.
- Voinnet, O., Rivas, S., Mestre, P., and Baulcombe, D.** (2003). An enhanced transient expression system in plants based on suppression of gene silencing by the p19 protein of tomato bushy stunt virus. *Plant J* **33**, 949-956.
- Walker, S.A., and Downie, J.A.** (2000). Entry of *Rhizobium leguminosarum* bv. *viciae* into root hairs requires minimal Nod factor specificity, but subsequent infection thread growth requires nodO or nodE. *Mol Plant Microbe Interact* **13**, 754-762.
- Wallin, E., and von Heijne, G.** (1998). Genome-wide analysis of integral membrane proteins from eubacterial, archaean, and eukaryotic organisms. *Protein Sci* **7**, 1029-1038.
- Wan, J., Tanaka, K., Zhang, X.C., Son, G.H., Brechenmacher, L., Nguyen, T.H., and Stacey, G.** (2012). LYK4, a lysin motif receptor-like kinase, is important for chitin signaling and plant innate immunity in *Arabidopsis*. *Plant Physiol* **160**, 396-406.
- Wan, J., Zhang, X.C., Neece, D., Ramonell, K.M., Clough, S., Kim, S.Y., Stacey, M.G., and Stacey, G.** (2008). A LysM receptor-like kinase plays a critical role in chitin signaling and fungal resistance in *Arabidopsis*. *Plant Cell* **20**, 471-481.
- Wang, B., and Qiu, Y.L.** (2006). Phylogenetic distribution and evolution of mycorrhizas in land plants. *Mycorrhiza* **16**, 299-363.
- Wang, C., Zhu, M., Duan, L., Yu, H., Chang, X., Li, L., Kang, H., Feng, Y., Zhu, H., Hong, Z., and Zhang, Z.** (2015a). Lotus japonicus clathrin heavy Chain1 is associated with Rho-Like GTPase ROP6 and involved in nodule formation. *Plant Physiol* **167**, 1497-1510.

References

- Wang, L., Li, H., Lv, X., Chen, T., Li, R., Xue, Y., Jiang, J., Jin, B., Baluska, F., Samaj, J., Wang, X., and Lin, J.** (2015b). Spatiotemporal Dynamics of the BRI1 Receptor and its Regulation by Membrane Microdomains in Living Arabidopsis Cells. *Mol Plant* **8**, 1334-1349.
- Wang, Q., Zhao, Y., Luo, W., Li, R., He, Q., Fang, X., Michele, R.D., Ast, C., von Wiren, N., and Lin, J.** (2013). Single-particle analysis reveals shutoff control of the Arabidopsis ammonium transporter AMT1;3 by clustering and internalization. *Proc Natl Acad Sci U S A* **110**, 13204-13209.
- Wang, W., Wen, Y., Berkey, R., and Xiao, S.** (2009). Specific targeting of the Arabidopsis resistance protein RPW8.2 to the interfacial membrane encasing the fungal Haustorium renders broad-spectrum resistance to powdery mildew. *Plant Cell* **21**, 2898-2913.
- Watanabe, Y., Meents, M.J., McDonnell, L.M., Barkwill, S., Sampathkumar, A., Cartwright, H.N., Demura, T., Ehrhardt, D.W., Samuels, A.L., and Mansfield, S.D.** (2015). Visualization of cellulose synthases in Arabidopsis secondary cell walls. *Science* **350**, 198-203.
- Whitehead, L.F., Young, S., and Day, D.A.** (1998). Aspartate and alanine movement across symbiotic membranes of soybean nodules. *Soil Biol Biochem* **30**, 1583-1589.
- Willemsen, V., Friml, J., Grebe, M., van den Toorn, A., Palme, K., and Scheres, B.** (2003). Cell polarity and PIN protein positioning in Arabidopsis require STEROL METHYLTRANSFERASE1 function. *Plant Cell* **15**, 612-625.
- Willige, B.C., Ahlers, S., Zourelidou, M., Barbosa, I.C., Demarsy, E., Trevisan, M., Davis, P.A., Roelfsema, M.R., Hangarter, R., Fankhauser, C., and Schwechheimer, C.** (2013). D6PK AGCVIII kinases are required for auxin transport and phototropic hypocotyl bending in Arabidopsis. *Plant Cell* **25**, 1674-1688.
- Willmann, R., Lajunen, H.M., Erbs, G., Newman, M.A., Kolb, D., Tsuda, K., Katagiri, F., Fliegmann, J., Bono, J.J., Cullimore, J.V., Jehle, A.K., Gotz, F., Kulik, A., Molinaro, A., Lipka, V., Gust, A.A., and Nurnberger, T.** (2011). Arabidopsis lysin-motif proteins LYM1 LYM3 CERK1 mediate bacterial peptidoglycan sensing and immunity to bacterial infection. *Proc Natl Acad Sci U S A* **108**, 19824-19829.
- Wisniewska, J., Xu, J., Seifertova, D., Brewer, P.B., Ruzicka, K., Blilou, I., Rouquie, D., Benkova, E., Scheres, B., and Friml, J.** (2006). Polar PIN localization directs auxin flow in plants. *Science* **312**, 883.
- Wolf, S., Hematy, K., and Hofte, H.** (2012). Growth control and cell wall signaling in plants. *Annu Rev Plant Biol* **63**, 381-407.
- Wright, P.E., and Dyson, H.J.** (1999). Intrinsically unstructured proteins: re-assessing the protein structure-function paradigm. *J Mol Biol* **293**, 321-331.
- Wunderlich, F., Ronai, A., Speth, V., Seelig, J., and Blume, A.** (1975). Thermotropic lipid clustering in tetrahymena membranes. *Biochemistry-U S* **14**, 3730-3735.
- Wunderlich, F., Kreutz, W., Mahler, P., Ronai, A., and Heppeler, G.** (1978). Thermotropic fluid goes to ordered "discontinuous" phase separation in microsomal lipids of Tetrahymena. An X-ray diffraction study. *Biochemistry-U S* **17**, 2005-2010.
- Wycoff, K.L., Hunt, S., Gonzales, M.B., VandenBosch, K.A., Layzell, D.B., and Hirsch, A.M.** (1998). Effects of oxygen on nodule physiology and expression of nodulins in alfalfa. *Plant Physiol* **117**, 385-395.
- Xie, F., Murray, J.D., Kim, J., Heckmann, A.B., Edwards, A., Oldroyd, G.E.D., and Downie, A.** (2012). Legume pectate lyase required for root infection by rhizobia. *Proc Natl Acad Sci USA* **109**, 633-638.

- Yang, W.L., Zhang, X., and Lin, H.K.** (2010). Emerging role of Lys-63 ubiquitination in protein kinase and phosphatase activation and cancer development. *Oncogene* **29**, 4493-4503.
- Yang, Z., and Fu, Y.** (2007). ROP/RAC GTPase signaling. *Curr Opin Plant Biol* **10**, 490-494.
- Yang, Z., and Lavagi, I.** (2012). Spatial control of plasma membrane domains: ROP GTPase-based symmetry breaking. *Curr Opin Plant Biol* **15**, 601-607.
- Yano, K., Shibata, S., Chen, W.L., Sato, S., Kaneko, T., Jurkiewicz, A., Sandal, N., Banba, M., Imaizumi-Anraku, H., Kojima, T., Ohtomo, R., Szczyglowski, K., Stougaard, J., Tabata, S., Hayashi, M., Kouchi, H., and Umehara, Y.** (2009). CERBERUS, a novel U-box protein containing WD-40 repeats, is required for formation of the infection thread and nodule development in the legume-Rhizobium symbiosis. *Plant J* **60**, 168-180.
- Yano, K., Yoshida, S., Muller, J., Singh, S., Banba, M., Vickers, K., Markmann, K., White, C., Schuller, B., Sato, S., Asamizu, E., Tabata, S., Murooka, Y., Perry, J., Wang, T.L., Kawaguchi, M., Imaizumi-Anraku, H., Hayashi, M., and Parniske, M.** (2008). CYCLOPS, a mediator of symbiotic intracellular accommodation. *Proc Natl Acad Sci U S A* **105**, 20540-20545.
- Yokota, K., Fukai, E., Madsen, L.H., Jurkiewicz, A., Rueda, P., Radutoiu, S., Held, M., Hossain, M.S., Szczyglowski, K., Morieri, G., Oldroyd, G.E.D., Downie, J.A., Nielsen, M.W., Rusek, A.M., Sato, S., Tabata, S., James, E.K., Oyaizu, H., Sandal, N., and Stougaard, J.** (2009). Rearrangement of Actin Cytoskeleton Mediates Invasion of Lotus japonicus Roots by Mesorhizobium loti. *Plant Cell* **21**, 267-284.
- Yuan, S., Zhu, H., Gou, H., Fu, W., Liu, L., Chen, T., Ke, D., Kang, H., Xie, Q., Hong, Z., and Zhang, Z.** (2012). A ubiquitin ligase of symbiosis receptor kinase involved in nodule organogenesis. *Plant Physiol* **160**, 106-117.
- Zeier, J., Ruel, K., Ryser, U., and Schreiber, L.** (1999). Chemical analysis and immunolocalisation of lignin and suberin in endodermal and hypodermal/rhizodermal cell walls of developing maize (*Zea mays* L.) primary roots. *Planta* **209**, 1-12.
- Zgadzaj, R., James, E.K., Kelly, S., Kawaharada, Y., de Jonge, N., Jensen, D.B., Madsen, L.H., and Radutoiu, S.** (2015). A legume genetic framework controls infection of nodules by symbiotic and endophytic bacteria. *Plos Genet* **11**, e1005280.
- Zhang, J., Nodzynski, T., Pencik, A., Rolcik, J., and Friml, J.** (2010). PIN phosphorylation is sufficient to mediate PIN polarity and direct auxin transport. *Proc Natl Acad Sci U S A* **107**, 918-922.
- Zhang, W., Tribble, R.P., and Samelson, L.E.** (1998). LAT palmitoylation: its essential role in membrane microdomain targeting and tyrosine phosphorylation during T cell activation. *Immunity* **9**, 239-246.
- Zhang, X.C., Cannon, S.B., and Stacey, G.** (2009). Evolutionary genomics of LysM genes in land plants. *Bmc Evol Biol* **9**.
- Zhao, X., Li, R., Lu, C., Baluska, F., and Wan, Y.** (2015). Di-4-ANEPPDHQ, a fluorescent probe for the visualisation of membrane microdomains in living *Arabidopsis thaliana* cells. *Plant Physiol Biochem* **87**, 53-60.
- Zidovetzki, R., and Levitan, I.** (2007). Use of cyclodextrins to manipulate plasma membrane cholesterol content: evidence, misconceptions and control strategies. *Biochim Biophys Acta* **1768**, 1311-1324.
- Zourelidou, M., Absmanner, B., Weller, B., Barbosa, I.C., Willige, B.C., Fastner, A., Streit, V., Port, S.A., Colcombet, J., de la Fuente van Bentem, S., Hirt, H., Kuster, B., Schulze, W.X., Hammes, U.Z., and Schwechheimer, C.** (2014). Auxin efflux by PIN-FORMED proteins is activated by two different protein kinases, D6 PROTEIN KINASE and PINOID. *Elife* **3**.

References

Zurzolo, C., van Meer, G., and Mayor, S. (2003). The order of rafts. Conference on microdomains, lipid rafts and caveolae. *EMBO Rep* **4**, 1117-1121.

Contributions to Publications

Tóth K*, **Stratil TF***, Madsen EB, Ye J, Popp C, et al. (2012). Functional Domain Analysis of the Remorin Protein LjSYMREM1 in *Lotus japonicus*. PLoS ONE 7(1): e30817. doi:10.1371/journal.pone.0030817. *equal contribution

In this manuscript, I cloned all constructs containing the LjSYMREM1_N- and C_terminal regions for BiFC, Y2H, FLIM-FRET, and protein purification analyses. Furthermore, I performed CLSM found in Figure 5, the Y2H drop tests of Figure 7, the protein purification experiments, and *in vitro* kinase assay of Figure 8 and S4. I also established, performed and analyzed the FLIM-FRET experiment in Table S2.

Jarsch IK, Konrad SSA, **Stratil TF**, et al (2014). Plasma Membranes Are Subcompartmentalized into a Plethora of Coexisting and Diverse Microdomains in *Arabidopsis* and *Nicotiana benthamiana*. The Plant Cell, 26: 1698–1711

For this manuscript, I performed FLIM-FRET analysis found in Figure 5. I also cloned the cytoskeleton markers and performed the CLSM, for the cytoskeleton disruption experiments of Supplemental Figure 5.

Konrad SSA*, Popp C*, **Stratil TF**, Jarsch IK, et al (2014). S-acylation anchors Remorin proteins to the plasma membrane but does not primarily determine their localization in membrane microdomains. New Phytologist, 203 (3): 758-769. *equal contribution

I transformed *Medicago* root cells and performed the CLSM localization analysis found in Figure 2b and Figure 6a, b, c.

Vaddepalli P, Herrmann A, Fulton L, Oelschner M, Hillmer S, **Stratil TF**, Fastner A, Hammes UZ, Ott T, Robinson DG, Schneitz K (2014) The C2-domain protein QUIRKY and the receptor-like kinase STRUBBELIG localize to plasmodesmata and mediate tissue morphogenesis in *Arabidopsis thaliana*. Development. doi: 10.1242/dev.113878

For this manuscript, I performed CLSM and FLIM-FRET analysis found in Figure 7 E, F.

Acknowledgments

First, I would like to thank Prof. Dr. Thomas Ott. Thank you Thomas, for providing me this opportunity to extend my diploma thesis project into a PhD project. Although project-wise some roadblocks were met, and some detours had to be taken, you continuously found the right words, showed lots of enthusiasm, and made problems seem like chances. I thank you for all the support and help you provided. Importantly, thank you for your great sense of humor; it made it very fun to work with you.

I thank Prof. Dr. Marc Bramkamp for providing the second expert opinion, and all other professors of the circulation committee for taking the time to read and evaluate this thesis.

I thank my great colleagues in the Ott group and from the Biocenter. I would specifically like to mention Jessica, Sandy, Uschi, Verena, Corinna, Addie, Iris, Katalin, Marion, Karl-Heinz, Andy, Marco, Ryan, Rosie, Felix, Paul, Esteban, and David. Thank you for providing scientific expertise, being helpful in the lab, and, more importantly, for making university-life as much fun as it was. Claudia, you were a great office mate, thank you for listening to my always-amazing stories and extremely funny jokes ;-)

Private acknowledgements were removed in this print-version.

Curriculum Vitae

THOMAS F. STRATIL

Born February 10, 1985

CURRENT

PhD Student, Faculty of Biology, Genetics, LMU Munich, Germany

Since September 2010, I am conducting doctoral research in the laboratory of Prof. Dr. Thomas Ott at the Genetics Institute of the Ludwigs- Maximilians University (LMU), Munich.

EDUCATION

2005 - 2010 **Diploma in Biology**, LMU, Munich, Germany

Major studies in Genetics

Minor studies in Biochemistry and Microbiology

2004 - 2005 **Military Service** (medics)

1996 - 2004 **High School Diploma, 'Abitur'**, Gisela Gymnasium, Munich, Germany